


2021

Novel Mammalian Models for Understanding and Treating Spinal Cord Injury

Michael B. Orr

University of Kentucky, michael.orr1991@gmail.com

Author ORCID Identifier:

 <https://orcid.org/0000-0001-5023-8197>

Digital Object Identifier: <https://doi.org/10.13023/etd.2021.341>

[Right click to open a feedback form in a new tab to let us know how this document benefits you.](#)

Recommended Citation

Orr, Michael B., "Novel Mammalian Models for Understanding and Treating Spinal Cord Injury" (2021).
Theses and Dissertations--Physiology. 52.
https://uknowledge.uky.edu/physiology_etds/52

This Doctoral Dissertation is brought to you for free and open access by the Physiology at UKnowledge. It has been accepted for inclusion in Theses and Dissertations--Physiology by an authorized administrator of UKnowledge. For more information, please contact UKnowledge@lsv.uky.edu.

STUDENT AGREEMENT:

I represent that my thesis or dissertation and abstract are my original work. Proper attribution has been given to all outside sources. I understand that I am solely responsible for obtaining any needed copyright permissions. I have obtained needed written permission statement(s) from the owner(s) of each third-party copyrighted matter to be included in my work, allowing electronic distribution (if such use is not permitted by the fair use doctrine) which will be submitted to UKnowledge as Additional File.

I hereby grant to The University of Kentucky and its agents the irrevocable, non-exclusive, and royalty-free license to archive and make accessible my work in whole or in part in all forms of media, now or hereafter known. I agree that the document mentioned above may be made available immediately for worldwide access unless an embargo applies.

I retain all other ownership rights to the copyright of my work. I also retain the right to use in future works (such as articles or books) all or part of my work. I understand that I am free to register the copyright to my work.

REVIEW, APPROVAL AND ACCEPTANCE

The document mentioned above has been reviewed and accepted by the student's advisor, on behalf of the advisory committee, and by the Director of Graduate Studies (DGS), on behalf of the program; we verify that this is the final, approved version of the student's thesis including all changes required by the advisory committee. The undersigned agree to abide by the statements above.

Michael B. Orr, Student

Dr. John C. Gensel, Major Professor

Dr. Kenneth S. Campbell, Director of Graduate Studies

NOVEL MAMMALIAN MODELS FOR UNDERSTANDING AND TREATING
SPINAL CORD INJURY

DISSERTATION

A dissertation submitted in partial fulfillment of the
requirements for the degree of Doctor of Philosophy in the
College of Medicine
at the University of Kentucky

By
Michael B. Orr

Lexington, Kentucky

Co-Directors: Dr. John Gensel, Professor of Physiology
and Dr. Kathryn Saatman, Professor of Physiology

Lexington, Kentucky

2021

Copyright © Michael B. Orr 2021
<https://orcid.org/0000-0001-5023-8197>

ABSTRACT OF DISSERTATION

Novel Mammalian Models for Understanding and Treating Spinal Cord Injury

Spinal cord injury (SCI) is devastating and often leaves the injured individual with persistent dysfunction. The injury persists because humans have poor wound repair and there are no pharmacologic treatments to induce wound repair after SCI. The continued efforts to discover therapeutic targets and develop treatments heavily relies on animal models. The purpose of this project is to develop and study novel mammalian models of SCI to provide insights for the development and effective implementation of SCI therapies.

Lab mice (*Mus musculus*) are a powerful tool for recapitulating the progression and persistent damage evident in human SCI, but our insight to naturally occurring wound repair because *Mus* recover poorly from SCI without intervention. Some non-mammalian species and neonates, on the other hand, can be used to identify therapeutic targets because they naturally regenerate spinal tissues. Unfortunately, translating therapeutic targets from non-mammalian or neonatal models to humans is onerous due to their phylogenetic and developmental disparity from adult mammals. One aspect of this project investigates SCI in the African spiny mouse (*Acomys cahirinus*), a rodent species with robust wound repair. In this investigation, I have identified enhanced functional recovery and tissue integrity in *Acomys* compared to *Mus*. Further investigations show that *Acomys* respond to injury with a dampened inflammatory and fibrotic scarring response, including a decrease in cells with fibroblast markers. The association of dampened inflammatory and fibrotic scarring responses with enhanced tissue integrity and functional recovery in the subacute window after SCI suggests that inhibiting subacute inflammatory and fibroblast proliferation and activation may be an effective strategy for inducing endogenous functional repair in the mammalian spinal cord. Further studies of SCI in *Acomys* can continue to illuminate the mechanism of endogenous repair in the mammalian spinal cord.

Effectively implementing therapies depends on accurately understanding the nature of the injury, which is doubly important in SCI because it is inherently heterogeneous. Several studies have suggested that the specific biomechanics of the initial SCI can influence overall outcomes of injury and perhaps even the secondary cellular responses to injury. While we have a broad understanding of these influences in SCI, the particular aspects of injury biomechanics and secondary injury responses have not been thoroughly investigated. In another aspect of my project, I investigate how subsequent compression affects the overall outcomes and inflammatory responses in *Mus* contusion SCI. This study identifies a unique injury progression specific to compression injuries, manifesting as a proportional increase in pathological macrophages, exacerbated tissue pathology, and a premature cessation of functional recovery in the subacute recovery window. Insights from this study provide strong rationale for the effectiveness of immunomodulatory therapies, particularly in SCI that involves sustained compression.

The novel mammalian models of SCI developed in this project point toward a strong influence of cellular dynamics in the subacute window after compression SCI. Insights across these studies can be applied to advance therapeutic development and to inform the effective application of these therapies.

KEYWORDS: Spinal cord injury, *Acomys*, wound repair, injury biomechanics, inflammation, fibrotic scarring

Michael B Orr

Author

May 19th, 2021

Date

Novel Mammalian Models for Understanding and Treating Spinal Cord Injury

By
Michael B Orr

Dr. John Gensel

Co-Director of Dissertation

Dr. Kathryn Saatman

Co-Director of Dissertation

Dr. Kenneth Campbell

Director of Graduate Studies

May 19th, 2021

Date

Dedicated to my wife, Molly Ann.
Your example inspires me to take joy in my studies,
and your unyielding support keeps me going even when that joy is hard to find.

ACKNOWLEDGMENTS

All that I have done and all that I am is the product of an incredibly blessed life filled with many loved ones. Mom and Dad, thank you for always prioritizing me and my education. You have been a constant source of support, encouragement, and love as I continue to learn and grow. Andrew and Stephen, thank you for being my best friends and confidants through all of life's seasons, especially when I need a diversion. Randolphs, thank you taking me in as one of your own and showing me all the love a son could ask for. Molly Ann, you deserve thanks for every word I have written and all the life that has been lived in their making.

My PhD would not be possible without the incredible advisors and co-workers with whom I have had the privilege to work. Dr. Gensel, you have a profound positive impact on my life, especially during this time of personal growth and development. I am continually reminded of how lucky I am to be working with you. Thank you to my many other mentors—especially those on my committee, in Physiology, and in SCoBIRC—who helped shape me as a professional and a scientist. Thank you to all my co-workers—especially Will, Tim, Andrew, Binoy, Zel, Bei, Jennifer, Chris, Sabryn, Kristin, and Corin—for your patience and tolerance, and for incredibly amount of work you have done to complete this project. My world is better for you all, and I hope you are proud of the fruits of all your hard work.

Finally, thank you to all my wonderful friends—especially Sarah, Shelby, Zach, Anthony, Chelsea, and Mitch—for lending an ear and inspiration on many occasions, and for helping me stay sane and smiling all along the way.

TABLE OF CONTENTS

ACKNOWLEDGMENTS	iii
TABLE OF CONTENTS	iv
LIST OF TABLES.....	vi
LIST OF FIGURES	vii
LIST OF ADDITIONAL FILES.....	ix
CHAPTER 1. An introduction to Understanding and Treating Spinal Cord Injury	1
1.1 <i>Clinical Presentation and Approaches for Spinal Cord Injury</i>	<i>1</i>
1.2 <i>Normal Function of the Spinal Cord</i>	<i>3</i>
1.3 <i>Endogenous Repair of the Damaged Spinal Cord.....</i>	<i>4</i>
1.4 <i>Pathological Responses to Spinal Cord Injury.....</i>	<i>5</i>
1.5 <i>Effects of Spinal Cord Injury Biomechanics.....</i>	<i>7</i>
1.6 <i>Understanding Spinal Cord Injury through Comparative Models.....</i>	<i>9</i>
CHAPTER 2. A Novel mammalian Model of Enhanced Recovery from Spinal Cord Injury, the African Spiny Mouse (<i>Acomys cahirinus</i>)	11
2.1 <i>Functional Deficits from Spinal Cord Injury in the Clinic.....</i>	<i>11</i>
2.2 <i>Open Field Testing of Motor Functional Recovery from Spinal Cord Injury.....</i>	<i>13</i>
2.3 <i>Acomys Show Enhanced Recovery from Spinal Cord Injury.....</i>	<i>15</i>
2.4 <i>Anatomical Damage from Spinal Cord Injury.....</i>	<i>27</i>
2.5 <i>Spinal Tissue Pathology in Acomys after Injury</i>	<i>30</i>
2.6 <i>Insights into Functional Recovery and Anatomical Pathology from Acomys Spinal Cord Injury</i>	<i>49</i>
CHAPTER 3. Dampened Inflammatory Response in Acomys Spinal Cord Injury.....	54
3.1 <i>Overview of Inflammation Following Spinal Cord Injury</i>	<i>54</i>
3.2 <i>Dual Role of Macrophages and Microglia in Secondary Damage and Wound Repair</i>	<i>56</i>
3.3 <i>Comparative Models Inform Our View of Macrophages in Wound Repair</i>	<i>58</i>
3.4 <i>Acomys Have Dampened Macrophage/Microglia Response to Spinal Cord Injury</i>	<i>61</i>
3.5 <i>Acomys Macrophages are Less Toxic to Neurons.....</i>	<i>70</i>
3.6 <i>Understanding the Role of Inflammation in Mammalian Spinal Repair through Acomys</i>	<i>76</i>
CHAPTER 4. Dampened Fibrotic Scarring in Acomys Spinal Cord Injury.....	80

4.1	<i>Glial and Fibrotic Scarring After Spinal Cord Injury</i>	80
4.2	<i>Comparative Models Reveal Importance of Glia and ECM in Wound Repair</i>	83
4.3	<i>Extracellular Matrix Molecules Affect Mammalian Neurite Growth</i>	85
4.4	<i>Acomys Have Dampened Fibrotic Scarring Response to SCI.....</i>	93
4.5	<i>Acomys Have Fewer PDGFRβ+ Cells in the Injured Spinal Cord</i>	101
4.6	<i>Understanding the Role of Fibrotic Scarring in Mammalian Spinal Cord Repair through Acomys</i> <i>115</i>	
CHAPTER 5. Injury Biomechanics Affect Spinal Cord Injury Progression		117
5.1	<i>Spinal Cord Injury is Meaningfully Heterogeneous.....</i>	117
5.2	<i>Experimental Design to Study the Effects of Compression in Spinal Cord Injury</i>	120
5.3	<i>Sustained Compression Decreases Functional Recovery from Contusion Spinal Cord Injury ...</i>	125
5.4	<i>Sustained Compression Decreases Tissue Sparing in Contusion Spinal Cord Injury.....</i>	133
5.5	<i>Sustained Compression Alters Inflammatory Response to Spinal Cord Injury</i>	140
CHAPTER 6. Conclusions on Targeting Secondary Injury Responses to Improve Recovery from Spinal Cord Injury 152		
6.1	<i>Crosstalk between macrophages and fibroblasts in injury responses</i>	152
6.2	<i>Role of PDGFRβ in tissue damage and repair.....</i>	156
6.3	<i>Hemodynamics and SCI progression</i>	160
6.4	<i>Summary of conclusions</i>	164
APPENDICES		166
1	<i>Appendix 1: Supplementary Figures</i>	166
2	<i>APPENDIX 2: Methods.....</i>	175
3	<i>APPENDIX 3: Materials</i>	192
4	<i>APPENDIX 4: Sample Sizes and Statistics</i>	198
Bibliography		207
Vita		234

LIST OF TABLES

<i>Table 5.2.1: Spinal Cord Injury Parameters</i>	<i>122</i>
<i>Table 5.3.1: Basso Mouse Scale Statistical Summary (p values).....</i>	<i>128</i>
<i>Table 5.4.1: Statistical summary (p values) for time course of epicenter tissue sparing</i>	<i>137</i>
<i>Table 5.4.2: Statistical summary (p values) for 28dpi rostral-caudal tissue sparing</i>	<i>138</i>

LIST OF FIGURES

<i>Figure 2.3.1: Acomys recover empty bladders and body weight more quickly than Mus.</i>	<i>18</i>
<i>Figure 2.3.2: Acomys and Mus have similar baseline hindlimb function and similar functional deficits from spinal crush.</i>	<i>22</i>
<i>Figure 2.3.3: Acomys exhibit enhanced functional recovery from SCI.</i>	<i>24</i>
<i>Figure 2.5.1: Chronic axon pathology in Mus.</i>	<i>33</i>
<i>Figure 2.5.2: Chronic axon pathology in Acomys.</i>	<i>35</i>
<i>Figure 2.5.3: Mus and Acomys axon pathology after SCI.</i>	<i>39</i>
<i>Figure 2.5.4: Mus and Acomys soma pathology after SCI.</i>	<i>42</i>
<i>Figure 2.5.5: Mus and Acomys have similar soma pathology after SCI.</i>	<i>43</i>
<i>Figure 2.5.6: Acomys have significantly more myelin sparing after SCI.</i>	<i>45</i>
<i>Figure 3.4.1: Acomys have a dampened immune response over time.</i>	<i>63</i>
<i>Figure 3.4.2: Acomys have a unique, dampened inflammatory response to SCI.</i>	<i>66</i>
<i>Figure 3.4.3: Acomys have a dampened inflammatory response with spatial restriction of macrophages/microglia.....</i>	<i>67</i>
<i>Figure 3.5.1: Activated Acomys macrophages are less neurotoxic than activated Mus macrophages.</i>	<i>74</i>
<i>Figure 4.3.1: Extracellular matrix molecules affect neurite growth.</i>	<i>90</i>
<i>Figure 4.4.1: Collagen IV histology after SCI in Mus and Acomys.</i>	<i>96</i>
<i>Figure 4.4.2: Acomys deposit significantly less collagen IV in the injured spinal cord than Mus.....</i>	<i>97</i>
<i>Figure 4.4.3: Acomys show dampened fibrotic scarring across various other ECM molecules.</i>	<i>99</i>
<i>Figure 4.5.1: Histological analysis of spinal PDGFRβ over time in the injured spinal cord.</i>	<i>105</i>
<i>Figure 4.5.2: Acomys have less spinal PDGFRβ at 2wpi.....</i>	<i>106</i>
<i>Figure 4.5.3: Acomys have less PDGFRβ chronically after SCI.</i>	<i>108</i>
<i>Figure 4.5.4: PDGFRβ+ staining has high overlap with alternative fibroblast marker, periostin.....</i>	<i>112</i>
<i>Figure 5.3.1: Compression impairs functional recovery from contusion SCI.....</i>	<i>127</i>
<i>Figure 5.3.2: Compression decreases functional recovery regardless of severity.</i>	<i>132</i>
<i>Figure 5.4.1: Compression significantly decreases anatomical recovery from contusion spinal cord injury.</i>	<i>136</i>
<i>Figure 5.4.2: Compression decreases anatomical recovery regardless of severity.</i>	<i>139</i>
<i>Figure 5.5.1: Representative images of macrophage/microglia phenotypic markers for histological analysis 7dpi and 14dpi.</i>	<i>143</i>
<i>Figure 5.5.2: Compression alters spinal cord injury macrophage activation at 7 dpi.....</i>	<i>146</i>
<i>Figure 5.5.3: Compression alters macrophage/microglia phenotypes 14 dpi.</i>	<i>147</i>

<i>Figure 5.5.4: Macrophage/microglia phenotypes are specifically regulated by compression independent of contusion severity.....</i>	<i>148</i>
---	------------

LIST OF ADDITIONAL FILES

Mus_HindlimbFunction_Uninjured.....	[MOV 119,841 KB]
Acomys_HindlimbFunction_Uninjured.....	[MOV 118,853 KB]
Mus_HindlimbFunction_3dpi.....	[MOV 67,682 KB]
Acomys_HindlimbFunction_3dpi.....	[MOV 62,399 KB]
Mus_HindlimbFunction_8wpi.....	[MOV 64,931 KB]
Acomys_HindlimbFunction_8wpi.....	[MOV 67,595 KB]
Rearing_HindlimbFunction_10wpi.....	[MOV 115,359 KB]

CHAPTER 1. AN INTRODUCTION TO UNDERSTANDING AND TREATING SPINAL CORD INJURY

Developing biomedical therapies requires researchers to discover physiologically-relevant targets and identify the proper contexts to enable efficacy of intervention. A critical first step toward developing therapies is building an understanding of the key differences between pathological and functional systems. This process is no less arduous or important than the creation of the intervention itself. Animal models are perhaps the most fundamental and powerful tools available to biomedical researchers because they provide the opportunity to create and test hypotheses in the complex contexts of a living creature. Throughout my doctoral training, I have developed and studied novel animal models of spinal cord injury (SCI) to identify potential therapeutic targets and the contexts in which these therapies would be efficacious.

1.1 Clinical Presentation and Approaches for Spinal Cord Injury

Each year in the United States, roughly 18,000 individuals survive a SCI and seek medical attention. Unfortunately, less than 1% experience complete neurological recovery by the time of discharge¹. This lack of recovery is due to an inability to naturally regenerate damaged spinal pathways and an absence of clinical treatments to induce robust reparative processes. The purpose of my research is to discover translatable therapeutic targets that will enable induction of endogenous repair processes after SCI, thereby improving the standard of care and standard of living for people with SCIs.

The inherently unexpected and heterogeneous nature of SCI makes the development of safe and effective therapies an onerous task for biomedical researchers. The most common stereotype is a young male suffering a SCI during an inherently

dangerous activity, but the reality of SCI is much more diverse. The most common causes of SCI are: vehicular crashes (39.2%), falls (31.8%), acts of violence (13.5%), sports/recreation activity (8.0%), and medical/surgery-related (3.1%)¹. These causes preclude preventative therapies due to their unexpected onset. Furthermore, the clinical presentation of injury is highly heterogeneous. Injuries vary in spinal location, injury severity, and injury type. Additionally, the patient population is not limited to any particular socioeconomic group, race, gender, or age. The sum of these factors means that biomedical researchers are striving to develop a therapy that can be administered after the SCI takes a place, and a therapy that will be efficacious across a spectrum of injury types and patients.

After the initial trauma inflicted by a SCI, resident neuronal and glial cells change physiological functions and peripheral cells cross the disrupted blood-spinal cord-barrier. The amalgamation of infiltrating and activated resident cells creates a complex SCI microenvironment. Some of these injury responses are critical for restoring and maintaining normal function of the spinal cord, but many aspects of these injury responses exacerbate the initial damage in a process known as secondary injury. The duality of this system allows researchers an opportunity to manipulate injury responses to better facilitate endogenous repair of spinal pathways. However, understanding each aspect of the injury response—both individually and within its greater microenvironmental context—is a challenging necessity to effectively employ therapies. The goal of this particular project is to understand how secondary injury responses contribute to reparative and pathological aspects of SCI, with the hope of identifying targets for therapies that will induce endogenous repair of damaged spinal pathways.

1.2 Normal Function of the Spinal Cord

The spinal cord is rich in neurons and glial cells. While glia are fairly ubiquitous throughout the cord, researchers have come to understand a fairly rigid organization of spinal neurons. Broadly speaking, the grey matter in the center of the spinal cord houses neuron cell bodies, called soma, and is surrounded by white matter that is rich in the axonal tracts that propagate information via action potentials. These action potentials carry information that governs sensory, motor, and autonomic function throughout the body.

Sensory information is carried through afferent pathways, which travel from peripheral tissues to the brain, while motor and autonomic control is carried through efferent pathways, which travel from the brain to peripheral targets. These pathways are strictly separated within the spinal cord and have distinct spinal exit points to preserve signal fidelity, but there is also controlled crosstalk between these pathways via interneurons that exist entirely within the spinal cord. Collectively, the afferent, efferent, and interneuron pathways facilitate transmission of sensory information, control autonomic function of involuntary actions, and perform controlled, voluntary motor functions.

In addition to neurons, a suite of glial cells are required for normal central nervous system (CNS) function. Oligodendrocytes wrap axons with myelin sheaths, insulating the axon to increase action potential conduction velocity and decrease signal decrement. Astrocytes interface with neurons and vasculature, where they sequester and transport neurotransmitters, ions, and nutrients to enable and optimize neuronal signaling. Pericytes ensheath endothelial cells of the CNS capillaries, where they optimize neurovascular function. Microglia patrol the CNS as resident immune cells, sampling the environment, destroying unwelcome constituents, phagocytosing pathogens and debris, and secreting

growth and supportive factors. Each of these glial cell types are necessary complements to their neuronal collaborators to maintain efficient signaling in the spinal cord².

1.3 Endogenous Repair of the Damaged Spinal Cord

While damage to the spinal cord causes neuron death and robust loss of axonal pathways, the injured spinal cord is capable of modest repair. In fact, there are several ways in which the spinal cord can re-establish functional pathways after injury. Damaged neurons can reform synaptic connections with the same or new targets or form similar or novel pathways. Additionally, axons can get to their destinations by regrowing directly through damaged areas or sprouting around the injury core³. Strict regeneration would form the same neuron-target connections through the same axonal pathways, but spinal repair through other means can elicit similar functional recovery.

One critical step in re-establishing spinal function is creating a permissive microenvironment for axon growth. For a long time, dogma dictated that CNS neurons were incapable of axon regrowth, unlike peripheral nervous system (PNS) neurons that readily regrow damaged axons. More recently, this dogma has been thoroughly overturned. Both CNS and PNS neurons are capable of robust axon regrowth *in vitro* and *in vivo*, but we have come to understand that the microenvironmental context is critical in determining the axon growth potential. When peripheral nerves are grafted onto the injured spinal cord, axons readily grow through the permissive PNS microenvironment⁴. Furthermore, specific manipulation of ECM proteoglycans allows enhanced axon regrowth into the SCI lesion⁵. While these studies indicate that adding a permissive environment or removing inhibitory factors allows regrowth, the unaltered SCI microenvironment is not completely inhibitory. Genetic manipulation of spinal neurons can induce axon regeneration through the unaltered

lesion core⁶. Collectively, we now understand that CNS are capable of axon regrowth, but the SCI microenvironment is a potent—though not insurmountable—barrier to axon regrowth.

It is critical to consider non-neuronal cells to create a spinal microenvironment that enables spinal repair. Upon injury, microglia transition from their quiescent, ramified morphology into activated states that are nearly indistinguishable from peripheral macrophages in their protein expression and morphology. These activated microglia, along with infiltrating neutrophils and macrophages, release proteolytic enzymes and reactive oxygen species (ROS) to break down debris and protect from potential invaders. In addition, fibroblasts proliferate and invade into the lesion core, where they deposit a variety of ECM molecules. Some posit that the provisional ECM scar serves a similar role in the CNS as in peripheral tissues, acting as a temporary scaffolding for cellular infiltration and facilitating eventual wound closure⁷⁻¹⁰. Astrocytes also play a critical role in the CNS injury response. Astrocytes proliferate, grow, and form a dense barrier at the edge of the lesion core to corral toxic species and limit the spread of damage into penumbral tissues¹¹. The functions of these resident glia and infiltrating cells, including other cell types not discussed above, are critical to clear the SCI site while preserving the structural integrity and protecting penumbral spared tissues.

1.4 Pathological Responses to Spinal Cord Injury

At the time of injury, synaptic connections are lost, axonal damage disrupts signal propagation, and neurons undergo mechanically-induced cell death. While some of this damage is immediately evident from blunt force mechanical trauma, much of the damage becomes evident over time through secondary cellular responses. One aspect of this

secondary damage is Wallerian Degeneration, where damaged axons and their associated myelin sheaths degrade away from the site of injury¹². This primary and secondary damage to axonal tracts is the most direct contributor to functional deficits from SCI.

Simply increasing spinal connectivity through inducing axon growth and synapse formation does not necessarily lead to improved outcomes, though. It is important to consider the dangerous dichotomy of novel synapse formation in the CNS, where the dense collection of potential neuronal targets can have myriad downstream effects. Synapses on random targets can give rise to maladaptive spasticity, which leads to complications including hypersensitivity, persistent pain, and autonomic dysreflexia^{13,14}. Therefore, truly beneficial spinal therapies must not only stabilize damaged neurons and re-establish functional pathways, but also ensure that only the right kind of spinal circuits are supported.

Non-neuronal cells also mount pathological responses to SCI. The primary injury triggers secondary injury responses, which are meant to clear debris, corral toxic species, and enable endogenous repair of damaged spinal pathways, but can also cause damage through a process known as secondary injury. In the injured spinal cord, resident glia secrete toxins and cytokines, which can damage tissue initially spared from mechanical trauma¹⁵. The diverse assemblage of glial cells, which is necessary to maintain healthy CNS function, becomes a complicated array of activated cells with pathological and reparative properties. Mechanical trauma and downstream signaling cascades further drive injury progression by facilitating infiltration of nonresident cells. Immune cells extravasate into the injury site and persist chronically within the injured spinal cord¹⁶⁻¹⁸. Fibroblasts infiltrate, proliferate, and deposit inhibitory ECM molecules within the injured spinal cord^{19,20}. Together, these resident and infiltrating cells facilitate the secondary injury.

1.5 Effects of Spinal Cord Injury Biomechanics

The accidental nature of SCI results in a wide variety of clinical presentations. Beyond the fact that any person—regardless of genetic background or lifestyle—can suffer a SCI, each injury can have distinct characteristics. Hereafter, I will refer to the specific aspects of the SCI as biomechanics. One of the most basic ways in which SCI biomechanics can differ is by severity. Many studies have shown that increasing the severity of the same type of SCI leads to worse damage to the spinal anatomy and worse subsequent motor function²¹⁻²⁵. While this is somewhat intuitive, it is important to understand that SCI is not an all-or-nothing system. Not only can deficits from injury manifest across a spectrum, but also benefits from treatment can provide meaningful improvements without achieving full anatomical or functional recovery. Indeed, people with lived experience specifically called for treatments that restore some, if not all, functionality at the National Institutes of Health-led conference “SCI 2020²⁶.”

Beyond severity, more specific SCI biomechanics can also affect the progression of injury. The initial SCI insult can result from fast or slow addition of force at a focal site or diffuse across the cord, which can be applied translationally (perpendicular or parallel with the cord) and/or rotationally. Each of these factors affect the deformation pattern of the soft spinal tissues, and can cause unique cellular dysfunction²⁷. These distinct biomechanics are at play in the heterogeneous clinical presentation of SCI. For example, consider two common types of SCI: gunshot wounds and fracture burst injury (vertebra breaks and presses into the cord). The gunshot wound would disrupt the blood-spinal cord-barrier (BSCB) in a penetrating injury with severe and transient application of force. The fracture burst injury, on the other hand, features rapid force generation across a greater surface area and sustained compressive force for a long period. Understanding the

similarities and differences in each of these injuries is key for effectively implementing therapies across this clinically heterogeneous condition.

Biomedical researchers are building an understanding of the effects of SCI biomechanics through animal models. A study of contusion (impacting), distraction (stretching), or dislocation (displacing) SCI reveals that these disparate biomechanics lead to unique lesion shapes and unique functional deficits²⁸. In another study, adding graded increases of compression to a contusion injury causes greater tissue damage and worsens functional recovery from injury²³. Counterintuitively, though, another study finds increased duration of compression does not affect anatomical or functional outcomes²⁹. Collectively, these studies show that specific SCI biomechanics are highly influential on the overall outcomes of SCI.

Decades of research have shown that the progression of SCI is largely determined by secondary injury responders. Unfortunately, little is known about how initial insult biomechanics affect secondary injury responses. Some studies have shown more severe injuries lead to more inflammation and fibrotic scarring^{21,30}. However, the little that we *do* understand is commonly investigated across various severities of the same injury type, not vice versa. It is reasonable to conceive that a particular injury biomechanic may play a specific role across a variety of injury severities. The very limited studies of this nature have shown that cellular function can be affected by injury biomechanics such as a direction of force application^{27,31}. The same may be true of another clinically-relevant injury biomechanic: compression. One aspect of my project investigates the role of compression, regardless of injury severity, in shaping the inflammatory response to SCI and the overall progression of injury.

1.6 Understanding Spinal Cord Injury through Comparative Models

The complexity and dynamic nature of SCI creates a challenge for deductive investigation by biomedical researchers. In one approach, researchers can take out specific cells to test their activity in a highly controlled environment (*in vitro*). Alternatively, researchers can test specific questions in live animals (*in vivo*) to gain insight in a more appropriately complex context. Rodents, including lab mice (*Mus musculus*) and lab rats (*Rattus norvegicus*), are perhaps the most common *in vivo* models for SCI. Using these rodent models allows researchers to test particular questions with the knowledge that general aspects of rodent SCI—including long-term deficits, the inflammatory response, and the scarring response—approximate the responses seen in human SCI.

While recapitulating the human condition is important, the fact that common rodent models do not naturally regenerate damage pathways limits the insight they can provide. Plainly, these rodents indicate intervention effectiveness, but do not naturally point the way *toward* effective therapeutic targets. Instead, researchers will often try to change the naturally-occurring systems in *Mus musculus*, commonly through genetic manipulation, in an attempt to induce regeneration. This approach can provide answers to very precise questions, but the genetic changes can also cause widespread, off-target effects by altering fundamental processes established over millions of years of evolution.

An alternative approach for identifying therapeutic interventions is to use naturally-occurring models of regeneration. Comparative biologists have studied SCI in regenerating animals such as salamanders, fish, newts, frogs, and neonatal opossums³². Unfortunately, we have only identified robust regeneration and spinal repair in these non-mammalian species and neonates. Translating therapeutic targets identified in non-mammalian species or neonates is incredibly difficult due to their phylogenetic or developmental differences

from adult humans. For instance, non-mammalian species have fundamentally different populations of glial cells and neuroarchitecture within the spinal cord³².

My project investigates SCI in a novel mammalian model, *Acomys cahirinus*, which shows enhanced repair after a wide variety of injuries. Thus far, *Acomys* have been shown to regenerate kidney, skeletal muscle, skin, glands, adipose tissue, cartilage, and axons³³⁻³⁷. Importantly, *Acomys* ear regeneration involves a unique, pro-regenerative deposition of ECM molecules³⁴, and requires a unique, pro-regenerative inflammatory response³⁸. The robust and wide-spread regeneration in *Acomys*, along with the importance of ECM and inflammation in SCI, provides strong rationale that *Acomys* may be a valuable comparative model to uncover therapeutic targets for inducing mammalian spinal repair.

CHAPTER 2. A NOVEL MAMMALIAN MODEL OF ENHANCED RECOVERY FROM SPINAL CORD INJURY, THE AFRICAN SPINY MOUSE (*ACOMYS CAHIRINUS*)

Neural information and control of the body's motor, sensory, and autonomic systems flow between peripheral systems and the brain through the spinal cord. Accordingly, SCI results in motor, sensory, and autonomic functional deficits. While the human body is capable of wound repair of many peripheral tissues, we exhibit poor spinal cord repair^{39,40}. Indeed, the initial SCI spreads to damage nearby spinal tissues and results in chronic anatomical damage and functional deficits^{41,42}. Limiting the spread of injury and inducing spinal repair has remained an elusive goal for biomedical researchers. One approach to uncovering novel therapeutic targets is to study animals with enhanced anatomical and/or functional recovery from SCI. Unfortunately we have only identified non-mammalian and neonatal model systems in which to study enhanced spinal repair³². In this chapter, I will discuss my investigations into the anatomy and functional recovery of *Acomys*, a novel mammalian model of enhanced repair⁴³, after SCI. By comparing *Acomys* to *Mus musculus*, a common rodent model of SCI, I will show that *Acomys* can serve as an informative model to better understand enhanced recovery from SCI in mammals.

2.1 Functional Deficits from Spinal Cord Injury in the Clinic

At least 99% of patients have functional deficits at the time of hospital discharge following SCI¹. For decades, the nominal and functional goal of SCI therapies has been to restore walking. Many consider wheelchairs as the hallmark of SCI, but motor functional deficits are much more widespread than the ability to walk. Injuries above the fourth cervical vertebrae can lead to dysfunctions of all 4 limbs (tetraplegia), while injuries at

thoracic spinal levels lead to dysfunctions in the mid-torso and lower limbs (paraplegia). Furthermore, high cervical injuries can prevent proper respiratory muscle function, leading to the necessity of consistent mechanical ventilation and a heightened propensity for respiratory infections. Therefore, therapeutic strategies improving motor function could have life-saving functional benefits beyond restoring the ability to walk.

Non-motor functional deficits are equally, if not more important after SCI. Dysregulation of autonomic control of circulation, known as autonomic dysreflexia, is a constant consideration and can prove fatal⁴⁴. Chronic pain from SCI often necessitates prescription pain medication and is associated with mortality⁴⁵. Non-fatal deficits are also widespread and critically important. Both paraplegics and quadraplegics prioritize sexual dysfunction, bladder/bowel control, and trunk stability above walking, while quadraplegics prioritize arm/hand function above all others⁴⁶. This is not meant to minimize any particular functional deficit from SCI, but it is important to remember that the functional detriments of SCI are widespread and devastating.

Personal accounts at national meetings from individuals living with SCI and research surveys gathering data on the true desires of the population have identified that autonomic and sensory functions are oftentimes a higher priority than motor function^{26,46}. Studying these pathways is difficult, due to their complicated nature, but is nonetheless critical. Voluntary bladder voiding is a key example. Proper function involves coordinated efforts from the sacral micturition center, pontine micturition center, and cerebral cortex, where parasympathetics provide excitatory input for muscle contraction, somatic nerves inhibit sphincters to allow fluid flow, and sympathetic nerves provide inhibition for relaxation⁴⁷. Immediately after injury, spinal shock can render these nerves inactive,

leaving no micturition reflex to void and no awareness of the bladder's fullness⁴⁸. Later after injury, the neurogenic bladder can recover some function, become overactive, or stay unresponsive⁴⁸. The complexity of these pathways make them both difficult to study, and vulnerable via multiple mechanisms to multiple types of dysfunction. Metanalysis estimates that urinary incontinence is present in 33.1% of individuals with SCI⁴⁹ and other studies estimate some sort of bladder dysfunction in up to 80% of individuals living with SCI⁴⁸. Unfortunately, those individuals without independent bladder and bowel control have lower physical independence, mobility, occupation function, and overall life satisfaction⁵⁰.

Collecting data on these motor, sensory, and autonomic functions is critical to diagnose the injury and to evaluate any therapeutic benefits of interventions. The most common clinical evaluation tool today is the American Spinal Injury Association (ASIA) Impairment Scale, which measures motor and sensory function at various dermatomes and classifies injury severity across 5 classes (A, B, C, D, or E)^{51,52}. The graded measurement across various dermatomes/myotomes is necessary because, as discussed above, functional deficits depend on many factors, including the location and severity of SCI. Collectively, these nuances are incredibly important for the individual living with SCI because deficits can persist for their entire life, and the nature of these deficits can have extreme impacts on their quality of life⁴⁶.

2.2 Open Field Testing of Motor Functional Recovery from Spinal Cord Injury

Preclinical research uses a wide battery of functional recovery outcomes, but perhaps the most common are open field tests. The Basso Battie Bresnahan (BBB) scale was developed for rats⁵³, followed by the Basso Mouse Scale (BMS) for mice⁵⁴. In these

tests, animals are allowed to roam freely in an open field and trained observers rate their hindlimb function based on a pre-determined set of movements. As these are among the most common outcomes for rodent SCI experiments, they have been well-described. Furthermore, centralized training courses have been established to ensure consistency amongst various labs in the field.

While the BMS is a powerful tool to describe the wide range of hindlimb motor function after SCI, the scale is not a perfect fit for all situations. Some animals may respond with an abnormal progression through the scale parameters, in which case BMS subscores are used to describe individual aspects of hindlimb function⁵³. BMS subscores provide the additional benefit of presenting data in a readily-interpretable state. Rather than showing a functional improvement from 2 to 3 on the BMS scale, a subscore can effectively relate that animals are able to plant their paw beneath their body. In this study, I use the total BMS scores and subscores derived from the BMS, thereby assessing the full spectrum of hindlimb motor function while also analyzing accessible and relevant functional outcomes individually.

One of the most difficult motor feats for a tetrapedal animal with a thoracic spinal cord injury is supporting its weight on solely on its hindlimbs, also known as “rearing”⁵⁵. Rodents readily perform the rearing action as part of normal exploration⁵⁵ (as shown in Figure 2.3.1). However, rearing is a complex motor challenge. Rearing requires the animals to have the proprioceptive ability to maintain balance while simultaneously supporting its own weight to move upward. Both of these complex motor tasks are important in SCI functional recovery. Proprioception is critical to initiate and maintain locomotor recovery⁵⁶ and body weight support has been heavily adopted as a means to induce functional recovery

in humans^{57,58}. Therefore, analyzing rearing in rodents gives insight into complex and critical aspects of motor functional recovery.

2.3 *Acomys* Show Enhanced Recovery from Spinal Cord Injury

Functional recovery is the clinical focus of SCI therapies and therefore is a critically important outcome for preclinical biomedical research. Spinal damage disrupts motor, sensory, and autonomic pathways, but motor functional deficits have historically received the most focus. Considering that *Acomys* exhibit regeneration of various tissues including functional recovery in the skin and kidney^{37,43}, I sought to test the functional recovery of *Acomys* after SCI. Here, I will describe the functional outcomes in *Acomys* compared to a standard mammalian model, *Mus*, after SCI. As discussed earlier, *Mus* are a useful control because they largely recapitulate human SCI responses and recovery and because they are among the most commonly employed *in vivo* SCI model systems. We matched animals based on developmental stage, using young sexually mature animals. Animals were 3-6 months old, which reaches well-established timelines for sexual maturity in *Mus*; *Acomys* were determined to be sexually mature based on changes in fur patterns that occurs upon sexual maturity⁵⁹. All male animals were used to preserve breeders for the *Acomys* colony. Our lab typically uses the *Mus* strain C57BL/6J, but for these experiments we used the Swiss Webster strain. Swiss Webster are a multipurpose model commonly used for safety and efficacy testing. I chose Swiss Webster because they are generally larger than C57BL/6 and were therefore closer to *Acomys* weight when developmentally matching animals.

Animals were tested for baseline function and acclimated to home cages before administering a spinal crush injury and allowing intervention-free recovery for specified days or weeks post injury (dpi or wpi, respectively). 10 animals of each species were deeply

anesthetized, the spinal cord was exposed, and modified forceps were used to administer a spinal crush for 1 second at thoracic level 9 (T9). The animals were allowed to recover from anesthesia and were returned to home cages, where they were checked twice daily and provided access to food and water ad libitum. Animals were given analgesic immediately after injury and antibiotic for the first 5 days after surgery, but were given no other treatments. 1 *Acomys* and 2 *Mus* died through the course of the study, leading to final sample sizes of 9 *Acomys* and 8 *Mus*.

Functional recovery data were collected longitudinally from animals until a chronic time point 12wpi. This time point was determined based on the a-priori criteria that both species had ceased recovering function, with a minimum time post-injury of 8wpi. To determine when both species had reached a functional recovery plateau, a blinded statistician reviewed longitudinally-collected functional recovery data and indicated to the researchers when hindlimb function did not change in both species over time. Therefore, animals were euthanized 12wpi, several weeks after statistically reaching a recovery plateau. Further details of the animal husbandry, SCI surgery, and functional testing are included in Appendix 2 (sections A2.1, A2.2, and A2.3, respectively).

I set out to evaluate both motor and sensory functional recovery in *Acomys*. Our approach to test mechanical and thermal sensitivity (Von Frey and Hargreave's, respectively) requires animals to be reliably capable of withdrawing their hindpaws from mechanical and thermal stimuli. Unfortunately, we were unable to perform these tests after injury because the animals did not recover sufficient motor control to reliably withdraw their paws. However, unexpected phenomena in *Acomys* routine care gave potential insights into autonomic functional recovery. As a part of routine animal care, I manually

palpated the lower abdomen to void the animal's bladder twice daily (described in more detail in Appendix 2). As described above, voluntary bladder voiding is controlled by both somatic and autonomic spinal pathways. Humans and other rodents have been shown to lose the ability to voluntarily void bladders either transiently or permanently after SCI^{48,60}. While *Mus* showed expected bladder dysfunction—recorded as small, medium, or large bladders at the time of routine voiding—*Acomys* unexpectedly returned to having empty bladders soon after injury. I quantified this phenomenon in retrospective analysis of these routine animal care sheets, recording bladder voiding as the first of 3 consecutive days with an empty bladder. These retrospective data show a significant improvement of bladder voiding in *Acomys* compared to *Mus* (Figure 2.4.1A, $p < 0.0001$).

Similarly, routine animal care involves weighing animals weekly as a gross indicator of health. Body weight was similar between *Acomys* and *Mus* both 1 week pre-injury and at the time of surgery (Supplementary Figure A1.1). As expected from historical rodent SCI experiments, animals lost ~10% of body weight immediately after SCI, and there was a significant change in body weight over time ($p < 0.0001$). However, *Acomys* recovered significantly more body weight (species effect $p < 0.05$) significantly quicker (interaction effect $p < 0.001$) than *Mus* (Figure 2.4.1B).

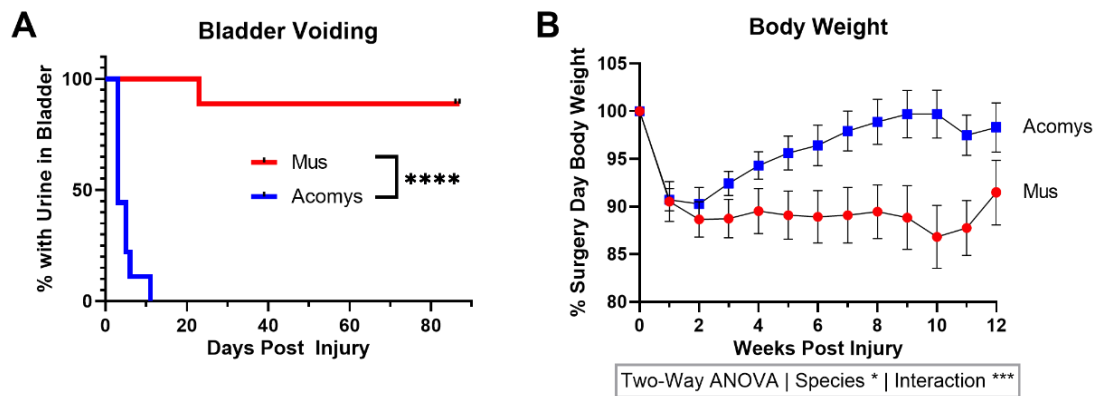


Figure 2.3.1: Acomys recover empty bladders and body weight more quickly than Mus.

A) Routine bladder care was unnecessary in all Acomys by 11dpi while 89% of Mus required manual bladder voiding for the full 12 week course of the study. Data analyzed as a log-rank using the Mantel-Cox test, **** $p < 0.0001$. B) Animals were weighed weekly throughout the study, and Acomys recovered closer to pre-injury body weight more quickly than Mus. $n=8$ Mus, $n=9$ Acomys. Bladder voiding analyzed by log-rank Mantel-Cox test. Body weight analyzed by two-way ANOVA with Sidak's multiple comparison correction. * $p < 0.05$, *** $p < 0.001$, **** $p < 0.0001$.

While these unexpected data are reflective of important and robust effects, it is important to note the caveats of these retrospective analyses. Interpretation of these results is difficult considering the number of factors that may affect bladder voiding and body weight. The bladder size of *Acomys* preinjury was not established, nor are the urodynamics well understood. Unlike *Mus*, *Acomys* are native to semi-arid climates and may therefore store water differently. Furthermore, while I administered saline injections for the first 5 days after injury as part of routine animal care, I did not control for water intake. While these are hefty considerations when interpreting the robust increase in bladder voiding in *Acomys*, the trend is consistent with an independent study of *Acomys* SCI⁶¹. Further study is warranted to understand if *Acomys* have improved bladder voiding, and these investigations could identify if *Acomys* could serve as a model of enhanced somatic and/or autonomic signaling to regain control of the bladder after SCI.

To evaluate hindlimb functional recovery, we employed open field tests including the BMS, BMS subscores, and rearing. Methods are detailed in Appendix 2. For BMS and BMS subscores, animals are allowed to roam freely in a large plastic environment for 4 minutes while at least 2 trained observers score the animal's hindlimb function according to the ability to perform each movement prescribed by Basso et al. in their original paper developing the scale⁶². These hindlimb scores are used to grade hindlimb motor function on a scale from complete paralysis (score = 0) to normal (score = 9). Alternatively, individual hindlimb functions can be analyzed independent of the full scale as a subscore. These subscores are particularly important in this study because they do not presume the ordered progression of functions originally created specifically for *Mus*. In this study, I analyze hindlimb plantar placement, plantar stepping, and coordination in outcomes

derived from the original BMS development publication. Additionally, I evaluated hindlimb function by measuring rearing, a difficult task that involves sophisticated motor and proprioceptive control. Briefly, I allowed animals to roam freely for 10 minutes in an activity box with an array of infrared beams. Movement across the ground—or horizontal movement—was measured by “beam breaks” on a lower row of infrared beams, while rearing—or vertical movement—was measured by “beam breaks” on a higher row of infrared beams. By analyzing the vertical/horizontal movement, I normalized the amount of rearing to the total amount of movement for each animal to avoid misinterpreting inactivity as less rearing.

Establishing baseline functional readouts was critical for this comparative study to ensure that proper hindlimb function was being analyzed for each species. Accordingly, trained observers watched *Acomys* and *Mus* hindlimb locomotion pre-injury. One important note is that some *Acomys* did not have tails before injury, so our subsequent analyses disregarded the final grading criteria, tail positioning, on the BMS scale. Otherwise, both animals were capable of performing all aspects of the BMS grading scale and exhibited normal scores, achieving a maximum score of 8 (normally 9 is achieved based on tail positioning)⁶². Allowing animals 10 minutes in the activity box showed that both species are both capable of measurable hindlimb rearing. Furthermore, both species were shown to rear a similar amount pre-injury, as shown by similar vertical/horizontal movement (*Mus* = 0.85 ± 0.35 vertical/horizontal episodes vs. *Acomys* = 0.74 ± 0.26 vertical/horizontal episodes; $p = 0.47$; Figure 2.3.2A). Collectively, these baseline measurements show that *Acomys* and *Mus* have similar scores on hindlimb functional assessments before injury.

Immediately after injury, animals typically show a rapid and robust loss of motor function. After spinal crush injury, both *Acomys* and *Mus* show similar hindlimb functional dysfunctions. Specifically, both species reach an average BMS score of about 1 at 3dpi, which is reflective of slight ankle movement (Figure 2.3.2B). Collectively, the data shown in Figure 2.3.2 show that *Acomys* and *Mus* have similar baseline functional ability (according to these measures), and that both species experience similar initial functional deficits from SCI.

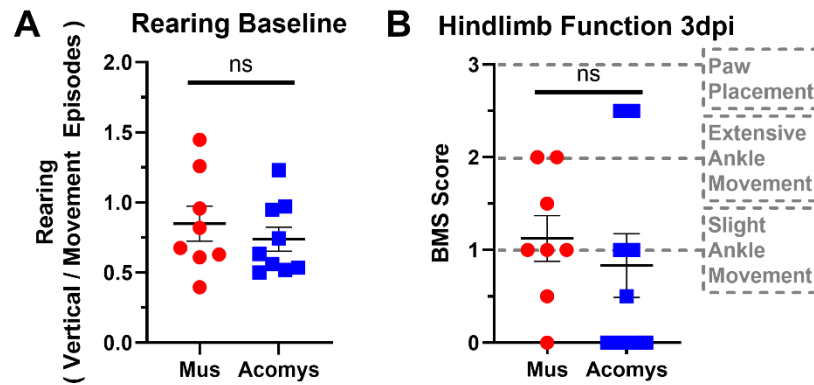


Figure 2.3.2: *Acomys* and *Mus* have similar baseline hindlimb function and similar functional deficits from spinal crush.

Open field tests were used to evaluate pre-injury (baseline) and post-injury (baseline) hindlimb function. A) *Acomys* and *Mus* have fully functional hindlimbs 1week before injury, including the ability and inclination to perform the “rearing” motion supporting themselves on their hindlimbs. B) However, at 3dpi both *Acomys* and *Mus* show diminished hindlimb function with an average score that reflects an average hindlimb functionality of “slight ankle movement.” n=8 *Mus*, n=9 *Acomys*. Analyzed by student’s T test, ns=no significant difference. Video of baseline (uninjured) and 3dpi hindlimb function is included as an additional file.

From previous experience in mammalian spinal cord injury, we expect to see some functional recovery during the first few weeks after injury. As expected, both *Mus* and *Acomys* recovered some hindlimb function over the first 2wpi. However, *Acomys* recovered significantly better hindlimb function, beginning around 2wpi, which resulted in significantly better hindlimb function at chronic time points after injury (Figure 2.3.3). At 11wpi, *Mus* reach a BMS score of ~3, which reflects plantar placing of the paw or dorsal (but not plantar) stepping, while *Acomys* reach a BMS score ~5, which reflects frequent or consistent stepping without coordination or with some coordination and improper paw rotation (Figure 2.3.3A). When analyzing specific individual hindlimb functions by BMS subscores at 11wpi, we see improvement in *Acomys* hindlimb plantar paw placement with weight support ($p < 0.001$, Figure 2.3.3C) and hindlimb plantar stepping ($p < 0.05$, Figure 2.3.3D), which is significantly different from *Mus*. It is important to note, though, that *Acomys* had improved but not completely recovered hindlimb function after injury. For example, *Acomys* do not have statistically significant improvements in coordination at chronic time points after injury (Figure 2.4.3E).

Although *Acomys* functional recovery is not perfect after SCI, the hindlimb function improvements are both robust and meaningful. This is perhaps most poignantly shown in rearing, which was measured longitudinally after animals first recovered the ability to step frequently. *Acomys* recover significantly better rearing than *Mus*, which is consistent from 4-10wpi (Figure 2.3.3B). Video collected 10wpi further illustrates the robust differences between species (videos included as additional files).

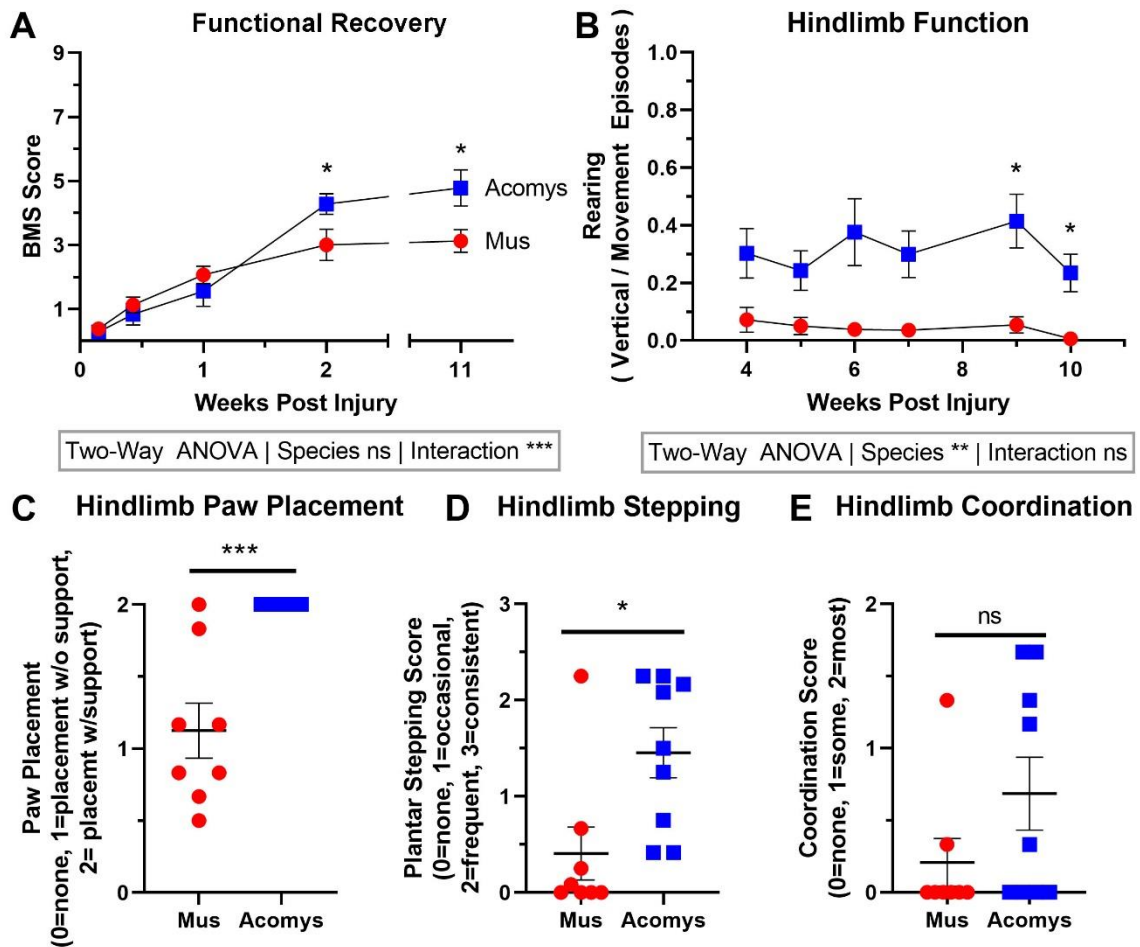


Figure 2.3.3: *Acomys* exhibit enhanced functional recovery from SCI.

A) *Acomys* recover significantly better hindlimb function according to the Basso Mouse Scale, which covers a wide variety of movements that span paralysis (score of 0.0) to normal hindlimb function (score of 8.0, excluding tail function). B) *Acomys* also recover significantly better rearing ability, beginning at 4wpi, after animals first recovered the ability to step on their hindlimbs. Subscores explicitly analyzing specific aspects of the Basso Mouse Scale at 11wpi show significantly better plantar placement (C) and plantar stepping (D) in *Acomys*, but both species fail to reach consistent coordination (E). $n=8$ *Mus*, $n=9$ *Acomys*. BMS (A) and Rearing (B) analyzed by two-way ANOVA with Sidak's multiple comparison test; subscores (C-E) analyzed by student's T-test. Species effect and interaction (species x time) effect displayed below graphs, ns=no significant difference, * $p<0.05$, ** $p<0.01$, *** $p<0.001$, **** $p<0.0001$. Video of hindlimb function is included as additional files.

The robust and consistent improvements in *Acomys* hindlimb motor function are unique amongst known mammals and provide incredible insight and promise for inducing endogenous mammalian functional recovery. Functional recovery is not only evident using the bins from BMS, but also specifically evident for specific hindlimb functions using the subscores. While these two findings are complementary, it is important to note the caveat that the BMS is somewhat subjective and based on the prior experience of the observers. Each trained observer used in this study was extensively trained for BMS using *Mus*. While the same movements are readily evident in *Acomys*, there may be subtle differences that affect the grading, especially concerning the stepping and coordination scores. For instance, differences in *Acomys* gait may lead an observer to judge that a normally-walking *Acomys* is not “coordinated”. However, the bias of observers to the natural *Mus* movements is more likely to lead to low *Acomys* scores. If this bias is influencing the functional recovery data, then *Acomys* would have an even greater improvement in functional recovery based on BMS.

Additionally, it is important to consider the potential for bias in data collectors, particularly considering that trained observers can readily tell the group difference based on phenotypic differences between species. The BMS outcome is limited by the repeated measures of individuals that are not blinded to the group code. To counteract this shortcoming, chronic BMS and subscores were graded by 6 trained observers that had not participated in longitudinal analysis. This approach aimed to circumnavigate any potential bias developed by longitudinal observation of animals obviously belonging to a particular group. Importantly, 2 of the 6 observers were blinded to the overall hypothesis in the study, and the scores from these individuals clustered well on an animal-by-animal basis with the

full cohort of 6 observers. Chronic BMS and subscore values displayed in Figure 3.3 are average values amongst the 6 novel observers. Therefore, while bias may be present based on obvious group code, steps were taken to validate the effects as best as possible.

The activity box rearing test was implemented at least in part because it is an unbiased test relying simply on “beam breaks” rather than any human grading. It is important to consider, though, that rearing involves both the ability and the inclination for each animal. It is possible that *Mus* were simply unmotivated to rear after injury. Furthermore, it is possible that *Mus* were simply unable to reach the higher row of beams to trigger a rearing episode. I ran several additional tests to ensure that these factors did not account for species differences in rearing. First, I suspended food above the apparatus to motivate animals to explore the vertical space. In a subsequent iteration, I moved the upper row of infrared beams to a lower position. In both tests, *Acomys* exhibited even more rearing, while *Mus* remained similarly disabled. Furthermore, considering the context of the BMS subscores, most *Mus* did not regain the ability to support their weight on plantar-placed paws; this logically precludes supporting the body on the hindlimbs alone. Finally, the baseline test shows a trend for slightly more rearing in the *Mus* than *Acomys*, which suggests that *Mus* do not have a decreased inclination to perform rearing. However, some studies have noted that rodents decrease rearing with familiarity of a location⁵⁵. While my additional investigations into rearing suggest that the above-mentioned factors are not likely to have affected my outcomes, it may be worthwhile to test baseline rearing in *Mus* and *Acomys* over time with repeated weekly measures.

As discussed above, SCI affects autonomic, motor, and sensory functions. While I have presented strong evidence for robust motor functional recovery in *Acomys* (Figure

2.3.3), the evidence for autonomic functional recovery (Figure 2.3.1) has many caveats, and I do not have evidence for improved sensory functional recovery. At the outset of these experiments, I intended to collect sensory functional recovery data. Indeed, I collected baseline measurements of mechanical and thermal sensitivity in the hindpaws of both *Mus* and *Acomys*. These baseline readings show that *Acomys* have significantly higher threshold to withdrawal from mechanical stimulus of the hindpaw ($p < 0.001$), but similar threshold to withdrawal from heat stimulus of the hindpaw (Supplementary Figure A1.2). As shown above, several *Mus* were unable to achieve plantar placement on the floor of the testing area, and it did not seem that most of the animals were capable of reliable withdrawal motions in response to stimuli. Therefore, we did not collect sensory functional recovery data in *Mus* and *Acomys* after injury. Future studies implementing a less severe SCI may allow animals to recover the ability to withdraw paws from mechanical and/or thermal stimuli, and these studies could identify if *Acomys* also show enhanced sensory functional recovery after SCI.

2.4 Anatomical Damage from Spinal Cord Injury

The functional deficits that follow SCI are oftentimes considered the symptoms of underlying anatomical pathology. The initial mechanical damage can sever axons and kill resident neurons and glia at the injury site. Subsequent cellular responses can further exacerbate tissue pathology by damaging surrounding cells and replacing functional tissue with non-functional fibrotic material. Indeed, spinal pathology is readily evident in rodents and humans at chronic times post injury⁴², and many note that anatomical pathology and functional deficits are oftentimes correlated^{21,22}. While some evidence identifies that anatomical and functional recovery can operate independently⁶³, it is difficult to imagine

normal motor, sensory, and/or autonomic function in the absence of functional spinal circuitry. Therefore, many biomedical scientists still focus on anatomical recovery as a complement to the critical goal of functional recovery.

Neurons are arguably the most commonly studied cell type within the spinal cord. The grey matter is rich with neural soma, including motor neurons of the ventral horn, sensory neurons of the dorsal horn, and interneurons interspersed throughout the grey matter. These neurons are long-lived and do not seem to be readily replenished by intraspinal stem cell pools, so neurotoxicity after SCI is a serious concern.

Unfortunately, there are many potential sources of neural damage during the spinal cord injury. Initial mechanical damage can destroy cells outright or cause more subtle shifts in cell membrane permeability that can lead to dysregulation and eventual neural death²⁷. Subsequently, environmental changes such as increasing pressure, hypoxia, or iron from hemorrhage can also lead to neuron death⁶⁴. Neurons can damage one another by releasing excessive neurotransmitter and over-activating targets in a deadly process known as excitotoxicity⁶⁵. To further complicate matters, there are a wide array of cellular effectors that can damage neurons after injury. Resident and infiltrating cells release toxic cytokines and factors that can lead to neuron death. For instance, while astrocytes of the glial scar form a barrier to isolate the lesion core and protect penumbral tissues, these astrocytes also exhibit concurrent neurotoxicity⁶⁶. This neurotoxicity is readily evident through a variety of histological stains, including immunolabeling of the neuronal nuclear antigen NeuN.

Even if neurons survive, the white matter on the edges of the spinal cord contains long axonal tracts that are subject to damage that could inhibit function. A process known as Wallerian degeneration occurs in neurons with damaged axons, where the axons retract,

losing their myelinated sections, and sometimes leading to total neuron death¹². Axons are capable of regrowth, as discussed earlier, but re-establishing full function requires concerted effort from both neurons and glial cells. For instance, myelination of axons in the spinal cord is critical to enabling and optimizing signal propagation^{67,68}. For this reason, stains of myelin have been employed to understand frank tissue pathology, or total tissue pathology that is likely to contribute to functional deficits^{69,70}. Other studies also use astrocytic scar formation as a measure of frank tissue pathology because GFAP+ astrocytes will form a stark delineation at the border of the lesion^{71,72}.

When investigating axons specifically, a useful approach is to target cytoskeletal components that provide structural support and facilitate intracellular transport. Neurons have some specific cytoskeletal components, including specialized intermediate filaments known as neurofilaments. Neurofilaments are composed of subunits, including high molecular weight NF (NF-H), which is a key cytoskeletal component commonly used to stain axons CNS⁷¹. High molecular weight NF is present in most axons, but is most highly expressed in mature, myelinated axons⁷³. Targeting NF-H for immunolabeling allows visualization of the full length of most axons. Because of this, I target NF-H to immunolabel mature axons in the injured spinal cord.

Alternatively, targeting neurotransmitters can provide more nuanced control by labeling specific neuron subpopulations. Serotonin (5-HT) is a monoamine neurotransmitter synthesized by a subset of CNS neurons primarily in the brainstem⁷⁴. Supraspinal serotonergic neurons project axons into the spinal cord, where they have axon terminals in the grey matter at all spinal levels^{75,76}. Serotonergic fibers are known to affect sensory and motor systems, and are involved in autonomic control⁷⁷. Specifically,

serotonin is known to regulate rhythm and coordinated movements through regulation of central pattern generators (CPGs)⁷⁸. In fact, administering serotonin to CPGs can improve hindlimb function and increase functional training-induced recovery⁷⁴. As a histological tool, serotonin has been previously used to evaluate axonal growth across spinal lesions because the supraspinal source of 5-HT means that caudal serotonergic fibers must traverse the lesion plane^{5,79,80}. Similarly, in this study I use 5-HT as a tool to immunolabel descending supraspinal pathways that can affect motor function to evaluate rostral-to-caudal regrowth of axons after injury.

2.5 Spinal Tissue Pathology in *Acomys* after Injury

Functional recovery is often attributed to increased axons or neurons available to propagate signal through the injured spinal cord. It is reasonable that sparing or recovering more neural tissues should improve functional outcomes from SCI. I investigated if robust functional improvements seen in *Acomys* could be attributed to improvements in decreased anatomical damage.

To better understand the spinal structure after injury, I stained and analyzed sagittal spinal sections harvested from animals euthanized 3 days, 1 week, 2 weeks, or 12 weeks after SCI (as described in Section 2.2 and Appendix 2.2). These spinal sections were stained with a variety of antibody- or chemical-based stains to visualize various aspects of the spinal cord, and images were collected using brightfield or fluorescent microscopy. These images were evaluated for qualitative differences in pathology and were analyzed on HALO histology analysis software to determine quantitative differences between species. Methods are described in more detail in Appendix 2, section 2.4.1.

Chronic spinal sections from 12wpi were evaluated to identify any long-term improvements in axon growth between species. The SCI lesion is easily identified using antibodies targeting glial fibrillary acidic protein (GFAP) to visualize astrocytes and the astrocytic scar that forms at the lesion border in mammals. Axons were visualized by targeting NF-H, which stains all mature axons in the spinal cord, and by targeting 5-HT, which stains serotonergic axons descending from the brain. Both *Mus* (Figure 2.5.1) and *Acomys* (Figure 2.5.2) have NF-H-positive axons traversing the injury. Few 5-HT-positive axons are evident in both species, but surprisingly it seems that *Mus* may have more 5-HT-positive axons than *Acomys* caudal to the injury site. In both cases, it seems that any axons have either been spared at the edges of the injury or have regrown around the edges of the spinal lesion.

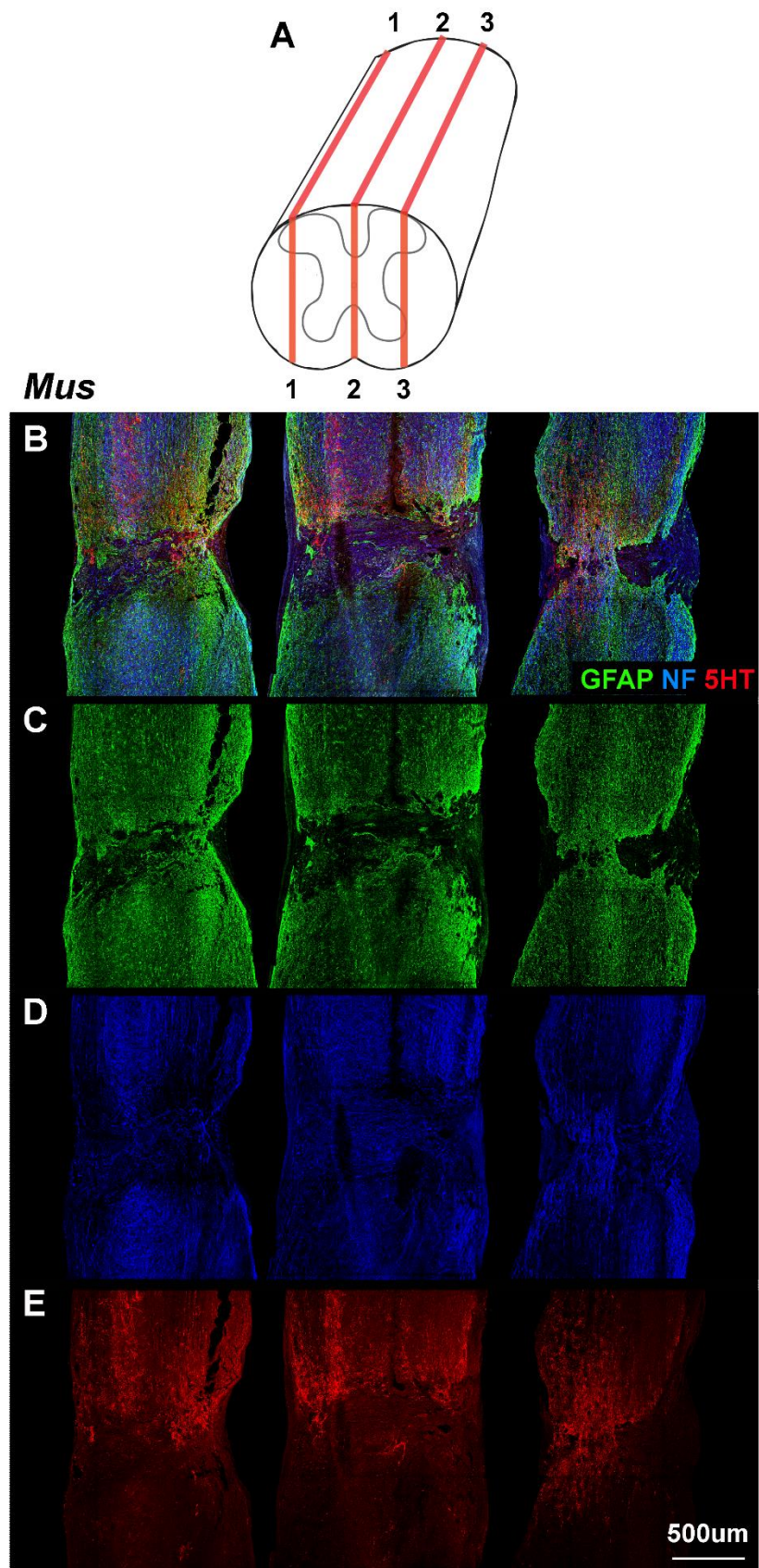


Figure 2.5.1: Chronic axon pathology in *Mus*.

Mus spinal cords isolated 12wpi were fluorescently immunostained for astrocytes (GFAP, Green), axons (NF-H, blue), and serotonergic axons (5HT, red). Three sagittal sections from a representative animal are shown in each column, which approximately correspond to spinal locations displayed in the top schematic (A). Each row shows images of merged channels (B) GFAP (C), NF-H (D), and 5HT (E). Scale bar for all images is 500 μ m.

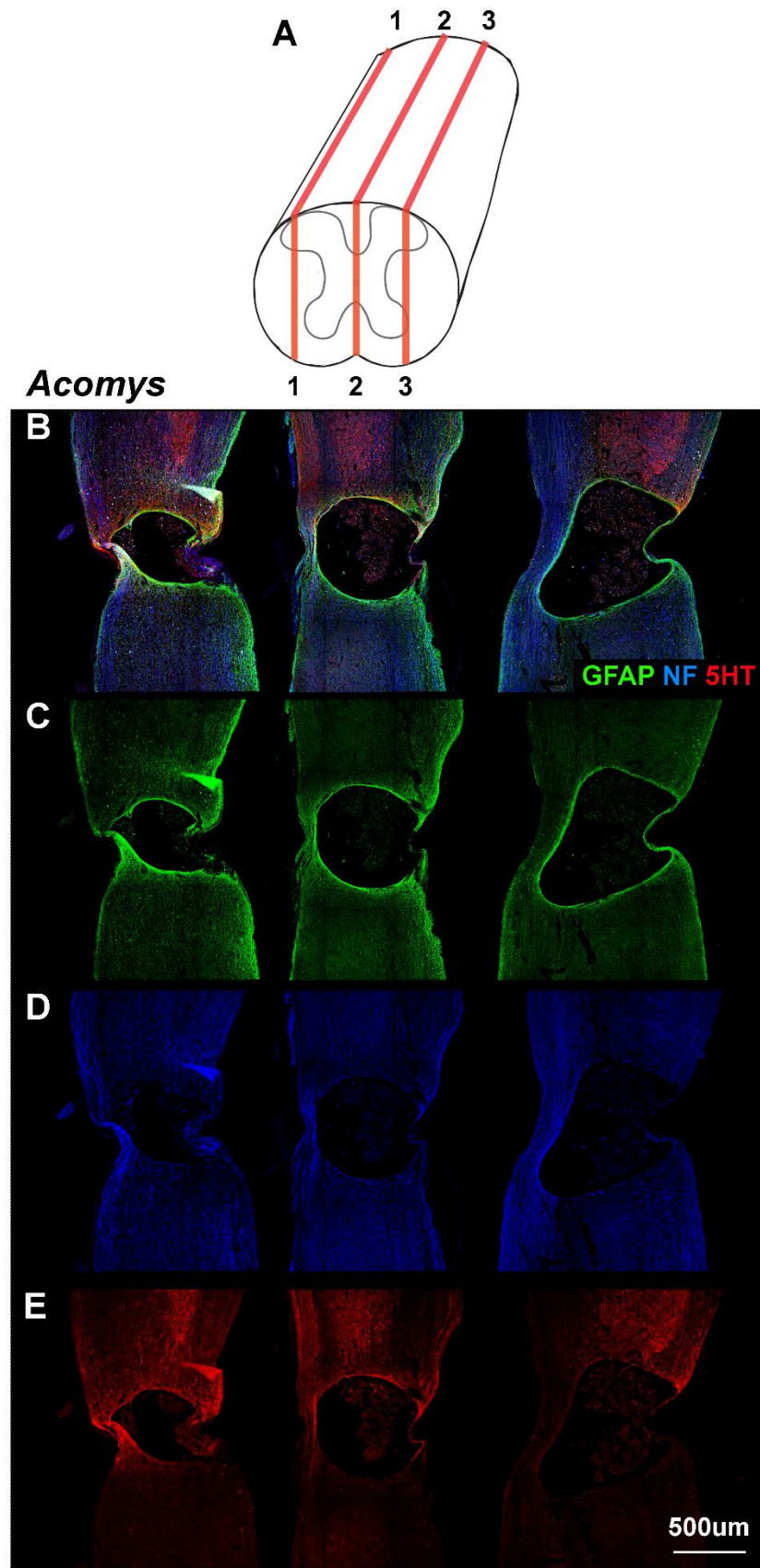


Figure 2.5.2: Chronic axon pathology in *Acomys*.

Acomys spinal cords isolated 12wpi were fluorescently immunostained for astrocytes (GFAP, Green), axons (NF-H, blue), and serotonergic axons (5HT, red). Three sagittal sections from a representative animal are shown in each column, which approximately correspond to spinal locations displayed in the top schematic (A). Each row shows images of merged channels (B) GFAP (C), NF-H (D), and 5HT (E). Scale bar for all images is 500 μ m.

Axon sparing is profoundly affected by acute injury responses after SCI. The expansion of spinal damage can be facilitated by secondary injury responses, as outlined in chapter 1. To evaluate axon sparing after injury, I immunostained for astrocytes (GFAP) to visualize the injury area, axons (NF-H), and cell nuclei (DAPI) in spinal sections isolated 3dpi, 1wpi, and 2wpi. At 3dpi the dynamic injury site has dystrophic axons with swollen endbulbs, likely in the beginning phases of Wallerian degeneration, and the GFAP+ glial scar border has not yet been established around the injury site (Figure 2.5.3A-F). By 1wpi the glial scar border has been established, and while some axons are growing past the glia limitans, they do not appear to reach the injury core (Figure 2.5.3G-L). Interestingly, *Mus* seems to send more axons past the glia limitans than *Acomys* (Figure 2.5.3I,L). This trend seems to hold at 2wpi, where both species have a strongly-established glial scar border. *Mus* axons abut and exceed this border while *Acomys* axons largely stay distant (Figure 2.5.3M-R).

Axon histology does not identify a robust decrease in axon pathology to complement the robust functional recovery in *Acomys*. Chronic histology shows axons do traverse the injury site around the edges of the lesion core, and these strips of astrocytes and axons are recognizable by 2wpi (illustrated in Figure 2.5.3P-R). While the strip is only readily evident in the representative image from *Acomys* at 2wpi (Figure 2.5.3P-R), it is important to note that this was evident in both species. Lateral spinal sections—analogueous to regions 1 and 3 in the schematic from Figure 2.5.1A—show very similar strips of intact tissue. Despite this similarity in strips of axon growth, *Mus* surprisingly have a slightly less axon pathology, as shown qualitatively by more axon growth into/near the lesion core at subacute time points and more serotonergic fibers in the caudal cord at the chronic time

point. Furthermore, by 2wpi it appears that there is a non-cellular cavity formed in the *Acomys* spinal cord whereas *Mus* have continuous cellular tissue throughout the lesion core. These are unexpected results given the context of robust *Acomys* functional recovery versus *Mus*.

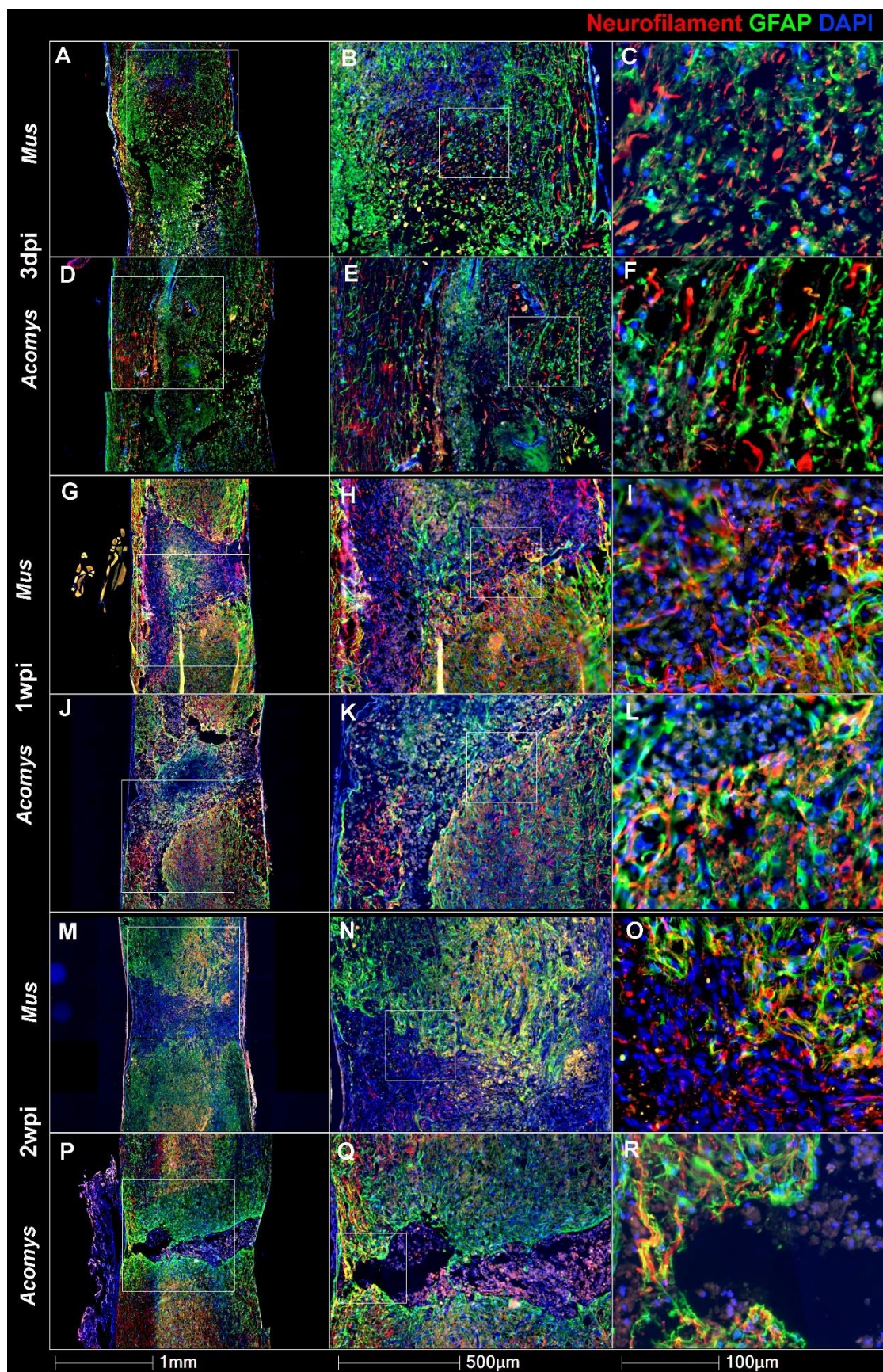


Figure 2.5.3: Mus and Acomys axon pathology after SCI.

Both species show significant pathology as visualized by immunostaining for axons (NF, red), astrocytes (GFAP, green), and nuclei (DAPI, blue). Axon pathology begins to become evident at 3dpi, but astrocytic borders show the lesion core established by 1wpi. Both species show significant axon pathology at 1 and 2wpi, but Mus show more axons unassociated with astrocytes in the lesion core at 1wpi and 2wpi. Scale bar listed at the bottom of each column. Species and timepoint listed to the left of each row.

Spinal cord injury incurs both axonal damage and neural cell death. Grey matter contains the soma of spinal neurons, and the death of these spinal neurons can be readily identified by staining the soma with NeuN⁸¹. I stained sagittal spinal sections from animals euthanized 3dpi, 1wpi, and 2wpi with antibodies targeted to NeuN and NF-H to gain a better understanding of neuron cell death after injury in each species (Figure 2.5.4). Subsequent analysis measuring the rostral-caudal distance between areas of NeuN+ soma quantifies the rostral-caudal spread of neuron pathology in each species. This quantification reveals a mild recovery of soma from 3dpi to 2wpi, but no statistical difference in the rostral-caudal spread of neuron pathology between species (Figure 2.5.5). Again, this finding is surprising considering the robust functional improvement in *Acomys* versus *Mus*.

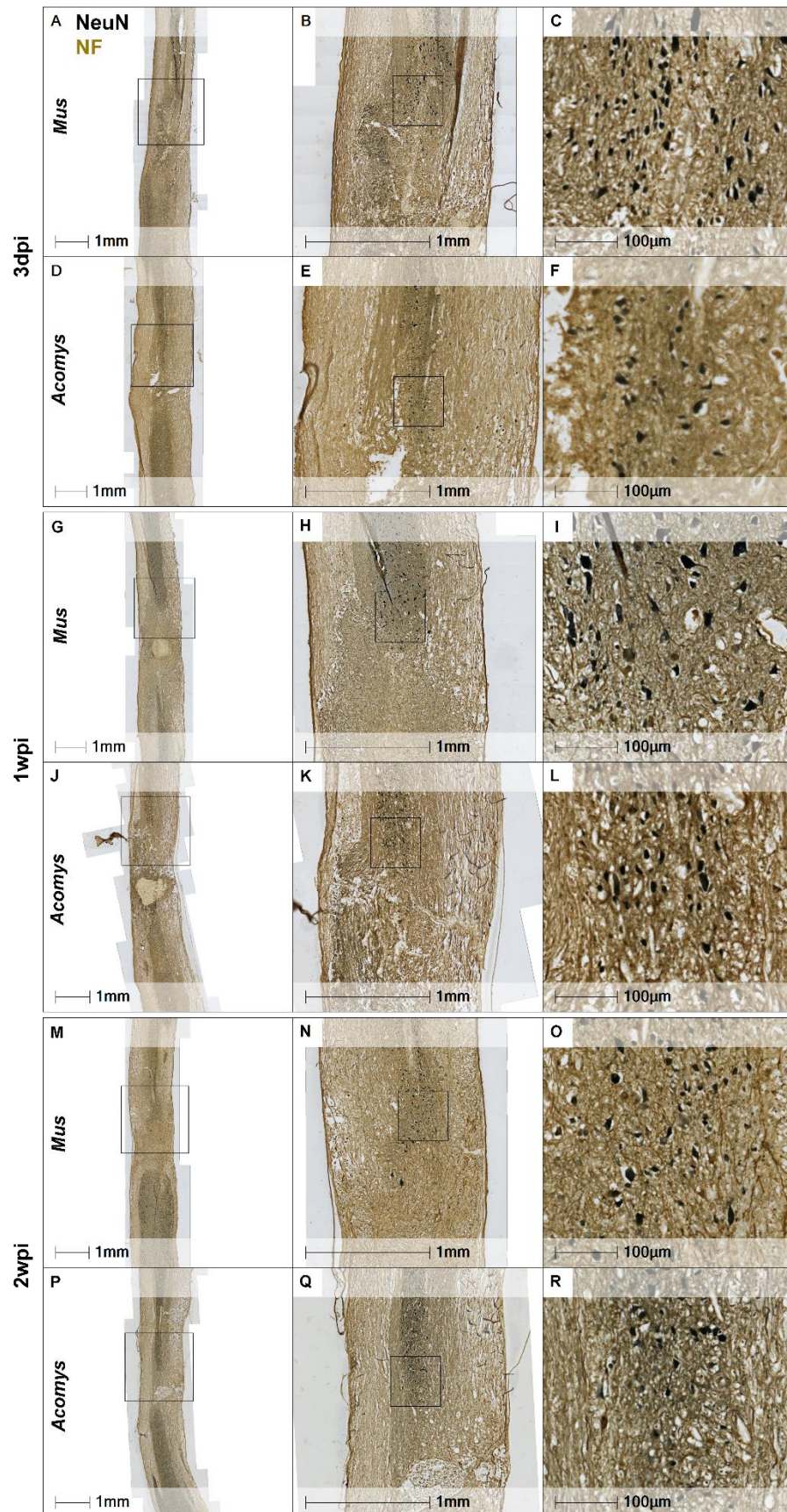


Figure 2.5.4: *Mus* and *Acomys* soma pathology after SCI.

Images are sagittal spinal sections isolated from injured animals and stained for neuron soma (NeuN, black) and axons (NF, brown). Each spinal section is representative of the average value for each species at 3dpi (A-F), 1wpi (G-L), and 2wpi (M-R). Scale bars provided at the bottom of each image pane.

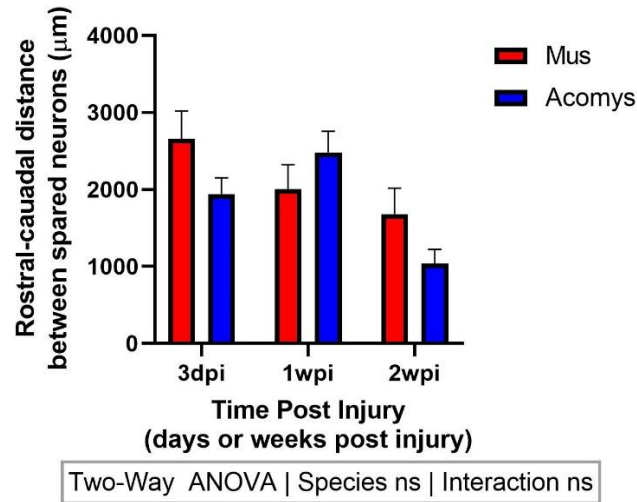


Figure 2.5.5: *Mus* and *Acomys* have similar soma pathology after SCI. Sagittal spinal sections were collected from injured animals 3dpi, 1wpi, or 2wpi, and were stained for neural soma by immunolabeling NeuN. The distance between areas of normal soma anatomy was measured, and analysis shows no statistical difference between species. *Mus* 3dpi (n=4), 1wpi (n=7), 2wpi (n=5); *Acomys* 3dpi (n=8), 1wpi (n=8), 2wpi (n=4). Data analyzed by two-way ANOVA with Sidak's multiple comparison correction, species effect and interaction (species x time) effect displayed below graphs, ns=no significant difference.

Non-axonal tissue pathology is equally important to understand after SCI, especially considering that non-axonal aspects are critical for proper spinal function. As such, I use Eriochrome Cyanine (EC) to stain myelin, along with a brightfield stain of NF-H-targeted antibodies. This combination of myelin and axon staining is common in the SCI field to assess frank tissue pathology^{69,70}. From this stain, I evaluated the frank spinal lesion as EC-negative area because the area of myelin loss are indicative of pathology, even if demyelinated axons are present. Analysis shows that *Acomys* had significantly smaller spinal lesions, as measured by lesion area (Figure 2.5.6A, species effect $p < 0.001$) and rostral-caudal lesion length (Figure 2.5.6B, species effect $p < 0.01$).

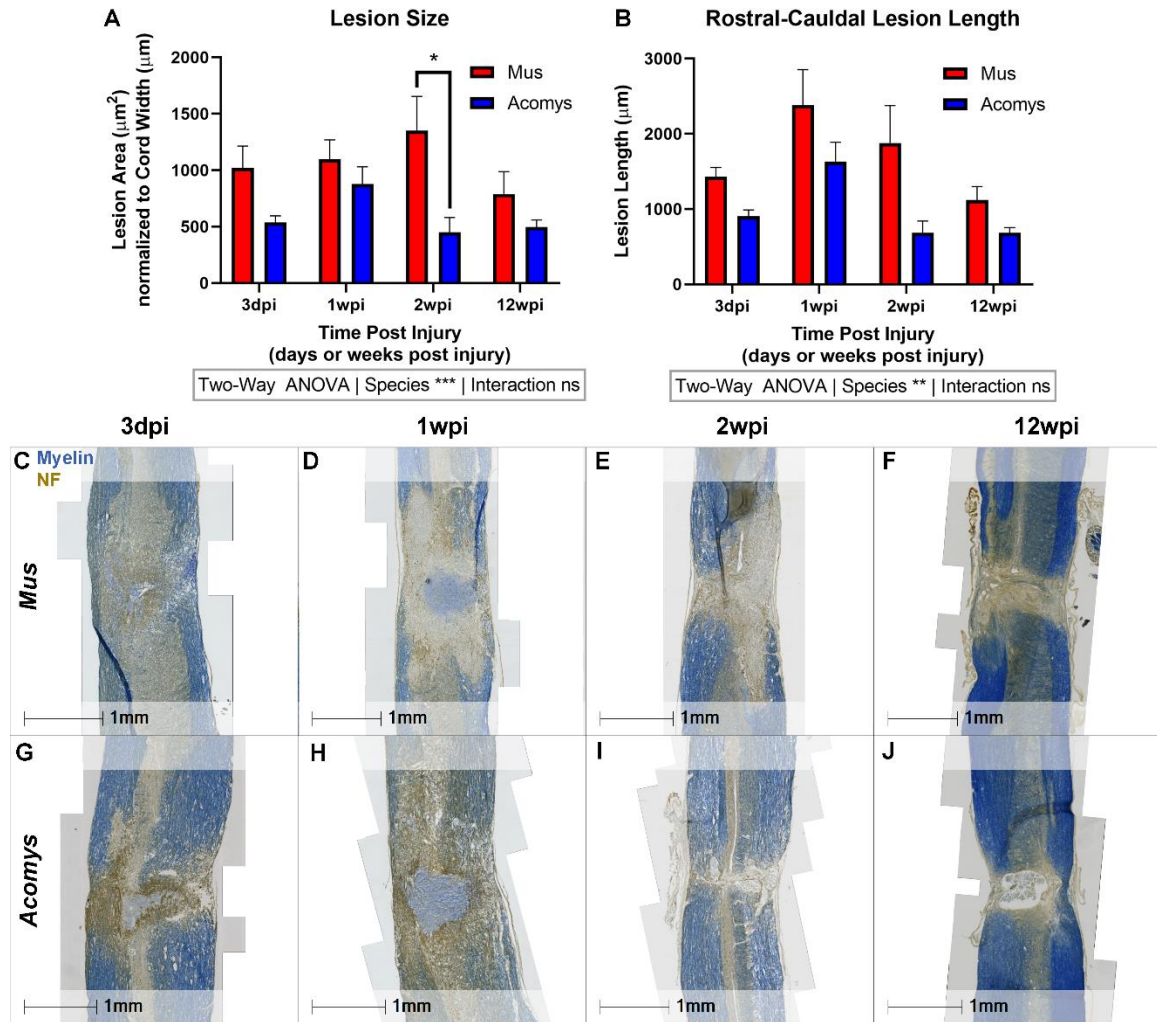


Figure 2.5.6: *Acomys* have significantly more myelin sparing after SCI.

Spinal cord sections from various times post injury were stained with EC and NF-H to label myelin (blue) and axons (brown), respectively. A) *Acomys* had significantly smaller spinal lesions, as determined by area of myelin pathology normalized to the total cord width at the epicenter of injury, at 2wpi and as a species effect across all time points. B) *Acomys* also had less rostral-caudal spread of myelin pathology as a species effect across all time points. C-J) Representative images from *Mus* and *Acomys* are representative of the mean tissue pathology at each time point. Lesion size (A) sample sizes: *Mus* 3dpi (n=4), 1wpi (n=10), 2wpi (n=4), 12wpi (n=8); for *Acomys* 3dpi (n=8), 1wpi (n=8), 2wpi (n=4), 12wpi (n=9). Lesion Length (B) sample sizes: *Mus* 3dpi (n=3), 1wpi (n=10), 2wpi (n=5), 12wpi (n=8); *Acomys* 3dpi (n=8), 1wpi (n=8), 2wpi (n=4), 12wpi (n=9). Data analyzed by two-way ANOVA with Sidak's multiple comparison correction, species effect and interaction (species x time) effect displayed below graphs, ns=no significant difference, * $p < 0.05$, ** $p < 0.01$, *** $p < 0.001$, **** $p < 0.0001$.

The rostral-caudal spread of pathology is used as a fundamental outcome in the quantification anatomical damage. This is an informative measure of lesion growth, sparing, or repair because both species were injured with the same modified forceps. Therefore, the initial spinal insult was delivered to the same rostral-caudal extent of the spinal cord and secondary physiological differences between the two species can therefore be assumed to account for differences in rostral-caudal neuron and/or frank tissue pathology. Due to the novel nature of *Acomys* SCI research, little is known about these subsequent injury responses. In fact, a paper from Streeter et al. is the only other study of SCI in *Acomys* to supplement findings of this document, and they show significant differences in post-injury responses of *Mus* vs. *Acomys*⁶¹. Therefore, while we may assume that secondary injury responses account for differences in *Acomys* spinal function and frank tissue pathology, it is unclear exactly what those responses are and how they work. More information to inform the interpretation of this chapter is included in chapters 3 and 4, where I investigate *Acomys* inflammatory and fibrotic response to SCI, respectively.

The histological approaches listed above give valuable insight into the frank tissue integrity, myelination, and axonal profile in the injured cord, but these stains are not perfect. High molecular weight NF is more highly expressed in mature axons, so NF-H stains may underestimate the total number of axons or neurites in the injury site. However, these immature axons are less likely to be facilitating proper function within the spinal cord, and a histological snapshot of these immature axons may misrepresent these highly transient neurites. Targeting 5-HT allows visualization of spinal pathways descending from the brain that facilitate motor function. However, it is important to note that 5-HT is a neurotransmitter rather than a structural protein (like NF-H), and may therefore reflect axon

terminals more robustly than axon tracts themselves. While this is true, 5-HT terminals are readily found throughout the grey matter of the spinal cord in non-human primates and rodents⁷⁴, so we would expect to see expression of either axons or their terminals throughout the intact cord. Finally, labeling with EC is a common practice for visualizing frank tissue pathology in SCI^{69,70}, but it is important to remember that this stain is specific to myelin. The pathology seen in EC-stained images can be influenced by the dynamic degradation and recovery of myelin independent of other cell types, as illustrated by nude axons in the injury site in the phenomenon of “myelin ghosts” that form in the absence of axonal counterparts⁸². That being said, oligodendrocytes in the spinal cord are critical for optimized neuron signaling, and are one of the better outcomes we have to assess “intact” spinal tissues.

When considering these histological outcomes, it is important to remember that tissue sections taken from different time points are simply snapshots from an individual animal at an individual time. While these investigations are helpful to understand generalized species effects at various times before/after injury, they do not allow for an understanding of the progression of injury/recovery within an individual animal. Further investigations that use longitudinal imaging methods would be highly informative to accurately establish immediate injury effects and subsequent lesion expansion and/or resolution at various times after injury. One relatively simple method to perform this analysis would be by ultrasound, where edema in the soft spinal tissues could be used as a generalized measure of tissue damage. Alternatively, magnetic resonance imaging (MRI) provides more powerful quantitative imaging methods to assess fluid dynamics within the cord. An optimal test for assessing spinal pathway integrity could be diffusor tensor

imaging (DTI), to visualize fiber tracts in the spinal cord before and after SCI⁸³. Both of these imaging techniques are complicated by the small size of the rodents and even smaller size of their spinal cords; imaging would require extremely high resolution to provide adequate voxel-to-voxel discrimination of lesion size with sufficient sensitivity to assess any subtle differences between groups. Additionally, the location of the SCI needs to be accessible to both imaging methods. The spinal cord is normally housed beneath layers of skin, fat, muscle, and bone. While the dorsal aspect of the vertebra is removed during the SCI surgery procedure, the spinal level varies in the amount of overlying muscle and bone. A low-thoracic injury may be optimal for minimizing the depth of the imaging plane, but many factors and outcomes must be considered in concert to ensure that a SCI experiment provides the most and best possible data for each animal used in the study. While longitudinal imaging methods would be onerous, these experiments would provide incredibly useful insight into the progression of anatomical pathology in *Acomys*.

While longitudinal imaging would be advantageous in future studies, the presented histological analysis can be used to focus these future investigations. This series of histological stains covers a wider range of time points than are typical for studies, and this canvassing of the acute (3dpi), subacute (1 and 2 wpi), and chronic (12wpi) time points identifies the subacute window as a key time for additional, more granular study. In my data, *Acomys* show robust improvements in myelin sparing and reverse unfavorable trends in neuron death between 1 and 2wpi. Concurrently, the glial scar matures into a robust delineation between the lesion core and penumbral tissues, while the *Acomys* lesion appears to shrink and develop into a cavity. Results presented in chapters 2-5 further bolster the

argument that there are interesting and meaningful secondary processes taking place in the subacute window that warrant more granular subsequent studies.

The formation of a cavity is an unexpected and interesting outcome of these histological investigations. Formation of cyst-like cavities typically occurs in the grey matter of the injury epicenter, where it is assumed that tissue is completely destroyed, leaving only a rim of subpial preserved tissue that can include myelinated axons⁸⁴. Cavity formation is actually rather common amongst mammals, including rats⁸⁵, hamsters⁸⁶, and humans⁸⁷. It would seem that the filled *Mus* injury core is somewhat unique amongst mammals^{86,88}. Here, we see that *Acomys* form a cavity in the subacute time points after injury, which persists and even expands chronically. The cavity in the central cord with EC/NF-H-positive tracts around the edges, seems analogous to the grey matter cavity with a rim of white matter sparing described by Guest and colleagues in humans⁸⁴. In terms of translation, this suggests that frank anatomical pathology of *Acomys* SCI more closely mimics humans than that of *Mus*.

Collectively, these histological investigations into *Acomys* anatomical response to SCI reveal that they do not have enhanced neuron or axon sparing after injury, but may have better preservation of spinal tissue than *Mus*. These results provide important insights for SCI researchers, especially when considered in the context of enhanced functional recovery in *Acomys*.

2.6 Insights into Functional Recovery and Anatomical Pathology from *Acomys* Spinal Cord Injury

Spinal crush results in some functional recovery in *Mus* over the first 2 weeks after SCI, after which functional recovery ceases and leaves animals with chronic functional

deficits. The moderate functional recovery in *Mus* is expected and in accordance with other studies of thoracic SCI using similar injury biomechanics (discussed in Chapter 5), namely contusion and compression^{70,89}. While *Acomys* do not fully recover from spinal crush, they recover significantly better hindlimb function compared to *Mus* beginning at 2wpi and sustaining to chronic time points. Interestingly, these robust and sustained functional improvements in motor function do not coincide with robust improvements in soma or axon pathology, but do coincide with decreased frank tissue pathology.

While we expect anatomical repair to underly functional recovery, a disconnect between anatomy and function is not unprecedented⁶³. In rats, injuries induced by graded increases in tissue displacement lead to graded spinal damage and motor deficits, but sensory deficits only manifested after reaching a threshold of white matter damage²⁴. Indeed, even in highly-controlled preclinical models, lesions of similar size can differ subtly in shape or location and thereby elicit significant differences in function⁶³. Furthermore, improvements in motor function can occur without any axon recovery⁹⁰. In humans, women have more natural neurologic recovery than men, but men tend to show better functional recovery from rehabilitation⁹¹. Individuals can manifest worsening functional status according to the ASIA impairment scale despite actual neurologic improvement⁵².

Perhaps the most relatable experiment showing a disconnect of anatomical and functional recovery from SCI is the comparative biology investigation of SCI in the MRL/MpJ mouse by Kostyk and colleagues. MRL/MpJ is a strain of *Mus musculus* noted for its enhanced wound repair. After SCI, the MRL/MpJ mouse had many more neurites growing through the lesion core, but did not exhibit greater tissue sparing (indicated by

Luxol Fast Blue staining of myelin) and exhibited significantly worse functional recovery (according to BMS) through 6wpi⁹². A subsequent study of MRL/MpJ mice contradicts Kostyk and colleagues by showing MRL/MpJ mice return to baseline function on a rotating rod and a grid walk, but these improvements can be attributed to worse functional performance of MRL/MpJ mice at baseline rather than superior post-injury hindlimb function compared to C57BL/6 controls⁹³.

Acomys show the inverse of MRL/MpJ mice, with significantly more tissue sparing and functional recovery, but no apparent improvements in axon growth out to 12wpi. Accordingly, while Kostyk et al. conclude that the permissive MRL/MpJ environment allows extensive axon growth but an inability to restore tissue integrity⁹², my data indicate that *Acomys* are able to maintain tissue integrity and thereby facilitate enhanced spinal signaling without similarly-robust increases in axon sparing or growth. This finding situates *Acomys* as a more valuable translational model for uncovering therapeutic targets for mammalian SCI considering that the primary goal of therapies is functional improvements for injured individuals.

There are several ways by which *Acomys* could be inducing functional recovery without robust neuronal or axonal sparing. Myelination of axons enhances signal propagation and axon stability, and this myelination is known to occur in both the subacute and chronic windows after SCI^{84,94}. This process depends on oligodendrocytes and oligodendrocyte precursor cells (OPCs) that are sensitive to secondary injury through processes such as hemorrhage⁹⁵ and inflammation^{96,97}, and can be influenced or stimulated by microenvironmental ECM molecules^{98,99} and growth factors^{100,101}. Later chapters will

further investigate these secondary processes that may be influencing oligodendrocyte and OPC survival and remyelination.

Alternatively, improvements in *Acomys* motor function could be facilitated by intra-spinal rather than supra-spinal pathways. Central pattern generators (CPGs) exist in the lumbar spinal cord and assist in the maintenance of rhythmic movement⁷⁸. While CPGs are typically under the control of supra-spinal pathways including serotonergic input⁷⁴, evidence suggests that CPGs can also operate independent of supra-spinal input¹⁰². Some studies have identified that enhanced functional recovery from interventions after SCI can rely solely on these intra-spinal pathways⁹⁰. In this investigation we do not observe enhanced 5HT growth across the lesion site. However, the robust—yet notably uncoordinated—hindlimb function in *Acomys* could potentially be facilitated by these intra-spinal pathways and CPGs rather than recovery of supra-spinal pathway recovery.

Further investigations could identify if the increased spinal function is occurring at the injury site by several methods. One straightforward way to assess the involvement of supra- vs. intra-spinal circuits is to allow animals to recover from a first SCI then performing a second SCI—preferably a transection⁹⁰. While this experiment would reveal if the functional recovery is attributable to caudal intraspinal circuits, it compromises the ability to analyze long-term sequelae by adding an additional injury. Alternatively, measuring electrical signaling through strategically-placed stimulating and recording electrodes, a process known as electrophysiology, could provide evidence for intra- or supra-spinal signal propagation^{103,104}. While this method provides important insight into the nature of supra- and/or intra-spinal signaling, stimulation changes the native spinal environment and electrode placement can destroy tissues, compromising the ability to

perform informative histological assessments. Future investigations could employ these spinal function assessments to better understand *Acomys* functional recovery on a tissue-specific level.

Mus are somewhat unique among mammals in that they do not form cavities after SCI. Some hypothesized that the *Mus* response to SCI, where the lesion site is moderately contracted and filled in with macrophages, fibroblasts, and fibrotic scar, is advantageous compared to cavity formation^{86,88}. Here, we observe that *Acomys* form cavities at subacute time points (2wpi), and that these cavities persist—perhaps even expand—chronically (12wpi). Considering this phenomena in the context of robust improvements in *Acomys* hindlimb function suggests that cavities are not inherently detrimental to functional recovery after injury. This assertion is supported by neonatal opossum models of SCI, where cavities form at the lesion site but animals still recover weight-bearing locomotion¹⁰⁵. Full regeneration of intact spinal tissues is surely an ideal goal for SCI wound repair. However, the insights gained from these models of enhanced mammalian repair suggest that filling in spinal cavities should not be a top priority when attempting to recover weight-bearing locomotion.

Collectively, this first investigation into *Acomys* functional and anatomical recovery after SCI develops our foundational understanding of enhanced repair of the mammalian spinal cord. It appears that salvaging tracts of tissue integrity, regardless of cavity formation and despite similar neuron and axon sparing, is sufficient to enable robust hindlimb functional recovery after thoracic spinal crush. Investigations in subsequent chapters will endeavor to understand the injury responses that underly *Acomys* functional recovery.

CHAPTER 3. DAMPENED INFLAMMATORY RESPONSE IN *ACOMYS* SPINAL CORD INJURY

Spinal cord injury evokes a robust inflammatory response at the injury site and distant spinal regions, which persists chronically^{18,106}. Recent research has revealed that the inflammatory response is highly nuanced, and that subtle shifts in the inflammatory profile can cause meaningful changes in outcomes of SCI^{2,107,108}. These studies primarily use rat and mouse models—which roughly recapitulate human SCI inflammation and outcomes—to evaluate how manipulating inflammation affects the progression of SCI. However, the field is still clarifying the exact role of inflammation. In this chapter, I will discuss my work studying inflammation in *Acomys* SCI, a novel model of enhanced recovery. These studies provide critical insight into mammalian inflammatory responses that allow or enable enhanced recovery from SCI, and can inform future efforts for therapeutic development.

3.1 Overview of Inflammation Following Spinal Cord Injury

Inflammation is critically important for clearing debris and is a normal phase of wound healing, preceding the proliferative phase and subsequent remodeling phase^{109,110}. Innate immune cells, including circulating macrophages and CNS-resident microglia, are key cellular mediators of the inflammatory response. Spinal cord injury creates cellular debris and releases intracellular proteins that act as potent inflammatory stimuli. These injury-exposed signals, also called damage-associated molecular patterns (DAMPs), are normally concealed from immune surveillance within the intact CNS¹¹¹. After injury, though, DAMPs engage pattern recognition receptors (PRRs) on inflammatory cells and mediate activation of resident inflammatory cells including astrocytes and microglia¹¹².

Reactive astrocytes and microglia release a wide variety of oxidative stress regulators, cytokines, chemokines, growth factors, and other inflammatory mediators¹¹³. Microglia also alter cellular morphology and protein expression profiles after SCI. Under normal conditions, microglia have long, thin processes that extend out from the central cell body to sample the extracellular environment. Following injury, microglia retract their processes and assume a more amoeboid morphology, better suited for phagocytosis and debris clearance. Visualizing these cells through F4/80-, Iba1-, and/or CD11b-targeted immunohistology shows that these activated microglia closely resemble circulating macrophage morphology¹¹⁴.

Along with the morphological changes comes the release of chemokines and cytokines which serve to recruit peripheral neutrophils and macrophages into the injured spinal cord¹¹⁵⁻¹¹⁸. Chemokines drive increased expression of selectins and cell adhesion proteins on nearby endothelial cells, and integrin-mediated adhesion of circulating immune cells facilitates extravasation of monocytes and neutrophils into the spinal cord¹¹⁹.

The first wave of infiltrating immune cells are neutrophils, which peak in rodent and human spinal cords around 1dpi^{16,18,106,120-123}. Neutrophils perform bactericidal functions as the first line of defense against invaders. However, neutrophil bactericidal mechanisms can contribute to SCI pathology. For instance, the oxidative burst of reactive oxygen species (ROS) can prove cytotoxic to otherwise-spared penumbral tissues^{80,117,124}. Conflicting studies report varying degrees of neutrophil-mediated oxidative damage following rodent SCI^{125,126}. Neutrophil levels drastically decrease in the rodent and human spinal cord within the first week post-injury, but low levels can persist

chronically^{16,121,127,128}. The resolution of neutrophils is coincident with increased monocyte-derived macrophage infiltration into the spinal cord¹²⁹.

Infiltrating macrophages contribute proteolytic enzymes, ROS, and inflammatory cytokines to the injury microenvironment, but also perform necessary functions of debris clearance, cellular remodeling, and production of pro-regenerative factors^{114,129,130}. The dual beneficial and reparative functions of macrophages make understanding their role in the injury response difficult. Endogenous microglia-derived and recruited monocyte-derived macrophages are also difficult to distinguish in the injured spinal cord. As discussed above, macrophages are very similar to microglia in morphology, protein expression, and function. Indeed, disentangling the two cell types required flow cytometry or genetic methods until very recent identification of protein markers distinct to the microglia^{131,132}.

Our understanding of the role of neuroinflammation is rapidly evolving to encompass detrimental and beneficial effects of each cell type during various phases post injury. Some studies show that monocyte depletion improves functional recovery from SCI^{119,133}, while others show that implanting macrophages or microglia improves function¹³⁴⁻¹³⁷. Understanding the role of neuroinflammation is critical for treating neurotrauma because human studies have shown us that neuroinflammation starkly increases within the first few days of SCI and persists for weeks to months after injury¹⁶.

3.2 Dual Role of Macrophages and Microglia in Secondary Damage and Wound Repair

Macrophages play diverse roles throughout the inflammatory, proliferation, and remodeling phases of wound healing. In the inflammatory phase, macrophage-mediated inflammation releases a slew of toxic products to clear debris and protect the injury from

potential infection. During this inflammatory phase, common cytotoxic products from macrophages include proinflammatory cytokines such as tumor necrosis factor- α (TNF α) and interleukin-1 β (IL-1 β), free radicals such as nitric oxide (NO) and ROS, and metabolites such as eicosanoids and quinolinic acid^{130,138,139}. However, macrophages and microglia are also critical for proliferative and remodeling phases of wound repair. Macrophages release pro-regenerative cytokines such as interleukin-4 (IL-4) and interleukin-10 (IL-10), and growth factors such as platelet derived growth factor (PDGF) and transforming growth factor- β (TGF β)¹⁴⁰⁻¹⁴². In an organized system, these macrophage functions complement one another over space and time to facilitate a cohesive and beneficial wound repair response^{107,143,144}.

Unfortunately, coordination of the complex macrophage-mediated wound healing response can be derailed and result in dysregulated damage. Macrophages are highly influenced by contextual cues¹⁴³, and evidence suggests that macrophages sustain a prolonged inflammatory response to SCI, which contrasts the peripheral wound healing response that features a more timely transition into proliferative and remodeling phases^{39,107,127}. Prolonged inflammation coincides with long-term ROS deposition^{145,146}, blood-spinal cord-barrier (BSCB) disruption^{147,148}, and proinflammatory cytokine deposition^{16,116}. Decreasing macrophage-mediated inflammation by depleting macrophages, inhibiting macrophage entry into the spinal cord, or pharmacologically limiting inflammation can improve anatomical and functional recovery from SCI^{80,117,119,133,149}.

While most studies point toward the detrimental effects of over-abundant and over-activated macrophages in the spinal cord, there are many that suggest a beneficial effect of

macrophages and microglia. Microglia-laden grafts allow enhanced axon growth¹³⁵ and injections of peripheral nerve-stimulated macrophages enhances functional recovery¹³⁶ in the injured rat spinal cord. Other studies show that depleting macrophages decreases tissue integrity and decreases functional recovery from SCI^{134,137}. The sum of these experiments suggests that limiting inflammation may be beneficial, but specifically harnessing inflammation—by maintaining strictly controlled cell numbers and activation states—is a more nuanced and powerful tool for maximizing endogenous repair mechanisms². To develop such therapies, we must gain a nuanced understanding of the role of inflammation in spinal repair.

3.3 Comparative Models Inform Our View of Macrophages in Wound Repair

Adult mammals are limited in their wound repair capabilities, which allows recapitulation of human healing responses but limits insight into naturally-occurring responses that facilitate enhanced repair. Comparative analysis of tissues and animals with enhanced repair, on the other hand, can illuminate a pathway for researchers to follow in pursuit of reparative therapeutic targets. These comparative studies across various organ systems, developmental stages, and animal species have highlighted a critical role of macrophages in injury responses and wound repair.

Macrophages are necessary for regeneration of various tissues across different animal models^{38,150-152}. While there are no studies definitively showing that macrophages are required for spinal cord regeneration, many lines of evidence point towards their importance in spinal repair. Resident inflammatory cells activate, migrate, and proliferate in response to SCI in lamprey^{153,154}, zebrafish¹⁵⁵, and salamanders¹⁵⁶. Studying these non-mammalian models of SCI repair has illuminated the importance of macrophage/microglia-

mediated inflammation in axon guidance^{153,154,157} and in supporting proliferation¹⁵⁸. However, inflammation is not ubiquitously beneficial for spinal regeneration in these animals. Regeneration can be increased by removing particular proinflammatory factors in the zebrafish¹⁵⁹ or by inhibiting microglial inflammation in salamanders¹⁶⁰. These results indicate that the non-mammalian inflammatory response is nuanced, and that the specific differences are critical in facilitating spinal repair.

While macrophages are present early in development and exist almost ubiquitously across vertebrates, these macrophages have distinct differences from adult mammalian analogues^{32,161}. Targets identified in neonatal or non-mammalian models may be vastly different or entirely absent in the adult mammal. Therefore, researchers have attempted to find comparative models within the adult mammal. Comparing the non-regenerating rat spinal cord to the rat sciatic nerve, which regenerates after injury, Leskovaara and colleagues see fewer macrophages and cytokines within the first 3 weeks of sciatic nerve injury¹⁶².

Other attempts to glean insight into adult mammalian repair have used the MRL/MpJ strain of *Mus*, which has been shown to respond with enhanced wound repair in the ear. Brain stab and dorsal hemisection show increased microglia response in the acute phases of injury (<2wpi)^{93,163}, while another study of spinal contusion injury shows decreased macrophage/microglia response at later time points (14-42dpi)⁹². Collectively, the MRL/MpJ CNS injury studies do not reach a consensus, but may indicate that a dampened inflammatory response at later time points may allow or enable greater axon growth in the damaged spinal cord.

This project investigates inflammatory response to SCI in *Acomys*, a rodent that responds to injury in multiple organs with robust wound repair. Importantly, *Acomys*

wound repair across each organ system coincides with a uniquely regulated inflammatory response, especially pertaining to macrophages. *Acomys* were first noted for regeneration of autotomized skin, which was hypothesized to be a defense mechanism akin to gekkos and lizards⁴³. Further investigations of *Acomys* skin regeneration show almost no F4/80+ macrophages enter the injury site, while there are many F4/80+ macrophages in the *Mus* injury and in the spleen of both species³³. A recent proteomic analysis also suggests that *Acomys* skin regeneration has lower levels of multiple components of the complement cascade, but many components were below a detectable threshold¹⁶⁴. Some data also suggest that *Acomys* have lower levels of inflammation-stimulating and chemotactic cytokines at the skin injury site, but these results are inconsistent and require further study^{165,166}. As the focus on *Acomys* as a mammalian model of regeneration has grown, evidence suggests that the dampened inflammatory responses to injury also applies to internal organ systems. Kidney and muscle injuries result in less F4/80+ staining for macrophages at the injury site compared *Mus*^{36,37}.

Perhaps the most thorough study of the *Acomys* inflammatory response was performed by Simkin and colleagues in the context of the ear hole punch injury. They note that while circulating levels of inflammatory cells are similar between *Acomys* and *Mus*, the *Acomys* ear injury site shows fewer Iba1+ macrophages than *Mus*³⁸. Furthermore, *Acomys* appear to achieve sophisticated spatial control of macrophage subsets. *Acomys* restrict pro-inflammatory (CD86+) macrophages from the leading edge of regeneration, while allowing pro-reparative (CD206+) macrophages access; *Mus*, on the other hand, have greater levels of both macrophage phenotypes without any apparent spatial restriction³⁸. Perhaps the most important takeaway from this study is the requirement of

macrophages for *Acomys* ear regeneration. Macrophage depletion with clodronate-loaded liposomes prevents ear hole closure in *Acomys*, but regeneration resumes after a washout period and return of macrophages³⁸. This study elegantly shows *Acomys* achieve sophisticated control of a blunted inflammatory response, which is required for repair of ear punch injuries.

3.4 *Acomys* Have Dampened Macrophage/Microglia Response to Spinal Cord Injury

As outlined earlier, injury causes macrophages and microglia to activate, migrate to the injury site, and proliferate. These inflammatory cells have both beneficial and detrimental effects on repair in the injured cord¹⁰⁷, but general trends indicate that robust, widespread inflammation exacerbates cellular damage and inhibits functional recovery^{119,133,167}. *Acomys* have shown a dampened inflammatory response with sophisticated control of macrophage localization^{33,37,38} in peripheral organ systems after injury. Considering this, along with the fact that *Acomys* show less frank tissue damage and better functional recovery from SCI compared to *Mus*, I sought to investigate macrophage/microglia-mediated inflammation in the injured *Acomys* spinal cord.

In lab mouse SCI, microglia respond within hours, macrophages begin infiltrating within 3 days, and inflammation reaches peak levels around 1wpi, but inflammation persists for months after injury¹²⁹. To analyze the spatiotemporal patterning of the inflammatory response, we created a time course of histological spinal samples from animals with mid-thoracic (T9) spinal crush injuries including acute (3dpi), subacute (1 and 2wpi), and chronic (12wpi) time points. These sagittal spinal sections were immunostained targeting allograft inflammatory factor 1 (Iba1), glial fibrillary acidic protein (GFAP), and DAPI to visualize macrophages/microglia, astrocytes, and nuclei,

respectively. Stained sections were then imaged using a “scan scope” to capture a full-tissue montage of 20x images, and these images were analyzed for staining density above threshold in a series of five 500 μm^2 square ROIs positioned at the injury epicenter and abutting one-another rostral and caudal to the injury epicenter. Whole cord staining was determined as the density of staining across all 5 ROIs. Collectively, this analysis method enables analysis of macrophage/microglia density across various times post-injury and over various rostral-caudal distances across the cord.

As expected, macrophage/microglia density increases from 3dpi to 1wpi in the injury epicenter (Figure 3.4.1B) and across the wider rostral-caudal extent of the cord (Figure 3.4.1A). Historical studies suggest this increase in inflammatory density is due to the infiltration of peripheral macrophages into the lesion core^{2,118}. *Acomys* show significantly lower density of macrophages/microglia across the whole cord (species effect $p < 0.001$) and specifically at the injury epicenter (species effect $p < 0.05$). Furthermore, there is a significant difference in the progression of whole-cord macrophage/microglia response between *Acomys* and *Mus* (interaction effect $p < 0.05$). This effect seems to be driven by a consistently sustained inflammatory response in *Mus* while *Acomys* have less inflammation at 2wpi ($p < 0.05$) that remains dampened at 12wpi ($p < 0.01$). Interestingly, these effects are less profound in the injury epicenter. While *Acomys* have less macrophage/microglia inflammation in the injury epicenter over time (species effect $p < 0.05$), there is no difference between species at subacute time points and a statistically significant difference only emerges at 12wpi ($p < 0.05$), although there is not a statistically significant difference over all time points (interaction [species x time]).

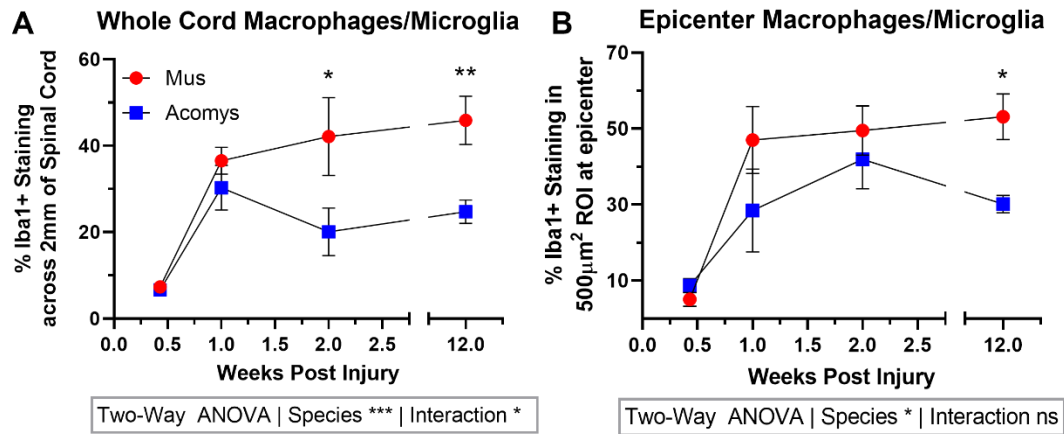


Figure 3.4.1: *Acomys* have a dampened immune response over time.

Spinal cords were harvested from injured animals 3dpi, 1wpi, 2wpi, and 12wpi, then sagittal sections were fluorescently immunostained for macrophages/microglia by labelling Iba1. Density of positive staining was analyzed in a single 500µm² square ROI at the injury epicenter (B) or in a series of five 500µm² square ROIs expanding rostral and caudal to the injury epicenter (A). *Acomys* have significantly less macrophage/microglia staining at the injury epicenter (B) and more broadly across the cord (A). *Mus* 3dpi (n=7), 1wpi (n=6), 2wpi (n=5), 12wpi (n=7); *Acomys* 3dpi (n=6), 1wpi (n=5), 2wpi (n=4), 12wpi (n=9). Data analyzed by two-way ANOVA with Sidak's multiple comparison correction, species effect and interaction (species x time) effect displayed below graphs, ns=no significant difference, *p<0.05, **p<0.01, ***p<0.001, ****p<0.0001.

Representative images the quantification of a less robust inflammatory response in *Acomys* compared to *Mus*. Amoeboid, activated macrophages/microglia are readily apparent in both *Acomys* and *Mus* lesion cores at all time points after injury, but the spread of these activated macrophages/microglia is more robust in *Mus* than *Acomys* (Figure 3.4.2). This trend of more widespread macrophage/microglia activity is particularly apparent in the subacute window 2wpi (Figure 3.4.2G-L). However, this spatial restriction is not apparent at chronic time points (Figure 3.4.2M-Q). Macrophages/microglia also appear to have a distinct morphologies between species. While we expect to see the more amoeboid shape in the lesion core with ramified, quiescent microglia further from the injury core, there are ramified microglia much closer to the injury site in *Acomys* and some macrophages/microglia appear to adopt an almost spheroid morphology in *Acomys* cords at chronic time points (Figure 3.4.2L,Q). These qualitative observations are valuable, but further analysis is necessary to confirm unique morphological or other phenotypic profiles in macrophages and microglia after *Acomys* SCI.

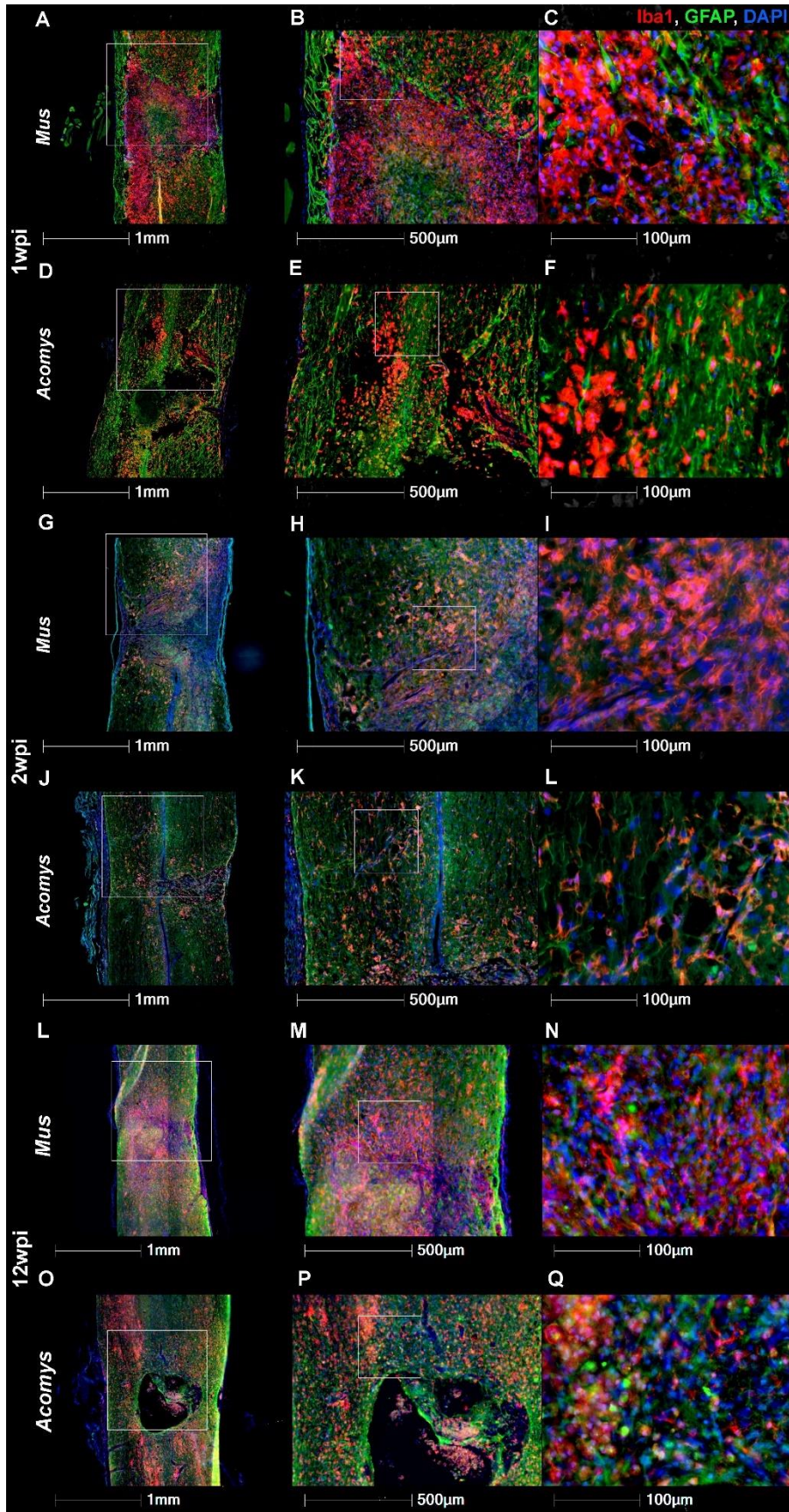


Figure 3.4.2: *Acomys* have a unique, dampened inflammatory response to SCI.

Representative images from histological samples of spinal cords 1, 2, and 12wpi immunostained for macrophages/microglia (Iba1, red), astrocytes (GFAP, green), and nuclei (DAPI, blue). Activated, amoeboid macrophages/microglia are readily apparent in the lesion core and in penumbral areas of the spinal cord.

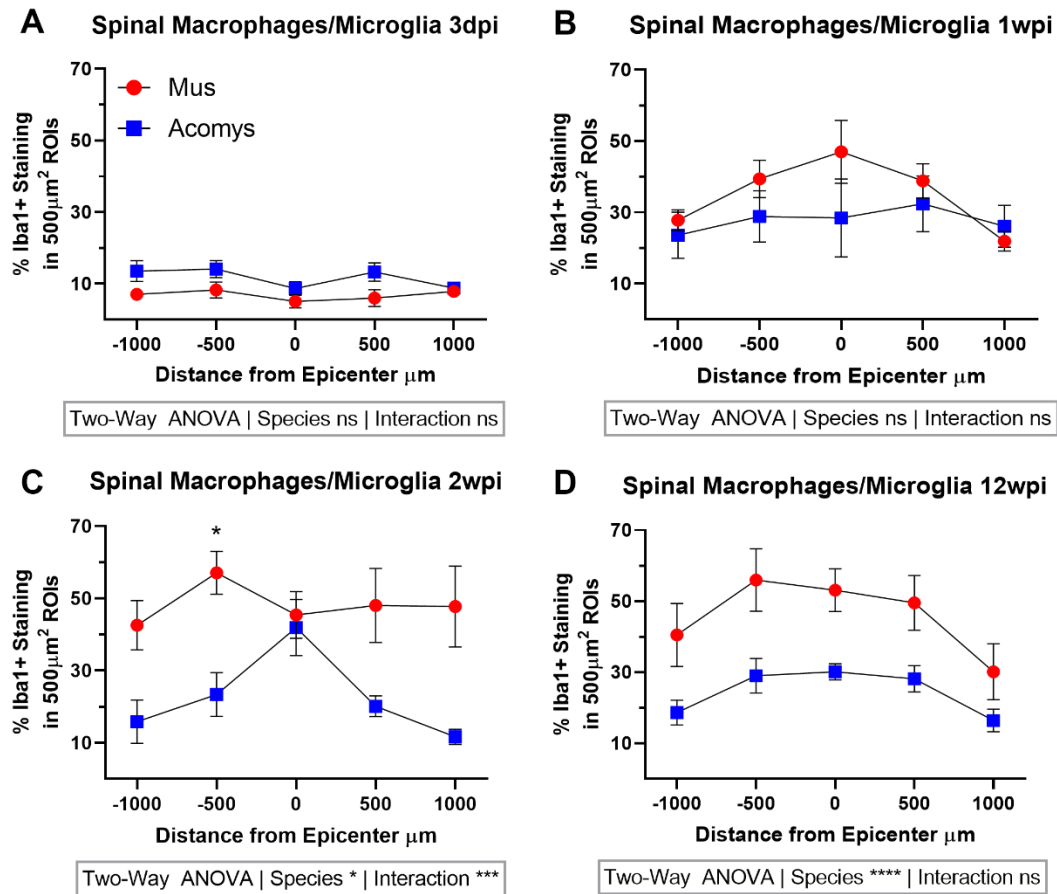


Figure 3.4.3: *Acomys* have a dampened inflammatory response with spatial restriction of macrophages/microglia.

Quantification of Iba1+ staining density at various times after injury show that *Acomys* have less macrophage/microglia density in the spinal cord 2wpi and 12wpi. Additionally, macrophage/microglia are more specifically localized to the *Acomys* injury epicenter at 2wpi while inflammation is widespread in *Mus*. *Mus* 3dpi (n=7), 1wpi (n=6), 2wpi (n=5), 12wpi (n=7); *Acomys* 3dpi (n=6), 1wpi (n=5), 2wpi (n=4), 12wpi (n=9). Data analyzed by two-way ANOVA with Sidak's multiple comparison correction, species effect and interaction (species x distance) effect displayed below graphs, ns=no significant difference, *p<0.05, **p<0.01, ***p<0.001, ****p<0.0001.

Analyzing macrophage/microglia density across various regions of the SCI site provides insight into the spatiotemporal patterning of the inflammatory response in *Acomys*. By analyzing Iba1+ density across the rostral-caudal extent of the spinal cord, we see that inflammation is generally increased at the injury epicenter in both *Acomys* and *Mus* with a dampened inflammatory response in *Acomys* at 2wpi (species effect $p < 0.05$) and 12wpi (species effect $p < 0.0001$; Figure 3.4.3). Interestingly, at 2wpi we see a significant difference in macrophage/microglia distribution between species (interaction effect $p < 0.001$). While both species have similar macrophage/microglia density at the injury epicenter, *Mus* have a similarly-robust macrophage/microglia response at areas more distant rostral and caudal to the injury site, while the *Acomys* rostral-caudal cord has less inflammation (Figure 3.4.3C). Widespread inflammation is considered to be a chief mediator of secondary damage and responsible for the spread of spinal pathology in the subacute windows of SCI, and these results may indicate a means by which *Acomys* limit subacute damage in the injured spinal cord.

As discussed earlier, it is important to consider that these histological samples are isolated from different animals at each time point when interpreting effects over time. While we would expect the group averages to normalize animal-to-animal differences and provide a snapshot of true group phenomenon at each time point, data should not be interpreted as changes over time within the same animal. Longitudinal imaging within the same animal would be favorable to see the dynamic shifts of macrophages/microglia over time, but these advanced techniques were not possible at this time for the *Acomys* study. Furthermore, spinal cords isolated at 12wpi were cut into 25 μ m-thick sections whereas all other time points were cut into 10 μ m-thick sections. This approach was taken to help

visualize full axon tracts in the histological analysis of axon sparing, but complicates interpretation of staining density. These caveats should be considered when interpreting data over time, especially chronic time points.

These results agree with previous studies in *Mus* showing excessive macrophage activation at the SCI epicenter and spread of inflammation distant to the epicenter. One other study has investigated macrophage/microglia activation in *Acomys* after SCI. Streeter and colleagues visualized macrophages and microglia in the *Acomys* and *Mus* spinal cords 4wpi using Iba1, and noted unique macrophage/microglia morphologies between species. Contrary to our results, they do not find a statistical difference in the density of Iba1+ staining between *Acomys* and *Mus*⁶¹. There are several potential contributors to these contrary findings. First, Streeter and colleagues use a unilateral dorsal crush injury in the cervical spinal cord. Previous data suggest that SCI responses in the cervical cord are distinct from those in the thoracic cord¹⁰³. Additionally, their data reflect a whole-cord analysis at a single time point after injury. While our data do reflect a species difference in our “whole cord” outcomes at 2wpi and 12wpi, Streeter et al. see only statistical trends for a difference in the “entire ipsilateral cord” at 4wpi. There is potential that the 4wpi time point may represent a unique inflammatory response compared to our 2 and 12wpi time points. Previous analysis of the time course of inflammation and immune responses suggests that macrophages and microglia respond to SCI with a multiphasic response, reaching multiple peaks over the course of a 180 days¹⁶. More likely, though, the sampling areas account for statistical inconsistencies. It is unclear exactly how large of an area is sampled by Streeter et al., but a large enough area may wash out the statistical effects that we see in our analysis. Judging from representative images in the Streeter et al. study, it

appears that there is a spatial restriction and a dampened inflammatory response similar to the response seen in our study. While this qualitative similarity is important and supportive of a uniform effect across studies in different labs, the statistical inconsistencies raise some concerns and merit further study of the macrophage/microglia inflammatory response in *Acomys* SCI. Third, their analysis method does not differentiate Iba1+ staining in various regions of the cord, but rather in a general ROI that is proportional to total cord size. This analysis method may wash out region-specific effects such as the ones we see at 2 wpi. Indeed, qualitative assessment of their representative images appear to have more widespread Iba1+ macrophages/microglia in the *Mus* cord than the *Acomys* cord, and the quantifications do have trends toward less Iba1+ staining in *Acomys*⁶¹.

Acomys appear to have sophisticated spatial regulation of inflammation. This study suggests that inflammation in the spinal cord is strictly localized to the SCI lesion epicenter. Simkin and colleagues show spatial restriction is also evident in ear injuries. While *Mus* have higher levels of all macrophage subtypes in the ear injury site, *Acomys* only allow pro-reparative macrophages to enter the leading edge of regeneration. Macrophage phenotypes are also critically important in determining axon growth and neurotoxicity in the injured spinal cord. Histological investigation of macrophage phenotypes in SCI could show if *Acomys* achieve a similar spatial restriction of macrophage subsets in CNS injury.

3.5 *Acomys* Macrophages are Less Toxic to Neurons

Researchers now discuss the beneficial versus pathological roles of macrophages in SCI through subcategorization of macrophages into a variety of activation states¹¹⁴. Categorization of these activation states in SCI has been revisited several times in recent years beginning with the identification of classically activated and alternatively activated

macrophages in the injured spinal cord, which have been shown to be pathological and reparative, respectively¹⁰⁷. While past classifications have listed macrophage phenotypes as M1 and M2, with further subdivisions into M2a, M2b, and M2c, more recent trends abandon strict classification because we now recognize that individual cells can exhibit a diversity of phenotypic markers over time, dynamically shifting through a spectrum of activation states^{107,114}.

Regardless of terminology, researchers recognize that macrophages can increase axon regeneration and neuronal function, but can also exacerbate tissue destruction¹⁶⁸. Unfortunately, pro-inflammatory macrophages predominate after injury in rodents¹⁰⁸ and there is evidence of a sustained pro-inflammatory monocyte activation after human SCI¹⁸. Clinicians and scientists are developing immunomodulatory therapies to target the dual roles of macrophages and potentiate reparative microglia and macrophage activation within the injured spinal cord. Past experimental and clinical attempts involved transplantation of pre-stimulated exogenous microglia or macrophages^{135,169}. With the identification of endogenously activated reparative macrophages and microglia after SCI¹⁰⁸, more recent immunomodulatory therapeutic approaches are instead focused on altering endogenous cells.

This study aims to understand the *Acomys* injury responses and overall outcomes of SCI. While we identify that *Acomys* respond to SCI with fewer macrophages, we must also understand how these macrophages affect neuron health. To investigate the effects of *Acomys* and *Mus* macrophages on neurons, we moved to an *in vitro* system. Well-established methods show that primary bone marrow stem cells can be isolated and induced to become bone marrow derived macrophages (BMDMs). Our lab and others use these

BMDMs as a system to investigate specifics of macrophage physiology without the extraneous variables that are inevitable in a whole-animal *in vivo* system.

We collected, grew, and stimulated macrophages from *Acomys* and *Mus* as previously described³⁸. Briefly, pluripotent bone marrow stem cells were isolated from *Acomys* and *Mus* femurs and tibias, promoted to differentiate into macrophages, and either activated or left unactivated before supernatants were collected. I chose to activate macrophages using lipopolysaccharide (LPS), a bacterial cell wall constituent normally used to achieve pro-inflammatory phenotype *in vitro*, and interleukin 4 (IL-4), a cytokine normally used to achieve an anti-inflammatory phenotype *in vitro*. These activated macrophages are intended to adopt an intermediate phenotype that may more closely resemble macrophages the activated macrophages we expect to see *in vivo*. After allowing the activated macrophages 24h to emit their normal milieu of cytokines, growth factors, oxidative species, etc., I collected the supernatant media. I applied the macrophage-conditioned media to N2A neurons to evaluate the effects of the macrophage-produced milieu on neuron health.

Neurons were exposed to macrophage-conditioned media for 32 hr then assessed for viability using the MTT assay, which provides a colorimetric measure of cell metabolic activity that is indicative of cell viability¹⁷⁰. As expected, media from activated *Mus* macrophages led to less neuron viability than media from unactivated *Mus* macrophages ($p < 0.0001$; Figure 3.5.1). However, media from activated *Acomys* macrophages did not result in decreased neuron viability compared to media from unactivated *Acomys* macrophages ($p = 0.968$). Furthermore, media from unactivated and activated *Acomys* macrophages led to more neuron viability than media from activated *Mus* macrophages

(both $p < 0.0001$). Interestingly, media from unactivated and activated *Acomys* macrophages resulted in slightly less neuron viability than supernatant from unactivated *Mus* macrophages. However, this trend was not statistically significant, and was marginal (6% and 5% reduction, respectively) especially when compared to supernatant from activated *Mus* macrophages (20% reduction). These results show that activation of macrophages in *Mus* increases neurotoxicity, but *Acomys* macrophages do not become more neurotoxic upon activation.

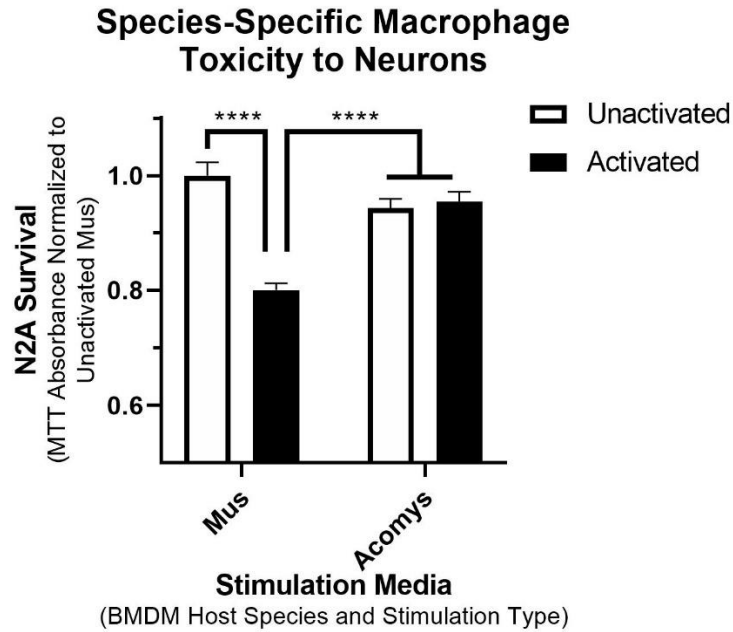


Figure 3.5.1: Activated *Acomys* macrophages are less neurotoxic than activated *Mus* macrophages.

Stimulating N2A neurons with supernatant from activated *Mus* macrophages causes significantly more neurotoxicity than supernatant from activated *Acomys* macrophages or from unactivated macrophages from either species. n=10 per stimulation type, data analyzed by two-way ANOVA with Sidak's multiple comparison correction, ****p<0.0001.

While this is the first investigation of *Acomys* macrophage neurotoxicity to our knowledge, the *Mus* neurotoxicity trend is consistent with past experiments in our lab and others. Activating *Mus* macrophages causes a shift in in the genetic profile, protein production, and production of toxic species^{107,114}. These activated macrophage products are likely to cause neurotoxicity, but the MTT assay is an indirect measure of neurotoxicity. The MTT assay measures the colorimetric reaction of mitochondrial succinate dehydrogenase catabolizing 3-[4,5-dimethylthiazole-2-yl]-2,5-diphenyltetrazolium bromide (MTT) to MTT-formazan. While this assay is commonly used to evaluate cell viability, the results may indicate a change in mitochondrial respiration that is not necessarily linked to either cell viability or cellular energy capacity. Future studies using a more direct and/or more sensitive measure of cell viability are warranted to provide more concrete evidence of species-specific macrophage neurotoxicity.

Our study uses a macrophage activation/stimulation paradigm that aims to elicit an “intermediate” phenotype. Past studies in our lab and others have used LPS + interferon gamma (IFN γ) to produce classically activated “M1” macrophages and IL-4 or IL-13 to produce alternatively activated “M2” macrophages^{71,171,172}. Simkin and colleagues have shown that *Acomys* BMDMs upregulate hallmark M1 and M2 protein markers similarly to *Mus* BMDMs in response to typical M1 and M2 stimulation³⁸. However, macrophages rarely, if ever, exhibit phenotypes that strictly adhere to M1 and M2 paradigms created *in vitro*¹⁷¹. As more stimulation paradigms are employed, more nuance and subdivision are added to the categories and the spectrum of macrophage activation¹¹⁴. We sought to more closely reflect *in vivo* conditions by activating macrophages with an intermediate phenotype, but our results may be specifically applicable to our particular stimulation

paradigm. Future studies could use spinal homogenates or specific spinal cord constituents to stimulate BMDMs to a phenotype more indicative of true *in vivo* activated spinal inflammatory phenotypes. For instance, a study in our lab performed by Tim Kopper shows that myelin exacerbates M1 toxicity in *Mus* BMDMs. Further study of spinal macrophage phenotypes in *Acomys* are warranted to better understand their contribution to neurotoxicity and/or repair in the spinal cord.

3.6 Understanding the Role of Inflammation in Mammalian Spinal Repair through *Acomys*

Macrophage- and microglia-mediated inflammation is an important part of secondary responses to mammalian SCI. These cells are thought to facilitate the clearance of debris and protect from foreign invaders in the injured cord, but are also capable of damaging previously spared tissues, thereby contributing to the spread of spinal pathology. Investigations outlined in chapter 2 show that *Acomys* exhibit enhanced functional recovery from SCI at the subacute and chronic time points after injury, which coincides with decreased frank tissue pathology. These findings suggest that secondary process in the *Acomys* spinal cord are able to enhance recovery. Histological analysis shows that *Acomys* have significantly less macrophage/microglia density in the injured spinal cord than *Mus* at subacute and chronic time points. Furthermore, these histological experiments show that there is a subacute spatial restriction of *Acomys* macrophages/microglia to the injury epicenter. Finally, *in vitro* experiments show that activated *Acomys* macrophages are less toxic to neurons. Collectively, these results suggest that spinal inflammation may be at least partially responsible for the enhanced *Acomys* recovery after SCI.

The association of a blunted inflammatory response and improved recovery from SCI has been thoroughly investigated in the past. Indeed, the only previously approved pharmacologic treatment for SCI was the immunosuppressant methylprednisolone¹⁷³. The addition of exogenous substances to inhibit macrophage entry into the spinal cord¹¹⁹ or to directly deplete circulating macrophages¹³³ have been shown to moderately improve functional recovery. This paradigm has been criticized, however, because some evidence suggests that macrophages aid in functional recovery¹³⁴. Indeed, insights from comparative studies show that macrophages are necessary for proper wound repair, including neonatal mouse heart regeneration¹⁵⁰ and *Acomys* ear regeneration³⁸. In perhaps the most relatable experiments, the MRL/MpJ mouse responds to SCI with a diminished macrophage/microglia response at subacute and chronic time points⁹². While the dampened inflammatory response in MRL/MpJ mice does correspond with increased axon growth in the lesion site, it results in worse functional outcomes⁹². These results stand in stark contrast to those in *Acomys*, where dampened inflammation results in no improvements to axon growth but robust improvements in functional recovery. Collectively, these results suggest that simple magnitude of inflammation is not the sole determinant of recovery, or that there is some deeper, more important aspect to inflammation that determines the subsequent effects on tissue sparing and functional recovery.

Temporal patterns of inflammation are a key detail determining the pathologic or reparative role after injury. One approach is to delay the onset of robust inflammation. Transient blockade of neutrophils has been shown to delay macrophage infiltration in rats and lead to improved sensory, autonomic, and motor function¹⁴⁹. Similarly, benefits of methylprednisolone were only evident when the drug was administered early and for a

short period of time¹⁷⁴. The results of experiments in *Acomys*, however, suggest that a shorter duration of macrophage/microglia inflammation is associated with favorable SCI outcomes. The *Acomys* inflammatory response is in line with a more traditional wound healing response in peripheral tissues—proceeding through 1) inflammation, 2) proliferation, and 3) remodeling phases—as opposed to the typical rodent SCI response which apparently fails to properly execute the remodeling phase^{85,107,127}. Inflammatory resolution in the later phases of wound repair is still an active area of investigation. Some posit that inflammatory resolution occurs when cells “fizzle out” in the absence of pro-inflammatory stimuli, while others suggest that the resolution is a much more active process of encouraging cell apoptosis or exit via vasculature and lymph^{175,176}. Recent investigations suggest that endogenous resolution mediators, such as Maresin 1, are not appropriately produced after SCI, and early application of these mediators can facilitate inflammatory resolution and improved recovery from SCI¹⁷⁷. *Acomys* provide an exciting new opportunity to uncover and understand these endogenous mechanisms that drive mammalian inflammatory resolution in the injured spinal cord.

The collective results of less inflammatory density, a spatial restriction of macrophages to the injury core, and less macrophage-mediated neurotoxicity intuitively suggests that *Acomys* should be less toxic to bystander tissues, particularly penumbral neurons^{108,170,171}. However, histological analysis of neural soma and axons in chapter 2 shows no benefit in *Acomys* neuron sparing. One potential explanation is that the *in vivo* SCI microenvironment is activating macrophages and microglia to an activation state that is distinct from the activation seen *in vitro*. Previous studies of *Acomys* ear injury show that *Acomys* macrophages also bear hallmarks of pathologic and reparative phenotypes, but

restrict pathological macrophages from the leading edge of the injury site³⁸. However, the spinal cord is a unique microenvironment that has equally unique effects on cellular activity. In the SCI microenvironment, *Acomys* macrophages could be more toxic, *Mus* macrophages could be less toxic, or both. Further investigation could not only uncover the true phenotype of the *Acomys* macrophages, but also provide insight into how these macrophages might interact with other components of the injury core.

The identification of spatial restriction of inflammation in *Acomys* has important implications for the maintenance of tissue integrity and the recovery of spinal function. Penumbral tissue is particularly important in SCI because small intact tracts of tissue are capable of creating novel downstream connections that can compensate for lost spinal pathways¹⁷⁸. Less inflammation in those penumbral tissues is potentially beneficial for many cell types, but is particularly important for oligodendrocytes and remyelination. Oligodendrocytes are lost over the first few weeks post injury, and surviving oligodendrocytes are limited in their remyelination because they are postmitotic^{179,180}. Therefore, OPCs are critical for the recovery of myelination and spinal function in the lesion border¹⁸¹. Unfortunately, these cells are particularly at risk of macrophage- and microglia-mediated inflammatory damage⁹⁶. As discussed in chapter 2, myelination of axons is critical for proper signal propagation and spinal function. Therefore, the restriction of macrophages from these oligodendrocytes and OPCs in penumbral tissues could help to facilitate spinal function in the absence of robust neuron or axon repair after injury.

CHAPTER 4. DAMPENED FIBROTIC SCARRING IN *ACOMYS* SPINAL CORD INJURY

In typical injury responses, extracellular matrix (ECM) molecules are deposited in a provisional scar to allow cellular infiltration and repair after injury, and in some cases a persistent ECM scar serves as a structural surrogate for properly regenerated tissue. In the mammalian CNS, tissue fails to regenerate and there is almost always chronic scar deposition at the injury epicenter. The fibrotic scar in the spinal lesion core is considered inhibitory to axon regrowth, and biomedical researchers have attempted degrading ECM as a therapeutic approach for SCI. However, the scarring response is a diverse and dynamic process that is facilitated by cells that are still being characterized in the injured spinal cord. In this chapter, I will discuss my investigations into scarring responses to SCI in *Acomys*, which identify dampened ECM deposition likely due to decreased density of ECM-producing cells in the injured cord. These findings provide unique insight into the development and consequences of fibrotic scarring, which can inform future therapeutic strategies for SCI.

4.1 Glial and Fibrotic Scarring After Spinal Cord Injury

SCI activates resident astrocytes and pericytes, and recruits infiltrating fibroblasts and Schwann cells from the periphery, leading to the development of lasting glial (cellular) and fibrotic (acellular) scars in the injured spinal cord. Astrocytes are perhaps the most abundant cell type composing the glial scar that surround the lesion site in an area referred to as the penumbra^{11,182}. Perivascular cells, particularly pericytes, expressing traditional fibroblast markers infiltrate into the lesion core where they are closely associated with ECM components, including laminin, fibronectin, and collagens^{19,20}. Schwann cells from

peripheral nerve roots infiltrate into the lesion epicenter where they also express fibroblast markers and closely associate with laminin, fibronectin, and collagen deposits¹⁸³⁻¹⁸⁵. In this chapter, I will discuss the *Acomys* fibrotic (ECM) scar and the fibroblast response following spinal cord injury.

The astrocytic and fibrotic components of the spinal scar are strictly separated to the penumbra and lesion core, respectively. In fact, many studies use astrocytic boundaries to demarcate regions of frank tissue pathology from more intact penumbral tissues⁷¹. The interface of the surrounding glial scar and the core fibrotic scar is sometimes referred to as the “glia limitans.” The strict sequestration is in stark contrast to regenerating species where both ECM components and glial cells cross the lesion site and precede neural regeneration^{32,156,186}. Formation of the glia limitans may be species-specific or driven by cellular interactions, as the phenomenon has been replicated *in vitro* by cocultures of mammalian astrocytes and fibroblasts, which naturally maintain spatial separation and inhibit neurite growth^{185,187,188}.

After injury, proliferating astrocytes thicken cellular processes and surround the lesion with a meshwork of overlapping outgrowths. Astrocyte activation and subsequent glial scar boundaries are enhanced by the addition of transforming growth factor-beta (TGF- β)^{187,189,190}. Signal transducer and activator of transcription 3 (STAT3) is also important for establishing the glial scar border that corrals infiltrating cells to the lesion epicenter^{11,182}. Previous schools of thought simply classified the glial scar as a maladaptation opposing neurite regrowth. More recently, evidence indicates that the glial scar is important for neurotrophin production, debris clearance, blood brain barrier repair, and sequestration of toxic species to the injury core^{72,191}.

The fibrotic scar, the acellular components of the scar consisting of deposited ECM materials, influences the cellular distribution of the glial scar. ECM molecules can increase the rigidity of the environment, create a physical barrier, and provide nonspecific topographical cues, all of which may affect cellular migration¹⁹²⁻¹⁹⁴. Additionally, ECM components signal through cell surface receptors to influence cellular activity. For example, tenascin and fibronectin increase matrix metalloproteases (MMPs) in various cell types¹⁹⁵⁻¹⁹⁷ and MMPs influence outcomes of SCI including the infiltration of cells into the injury core¹⁹⁸⁻²⁰¹. Despite the presence of tenascin, fibronectin, and MMPs at the glia limitans, the demarcation remains intact chronically. Overall, investigations into the glia limitans provide interesting pathophysiological descriptions, but have not led to therapeutic strategies that interfere with the establishment of the scar demarcations.

The fibrotic scar is also a critical regulator of axonal regeneration and growth after SCI. Cells within the lesion core mediate ECM dynamics through production of ECM components and proteolytic enzymes²⁰²⁻²⁰⁴. MMPs degrade ECM molecules, allowing receptor mediated assembly into dense matrices²⁰². Several of the ECM components, such as chondroitin sulfate proteoglycans (CSPGs) and fibronectin, inhibit neurite regrowth *in vitro*; others, such as laminin, promote greater neurite outgrowth^{8,205-208}. Removal of inhibitory ECM components, such as CSPGs, improves neurite growth *in vivo*^{5,209-212}. Alternatively, altering the physical properties of ECM components, such as orientation and stiffness, can promote directional axon growth^{8,193,194,205,213}. Collectively, these results indicate that ECM of the fibrotic scar is dynamic, nuanced, and can be harnessed to promote functional regrowth in the injured cord.

The above components of the glial and fibrotic scar are primarily derived from observations made in rodent SCI models. By comparison, data is limited regarding SCI scar formation in humans. As in rodents, there is clear cellular demarcation of the glial scar with astrocytes around the lesion border and fibroblasts, Schwann cells, and meningeal cells sequestered within the lesion core^{106,183,214,215}. However, some studies suggest that the prominence of the astrocytic glial scar varies between species with less astrocytosis in humans^{106,184}.

4.2 Comparative Models Reveal Importance of Glia and ECM in Wound Repair

Using transgenic models, researchers have gained insight into therapeutic targets that reduce the inhibitory effects of scarring on SCI repair. Targeted suppression of astrocyte signaling pathways reduces scar formation and facilitates axon growth and functional recovery from SCI²¹⁶. Specifically, transgenic approaches have identified astrocyte inhibition of TGF- β /Smad, TLR, JAK/STAT3, and JNK/c-Jun signaling cascades, among others, as potential SCI therapies¹⁸². However, depending on the timing post-injury, astrocyte inhibition also interferes with deposition of ECM, growth supportive substrates, and neurotrophins (e.g., laminin, fibronectin, growth factors) thereby reducing endogenous repair processes²¹⁷. Indeed, transgenic models demonstrate that astrocytes play an important role in limiting the spread of secondary injury events early after injury^{11,72}. Although these transgenic models are a powerful tool for investigating particular aspects of the glial and fibrotic scars, they often incur off-target effects and induce changes that disrupt homeostasis that is carefully engineered over millions of years of evolution.

Naturally-occurring models of enhanced repair offer the opportunity to understand a roadmap to physiologically feasible endogenous repair. For instance, a common trend

amongst non-mammalian models of spinal regeneration is the formation of a glial bridge preceding axon regeneration³². Indeed, migration and alignment of glial cells that closely resemble astrocytes or oligodendrocyte precursor cells (OPCs) is necessary for axon regeneration in the goldfish, zebrafish, and turtle^{186,218,219}. These findings stand in stark contrast to the adult mammalian glial scar response to SCI, where glia form an opposing wall against spread of injury and axonal regrowth. Indeed, evidence suggests that axonal regrowth in the rat spinal cord coincides with incidences where astrocytes achieve proper alignment along the rostral-caudal axis of the cord⁴.

Non-mammalian models of regeneration also provide insight into the importance of ECM in wound repair, but the fibrotic scar in SCI is less thoroughly studied. Nevertheless, studies in non-mammalian models of skin, limb, heart, and tail regeneration consistently show a dependence on ECM molecule expression and ECM remodeling. In peripheral nerve regeneration, ECM molecules such as collagen, laminin, and fibronectin are key to providing a permissive environment at the distal stump⁸. Zebrafish normally upregulate the ECM molecule tenascin-C when regenerating axons, but inhibiting expression of this ECM molecule decreases axon growth, synapse formation, and locomotor recovery²²⁰. Furthermore, axolotl spinal cords show dramatic increases in MMP production during regeneration, implying that ECM remodeling is an important aspect of spinal regeneration²²¹. Collectively, these comparative models show that regeneration of many tissues, including the spinal cord, require the right kind of ECM substrates rather than a lack of ECM response.

Researchers investigated the MRL/MpJ strain of lab mouse in a comparative study aimed to better understand the interplay of fibrosis and recovery from spinal cord injury.

The MRL/MpJ mouse deposits less ECM scar molecules in response to peripheral injuries, and the same trend held for CSPGs stained in the spinal cord after contusion injury⁹². However, fibronectin scarring in the contused spinal cord was more widespread but less dense than C57BL/6J control mice⁹². These changes in MRL/MpJ fibrosis are associated with widespread axon growth in the lesion epicenter, but do not result in enhanced recovery of hindlimb function⁹². This improvement in axon growth is supported by studies of brain injury that suggest fibronectin promotes axon growth²²². Indeed, *Acomys* repair of ear punch injuries also includes more fibronectin and less collagen than *Mus*, and the repaired ear tissue is full of regrown axons³⁴.

4.3 Extracellular Matrix Molecules Affect Mammalian Neurite Growth

To test the effects of key ECM molecules in axonal regrowth, I performed *in vitro* experiments with dorsal root ganglion (DRG) neurons, testing their neurite regrowth on coverslips coated with poly-D-lysine and specific ECM substrates. These DRG neurons isolated from ganglia nestled just beside the spinal cord are often used as surrogates for CNS neurons during *in vitro* experiments^{222,223}. After isolating DRGs from the animal, the neurons can be cultured in a highly controlled environment to test the effects of various stimuli and/or treatments on neurite growth^{222,224}. In our experiment, we used poly-D-lysine and laminin-coated coverslips to allow DRG neuron adhesion and axon growth, and added fibronectin, collagen IV, or aggrecan to evaluate the effects of each ECM substrate on neurons from each species.

Laminins are protein constituents of the lamina lucida, which is part of the basal lamina that lines body surfaces including blood vessels. Laminin self-assembles into trimers that are readily bound by cells and contribute to cell attachment, differentiation,

movement, and survival²²⁵. Laminin seems to play a critical role in the myelination of axons in the peripheral nervous system^{98,99,226}. *In vitro* experiments often use laminin as an adhesive molecule for neurons, and coating a 2D or 3D environment with laminin increases neurite growth from DRG neurons^{10,207}. After CNS injury, laminin is readily deposited into the injury core either in association with neovasculature or independent of vasculature as a general connective tissue matrix^{227,228}. Axon growth appears to be directed by laminin both *in vitro*²⁰⁵ and in the injured spinal cord²²⁹.

Fibronectin is an ECM protein that acts as a “biological glue”, and in both its soluble fibrils and insoluble matrices it provides binding sites for additional fibronectin, other ECM molecules, and cells^{230,231}. Consistent with its characterization as a sticky scaffolding, fibronectin is important for the attachment and migration of cells in the early wound healing process^{7,232}. Fibronectin is readily deposited in the lesion core after CNS injury^{19,202,233}, but its role is complex and incompletely understood. While fibronectin appears to aid axon regrowth after brain injury²²², it is also implicated as a barrier to regeneration in the spinal cord²³⁴. Similarly, there is not consensus on the effects of fibronectin on neurite growth *in vitro*. Petri dishes covered with fibronectin allow DRG neuron adhesion and allow robust DRG neurite growth, but do not allow retinal or spinal neuron adhesion²⁰⁸. Similarly, DRG neurons adhere and readily grow neurites on fibronectin-coated coverslips and blocking fibronectin with antibodies prevents neurite growth²²². However, fibronectin in hydrogels slightly decreases DRG neurite growth and neurite length¹⁰.

Collagens are extremely common structural ECM proteins composing up to 25-35% of mammals’ whole-body protein content²²⁷. There are 27 currently recognized types

of collagens that exhibit unique peptide sequences, physical characteristics, and distribution throughout the body. Type IV collagen (collagen IV) is primarily found in the basal lamina, an ECM-rich layer of the basement membrane, that acts as lining for surfaces such as the endothelium of blood vessels²³⁵. After CNS injury, collagen IV is found in the injury core both associated with neovasculature and in matrix independent of endothelial cells²²⁸. In some experiments inhibiting collagen IV decreases levels of accompanying inhibitory ECM molecules and improves axon growth over glial cells²³⁶⁻²³⁸, implying that collagen IV serves as a scaffold for inhibitory cues in the lesion epicenter. However, other experiments fail to elicit axon regrowth by inhibiting basal lamina constituents, including collagen IV²²⁷.

Chondroitin sulfate proteoglycans (CSPGs) are perhaps the most thoroughly-studied ECM constituents in SCI due to their potent inhibition of neurite growth. Aggrecan is a core glycoprotein to which glycosaminoglycans (GAGs), such as CSPGs, can attach²³⁹. Aggrecan and CSPGs normally form a perineuronal net around neuron soma²⁴⁰, and the aggrecan core is present with or without its additional GAG chains after SCI²⁴¹. The cellular source of spinal CSPGs after injury is currently believed to be astrocytes of the glial scar borders^{79,242}, and the production of CSPGs begins within the first week and continues to chronic time points after injury^{242,243}. Actively degrading CSPGs with chondroitinase ABC has shown profound improvements in axon growth and invasion into the lesion core^{5,211}. Aggrecan, specifically, inhibits axonal growth in the injured CNS²⁴¹, decreases neuronal plasticity²⁴⁰, and potently inhibits DRG neurite growth *in vitro*^{239,244,245}. In this experiment, we use aggrecan as a control to validate that our ECM coatings are able to inhibit DRG neurite growth *in vitro*.

Acomys have been shown to deposit less collagen and more fibronectin during tissue regeneration than the non-regenerating *Mus*^{34,164}. Furthermore, this “pro-regenerative” ECM microenvironment coincides with extensive neurite regrowth in the regenerated ear³⁴. Therefore, I sought to test how these ECM molecules affected neurite growth and if *Acomys* and *Mus* neurons differ in their intrinsic growth potential over these specific ECM substrates. In order to test the effects of the substrates themselves, we collected DRG neurons from each species and allowed them to grow neurites on coverslips coated with our substrates of interest. Then we analyzed their neurite growth using sholl analysis, as previously described^{246,247}. Briefly, we fixed the cells after 36hr of growth, stained neurons using antibodies targeted to the cytoskeleton (β -tubulin), and counted the number of neurites from each neuron crossing concentric circles. These data were plotted as number of crossings (y coordinate) at each circle diameter (x coordinate), and analyzed as the area under the curve.

In this experiment, laminin was intended as a positive control because it is the standard ECM molecule used to promote axon growth, while aggrecan was intended as a negative control because it is known as a potent axon growth inhibitor^{239,244,245}. As expected, the addition of aggrecan inhibited neurite growth in both *Acomys* and *Mus*. While *Mus* neurites grew best on laminin, *Acomys* neurites unexpectedly tended to grow better on fibronectin than on laminin—though this trend was not statistically significant (Figure 4.3.1). In fact, *Acomys* neurites grew best on fibronectin-coated coverslips, while fibronectin only mildly inhibited neurite growth in *Mus* (Figure 4.3.1). Collagen IV, on the other hand, significantly decreases neurite growth in both *Mus* and *Acomys* when compared to the most growth-permissive ECM substrate for each species—laminin and fibronectin,

respectively (Figure 4.3.1). Comparing between both species, it appears that *Acomys* DRGs exhibit significantly less neurite growth on laminin ($p < 0.05$) and aggrecan ($p < 0.0001$) than *Mus* DRGs, with slightly less growth on collagen IV ($p = 0.07$). Neurite growth from *Acomys* and *Mus* DRGs on fibronectin was very similar ($p = 0.51$). Collectively, these data indicate that collagen IV and aggrecan inhibit neurite growth in both species, and suggest that laminin and aggrecan are more growth-restrictive in *Acomys* than in *Mus*.

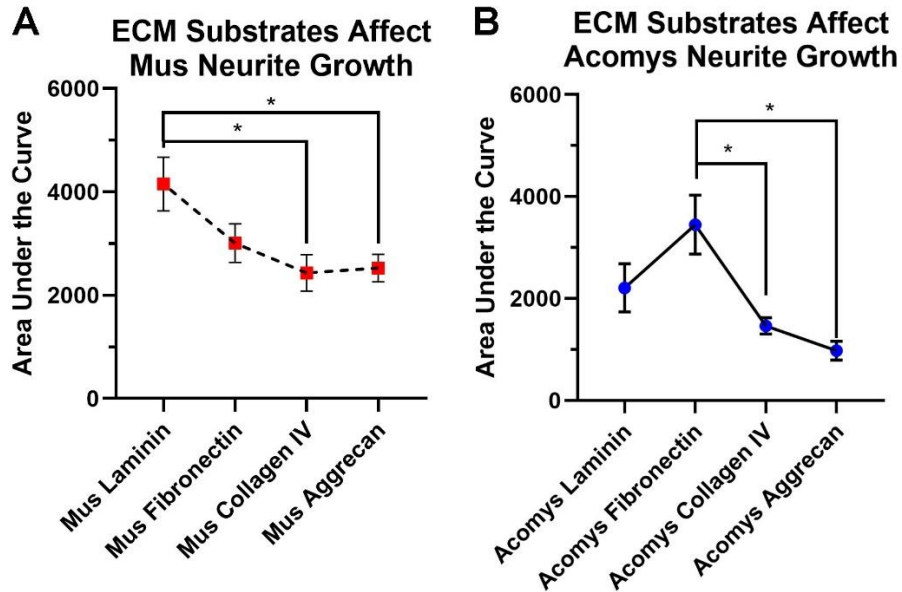


Figure 4.3.1: Extracellular matrix molecules affect neurite growth.

Data collected by sholl analysis of DRG neurons grown on coverslips coated with various ECM substrates. Collagen IV and aggrecan decrease neurite growth in both species. Interestingly, both aggrecan and laminin appear to be less growth-permissive to *Acomys* DRG neurites than those of *Mus*. * $p < 0.05$. *Mus* laminin (n=38), *Mus* fibronectin (n=64), *Mus* collagen IV (n=51), *Mus* aggrecan (n=63), *Acomys* laminin (n=13), *Acomys* fibronectin (n=47), *Acomys* collagen IV (n=24), *Acomys* aggrecan (n=39). Data analyzed by one-way ANOVA with Tukey's multiple comparison correction, * $p < 0.05$.

This experiment provides important information about the growth potential of *Acomys* and *Mus* neurons on various ECM substrates. My original hypothesis was that *Acomys* would deposit an ECM profile that favors more axon growth in the injured cord than *Mus*. If *Acomys* were to deposit more fibronectin and less collagen in the injured cord, as they do in the ear³⁴, these *in vitro* data suggest that ECM profile would support more neurite growth. I did expect collagen IV to be more inhibitory to axon growth than fibronectin, based on the historical context outlined above. However, less neurite growth on laminin than fibronectin in *Acomys* is unexpected and merits further investigation.

There are some important considerations when translating the *in vitro* findings to *in vivo* implications. First, DRGs contain sensory neurons that participate in afferent signaling and therefore only represent a subset of axons that exist within the spinal cord. Some studies suggest that these sensory afferent neurites show more robust growth over ECM substrates after SCI than efferent motor pathways²⁴⁸. Furthermore, dissociated DRG neurons consist of a wide variety of neuron subtypes that vary in receptor profiles, injury response, and neurite growth²⁴⁹⁻²⁵¹. There is potential for species differences in the proportion of DRG neuron subtypes; which may account for the differences in neurite growth between *Acomys* and *Mus*. Finally, the DRG neurons are located just outside the spinal cord and project axons into the spinal cord, but they are still peripheral neurons and are likely to behave differently than true CNS neurons. Previous experiments specifically note that DRG neurons attach and extend neurites more readily on fibronectin than spinal neurons²⁰⁸. Further investigations identifying the relative distribution of DRG neuron subtypes in *Acomys*, the growth potential of these subtypes, and the growth potential of

CNS neurons vs. DRG neurons would give further insight into the intrinsic ability of *Acomys* neurons to regrow axons on ECM substrates.

Additionally, it is important to consider that these experiments were performed on glass coverslips with poly-D-lysine and laminin coating in each experimental group. While I considered poly-D-lysine and laminin necessary to encourage neuron attachment, these substrates provide additional variables that may dilute or alter the effects of fibronectin, collagen IV, and/or aggrecan alone. Indeed, Tong and colleagues find that double-coating collagen I grafts with laminin and fibronectin improves sciatic nerve growth *in vivo*, suggesting that these ECM molecules can synergize to change neurite growth potential²⁵². Additionally, these substrates are likely to affect axon growth differently in alternative culture environments. For example, growing cells in planar vs. 3-dimensional matrices changes cellular morphology, protein profile, and migration characteristics²⁵³⁻²⁵⁵. Furthermore, microenvironmental factors such as stiffness and topographical cues can affect neurite growth in a 3-dimensional culture²⁵⁶⁻²⁵⁸. While this study was designed to specifically test the outgrowth potential of *Mus* and *Acomys* neurons in a controlled microenvironment, future studies could identify if our results can be replicated in additional contexts. Particularly, mirroring *in vivo* spinal ECM proportions could provide interesting insight into neurite growth potential in the SCI-specific context.

Finally, it is important to consider these findings in the greater context of the whole project. In chapter 2 I outline that *Acomys* do not have enhanced axon sparing or growth following SCI. These data suggest that the presence of ECM molecules such as laminin, collagen IV, or aggrecan may not permit as much *Acomys* neurite growth as in *Mus*. In the

next section, I will investigate the actual *Acomys* ECM deposition in the injured spinal cord to understand what the true scarring responses are after *Acomys* SCI.

4.4 *Acomys* Have Dampened Fibrotic Scarring Response to SCI

The intact spinal cord typically has low levels of ECM molecule expression, largely limited to the neurovasculature²⁴³. However, resident cells activate and fibroblasts invade the injury core to deposit a dense meshwork of ECM known as the fibrotic scar². The formation of this dense fibrotic scar occurs within the subacute window after injury and persists to chronic time points in both rodent and human SCI^{106,202,235}. Researchers currently consider this chronic scar tissue an impediment to axon growth¹⁰⁶, which is substantiated by approaches that have induced axon regrowth and functional recovery by inhibiting deposition of ECM in the injured cord^{211,236,259}. *Acomys* have now been documented to deposit significantly less fibrotic scar, especially collagen, during the regeneration of peripheral tissues, including the ear³⁴, kidney³⁷, and muscle³⁶. Here, I use histological analysis to determine the fibrotic scarring profile in *Acomys* over time after thoracic spinal crush.

Collagen IV is a major component of the fibrotic scar in rodents and humans²³⁵, and I show that collagen IV inhibits neurite growth in *Acomys* and *Mus* DRG neurons *in vitro*. I histologically assessed collagen IV scarring in sagittal spinal sections collected 3 days, 1 week, 2 weeks, and 12 weeks after thoracic spinal crush, and immunostained for collagen IV, astrocytes (GFAP), and nuclei (DAPI). As expected, initial observations of the histology images show a robust deposition of collagen IV in the injury epicenter of *Mus* spinal cords at 1, 2, and 12wpi (Figure 4.4.1). *Acomys* also have collagen IV deposition at the injury epicenter, but there appears to be far less collagen IV density in *Acomys*

compared to *Mus*, and *Acomys* collagen appears in vascular-like structures (Figure 4.4.1). As a constituent of the basal membrane, collagen IV is expected to be present surrounding vasculature. Indeed, collagen IV appears to follow this morphology in sections 3dpi (Supplementary Figure A.1.6) and in regions distant from the injury epicenter in both species. However, the maintenance of vascular-like morphology in *Acomys* at subacute and chronic time points after SCI is surprising.

Quantification of histological samples shows that density of collagen IV increases over time in the whole cord (Figure 4.4.2A), including the injury epicenter (Figure 4.4.2B), in both species. However, *Acomys* have significantly less collagen IV density in both the whole cord (species effect $p < 0.0001$) and the injury epicenter (species effect $p < 0.0001$). Analyzing the collagen IV deposition at various distances across the rostral-caudal extent of the injured cord shows that collagen deposition is most dense at the injury epicenter, beginning at 1wpi in *Mus* (Figure 4.4.2D) and at 2wpi in *Acomys* (Figure 4.4.2E), and continuing out to 12wpi in both species (Figure 4.4.2F). Interestingly, while there is no significant difference in the progression of whole-cord collagen IV deposition between species (interaction effect $p = 0.094$), there is a significant difference in the injury epicenter (interaction effect $p < 0.01$). This difference in epicenter-specific collagen may be driven by early subacute deposition. *Acomys* appear to maintain low collagen IV density across the spinal cord without a noticeable increase at the injury epicenter at 3dpi or 1wpi, while *Mus* show a significant increase in spinal collagen IV at the injury epicenter 1wpi (Figure 4.4.2D, interaction effect $p < 0.001$).

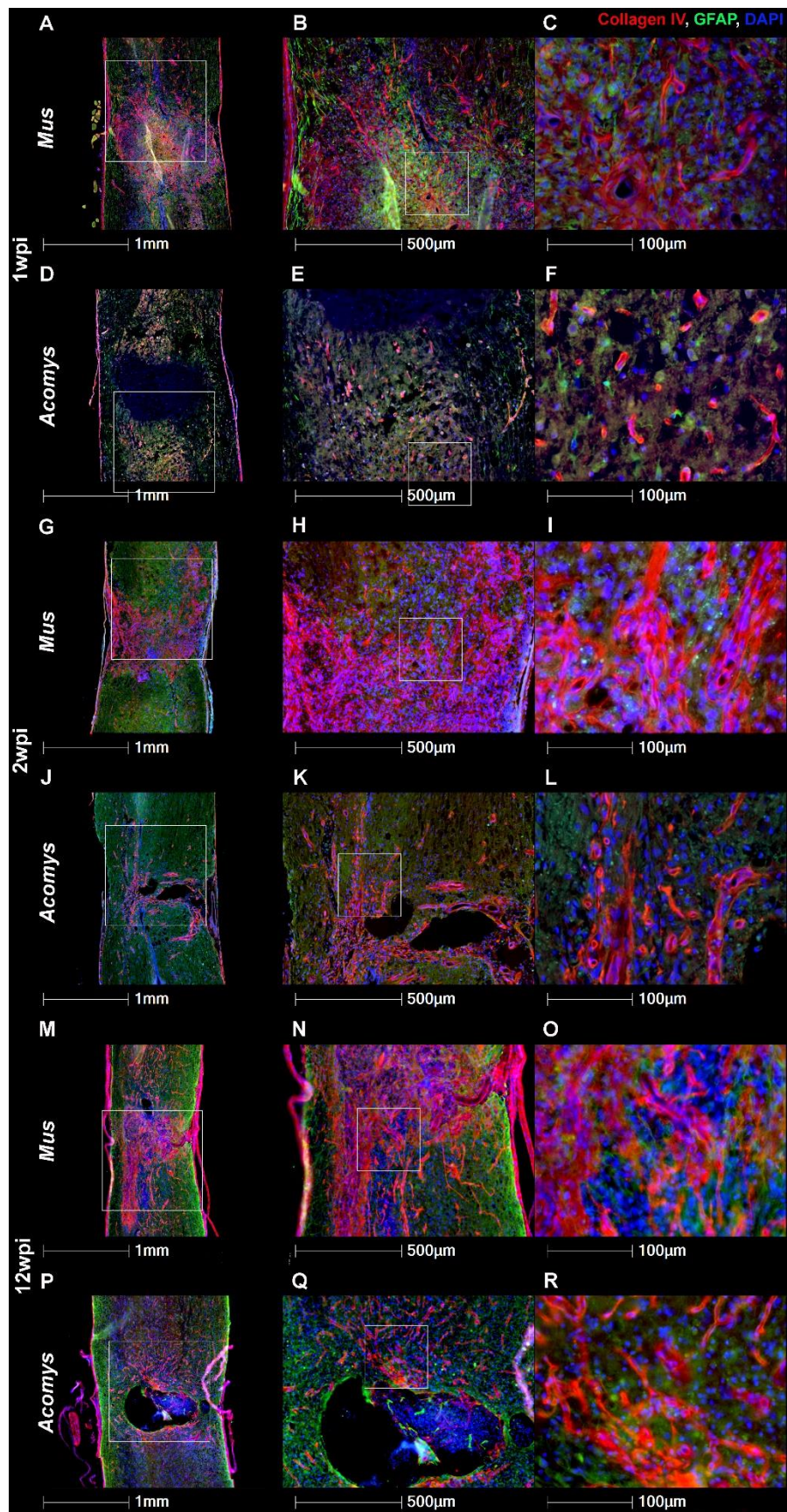


Figure 4.4.1: Collagen IV histology after SCI in *Mus* and *Acomys*.

Immunostaining was used to visualize the fibrotic scar (collagen IV, red), astrocytes (GFAP, green), and nuclei (DAPI, blue) at various times after SCI in *Acomys* and *Mus*. This histological analysis reveals the blunted collagen IV deposition in *Acomys*. While *Mus* form a dense, disordered fibrotic scar in the injury core from subacute to chronic timepoints, *Acomys* remain in a vessel-like orientation with only little mesh-like fibrotic scar formation at the lesion epicenter. Each row contains images from a representative animal from each species and time point. Species and time point are listed on the left. Panes include an inset to indicate the location of magnified image to the right, and a scale bar in the bottom of each pane.

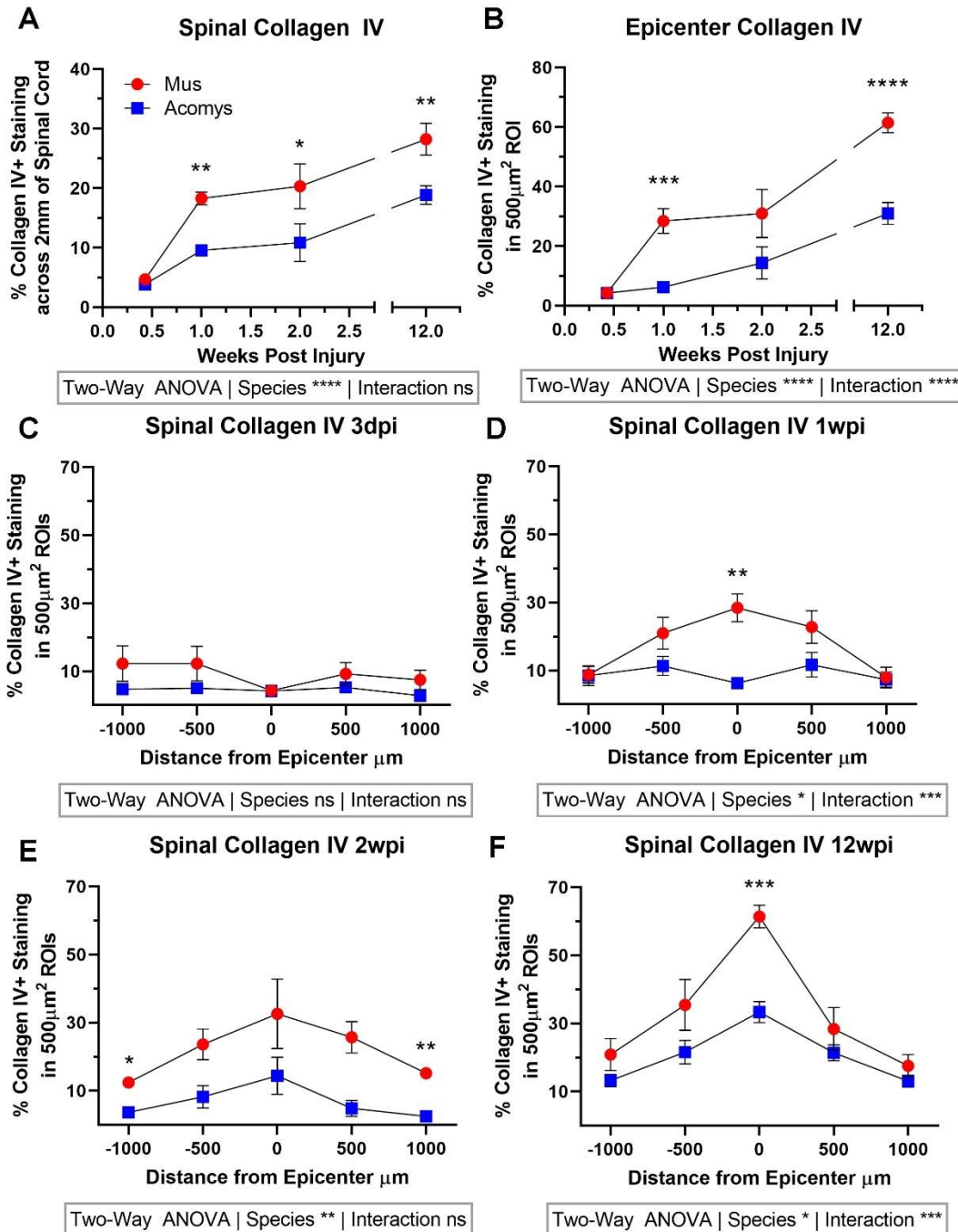


Figure 4.4.2: *Acomys* deposit significantly less collagen IV in the injured spinal cord than *Mus*.

Histology was quantified as density of collagen IV+ staining in 500 μ m² square ROIs oriented at the epicenter and radiating out rostral and caudal to the epicenter. Data from all 5 ROIs (A) and the injury epicenter ROI (B) show progressive deposition of collagen IV in the injury site, with particularly dense collagen IV deposition at the injury epicenter (D-F). *Mus* 3dpi (n=5), 1wpi (n=8), 2wpi (n=5), 12wpi (n=8); *Acomys* 3dpi (n=8), 1wpi (n=8), 2wpi

(n=4), 12wpi (n=9). Data analyzed by two-way ANOVA with Sidak's multiple comparison correction, species effect and interaction (species x time A-B, species x distance C-F) effect displayed below graphs, ns=no significant difference, * $p<0.05$, ** $p<0.01$, *** $p<0.001$, **** $p<0.0001$.

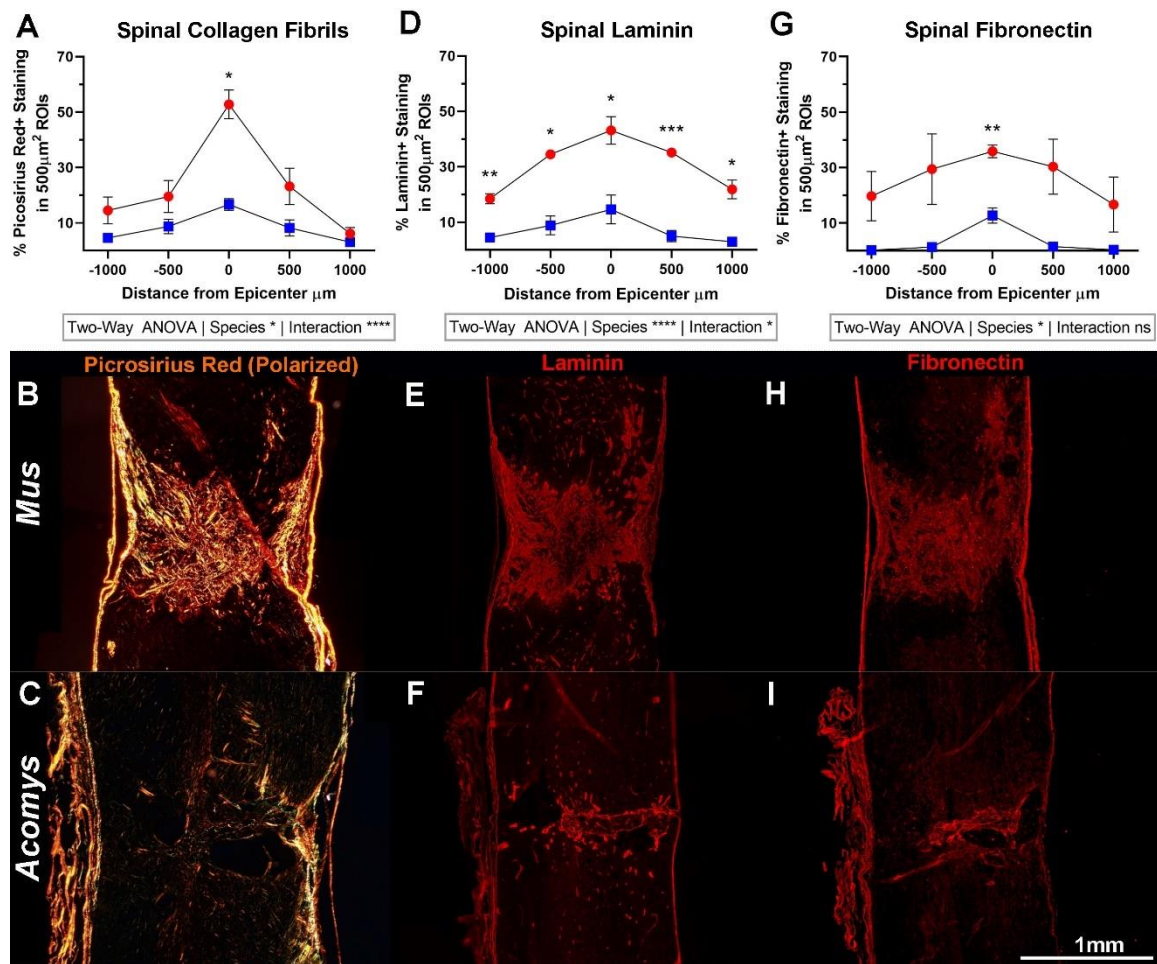


Figure 4.4.3: *Acomys* show dampened fibrotic scarring across various other ECM molecules.

Histological analysis shows that the dampened fibrotic scar extends to other ECM molecules, including collagen fibrils (A-C), laminin (D-F), and fibronectin (G-I). Data are quantified as density of staining above threshold in $500\mu\text{m}^2$ square ROIs at various distances from the lesion epicenter in cords isolated 2wpi. $n=4$ for each species with each ECM target. Data analyzed by two-way ANOVA with Sidak's multiple comparison correction, species effect and interaction (species x distance) effect displayed below graphs, ns=no significant difference, * $p<0.05$, ** $p<0.01$, *** $p<0.001$, **** $p<0.0001$.

Many different ECM molecules are deposited in the injured spinal cord, including other types of collagens²³⁵, laminin²²⁸, and fibronectin²⁰². While collagen IV forms dense networks in the basal lamina, other types of collagens—namely types I, II, III, V, and XI—form fibril structures that can be visualized by shining polarized light on sections stained with the birefringent dye, picrosirius red^{260,261}. I used picrosirius red and fluorescent immunostaining targeted to laminin and fibronectin proteins to evaluate the density of other ECM constituents within the injured cord 2wpi. Histological analysis reveals lower density of collagen fibrils (species effect $p < 0.05$), laminin (species effect $p < 0.0001$), and fibronectin (species effect $p < 0.05$) in the injured cord of *Acomys* compared to *Mus* (Figure 4.4.3).

Collectively, these histological assessments identify a significantly lower density of collagen IV, collagen fibrils, laminin, and fibronectin in the injured *Acomys* spinal cord compared to *Mus*. The results do not support my original hypothesis that *Acomys* would respond to SCI with a growth-permissive fibrotic scar that mimicked trends seen in the ear, with less collagen and more fibronectin. Rather, these results suggest that *Acomys* have a dampened fibrotic scarring response across all tested ECM molecules. While the global effects on ECM molecules is somewhat simpler than selective up- and down-regulation of specific ECM constituents, this result is complicated by the diverse and divergent effects of each of these ECM molecules on recovery from SCI. As discussed before, studies suggest that collagens are detrimental to recovery from SCI²³⁵, but laminin is viewed as beneficial for axon growth and remyelination^{99,229}, and fibronectin has been identified as beneficial and detrimental in different contexts^{222,234}.

In addition to considering the dichotomous theoretical effects of various ECM molecules and subtypes, it is important to consider the limitations imposed by these specific histological methods. While collagen IV and laminin staining do appear to follow vascular-like morphologies and are known constituents of the perivascular basal lamina, it is possible that this is an overinterpretation of the observation. A subsequent study that pairs a vascular stain in the form of an epithelial marker or a circulatory dye—paired with these ECM-targeted stains—could identify if these ECM molecules are indeed more tightly restricted to vasculature in *Acomys*. Furthermore, as with the inflammatory histology in chapter 3, it is important to remember that a time course of histological samples is collected from different animals at each time point rather than a single animal longitudinally. Overinterpretation of histological trends over time is possible, especially for the 12wpi tissue that is cut to a different thickness from the earlier timepoints. Regardless, the effect of a dampened fibrotic scarring response is robust at each time point individually and independent of vascular associations. Furthermore, the dampened fibrotic scar response is supported by an independent study by Streeter et al. that shows less collagen IV deposition in the injured cord of *Acomys* compared to *Mus*⁶¹.

4.5 *Acomys* Have Fewer PDGFR β + Cells in the Injured Spinal Cord

Considering the robust effects of dampened ECM deposition within the injured *Acomys* spinal cord, I sought to determine if this was attributable to a decrease in cells that deposit ECM. The general term used for the fibrotic tissue-depositing cells is fibroblasts, but fibroblasts are difficult to define and label²⁶². The particular origin of ECM-depositing fibroblasts within the injured spinal cord is still an area of active debate. Astrocytes have long been studied for their deposition of ECM molecules, especially CSPGs^{79,210,217}. Some

point toward infiltrating schwann cells that express high levels of growth-modulating ECM molecules, especially in the human cord^{106,183}. Perhaps the most thoroughly-studied cellular source of ECM, though, is the pericyte. Multiple genetic studies have shown that perivascular cells, likely subsets of pericytes, enter the lesion core after injury and deposit ECM^{19,20,263}. Genetically depleting these cells decreases ECM deposition within the injured cord²⁶⁴, and allowing the return can resume ECM deposition at subacute time points²⁶³. Collectively, it seems multiple cell types contribute to the fibrotic scar after SCI but pericytes are likely the primary cellular source of spinal fibroblasts.

Göritz and colleagues genetically labelled a specific GLAST+ subset of pericytes that abandon blood vessels to invade the lesion core, and deposit ECM within the injured cord²⁰. Furthermore, genetic deletion of this pericyte subset decreases cellular infiltration and ECM deposition in the lesion core after SCI²⁰. Soderblom and colleagues also find that perivascular cells—potentially the same subset identified by Göritz and colleagues—are a key source of ECM in the injured cord. Using light-sheet microscopy to evaluate colocalization of genetically-labelled collagen-producing cells (Coll α 1+) and a suite of histological markers, Soderblom and colleagues conclude that fibroblasts migrate into the injury site as early as 5dpi, peak around 7dpi, and persist in the injury core until at least 56dpi¹⁹. While Soderblom and colleagues show that their Coll α 1+ fibroblasts are distinct from NG2+ pericytes, Hesp and colleagues show that inhibiting NG2+ proliferation decreases fibroblast levels and ECM in the injured cord²⁶³. They suggest that non-fibroblast pericytes may provide a necessary substrate for fibroblasts to enter the lesion core²⁶³. Together, these studies identify an important role for fibroblasts of a pericyte origin in establishing a robust fibrotic scar in the injured rodent spinal cord. Unfortunately, the

genetic labelling strategies employed in these investigations are currently unavailable in the burgeoning model system of *Acomys*, and histological assessments of fibroblasts in SCI is not straightforward.

Platelet-derived growth factor receptor (PDGFR) is a common receptor among fibroblasts and is key in regulating fibroblast behavior following injury. The receptor itself is a dimer composed of any combination of α and β subunits (PDGFR α and PDGFR β , respectively). While both are responsible for propagating signals for cell differentiation, cell growth, and development, we focus on PDGFR β because it has been specifically identified in genetically labelled fibroblasts after SCI. Soderblom et al. identify that 96% of their genetically labelled (Col1 α 1+) fibroblasts express PDGFR β ^{19,20}. Göritz et al. show that fibroblasts express both PDGFR α and PDGFR β while in contact with blood vessels, but express only PDGFR β when they have abandoned vessels and infiltrated into the spinal lesion core²⁰. PDGFR β + pericytes are similarly seen “lifting away” from the vasculature while migrating and proliferating after penetrating injuries to the human brain²⁶⁵. PDGFR β is also a functionally relevant marker for fibroblasts. Studies show that inhibiting PDGFR β *in vivo* and *in vitro* decreases fibroblast and pericyte proliferation and migration into injury sites²⁶⁶. In this study I use PDGFR β as a histological marker of ECM-producing cells. While this marker is not perfect, and will not solely identify fibroblasts²⁶², PDGFR β histology is an informative surrogate for genetic studies of fibroblasts.

I performed histological assessment of PDGFR β and other fibroblast markers in spinal cords isolated 3 days, 1 week, 2 weeks, and 12 weeks post spinal crush in *Mus* and *Acomys* to gain a better understanding of the cells that may be contributing to the fibrotic scar after SCI. Before injury there are very few PDGFR β + cells in the injured cord and

these cells are largely isolated to the vasculature^{19,20}. Levels of PDGFR β are similarly low at 3dpi, but upregulate in the whole cord (Figure 4.5.1A) and injury epicenter (Figure 4.5.1B) by 1wpi. However, *Mus* maintain a significantly higher density of PDGFR β + staining at 2wpi and 12wpi, while *Acomys* return to a lower level of PDGFR β + staining density (Figure 4.5.1). Indeed, *Acomys* have significantly lower PDGFR β + staining density in the whole cord (species effect $p < 0.01$) and injury epicenter (species effect $p < 0.0001$).

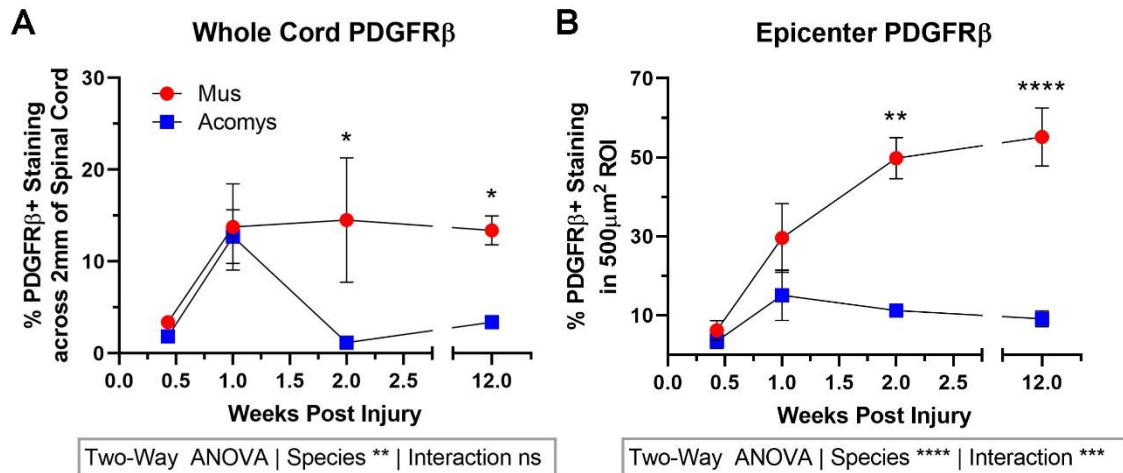


Figure 4.5.1: Histological analysis of spinal PDGFRβ over time in the injured spinal cord.

Histological analysis of spinal sections 3dpi, 1wpi, 2wpi, and 12wpi shows that whole-cord (A) and epicenter (B) PDGFRβ expression increases after SCI. While *Mus* maintain high PDGFRβ through chronic time points, *Acomys* have significantly less PDGFRβ, which seems to be driven by a decrease at 2wpi and 12wpi. *Mus* 3dpi (n=6), 1wpi (n=8), 2wpi (n=5), 12wpi (n=8); *Acomys* 3dpi (n=8), 1wpi (n=7), 2wpi (n=4), 12wpi (n=9). Data analyzed by two-way ANOVA with Sidak's multiple comparison correction, species effect and interaction (species x time) effect displayed below graphs, ns=no significant difference, *p<0.05, **p<0.01, ***p<0.001, ****p<0.0001.

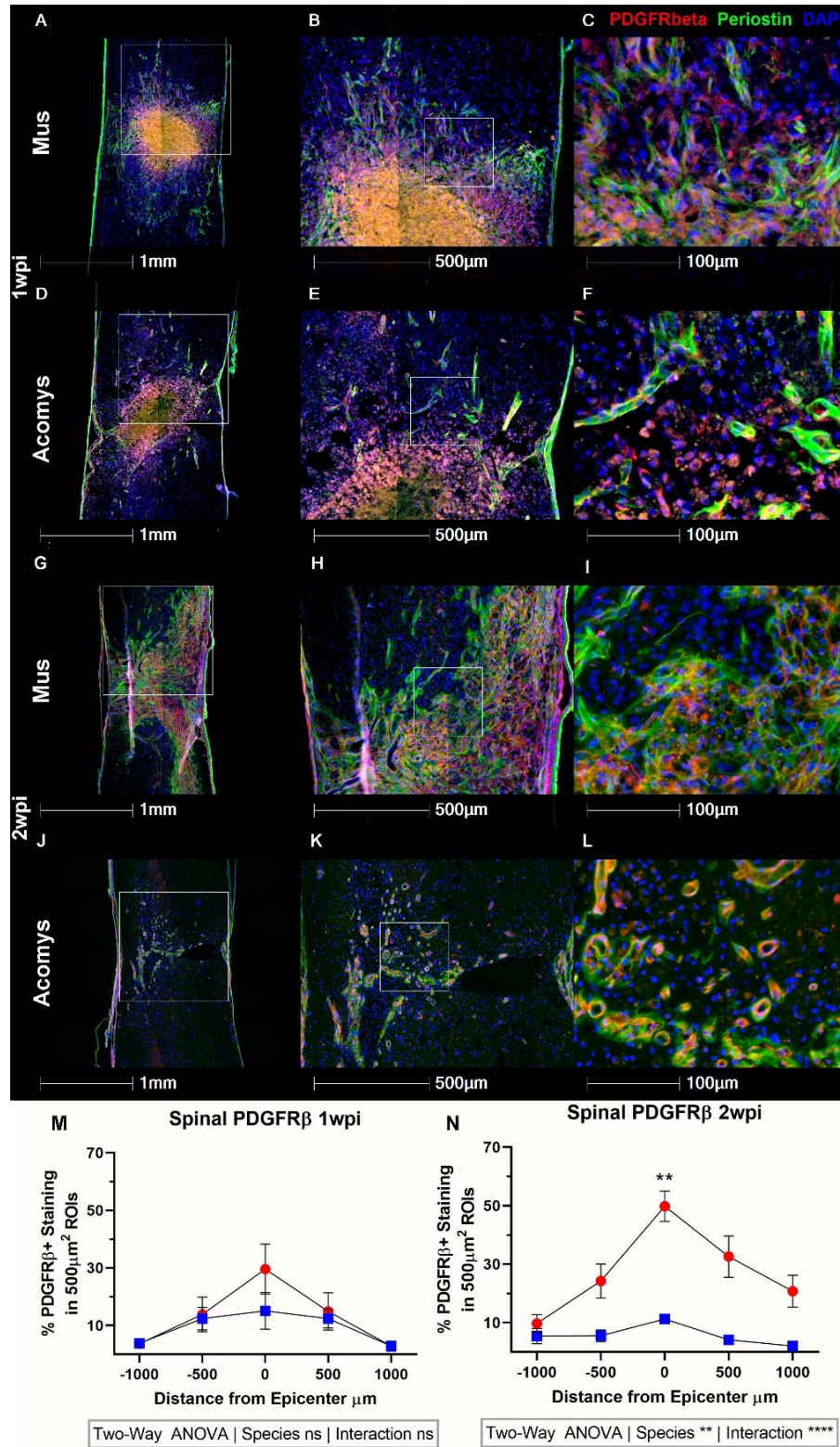
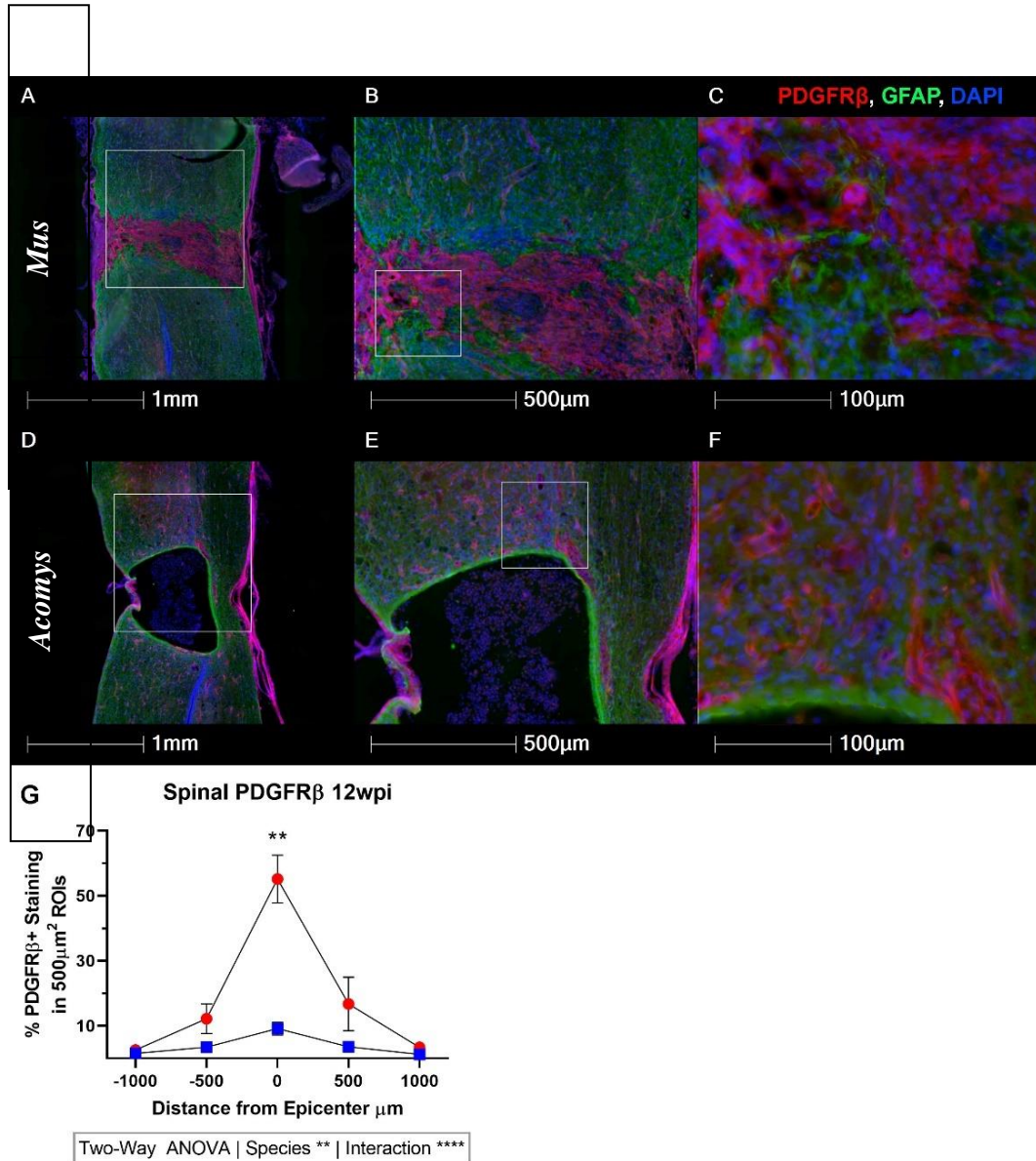


Figure 4.5.2: *Acomys* have less spinal PDGFRβ at 2wpi.
Representative images from each species suggest that while both species may have a dense accumulation of PDGFRβ in the lesion core 1wpi (A-F),

expression spreads across the cord in *Mus* at 2wpi (G-I) while it decreases in *Acomys* (J-L). Histological analysis of injured spinal cords harvested 1 and 2wpi shows similar PDGFR β density between species at 1wpi (M), but a significant decrease in PDGFR β density in *Acomys* 2wpi (N). *Mus* 1wpi (n=8), 2wpi (n=5); *Acomys* 1wpi (n=7), 2wpi (n=4). Data analyzed by two-way ANOVA with Sidak's multiple comparison correction, species effect and interaction (species x distance) effect displayed below graphs, ns=no significant difference, **p<0.01, ****p<0.0001.



When analyzing individual ROIs at various distances rostral and caudal to the injury epicenter, both species show an upregulation of PDGFR β + staining at the injury epicenter (Figure 4.5.2 and Figure 4.5.3). However, *Mus* have significantly higher PDGFR β density at the injury epicenter 2wpi (Figure 4.5.2N, $p < 0.01$) and 12wpi (Figure 4.5.3G $p < 0.01$). At 2 and 12wpi *Acomys* have significantly less PDGFR β density in the injured cord (species effect $p < 0.01$) and a significant difference in the patterning of PDGFR β + density (interaction effect $p < 0.0001$; Figure 4.5.2N, Figure 4.5.3G). Representative images from each species reflect these differences, with generalized staining in the lesion epicenter in both species 1wpi, followed by more discrete areas of staining at 2 and 12wpi. *Mus* appear to fill in the lesion core with generalized mesh-like patterning (Figure 4.5.2G-I and Figure 4.5.3A-C), as expected from previous investigations^{19,20,263}, while *Acomys* PDGFR β staining appears to adopt a more vessel-like morphology at 2wpi (Figure 4.5.2J-L) and 12wpi (Figure 4.5.3D-F).

As discussed above, PDGFR β staining is an imperfect indicator of fibroblasts in SCI. While the vast majority of Coll α 1+ fibroblasts express PDGFR β , it is not necessarily restricted to fibroblasts alone¹⁹. To better understand the identity of these PDGFR β + cells, I sought converging evidence with an alternative fibroblast marker, periostin. Periostin is an ECM protein that plays a role in bone, tooth, and heart morphogenesis in embryonic development, but is downregulated in adulthood outside the context of an insult or injury^{267,268}. Specifically, periostin has been used as a cardiac²⁶⁹ and CNS²⁷⁰ fibroblast marker, including specific association with ECM-producing pericytes²⁷¹. Co-staining for PDGFR β and periostin shows similar species trends at 1wpi (Figure 4.5.4A,B) and 2wpi (Figure 4.5.4C,D). Representative images also show similar staining patterns for PDGFR β

and periostin in both species 2wpi (Figure 4.5.4E, left column). This converging evidence suggests that *Acomys* have a lower fibroblast density in the injured cord. Further immunostaining with periostin and α -smooth muscle actin (aSMA), a marker of myofibroblasts, shows that only a small proportion of these cells are likely myofibroblasts (Figure 4.5.4E, right column).

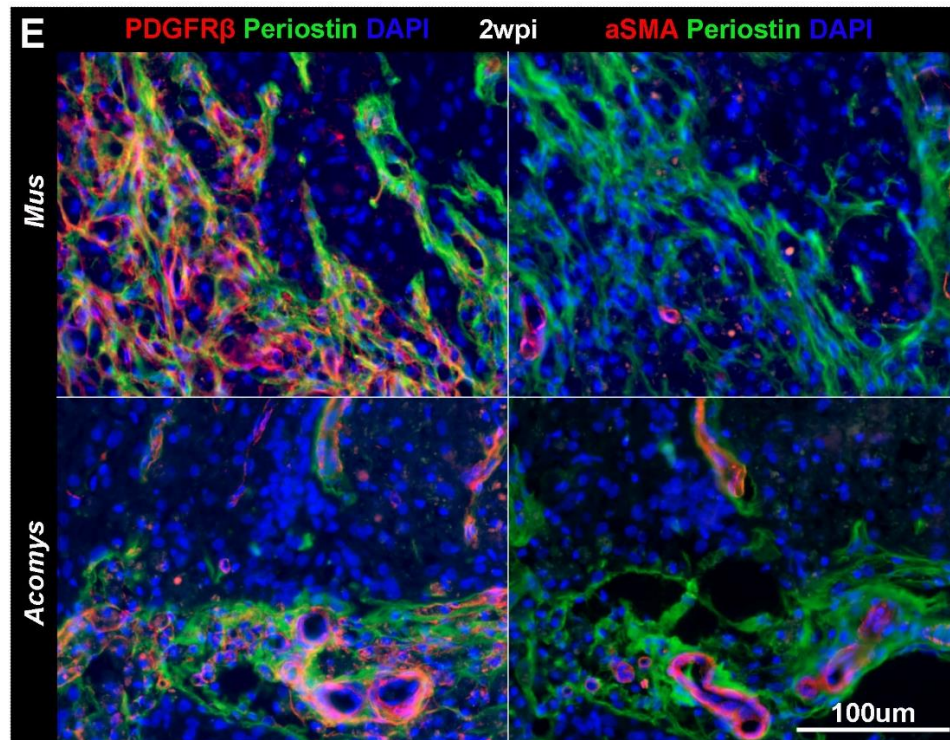
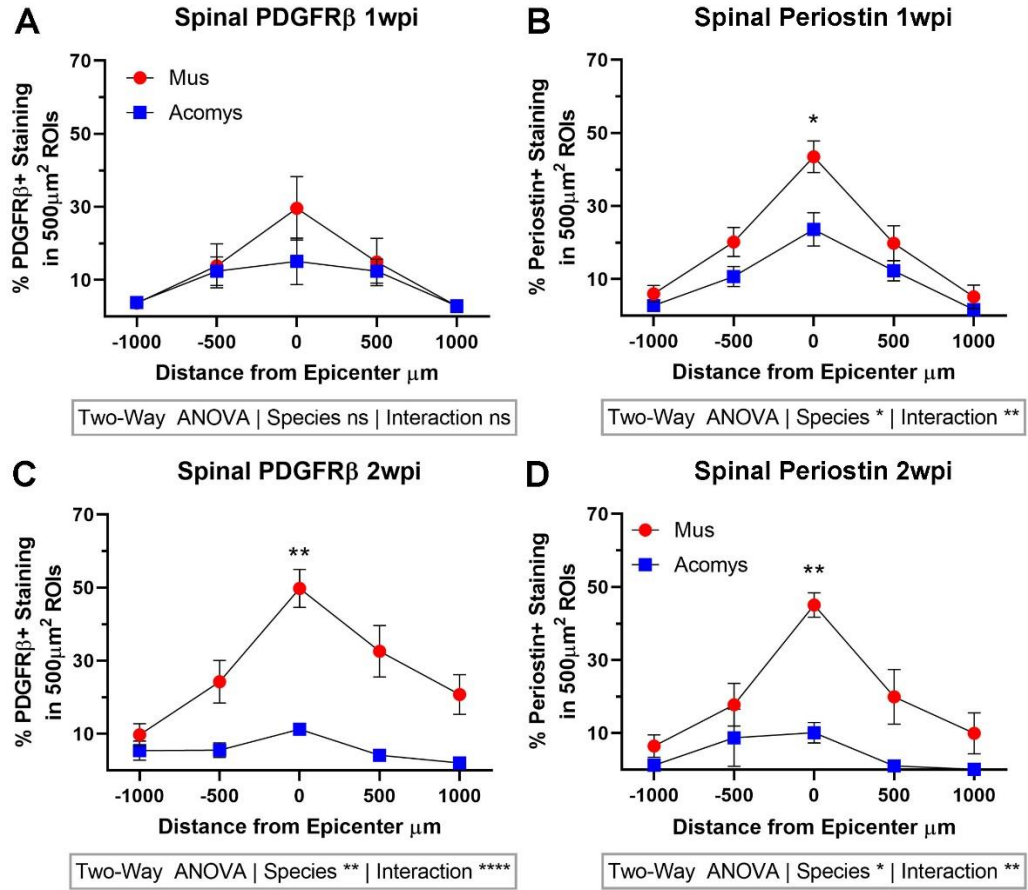


Figure 4.5.4: PDGFR β + staining has high overlap with alternative fibroblast marker, periostin.

Periostin, a fibroblast marker, shows similar expression patterns at subacute time points to PDGFR β (A-D). Representative images from spinal cords 2wpi show that PDGFR β and periostin are closely associated and may be co-expressed within the same cells (E). On the other hand, there is far less aSMA expression with only some co-expression with periostin, suggesting there are few myofibroblasts in the injured spinal cord of *Mus* and *Acomys* 2wpi. *Mus* PDGFR β 1wpi n=8, *Mus* PDGFR β 2wpi n=5, *Mus* periostin 1wpi n=8, *Mus* periostin 2wpi n=4; *Acomys* PDGFR β 1wpi n=7, *Acomys* PDGFR β 2wpi n=4, *Acomys* periostin 1wpi n=7, *Acomys* periostin 2wpi n=4. Data analyzed by two-way ANOVA with Sidak's multiple comparison correction, species effect and interaction (species x distance) effect displayed below graphs, ns=no significant difference, *p<0.05, **p<0.01, ****p<0.0001.

Converging evidence from PDGFR β and periostin histology suggests that *Acomys* may have fewer fibroblast in the lesion epicenter after SCI. The presence of a dense, mesh-like accumulation of PDGFR β + cells in the *Mus* injury site is supported by previous studies, where similar spinal histology is seen 2 weeks¹⁹ and 3 weeks²⁶³ after contusion injury. Furthermore, the upregulation of PDGFR β between 3dpi and 1wpi is supported by studies showing a robust increase in genetically labeled spinal fibroblasts between 4-9dpi^{19,20}. Finally, the spatial profile of *Mus* PDGFR β + cells—where widespread expression is condensed into persistent expression in the lesion core—is consistent with studies of genetically labeled fibroblasts¹⁹ and general PDGFR β ^{265,272} expression in the injured CNS. However, the resolution of lesion core PDGFR β expression in *Acomys* is unique amongst mammalian models of CNS injury.

When interpreting these data, it is important to remember that both PDGFR β and periostin are imperfect histological markers of fibroblasts. PDGFR β expression is robust in fibroblasts^{19,20} but is also present in vascular pericytes²⁷³, vascular smooth muscle²⁷⁴, and neurons^{275,276}. While periostin was seen in astrocytes, macrophage/microglia, periendothelium, and fibroblasts in the first week after ischemic stroke, periostin was only found in fibroblasts in the peri-infarct and lesion core 2wpi and 4wpi²⁷⁰. However, it is unlikely that the robust lesion core PDGFR β and periostin staining is reflective of neurons, as we see neuron soma are not present in the lesion core (Figure 2.5.4). The spatiotemporal patterning also suggests that PDGFR β and periostin staining are unlikely to be solely attributable to vasculature or neovasculature in the injured cord. Neovascularization in the injured rodent cord occurs mostly within the first week post injury^{228,277} and this neovascularization is primarily in areas distant to the injury epicenter (1000 μ m rostral and

caudal)²⁷⁷, where we see the least PDGFR β and periostin staining. There are mature vessels that appear in the epicenter of injured *Mus* spinal cords at subacute and chronic time points after injury, but these vessels are distinct in both their spacing and morphology^{147,278}. Indeed, high-powered fluorescence and electron microscopy has been used to show PDGFR β + cells abandon vessels and adopt the sheet-like meshwork in the later stages of CNS injury^{20,272}. Therefore, while some PDGFR β and periostin staining may be attributable to vasculature and vessel-associated cells in the injured spinal cord, historical evidence suggests that the majority of PDGFR β and periostin staining in the subacute injury core is reflective of extravascular, non-neuronal cells.

Decreased PDGFR β + and periostin+ staining density in the injured *Acomys* cord can be attributed to less cell proliferation, less cell infiltration, or less cell-to-cell protein expression. The diverse assemblage of cells and microenvironmental stimuli provides many factors to drive fibroblast proliferation, infiltration, and/or protein expression. Fibroblasts are highly responsive to growth factors²⁷⁹, cytokines^{140,280}, ECM components^{196,281}, and topographical cues²⁸² both *in vivo* and *in vitro*¹¹⁰. Many believe that the primary chemotactic signal for invading fibroblasts is PDGF released by platelets and macrophages²⁸³. Macrophage-induced fibroblast infiltration and proliferation is part of the normal course of wound healing for peripheral injuries¹⁴⁰. Accordingly, inhibiting PDGFR β activation prevents fibroblast proliferation and infiltration in a mouse model of cutaneous wound repair²⁶⁶. Similarly, periostin has been suggested as a regulator of fibroblast function in SCI. Using a genetic deletion model, Yokota and colleagues show that inhibiting periostin decreases total PDGFR β staining and ECM deposition in mouse

SCI²⁷¹. The functional role of these fibroblast markers is discussed in further detail in chapter 6.

4.6 Understanding the Role of Fibrotic Scarring in Mammalian Spinal Cord Repair through *Acomys*

Extracellular matrix is a key part of normal physiological function, but some injuries evoke an overactive fibrotic scarring response that does not facilitate repair. Many have suggested that the fibrotic scar, deposited by fibroblasts in the lesion core, prevents spinal repair after injury^{2,235,238,284}. In this chapter, I describe a dampened fibrotic scarring response in the injured spinal cord of *Acomys*, a mammalian model of enhanced functional recovery from SCI. Histological analysis suggests that less ECM deposition—specifically, less collagen IV, collagen fibrils, laminin, and fibronectin—is likely underpinned by fewer ECM-depositing cells, as indicated by less PDGFR β and periostin staining in *Acomys* SCI than than in *Mus*.

One unifying factor for several of these stains is the traditional association with vasculature. Basal lamina constituents, collagen IV and laminin, and PDGFR β + pericytes typically surround vascular endothelium in the CNS. While evidence from past studies shows a profound upregulation of extravascular collagen IV, laminin, and PDGFR β staining in rodent models of SCI^{20,228,235,265}, this study does not include endothelial or other vascular markers. Histological markers of endothelial cells, particularly PECAM/CD31, would enable visualization of the vascular endothelium. Pairing these stains with proliferative markers would give further indication of neovascularization in the injured cord^{228,277}. Alternatively, circulatory dyes and dextrans can be used to mark intact vasculature. Qualitatively, basal lamina constituents, PDGFR β , and periostin appear to be

restricted to a vessel-like morphology in *Acomys*. Pairing vascular labeling methods with basal lamina and fibroblast markers would provide valuable insight into the extravasation (or lack thereof) that underlies the robust effects seen in this investigation.

While the vascular dynamics in the injured *Mus* vs. *Acomys* spinal cord may underlie some effects, I hypothesize that ECM trends are driven by non-vascular ECM production of these PDGFR β +/*periostin*+ cells in their functions as fibroblasts. Results in *Acomys* seem similar to genetic studies in the mouse that limit PDGFR β and ECM in the injury core^{20,263}. Limiting the proliferation of PDGFR β + fibroblasts leads to a profound decrease in fibronectin deposition at SCI site²⁰. Indirectly preventing PDGFR β + cell expansion in the injured cord—likely by preventing entry into the injury core—leads to dramatic decreases in laminin deposition²⁶³. Inhibiting *periostin* causes a decrease in PDGFR β and collagen fibrils in the injured cord²⁷¹. As in *Acomys*, these models of decreased PDGFR β and ECM in the injured cord show increased functional recovery from SCI^{263,271}. While genetic and antibody-based inhibition studies support our results to show the importance of fibroblasts in functional recovery of the injured spinal cord, the common therapeutic approach in SCI is to target ECM directly rather than targeting ECM-depositing cells. By altering the activity of spinal fibroblasts, biomedical researchers may be able to facilitate endogenous repair rather than fighting against a maladaptive system. *Acomys* provide an exciting opportunity to better understand naturally occurring endogenous mechanisms of fibrosis that can facilitate enhanced recovery.

CHAPTER 5. INJURY BIOMECHANICS AFFECT SPINAL CORD INJURY PROGRESSION

Identifying key cellular and molecular pathways that facilitate pathology and repair is a key first step in developing biomedical therapies. An equally important aspect, though, is identifying the contexts in which these therapies will be beneficial. Context is doubly important in the extremely heterogeneous condition of SCI. In this chapter I will discuss additional studies in a novel SCI paradigm developed to study mammalian SCI progression. By specifically controlling the parameters of the SCI insult, I was able to identify how these initial injury biomechanics affect downstream secondary injury responses and the overall outcomes of SCI. This project, which has previously been published in the *Journal of Neurotrauma*⁷⁰, provides important contextual information to identify when immunomodulatory therapies would be most efficacious for treating SCI.

5.1 Spinal Cord Injury is Meaningfully Heterogeneous

Spinal cord injury is not bound by any demographic or specific injury biomechanics. Clinically, traumatic SCI involves a wide array biomechanical variables, each of which can vary broadly. For instance, the force applied to the cord can vary in velocity, acceleration, duration, direction, distribution, and magnitude. Each of these biomechanical details are clinically meaningful to the clinical presentation of SCI and are readily apparent in typical SCI cases. SCI can occur abruptly due to motor vehicle accidents, falls, and sport injuries, or it can occur gradually as a result of spinal stenosis, osteoarthritis, abscess, and tumors¹. The speed of force application can affect the deformation of the soft spinal tissues as they absorb and diffuse the force²⁷. Unfortunately, the overt heterogeneity of SCI is at odds with efforts of researchers who strive to minimize

extraneous variables and create consistent injuries to derive reproducible results. In this chapter, I will discuss how different SCI biomechanics can affect injury progression and the implications of these differences both in the laboratory and in the clinic.

Severity of injury is one of the more foundational and straight-forward aspects of SCI. In the clinic, physicians will commonly classify SCI based on the American Spinal Injury Association (ASIA) Impairment Scale as A, B, C, D, or E which represent functional deficits from most to least severe, respectively⁵¹. While the ASIA scale is fairly obtuse and has been criticized for failing to account for many granular aspects of injury²⁸⁵, it provides evidence of the non-binary nature of clinical deficits after SCI. Many research groups have investigated the effects of varying severities of their particular animal SCI paradigms. Greater force applied to the cord in contusion injuries can cause greater anatomical and functional deficits^{22,286,287}. Similarly, greater contusion-induced tissue displacement results in decreased tissue sparing and functional recovery²⁵. Severity-dependent deficits are not unique to contusion injury. Stepwise compression injury also causes stepwise decreases in tissue sparing and function, as shown in a model of spinal crush with forceps restricted to various maximum closure distances²³. Thus, the severity of contusion and compression injuries plays a key role in determining overall anatomical and functional outcomes in SCI.

Subtle differences in injury biomechanics also affect SCI progression. The direction of force application affects neuron permeability. Shear force (applied parallel to the hydrogel surface) causes more cellular permeability than the same cultures loaded with compressive force (applied perpendicular)²⁷. Furthermore, in vivo experiments identify that these various directions of force loading are evident even within different regions of the same injury²⁷. Oxland and colleagues created sophisticated, clinically relevant injury

paradigms to further investigate SCI biomechanics, which include dislocation (shifting vertebra outside of spinal axis), distraction (pulling vertebra apart along the spinal axis), and contusion (exposing and impacting the spinal cord) injures. Dislocation, distraction, and contusion SCI each produced unique histological and functional deficits and at a cellular level, affecting apoptosis, permeability, and axon degeneration²⁸⁸. Collectively, these experiments show that highly specific aspects of injury biomechanics, such as direction of force application, can affect the progression of SCI pathology on a organ-wide and cellular level.

Beyond the direct effects on pathology, it is also important to understand how SCI biomechanics affect secondary injury responses and shape the SCI microenvironment over time. As discussed earlier, the overall outcomes of SCI are heavily influenced by the complex secondary injury cascades that can serve protective and reparative roles but can also exacerbate damage and contribute to progressive injury. Macrophages and microglia, in particular, are major mediators of spinal inflammation and exhibit high levels of context-dependent plasticity. Specific stimuli shift macrophage and microglia along a spectrum of phenotypes ranging from pro-reparative to pathological^{143,289}. Injury biomechanics establish the SCI microenvironment and can dictate the contextual cues for macrophages and microglia. For instance, residual compression increases hemorrhage²⁹⁰, and hemorrhage-induced hypoxia alters cellular bioenergetics²⁹¹. The implications of these relationships should be considered both in the lab and in the clinic.

In this chapter, I will discuss our study investigating the effects of residual compression on spinal inflammation and progression of SCI. Importantly, this study investigates residual compression across various injury severities in an effort to disentangle

effects specific to compression from effects of injury severity. We used the Infinite Horizons (IH) impactor²⁸⁶ to deliver spinal contusion to mice with specifically controlled impact force and duration, effectively created injuries of various severity with and without residual compression. Then, we analyzed locomotor function, anatomical deficits, and inflammatory profiles of mice at various times after injury. These experiments show that residual compression causes exacerbated spinal pathology, a premature cessation of functional recovery, and a downstream shift in macrophage/microglia phenotypes.

5.2 Experimental Design to Study the Effects of Compression in Spinal Cord Injury

We set out to understand the effects of compression on SCI progression and injury responses by designing our experiment with moderate (50 kdyn) and severe (75 kdyn) contusion injuries with or without 20 sec of sustained compression after contusion. This gives us 4 injury groups, which will hereafter be labelled as (1) 75 kdyn, (2) 75 kdyn 20 sec, (3) 50 kdyn, and (4) 50 kdyn 20 sec. Using these four injury groups, we were able to investigate the effects of compression in moderate and severe injuries specifically, but could also investigate effects of compression regardless of injury severity.

We performed our experiments using 90 3–4 month old female C57BL/6 mice (Jackson Laboratory, Bar Harbor, Maine), a common species and strain for SCI research. Animals were housed in individually ventilated cages with ad libitum access to food and water. All procedures were performed in accordance with the guidelines of the Office of Responsible Research Practices and with the approval of the Institutional Animal Care and Use Committee at the University of Kentucky.

Mice were anesthetized via intraperitoneal (ip) injections of ketamine (100 mg/kg) and xylazine (10 mg/kg). After a T9 laminectomy, a mid-thoracic SCI was produced using

the IH injury device²⁸⁶. A previous study suggests that the duration of compression has negligible effects on outcomes²⁹. Based on these findings, we performed pilot studies examining different compression times and found no obvious differences in injury severity between groups. This finding is consistent with a previous study reporting an injury threshold at 15 sec of sustained compression after IH contusion SCI²⁹². Thus, we determined a 20 sec sustained compression was sufficient and reproducible within our stereotaxic mode of injury application.

Mice were divided randomly to receive SCI with varying impact force (50 or 75 kdyn) and duration of maintained compression (i.e., dwell time: 0sec or 20sec), yielding four groups: 50 kdyn, 50 kdyn 20 sec, 75 kdyn, and 75 kdyn 20 sec. After injury, muscle and skin incisions were closed using monofilament suture. Post-surgically, animals received one subcutaneous injection of buprenorphine-SR (1 mg/kg) for pain and 2 mL of saline + antibiotic (5 mg/kg, enroloxacin 2.27%: Norbook Inc, Lenexa, KS); buprenorphine has been shown to produce analgesic effects without affecting molecular, anatomical, behavioral, or physiological parameters after SCI²⁹³. Animals were housed in warming cages overnight. Animals continued to received 1mL saline + prophylactic antibiotics subcutaneously for five days. Food and water intake and the incision site were monitored throughout the course of the study. Bladder expression was performed on injured mice twice daily until mice reached voluntary evacuation. Two mice received SCI with abnormalities in the force versus time curve generated by the IH device, indicating bone contact or spinal cord movement during impact. Based on these pre-determined exclusion criteria, these two mice were excluded from further analyses. Groupwise spinal cord injury parameters are summarized in (Table 5.2.1).

Table 5.2.1: Spinal Cord Injury Parameters

<i>Group</i>	<i>Set force (kdyn)</i>	<i>Actual force Avg. (kdyn) ± SD</i>	<i>Displacement Avg. (μm) ± SD</i>	<i>Compression time (s)</i>
50 kdyn	50	54 ± 2	429 ± 88	0
50 kdyn 20 sec	50	53 ± 2	398 ± 99	20
75 kdyn	75	78 ± 2	566 ± 99	0
75 kdyn 20 sec	75	78 ± 2	492 ± 76	20

Animals (n=9-11/group) were tested for functional recovery of hindlimb locomotion using the Basso Mouse Scale (BMS) before euthanizing the animal to collect spinal tissue at 28 days post injury (dpi). Behavioral testing with BMS is described in more detail later in Appendix 2. Separate cohorts were injured and euthanized for spinal tissue collection 3, 7, or 14 dpi (n=4-6 per time point).

We analyze the anatomical responses to injury 3, 7, 14, or 28 dpi by collecting spinal tissues from injured mice. To collect these tissues, mice were anesthetized with a lethal dose of ketamine (150 mg/kg) and xylazine (15 mg/kg), then transcardially perfused with cold phosphate buffered saline (PBS) (0.1 M, pH 7.4), followed by perfusion with cold 4% paraformaldehyde (PFA). Dissected spinal cords (1 cm) were post-fixed for 2hr in 4% PFA, then rinsed and stored in cold phosphate buffer (0.2 M, pH 7.4) overnight at 4°C. Tissue was cryoprotected in 30% sucrose at 4°C for one week, then rapidly frozen using optimal cutting temperature compound (Sakura Finetek USA, Inc., Torrance, CA) on dry ice. Tissue was systematically randomized into blocks with equal group distribution in each block to ensure uniformity of staining across groups. Tissue was stored at -80°C before sectioning. Tissue blocks were cut in 10µm thick serial cross sections and mounted onto Colorfrost plus slides (Fisher #12-550-17).

Spinal tissue was stained for visualization through chemical or antibody-based stains specifically described in Appendices 2 and 3. Briefly, brightfield chemical staining with eriochrome cyanine (EC) and neurofilament (NF-H; Aves Labs, #NFH) was used to visualize spared tissue as described previously^{69,71}, while antibody-mediated fluorescent staining of various macrophage/microglia phenotypic markers were employed to visualize the macrophage/microglia responses to injury. Stained spinal tissue was then imaged and

analyzed using semi-automated analysis processes on the MetaMorph analysis program (Molecular Devices, Sunnyvale, CA).

Because of unknown, at the time, temperature inconsistencies during tissue processing and sectioning, some cross sections were lost or folded during staining, making analysis impossible. Mice without an obvious and fully intact epicenter were not included for histological analysis, decreasing the total number of mice analyzed for histological analyses from 88 to 71.

Investigators blinded to experimental groups performed all data acquisition and analysis. Statistical analyses were completed using GraphPad Prism 6.0 (GraphPad Software). Data were analyzed using one- or two-way analysis of variance (ANOVA) followed by the Holm-Sidak test for multiple comparisons. Specifically, repeated measures two-way ANOVA was used to analyze BMS (time [repeated] x injury), 28d tissue sparing (distance [repeated] x injury), and macrophage phenotype (ROI [repeated] x injury). Ordinary two-way ANOVA was used to analyze tissue sparing over time (time x injury). All other outcomes were analyzed using one- way ANOVA or independent sample t tests when appropriate. Comparisons include groups differing only in contusion force (50 kdyn vs. 75 kdyn, 50 kdyn 20 sec vs. 75 kdyn 20 sec) or compression (50 kdyn vs. 50 kdyn 20 sec, 75 kdyn vs. 75 kdyn 20 sec); other groups were not analyzed statistically to avoid comparing across multiple independent variables. The robust regression and outlier removal method with a false positive rate for detecting outliers (Q-value) of 1% was used to automatically identify outliers, and imputed mean values were used when necessary for repeated measures²⁹⁴. Results were considered statistically significant at $p < 0.05$. All data

are presented as mean \pm standard error of the mean unless otherwise noted. Figures were prepared using Adobe Photoshop CS6 (Adobe Systems) and Prism 6.0.

5.3 Sustained Compression Decreases Functional Recovery from Contusion Spinal Cord Injury

Initial injury biomechanics are highly influential on the progression of pathology and recovery from SCI. Clinically, function is used to categorize the severity of injury on the ASIA scale⁵¹. In the lab, behavioral outcomes have been similarly evaluated on their ability to detect differences between animals injured with graded contusion severities²². Several studies have shown that graded increases in compression cause progressive functional deficits^{23,295}, but this is the first study to investigate if compression, as a unique injury biomechanic independent of injury severity, causes unique progression of injury and/or recovery.

We assessed locomotor hindlimb function in injured mice using the BMS as described previously⁵⁴. Two observers blinded to group inclusion observed and scored mice in an open field for 4 min at 1, 3, 7, 14, 21, and 28dpi. Each hindlimb was scored separately based on hindlimb movement (e.g., ankle placement and stepping), coordination, and trunk stability, then averaged to generate a single score for each animal. A score of 0 indicates complete paralysis while a score of 9 indicates normal locomotion. The BMS subscore is sensitive to atypical patterns of locomotor recovery⁵⁴ and was used to analyze specific aspects of locomotion (e.g., paw placement and coordination).

Our injury model was consistent with previous reports that locomotor function varied significantly depending on the contusion force^{25,54}. Specifically, recovery was significantly worse for animals receiving 75 kdyn versus 50 kdyn contusions regardless of

compression (main effect of 50 kdyn vs. 75 kdyn or 50 kdyn 20 sec vs. 75 kdyn 20 sec $p < 0.01$; Table 5.3.1 and Figure 5.3.1). Compression also significantly decreased recovery independent of contusion severity (main effect of 50 kdyn vs. 50 kdyn 20 sec or 75 kdyn vs. 75 kdyn 20 sec $p < 0.0001$). These data help support previous data indicating that both increased severity and the addition of compression contribute to functional deficits from SCI.

To account for atypical patterns of recovery that may occur with sustained compression, we further investigated recovery using the BMS subscore at 28dpi. This composite score is based on the functional levels achieved for stepping, coordination, paw position, trunk stability, and tail placement independent of the pattern of recovery⁵⁴. Figure 5.3.1B shows that the total BMS subscore is decreased by increased contusion force (50 kdyn vs. 75 kdyn, $p < 0.05$), and with the addition of compression at each contusion force (50 kdyn vs. 50 kdyn 20 sec, $p < 0.0001$; 75 kdyn vs. 75 kdyn 20 sec, $p < 0.01$). Particular aspects of the BMS subscore highlight specific functional tasks, all of which follow a similar pattern to the overall BMS subscore and functional outcomes at 28dpi.

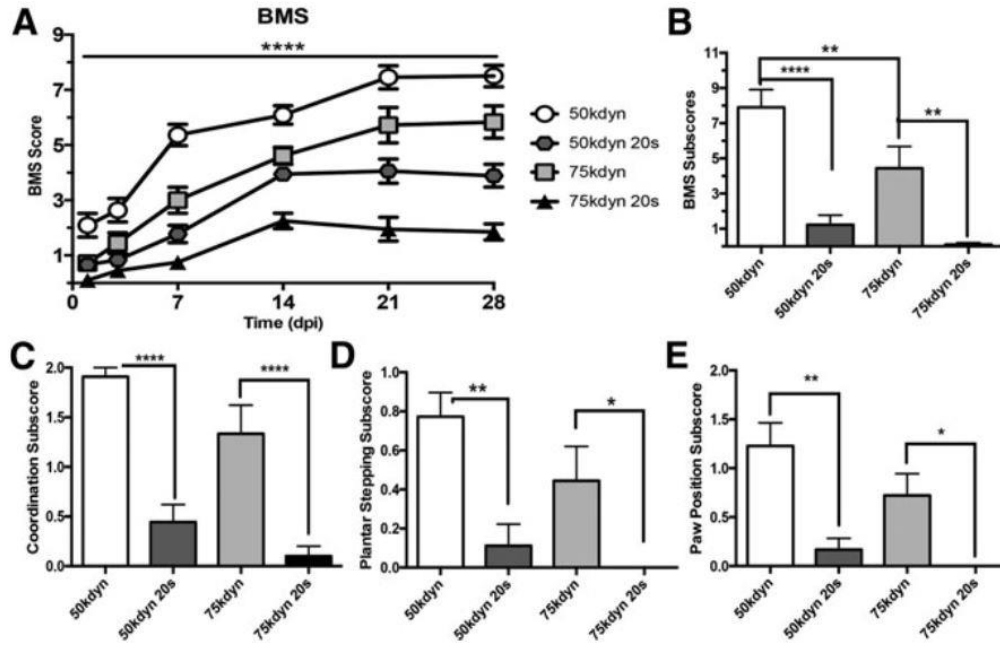


Figure 5.3.1: Compression impairs functional recovery from contusion SCI.

A) Over a 28-day period, groups with higher impact force have worse hindlimb function than groups with lower impact force and groups with compression had worse hindlimb function than groups without compression (statistics detailed in Table 5.3.1). Specifics of hindlimb function are detailed in 28dpi BMS subscores. Groups with compression performed significantly worse than force-matched counterparts for every subscore. (B) Composite BMS subscore is significantly decreased by increased severity and compression. (C) Coordination is graded as 2 = mostly coordinated (>50%), 1 = some coordination (<50%), or 0 = no coordination. (D) Plantar stepping is graded as 1 = consistent or 0 = less than consistent. (E) Paw position is graded as 2 = parallel throughout, 1 = parallel and rotated, or 0 = rotated throughout. * $p < 0.05$, ** $p < 0.01$, **** $p < 0.0001$.

Table 5.3.1: Basso Mouse Scale Statistical Summary (p values)

<i>Groups (n)</i>	<i>Main</i>	<i>1 dpi</i>	<i>3 dpi</i>	<i>7dpi</i>	<i>14 dpi</i>	<i>21 dpi</i>	<i>28 dpi</i>
50 kdyn (<i>n</i> = 11) vs. 75 kdyn (<i>n</i> = 9)	**	0.14	0.27	***	0.09	*	*
50 kdyn 20 sec (<i>n</i> = 9) vs. 75 kdyn 20 sec (<i>n</i> = 10)	***	0.65	0.92	0.07	***	****	****
50 kdyn (<i>n</i> = 11) vs. 50 kdyn 20 sec (<i>n</i> = 10)	****	*	**	****	***	****	****
75 kdyn (<i>n</i> = 9) vs. 75 kdyn 20 sec (<i>n</i> = 10)	****	0.78	0.27	***	****	****	****

*, **, ***, **** $p < 0.05, 0.01, 0.001, 0.0001$.

Coordination of stepping is significantly compromised in animals whose injuries include compression. Figure 5.3.1C shows the coordination subscore that quantifies forelimb-hindlimb stepping as mostly coordinated (at least 50% coordinated, score = 2), some coordination (at least 1 coordinated pass, score = 1), or no coordination (score = 0). Compression significantly decreased forelimb-hindlimb stepping coordination (50 kdyn vs. 50 kdyn 20 sec, $p < 0.0001$; 75 kdyn vs. 75 kdyn 20 sec, $p < 0.0001$). Figure 5.3.1D shows the plantar stepping subscore that distinguishes between frequent hindlimb plantar stepping (at least 50% stepping, score = 1) and occasional/no hindlimb plantar stepping (<50% stepping, score = 0). Compression significantly decreased hindlimb plantar stepping performance (50 kdyn vs. 50 kdyn 20 sec, $p < 0.01$; 75 kdyn vs. 75 kdyn 20 sec, $p < 0.05$).

Positioning of the paw during hindlimb stepping is significantly impaired in animals with injuries including compression. The paw position subscore included in Figure 5.3.1E quantifies paw rotation during stepping from the initial contact through liftoff as parallel throughout (score = 2), parallel and rotated (score = 1), or rotated throughout (score = 0). Animals that have injuries without compression sometimes achieve parallel paw positioning while stepping, but animals with compression injuries cannot achieve parallel paw placement while stepping (50 kdyn vs. 50 kdyn 20 sec, $p < 0.001$; 75 kdyn vs. 75 kdyn 20 sec, $p < 0.05$). Collectively, BMS score and subscore indicate that functional recovery is impaired by additional compression at the time of contusion regardless of impact force.

Only a few studies have reported long-term recovery after contusion injury with or without subsequent compression. For example, Streijger and colleagues examined fore- and hindlimb recovery after cervical IH contusion in mice with or with subsequent

compression (0, 15, or 30 sec)²⁹². Depending on the outcome measure, recovery was noted in the contusion alone group after two weeks (e.g., forelimb grip strength); however, little recovery was observed within the first month across a range of functional measures in combined contusion-compression groups²⁹². Chronically (12 wks), some behaviors did improve across all groups; however, functional decline was noted only in the combined contusion/compression groups over this period.

The behavioral results are less consistent in rat models of contusion with subsequent compression injury. When a spacer was placed on the dura after contusion SCI to maintain compression for various periods (hours to weeks), the rate and overall extent of recovery varied with spacer size and compression duration^{296,297}. These data, along with a rat study with various compression times after IH contusion²⁹, indicate that the compression itself, and not the duration of the compression, worsens functional outcome. Collectively, these published results, along with the results of the current study, indicate that the mode of injury is an important determinant of functional recovery. Indeed, a recent comparison across contusion, dislocation, and distraction SCI reported different rates of recovery depending on the mode of SCI²⁸.

Our study was specifically designed to disentangle the injury biomechanics of severity and compression. Adding compression to a contusion injury could lead to effects due to increasing injury severity or due compression itself. However, by collapsing groups of moderate (50 kdyn) and severe (75 kdyn) injuries to create two groups (with 20 sec compression and without 20 sec compression), we can gain insight into the effects generalized effects of compression in contusion injury regardless of severity. Through this analysis, we uncover that compression significantly impairs hindlimb function, as

quantified on the BMS, at all time points (Figure 5.3.2A; $p < 0.0001$, main effect of compression). Furthermore, this analysis highlights the fact that compression causes early cessation in functional recovery, resulting in a premature recovery plateau 14 dpi. Specifically, mice injured without compression improved an average of 1.5 points on the BMS scale between 14 dpi and 28 dpi (Figure 5.3.2B). On the other hand, mice injured with sustained compression after contusion SCI improve significantly less ($p < 0.005$), only increasing their BMS score an average of 0.3 points between 14 and 28 dpi (Figure 5.3.2B).

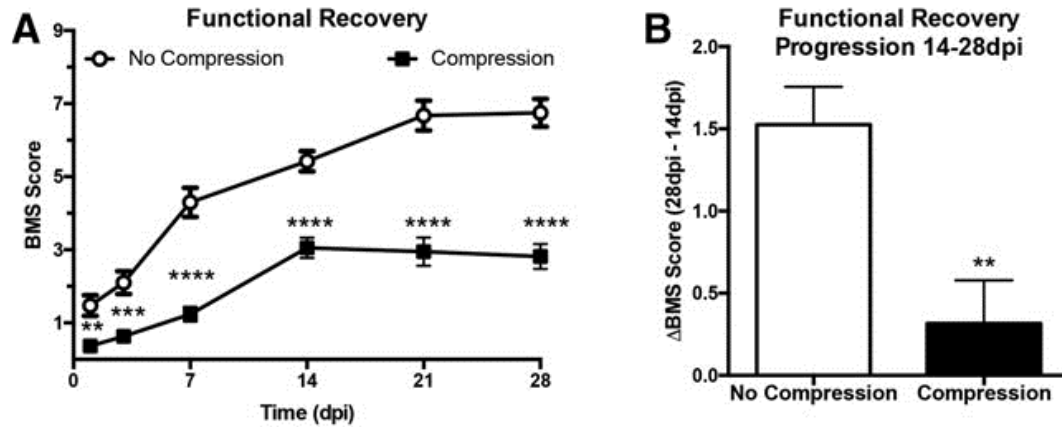


Figure 5.3.2: Compression decreases functional recovery regardless of severity.

Both 50 and 75 kdyn spinal cord injury contusion groups were collapsed and the effect of 20 sec of sustained compression was compared between aggregate groups. (A) Animals with compression injuries do not recover as much hindlimb function, according to the Basso Mouse Scale, as counterparts whose injuries did not include compression ($n=19-20$; main effect $p < 0.0001$). In addition, (B) animals injured without compression demonstrate improved function from 14 to 28 dpi, while animals whose injuries included subsequent compression prematurely cease recovery after 14 dpi. ** $p < 0.01$, *** $p < 0.001$, **** $p < 0.0001$.

Interestingly, a similar two-week plateau in functional recovery has been reported after varying degrees of compression injury alone and after severe IH contusion injury^{25,298}. While it is not surprising that little recovery would be detectable after severe injuries, it is interesting to note that clip-compression SCI, a form of contusion with sustained compression, results in little recovery after the first few weeks of injury in both rats and mice^{89,295}. Collectively these data indicate that compression significantly impairs functional recovery from SCI, potentially by creating a premature cessation in the progression of functional recovery.

5.4 Sustained Compression Decreases Tissue Sparing in Contusion Spinal Cord Injury

Previous studies have shown that injury biomechanics affect lesion size and tissue sparing^{22,28}. Additionally, studies show adding compression²⁹² and increasing the extent of compression²⁹⁰ can cause increased tissue pathology in contusion spinal cord injury. However, our study is the first to investigate effects of compression across various contusion severities. Understanding the effects of compression on tissue pathology independent of injury severity is critical to building a better understanding of the interplay of these clinically relevant injury biomechanics.

To determine whether long-term anatomical recovery was affected by the addition of compression to a contusion SCI, we investigated tissue changes through histological analysis of serial spinal cord cross sections. As validated and described previously, spared tissue was identified using a combination of eriochrome cyanine (EC) and NF-H to label myelin and axons, respectively^{69,71}. Tissue sparing images were collected using an Olympus AX-80 and Aperio Scanscope, and images were analyzed using the MetaMorph analysis to create custom regions of interest (ROIs) outlining areas of frank pathology that

quantified spared and lesioned area. We performed tissue sparing analysis at 28 dpi on sections identified as the lesion epicenter as well as sections 0.2 mm, 0.5 mm, and 1.0 mm rostral and caudal to the lesion epicenter.

Our histological results were consistent with previous reports^{22,286} in showing decrease epicenter tissue sparing with increased contusion severity (50 kdyn vs. 75 kdyn $p = 0.03$; Figure 5.4.1 and Table 5.4.1). Further, our data reveal that compression significantly decreases tissue sparing at the lesion epicenter of animals at both injury severities (50 kdyn vs. 50 kdyn 20 sec and 75 kdyn vs. 75 kdyn 20 sec $p < 0.0001$). These lesions consumed a larger portion of the cord at the injury epicenter, but analysis of sections rostral and caudal to the immediate injury site also reveal that tissue pathology spread throughout the cord (Figure 5.4.1A and Table 5.4.2).

To gain insight into the progression of tissue damage, additional epicenter tissue sparing data were gathered at 3, 7, and 14 dpi. The proportional area data reflect a highly dynamic spinal lesion, which changes over time due to transient edema and active clearance of debris. Still, our longitudinal histology reveals compression causes long-term (28 dpi) tissue loss that is similar to acute (7 dpi) pathology, while tissue pathology in spinal cords injured without compression recover to a greater proportional area of spared tissue (Figure 5.4.1). This trend for compression-induced sustained tissue pathology is more evident and is statistically significant when analyzing groups collapsed across contusion severities (Figure 5.4.2; effect of compression $p < 0.001$).

Penumbral areas are often spared from the initial mechanical damage but are still susceptible to secondary injury. Considering the body of evidence suggesting that primary biomechanics affect secondary injury progression^{31,288}, it is likely that compression

influences these secondary injury cascades and thereby the overall progression of SCI. Indeed, previous studies show that compression after contusion induces increased hemorrhage, decreases spinal cord perfusion, and increases indicators of hypoxia in penumbral and distal areas of the spinal cord relative to the lesion epicenter^{290,291,297}. These changes can have widespread effects, including effects on the macrophages and microglia, which are especially responsive to hemorrhage and its accompanying blood components^{299,300}.

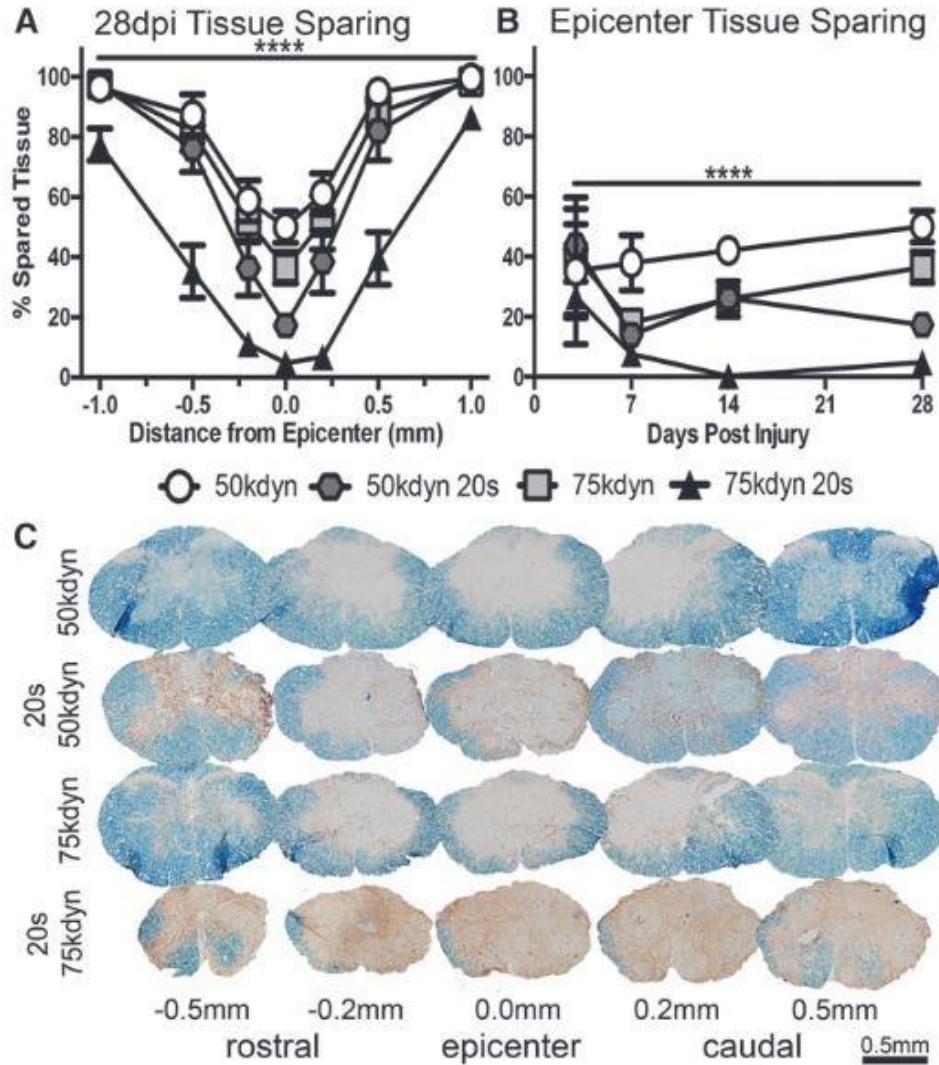


Figure 5.4.1: Compression significantly decreases anatomical recovery from contusion spinal cord injury.

A) Tissue sparing at 28 dpi is decreased by both increased force and compression at the epicenter and at regions rostral and caudal to the epicenter. (B) Tissue sparing at 3, 7, 14, and 28dpi, reflected by myelin (EC, blue) and axon (NF-H, brown) at the lesion epicenter is decreased by both increased impact force and compression. (C) Representative images reflect decreased tissue sparing in groups that receive compression. Scale bar, 400 μ m. Statistical details are included Tables 5.4.1 and 5.4.2.

Table 5.4.1: Statistical summary (p values) for time course of epicenter tissue sparing

<i>Groups</i>	<i>p value</i>				
	<i>Main</i>	<i>3 dpi</i> (n=2–4)	<i>7 dpi</i> (n=3)	<i>14 dpi</i> (n=5)	<i>28 dpi</i> (n=8–9)
50 kdyn vs. 75 kdyn	**	0.99	0.29	0.25	0.18
50 kdyn 20 sec vs. 75 kdyn 20 sec	****	0.52	0.74	****	**
50 kdyn vs. 50 kdyn 20 sec	****	0.90	0.07	0.16	****
75 kdyn vs. 75 kdyn 20 sec	****	0.58	0.60	***	****

*, **, ***, **** $p < 0.05, 0.01, 0.001, 0.0001$.

Table 5.4.2: Statistical summary (p values) for 28dpi rostral-caudal tissue sparing

<i>Groups (n)</i>	<i>Main</i>	<i>Rostral (mm)</i>			<i>Epicenter</i> <i>0</i>	<i>Caudal (mm)</i>		
		<i>1</i>	<i>0.5</i>	<i>0.2</i>		<i>0.2</i>	<i>0.5</i>	<i>1</i>
50 kdyn (<i>n</i> =8) vs. 75 kdyn (<i>n</i> =9)	0.28	>0.99	0.99	0.97	0.46	0.84	0.97	>0.99
50 kdyn 20 sec (<i>n</i> =8) vs. 75 kdyn 20 sec (<i>n</i> =9)	***	0.16	****	*	0.72	**	***	0.63
50 kdyn (<i>n</i> =8) vs. 50 kdyn 20 sec (<i>n</i> =8)	**	>0.99	0.78	0.08	**	0.07	0.48	>0.99
75 kdyn (<i>n</i> =9) vs. 75 kdyn 20 sec (<i>n</i> =9)	****	0.10	****	****	**	****	****	0.65

*, **, ***, **** $p < 0.05, 0.01, 0.001, 0.0001$.

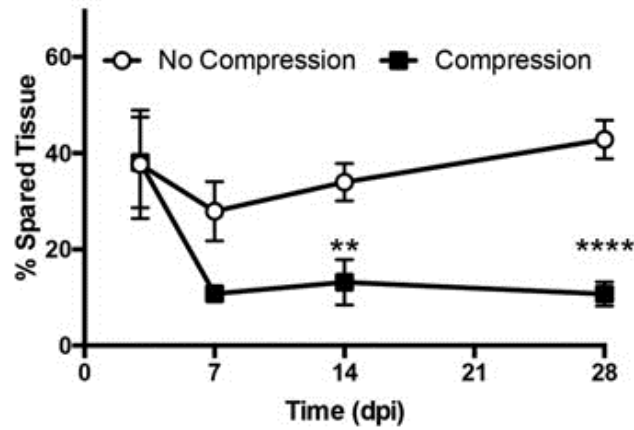
A**Anatomical Recovery**

Figure 5.4.2: Compression decreases anatomical recovery regardless of severity.

Both 50 and 75 kdyn SCI contusion groups were collapsed and the effect of 20sec of sustained compression was compared between aggregate groups. Frank tissue pathology at the lesion epicenter, determined by myelin (EC) and axon (NF-H) stains, is significantly worse with compression at 14 and 28dpi. ** $p < 0.01$, **** $p < 0.0001$.

5.5 Sustained Compression Alters Inflammatory Response to Spinal Cord Injury

We began to observe significant compression-mediated differences in tissue sparing and functional recovery at 7dpi with a clear plateau by 14dpi. These time points coincide with the peak of SCI macrophage infiltration and subsequent predominance of proinflammatory activation^{107,129}. The inflammatory response at these time points is dominated by infiltrating, hematogeneous macrophages and resident microglia. Once activated, macrophage and microglia adopt amoeboid morphologies and upregulate specific protein expression profiles. Macrophages and microglia are nearly indistinguishable from one another, but both cell types adopt a spectrum of activation states characterized by gene and protein expression profiles that indicate their propensity to promote tissue recovery or exacerbate tissue pathology^{2,301}. These phenotypes are dynamically controlled by microenvironmental cues. Therefore, we investigated the effects of compression and injury severity on macrophage/microglia polarization 7 and 14dpi.

We used previously described histological markers to evaluate macrophage polarization within the lesioned spinal cord. Macrophages and microglia were assessed for hallmarks of alternatively activated, reparative phenotypes and classically activated, cytotoxic phenotypes. Each of these markers are analyzed on cells labeled with Tomato Lectin (TomL) staining. Lectins are carbohydrate-binding proteins that can be conjugated to biotin or fluorescent components to visualize carbohydrate-expressing cells. Tomato lectin is a well-known product of *Lycopersicon esculentum*, which binds to carbohydrates on macrophages and microglia³⁰². Therefore, we captured a snapshot of the macrophage/microglia inflammatory response at specific timepoints with TomL, and then assessed these inflammatory cells for hallmarks of their activation state and phenotype.

Alternatively activated, reparative macrophages and microglia express mannose receptor (CD206) and Arginase 1 (Arg1)¹¹⁴. CD206 is a lectin that recognizes terminal mannose and facilitates phagocytosis for antigen presentation and evaluation of potential pathogens. CD206 performs anti-inflammatory functions indirectly by clearing glycoprotein stimuli and directly by altering cytokine production^{303,304}. Arginase 1 is an enzyme responsible for converting L-arginine to ornithine and urea in the final step of the urea cycle. Arginase has been proposed to facilitate anti-inflammatory effects via several mechanisms. One potential mechanism is Arg1 inhibition of oxidative damage through substrate competition with nitric oxide synthase. Arginase consumption of L-arginine is associated with a decreased production of the potent oxidative molecule, nitric oxide, in various contexts, including SCI^{305,306}. Alternatively, Arg may achieve anti-inflammatory effects through affecting autophagy. Immunosuppression elicited by Arg administration mimics chemical inhibition of autophagy³⁰⁷. Both CD206 and Arg1 have been found to be upregulated in alternatively activated macrophages and microglia *in vitro* and *in vivo*, and these cells are associated with pro-growth and reparative functions in many contexts, including SCI^{107,144}.

Classically activated, cytotoxic macrophages and microglia express CD86 and macrophage receptor with collagenous structure (MARCO)³⁰⁸. CD86 performs antigen presentation to adaptive immune cells, and is a costimulatory protein (acting with CD80) responsible for T-cell activation and survival. Upon stimulation, CD86 signals through NF- κ B to cause production of pro-inflammatory cytokines^{309,310}. MARCO is a class A scavenger receptor that assists in the phagocytosis of a wide variety of particles and promotes production of proinflammatory cytokines mediated through TLR2

signaling^{311,312}. The binding properties of MARCO enable this cell surface receptor to recognize pathogen- and damage-associated molecular patterns with polyanionic properties. Specifically, MARCO can recognize lipopolysaccharides, nucleic acids, and modified lipids³¹³⁻³¹⁵, and the loss of macrophage-specific MARCO expression leads to accumulation of oxidized lipids in lung models of oxidant inhalation³¹⁶. Representative images show spinal macrophages/microglia expressing these hallmarks of cytotoxic (Figure 5.5.1A,B) and reparative (Figure 5.5.1C,D) phenotypes.

For immunohistochemical analyses of macrophage/microglia phenotypes, sections were incubated with goat anti-CD206 (1:100 dilution, AF2535, R&D Systems, Minneapolis, MN), goat anti-Arg1 (1:100, SC-18354, Santa Cruz Biotechnology, Dallas, TX), rat anti-CD86 (1:100, 553689, BD Biosciences, San Jose, CA), or rat anti- MARCO (1:1000, MCA1849, BioRad, Hercules, CA). Slides were incubated with these primary antibodies overnight at 4°C in 0.1M PBS with 5% normal donkey serum, 0.1% fish gelatin (Sigma- Aldrich, G7765), 1% BSA and 0.1% Triton X-100. Sections were subsequently incubated with a biotinylated tomato lectin (1:1000, L0651; Sigma-Aldrich, St. Louis, MO) to counterstain for total macrophage numbers. Detection of primary antibodies was performed with donkey anti-rat Alexa Fluor (AF) 488, donkey anti-goat AF 568, and streptavidin AF 647 (all secondaries at 1:1000 dilution, Life Technologies, Carlsbad, CA) for 1 hr at room temperature. To validate antibody staining, negative controls were run without primary antibody, and full dilution curves were analyzed.

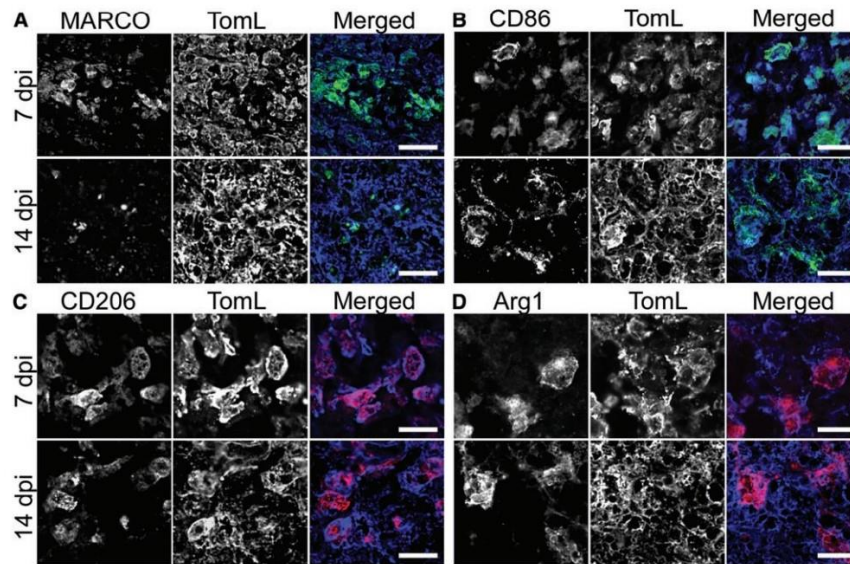


Figure 5.5.1: Representative images of macrophage/microglia phenotypic markers for histological analysis 7dpi and 14dpi.

All images are collected from the epicenter of the spinal cord injury of animals in the 50 kdyn 20 sec group. (A) Macrophage receptor with collagenous structure (MARCO; panel 1 and panel 3, green) and tomato lectin (TomL; panel 2 and panel 3, blue) positive cells at 7dpi (top panels) compared with fractured, noncellular MARCO staining at 14dpi (bottom panels). (B) CD86 (green) and TomL (blue) positive cells observed at 7 and 14 dpi. (C) CD206 (red) and TomL (blue) positive cells observed at 7 and 14 dpi. (D) Arginase 1 (Arg-1; red) and TomL (blue) positive cells observed at 7 and 14dpi. Scale bars = 20mm.

Macrophage/microglia images were collected using an Axioplan 2 imaging microscope (Carl Zeiss) at 20x magnification, and were analyzed via MetaMorph. We collected three or four images per subject within the lesion epicenter, as visualized in Figure 5.5.2A. Injury epicenter section selection was accomplished by evaluating serial sections from EC/NF staining to identify the section with the least proportional spared tissue. Macrophage phenotypic marker (Arg1, CD206, MARCO, and CD86) expression was evaluated via threshold-based positive staining within each of these images from the injury epicenter. The total area of positive signal for macrophage markers was then normalized to total TomL-positive area for each image to determine proportion of positive macrophages within the lesion. Although lesion size varied across groups, we observed a similar macrophage density within the lesion epicenter in all injury groups at both time points (Figure 5.5.2A and Figure 5.5.3A; $p > 0.4$ main effect injury, $n = 3-5$ per group).

At 7 dpi, there was no effect of force or compression on the percentage of macrophages positive for protective markers, CD206 ($p = 0.4$ and 0.6 , main effect of force and compression, respectively) and Arg1 ($p = 0.7$ and 0.5 , main effect of force and compression, respectively) (Figure 5.5.2B,C). Similarly, macrophages positive for the proinflammatory marker, CD86, are present at comparable levels with a force-dependent trend toward increased expression after 50 kdyn injuries ($p = 0.1$ and 0.5 , main effect of force and compression, respectively, Figure 5.5.2D,E). We observed a significant difference, however, in the percent of macrophage positive for MARCO (Figure 5.5.2E,F) with compression at the time of contusion increasing the proportion of MARCO+ cells twofold to threefold compared with contusion alone (50 kdyn 20 sec = 10.3% and 75 kdyn

20 sec = 14.0% vs. 50 kdyn = 2.4% and 75 kdyn = 3.6%; main effect of compression $p = 0.02$, main effect of force $p = 0.5$).

At 14 dpi, we observed that compression at the time of contusion decreased the proportion of Arg1+ macrophages one and one half to twofold compared with contusion alone (50 kdyn 20 sec = 13.0% and 75 kdyn 20 sec = 17.8% vs. 50 kdyn = 23.8% and 75 kdyn = 29.05%; main effect of compression $p = 0.04$, main effect of force, $p = 0.4$) (Figure 5.5.3B,C). We observed no effect of injury type on the percentage of macrophages positive for CD206 ($p = 0.3$ and $p = 0.5$, main effect force and compression, respectively; Figure 5.5.3D) or CD86 ($p = 0.3$ and $p = 0.3$; main effect force and compression, respectively; Figure 5.5.3E). In addition, whereas MARCO staining was observed on the cell surface of macrophages cells at 7 dpi (Figure 5.5.2E), by 14 dpi, MARCO displayed fractured staining with no definitive localization in all treatment samples. Thus, we did not observe any MARCO+/TomL+ cells at 14 dpi.

We collapsed groups across both contusion injury severities (50 kdyn and 75 kdyn) to perform comparisons in groups injured with vs. without sustained compression. When performing this analysis, we uncover that residual compression, regardless of contusion severity, significantly alters markers of macrophage/microglia phenotype. Compression significantly increased MARCO expression 7dpi (Figure 5.5.4A) and significantly decreased Arg1 expression 14dpi (Figure 5.5.4B). Collectively, these data show that compression alters the inflammatory profile of macrophages/microglia in the injured spinal cord.

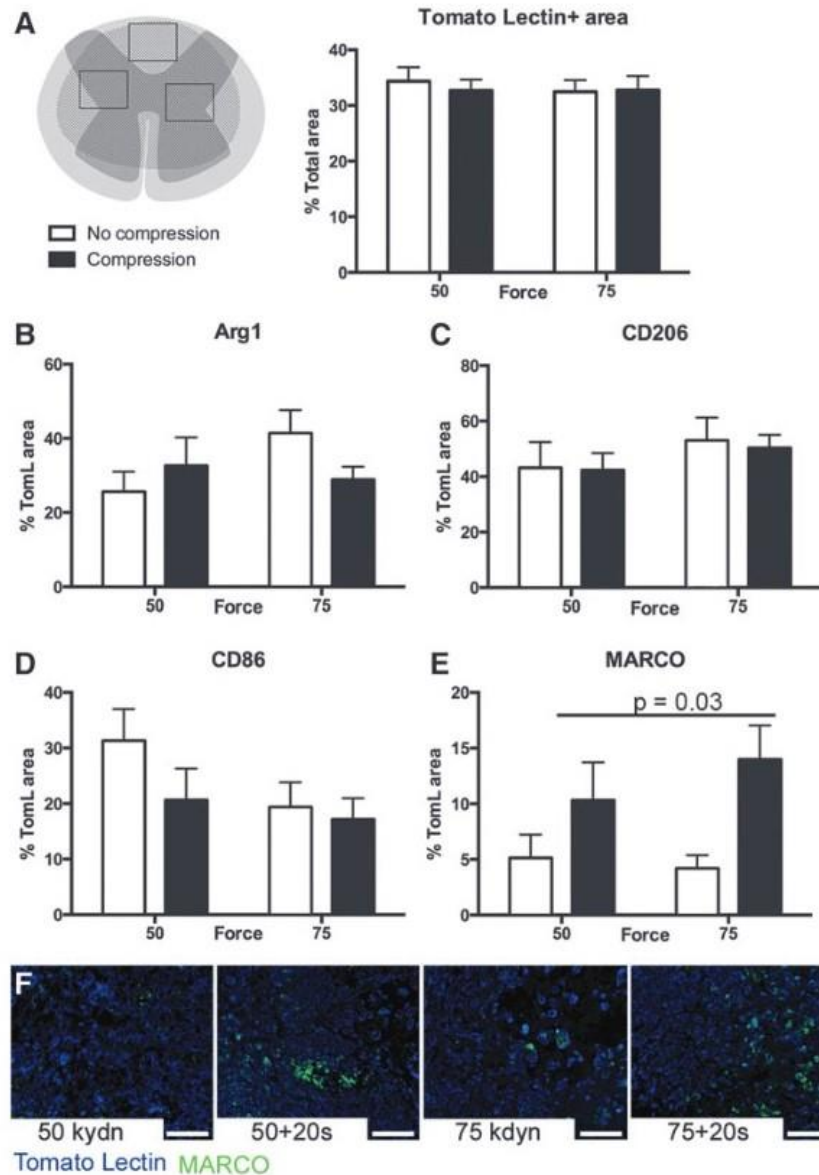


Figure 5.5.2: Compression alters spinal cord injury macrophage activation at 7 dpi.

A) Three regions of interest (dorsal, left, and right) within the lesion epicenter of each animal were analyzed at 7 dpi for macrophage (TomL) density. The TomL+ area was similar across the four injury paradigms: 50 kdyn, 75 kdyn without compression (open bars) and 50 kdyn, 75 kdyn with compression (black bars). (B) Percent of TomL+ cells positive for Arg1 across treatments. (C) Percent of TomL+ cells positive for CD206 across treatments. (D) Percent of TomL+ cells positive for CD86, and (E) percent of TomL+ cells positive for MARCO ($p=0.03$ main effect of compression). (F) Representative images for analysis of TomL+ (blue)/MARCO+ (green) cells across treatments. Scale bar = 50 μ m; $n=3-4$ per group; error bars = SEM.

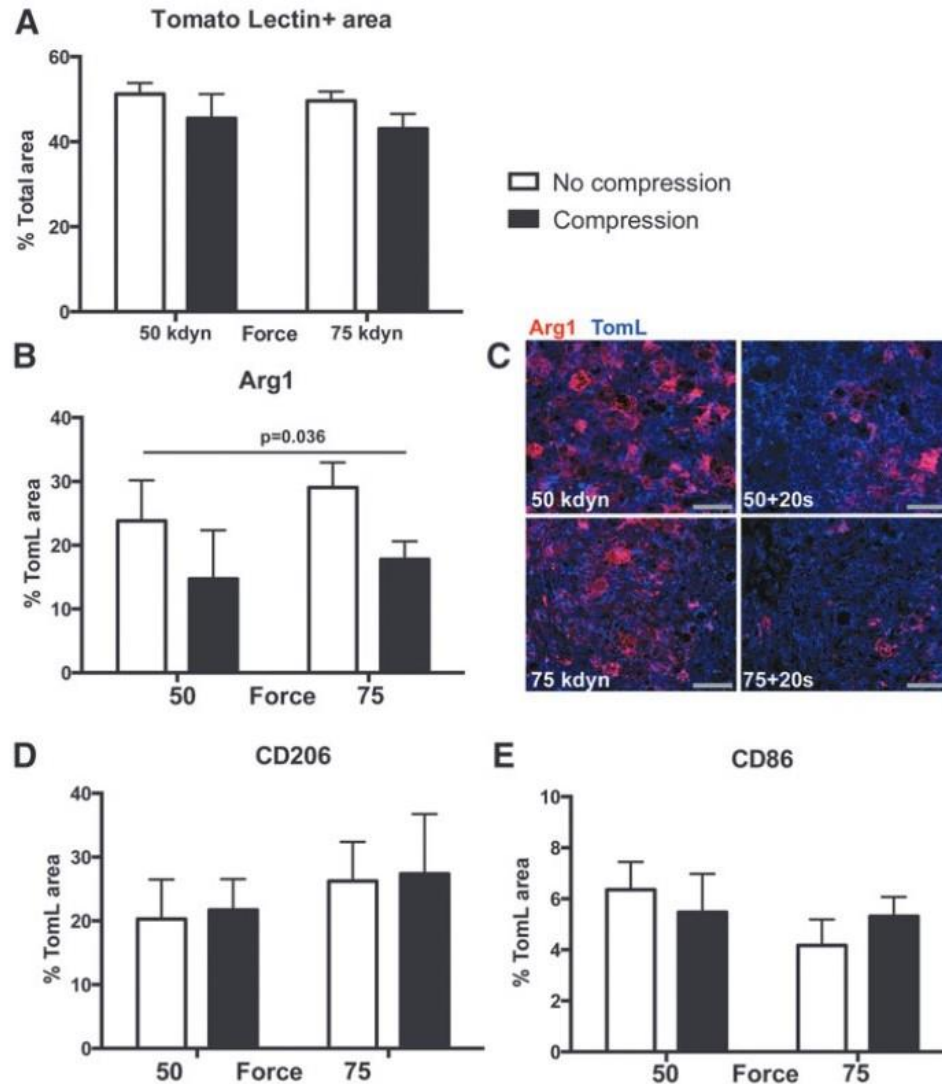


Figure 5.5.3: Compression alters macrophage/microglia phenotypes 14 dpi.

A) Four regions of interest within the lesion epicenter of each animal (as depicted in Figure 7.6A and ventral) were analyzed at 14 dpi for TomL+ density. The TomL+ area was comparable across all four injuries: 50 kdyn, 75 kdyn without compression (open bars) and 50 kdyn, 75 kdyn with compression (black bars). (B) Percent of TomL+ cells positive for Arg1 across treatments (p=0.036 main effect compression). (C) Representative images for analysis of tomato lectin+(blue)/Arg1+(red) cells across treatments. Scale bar=50µm. (D) Percent of TomL+ cells positive for CD206, and (E) percent of TomL+ cells positive for CD86. n=5, error bars=standard error of the mean.

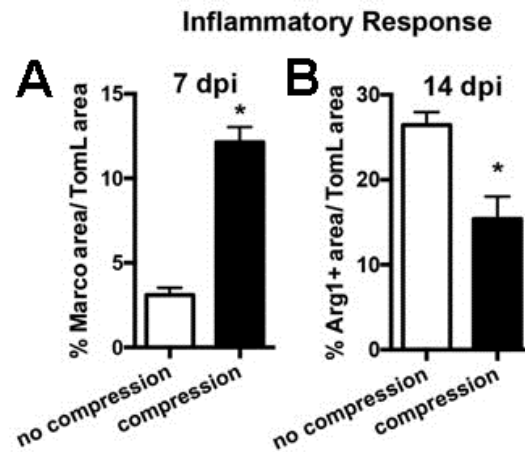


Figure 5.5.4: Macrophage/microglia phenotypes are specifically regulated by compression independent of contusion severity.

Both 50 and 75 kdyn spinal cord injury contusion groups were collapsed, and the effect of 20s of sustained compression was compared between aggregate groups. (A) Tomato lectin (TomL)+ macrophages in spinal cords injured with compression show increased MARCO expression 7 dpi (A) and decrease Arg1 expression 14 dpi (B) compared to spinal cords injured without sustained compression. * $p < 0.05$

Neuroinflammation plays a major role in orchestrating secondary injury mechanisms¹⁰⁹. Specifically, macrophage activation is dictated, in part, by the microenvironment, and macrophages can adopt proinflammatory, neurotoxic phenotypes or purportedly reparative phenotypes depending on the stimuli present in the injured spinal cord¹⁰⁸. A novel observation in the current study is that the proportion of macrophage phenotypes shift to displaying more pathological and less reparative markers after contusion-compression SCI than after contusion-alone injuries. It is important to note that we normalized to the overall magnitude of the macrophage response, thereby concluding that biomechanics, and not injury sizes are likely driving this unique macrophage profile.

In support of this idea, it was previously observed that the extent of macrophage/microglia activation after SCI varied across contusion, dislocation, and distraction injuries³¹. Differences have also been observed in the immune system response to brain injury versus SCI³¹⁷. Indeed, while both central nervous system organs are extremely similar, subtle differences in blood barriers and resident glial cells can lead to robust differences in immune cell activity and distribution^{148,301}. In addition, Zhang and colleagues²⁹⁹ show microenvironment-specific differences in toll-like receptor 4 (TLR4) expression on activated macrophages after compression SCI. TLR4 is important for lipopolysaccharide-mediated proinflammatory macrophage activation, and that article demonstrated that even within the same organ with the same injury, microenvironmental conditions significantly impact proinflammatory responses.

It is also important to consider that although microglia and monocyte-derived macrophages express similar histological markers of myeloid cells, they are distinct populations and may play distinct roles in SCI pathophysiology. We observed

compression-specific changes in MARCO and Arg1. Interestingly, both phenotypic markers are predominantly expressed in monocyte-derived macrophages. Specifically, using a transgenic model to label infiltrating cells, Greenhalgh and colleagues¹³² detected Arg1 exclusively on monocyte-derived macrophages after contusion SCI.

Targeting MARCO reduces monocyte trafficking in models of myocardial infarction, experimental autoimmune encephalomyelitis, colitis, peritonitis, and encephalitis³¹⁸. Therefore, MARCO may be a hallmark for proinflammatory monocytes. Indeed, in the current study we focused our analyses on the lesion core, an area predominantly populated by monocyte-derived macrophages after contusion SCI¹³¹. Collectively, our observations suggest that compression polarizes monocyte-derived macrophages toward a proinflammatory phenotype. It is also possible the compression alters the distribution of microglia after injury or upregulates markers in microglia not normally expressed after contusion SCI. Further studies are warranted to parse out the specific contribution of injury biomechanics to environmental and chemotactic cues for macrophages and microglia independently.

In the current study, we detected a compression-specific increase in the proportion of macrophages expressing MARCO. This finding is especially interesting when considering the role of MARCO as a scavenger receptor that binds DAMPs, including oxidized targets^{314,319}. SCI biomechanics influence microenvironmental factors such as 3-NT, cytochrome c, and membrane permeability^{31,288}. Compression specifically adds a component of reperfusion and hemorrhage that alters fluid dynamics^{290,320}. Collectively, these published data and the increased MARCO+ macrophages observed with compression in the current study, suggest that macrophages may be specifically upregulating receptors

to bind to the specific type of damage caused by reperfusion, excessive oxidants, and oxidized lipids in contusion-compression SCI.

The shift in MARCO and Arg1 macrophages not only reflects differences in the microenvironment after a compression-contusion injury, but also is a likely player in secondary pathology. MARCO is specifically expressed by proinflammatory, neurotoxic macrophages³⁰⁸ and is integral in the uptake of immune-modifying microparticles, which subsequently inhibits trafficking of pathological macrophages³¹⁸. Our lab previously observed an age-dependent decrease in recovery and increase in tissue pathology coincident with decreased Arg1 expression in macrophages/microglia³²¹. Whether MARCO and Arg1 alone or a large repertoire of proteins are affected by the compression microenvironment, these secondary responses are likely critical to overall outcomes of SCI, and thus are important targets for therapeutic intervention.

The heterogeneous nature of human SCI creates a challenge for recapitulation in controlled experimental models. Resolving SCI into its composite parts has provided valuable insight, but extrapolating findings from oversimplified injury paradigms risks erroneous inductive generalizations. The model employed in this study provides valuable information about the interaction of biomechanics common to clinical SCI. It shows that compression affects overall outcomes of SCI and specifically alters at least one secondary injury response. These results simply introduce additional questions as to how contusion, compression, and other injury biomechanics affect other secondary responses to injury. Developing a deeper understanding of how specific injury biomechanics affect specific injury responses will help us develop and implement more effective therapies for SCI.

CHAPTER 6. CONCLUSIONS ON TARGETING SECONDARY INJURY RESPONSES TO IMPROVE RECOVERY FROM SPINAL CORD INJURY

Many factors that can influence the progression SCI pathology and repair. Chapters 2-5 describe novel mammalian models of SCI I employed to better understand the role of secondary injury responders—particularly spinal inflammation and scarring—with the intent of informing future therapeutic development. Considering these studies together provides interesting perspectives on how to effectively facilitate endogenous repair in the mammalian spinal cord. Here, I will discuss insights gained from my graduate studies, and how these insights may contribute to SCI therapeutic development.

6.1 Crosstalk between macrophages and fibroblasts in injury responses

Proper wound healing involves concerted responses of many different cell types, including inflammatory cells and fibroblasts. Inflammatory cells and fibroblasts enter into the injury site and begin secreting a suite of growth factors and cytokines, which exert autocrine and paracrine effects that are highly influential on the inflammatory and fibrotic profile³²². In typical peripheral wound healing, this cellular response orchestrates proper progression through inflammatory, proliferative, and remodeling phases of tissue repair^{144,323,324}. However, these responses are dysregulated in SCI and result in a persistent inflammation and a fibrotic scar¹⁰⁷. Many lines of evidence point toward crosstalk between macrophages and fibroblasts as a lynchpin for proper wound healing progression³²⁵.

The phenotypic profiles of macrophages and fibroblasts, particularly their secreted factors, are highly influential on the progression and degree of wound healing. Macrophage-derived interleukins are known to play a key role in fibroblast recruitment and macrophage-derived tumor necrosis factor α (TNF α) triggers collagen synthesis³²².

Similarly, fibroblasts can recruit macrophages through secretion of interleukins and other chemokines, while simultaneously affecting fibroblast and macrophage phenotype through factors such as transforming growth factor β (TGF β)^{322,326,327}. The cytokines are not solely deleterious. Persistent high levels of pro-inflammatory cytokines leads to poor recovery and chronic wounds³²⁸, but proper cytokine signaling is necessary to facilitate repair¹⁴⁰. Furthermore, these macrophages and fibroblasts also produce growth factors, including PDGF, which are necessary for wound healing³²⁹. Macrophages and fibroblasts exist in a delicate balance to facilitate repair, but can easily slip into a vicious cycle that self-sustaining inflammatory damage. Perhaps this vicious cycle is a main driver in the increased pro-inflammatory and decreased pro-reparative macrophage profile we see in the contusion-compression injuries vs. contusion-alone.

Studies in models of regeneration show that macrophages are necessary to facilitate wound repair at least partially through their effects on fibroblasts. Godwin and colleagues show that early depletion of macrophages in axolotl limb amputation inhibits the normal limb regeneration. Furthermore, the macrophage-depleted injury site features a significant increase in pro-inflammatory cytokines, myofibroblasts, and collagen deposition, suggesting that the macrophages regulate both inflammation and fibrosis after injury¹⁵². In a similar series of experiments, Godwin and colleagues show that macrophage depletion also impairs axolotl regeneration from cryo-injury of the heart. The macrophage-depleted axolotl heart also has a robust increase in myofibroblasts and collagens, as well as lower levels of growth factors that aid heart regeneration¹⁵¹. These non-mammalian results have been replicated in the neonatal *Mus*, where macrophage depletion inhibits heart regeneration and results in the formation of a robust fibrotic scar¹⁵⁰. Furthermore,

macrophage depletion inhibits *Acomys* ear regeneration³⁸. The exact nature of macrophage and fibroblast crosstalk is an area of active investigation, and understanding the context of this interplay is incredibly important. For instance, Zhu and colleagues show that macrophage depletion in mouse SCI leads to fewer genetically labelled (Coll α 1+) fibroblasts in the spinal cord 1 and 2wpi¹⁶⁷. This phenomena is more in line with trends seen in *Acomys*, where there are fewer macrophages/microglia *and* fewer cells expressing fibroblast markers at subacute time points. This suggests that macrophage-fibroblast interactions are likely unique in the *Acomys* spinal cord, and merit further study to understand how they contribute to enhanced recovery from SCI.

In addition to the general organ environment, macrophage and fibroblast crosstalk may also be influenced by local ECM. Fibroblasts are key players in establishing the ECM microenvironment, which has subsequent effects on cellular dynamics, particularly those of the highly responsive macrophage. For instance, periostin induces macrophage migration and expression of TNF- α in a mouse model of SCI²⁷¹. These ECM-induced changes in macrophage phenotype are thought to be primarily mediated by integrin receptors, which can induce macrophage chemotaxis¹¹⁹, reactive oxygen species production¹¹⁷, and cytokine production³³⁰ after SCI. Preclinical efforts have reduced early inflammation and improved recovery from SCI by acute inhibiting integrin binding using monoclonal antibodies^{117,119,149}. Specific ECM components do have specific integrin counterparts³³¹. For instance, stimulating α 9 β 1 integrin binding improves DRG axon growth over Tenascin-C³³². On the other hand, fibroblast-produced fibronectin binds α 5 β 1 integrins on macrophages and fibroblasts in the injured cord, and may provide an opportunity to limit cellular infiltration²⁰².

Macrophages and fibroblasts also collaborate in the remodeling of the ECM microenvironment through release of proteolytic enzymes, such as matrix metalloproteinases (MMPs)³³³, and tissue inhibitors of these proteases (TIMPs)³²². While macrophages/microglia are identified as the major source of MMPs and TIMPs in the injured spinal cord, fibroblasts are also known to release a wide variety of MMPs that can cleave and rearrange various ECM constituents³³³. MMP release by either cell type can affect cell migration through the dense meshwork of ECM, including axon growth and revascularization^{199,334,335}. Furthermore, the effects of proteolytic enzymes affect ECM stiffness, which is a key determinant for fibroblast proliferation^{192,336} and ECM deposition profile³³⁷. Interestingly, *Acomys* produce significantly more MMPs than *Mus* in skin¹⁶⁴ and ear³⁴ injuries. Extracellular matrix remodeling may therefore be another mediator of divergent inflammatory and fibrotic responses to SCI in *Acomys*.

The collective evidence suggests that macrophages and fibroblasts coexist in injury responses, and that their crosstalk dynamically influences self- and cross-regulation. For example, fibroblasts are instrumental in establishing the ECM microenvironment, including the deposition of periostin³³⁸, which causes macrophages to produce more TNF- α , which in turn promotes proliferation of ECM-producing pericytes²⁷¹. Misbalance of macrophage and fibroblast interactions may inhibit proper progression through wound healing, leading to improper tissue repair and the establishment of chronic fibrotic scar and inflammation^{2,107}. The microenvironmental context during spinal cord injury leads to a vicious cycle^{2,107}. One of the few studies investigating macrophage-fibroblast interactions in SCI suggests that disrupting the interaction between these two cell types can decrease inflammation and scarring while increasing axon growth¹⁶⁷. My investigations into *Acomys*

SCI show that enhanced functional recovery is associated with a dampened inflammatory and fibrotic response to injury. Future studies to more deeply understand the cross-talk between these two injury responses could identify if one or both of the cell types are driving the dampened response. Understanding this phenomenon in a naturally occurring system of enhanced recovery provides an excellent opportunity to illuminate a path for inducing endogenous spinal repair after injury.

6.2 Role of PDGFR β in tissue damage and repair

An important regulator of wound healing responses is platelet-derived growth factor (PDGF) and its receptor (PDGFR). This growth factor has long been recognized for its importance to wound healing. Healing-impaired diabetic and glucocorticoid-treated mice have lower expression of PDGFs and PDGFRs^{329,339}, and a delayed appearance of PDGF and PDGFRs in age is associated with impaired wound healing³⁴⁰. Furthermore, it likely sits at the intersection of macrophage and fibroblast responses to injury. Studies of pulmonary fibrosis have shown that alveolar macrophages produce PDGF, the majority of which is PDGF-B, that acts on pulmonary fibroblasts and contributes to fibrotic deposition^{276,341,342}. These examples effectively reflect our understanding of PDGF and PDGFR in wound repair: they are necessary to facilitate proper wound healing, but can lead to improper repair (e.g. fibrosis) when overexpressed.

Some suggest replacing damaged tissues in the injured cord with newly proliferated cells would be advantageous compared to the absence of cells in spinal cysts^{88,248}. However, evidence from our study and a study in neonatal opossums¹⁰⁵ shows that the formation of fluid-filled cysts does not necessarily preclude robust functional recovery. PDGF and PDGFR are important for the migration and proliferation of cells in the injured

cord, and several studies, including mine, show that PDGFR β is robustly expressed in the chronic SCI core where there is inflammation and fibrotic scarring^{20,263}. Targeting PDGFR, and PDGFR β in particular, may provide a powerful tool for decreasing inflammatory and fibrotic cell infiltration and proliferation in the injured cord.

Directly targeting PDGFRs has led to improved recovery from CNS trauma. In a mouse model of seizure, the fibrotic scar is associated with PDGFR β and can be activated by the PDGFR β agonist PDGF-BB and inhibited by the PDGFR β antagonist, imatinib³⁴³. Indeed, the tyrosine kinase inhibitor, imatinib, has also shown benefits in rodent models of traumatic brain injury (TBI) and SCI. Administration of imatinib for the first 5 days after TBI and SCI improves functional recovery, likely by reducing BBB and BSCB breakdown and reducing inflammation³⁴⁴⁻³⁴⁶. These results have even led to a phase 2 clinical trial in SCI (NCT02363361). However, it is important to note that an independent lab failed to reproduce improvements in SCI with imatinib administration³⁴⁷.

An important consideration is the timing of imatinib administration. Dosing for the first 5 days after injury is expected to inhibit early inflammation, as reported by tracking inflammatory biomarkers³⁴⁴, and vascular dynamics. Indeed, while some reports indicate decreased hemorrhage by tyrosine kinase inhibition with imatinib³⁴⁶, other studies identify an important role for PDGFR β , in particular, in limiting hemorrhage²⁷⁵. Shen and colleagues show that PDGFR β is protective in mouse middle cerebral artery occlusion because PDGFR β knockout mice have delayed recovery and more hemorrhage after injury²⁷⁵. Histological investigations show that PDGFR β knockout mice have significantly fewer myofibroblasts and significantly less astrocytic scar density than wildtype mice after ischemic brain injury²⁷⁵. These results are in line with the general theme that vascular

stability and astrocytic scarring helps protect from the spread of CNS injury^{11,182}, and identify an important role for PDGFR β in those beneficial injury responses. However, the lack of a fibrotic scar formation in this injury model²⁷⁵ begs the question whether PDGFR β and PDGFR β -expressing cells are protective in injuries that do evoke a robust fibrotic response, like TBI and SCI.

Alternatively, it may be possible to indirectly target PDGFR β ⁺ cells in the injured cord. Hesp and colleagues show that genetic inhibition of NG2⁺ pericytes leads to decreased PDGFR β ⁺ staining, increased axon growth, and improved locomotor function after mouse cervical hemicontusion SCI²⁶³. These results are somewhat distinct from results in *Acomys* presented in chapters 2 and 4, where *Acomys* show a decrease in PDGFR β ⁺ density and an improvement in locomotor function, but no notable increase in axon growth. Hesp and colleagues suggest that the genetic inhibition of NG2⁺ cell proliferation acts on axon growth and fibrotic scarring independently through effects on NG2⁺ glia and NG2⁺ pericytes, respectively. They hypothesize that inhibiting NG2⁺ glia proliferation disrupts the glial scar formation over the first 11 dpi and allows enhanced axon growth, while inhibiting NG2⁺ pericyte proliferation prevents angiogenesis that deprives a physical substrate for PDGFR β ⁺ fibroblast infiltration into the lesion core²⁶³. According to this hypothesis, inhibited pericyte proliferation could underlie dampened PDGFR β and ECM responses in the injured *Acomys* cord without any robust effects on axon growth. Furthermore, this trend could be specifically driven by NG2⁺ pericytes that are distinct from the PDGFR β ⁺ pool visualized in our studies. This line of reasoning offers an interesting prospect for therapeutic development, but undoubtedly requires further

investigation to better understand underlying NG2+ cell and vascular biology in *Acomys* SCI.

I propose that targeting PDGFR β signaling, either directly or indirectly, at subacute time points would be preferable to early acute administration. Studies of PDGFR β in CNS injury consistently show increased expression in the subacute window as opposed to early acute time points^{19,20,263,265}. The disconnect between imatinib studies across different labs, in particular, may be affected by a small effect size given the smaller potential pool of tyrosine kinase receptors in the injured cord^{347,348}. Furthermore, delaying to a subacute administration would circumvent potential negative effects on vascular stability in the acutely injured cord. Neovascularization has mostly occurred before 1wpi^{147,228}, while the peak of inflammation, fibroblast recruitment to the lesion core, and deposition of ECM in fibrotic scarring occurs after 1wpi^{19,107,167}. Overall, delaying treatment to the subacute window would be preferable to disrupt the vicious cycle of inflammation and fibrosis in the injured cord.

The results of my graduate studies are highly informative for the role of cell expansion in SCI. In my studies, I see a divergence of *Acomys* from *Mus* and non-compression from compression-involving injuries in the subacute phase (1-2wpi) of injury responses. Specifically, macrophages/microglia and PDGFR β + cells in the *Mus* cord are maintained or expand after this 1wpi point, while *Acomys* have a dampened response and improved recovery from SCI. Growth factors, and PDGFR β in particular, are recognized for being highly influential in inflammatory and fibrotic cell migration and proliferation. Future studies are warranted for the cell-to-cell crosstalk in the injured *Acomys* cord, and specifically investigating the role of PDGFR β in this cell-to-cell crosstalk is a reasonable

place to start. Studying this system of enhanced spinal repair will give us a deeper understanding of these injury responses and how they contribute to endogenous repair of the injured cord.

6.3 Hemodynamics and SCI progression

Another potential link between inflammation, fibrosis, and overall outcomes of SCI are hemodynamics in the injured cord. Because of the toxic nature of blood, coagulation is a critical first step in the wound healing process. Release of tissue factors begins a coagulation cascade that leads to the eventual activation of thrombin, which cleaves fibrinogen into its active form of fibrin³⁴⁹. Fibrin quickly polymerizes and serves as a scaffolding for the accumulation of platelets, which degranulate to provide a rich source of cytokines and growth factors, including PDGF²⁷⁶. The dissolution of clots is similarly important for wound healing processes. Plasmin, which is controlled by a wide variety of activators and inhibitors, is the primary enzyme responsible for dissolving clots by cleaving fibrin crosslinks³⁴⁹. Notably, plasmin can have direct influences on inflammatory cells at the injury site³⁵⁰. The delicate balance of coagulation and fibrinolysis plays a major role in wound healing processes.

Hemorrhage, coagulation, and fibrinolysis are particularly important to CNS injuries. The immediate blood-spinal cord-barrier (BSCB) or blood-brain-barrier (BBB) breakdown allows free hemorrhage into CNS, but this bleeding is prolonged during subsequent neovascularization^{64,147}. The toxic nature of dysfunctional hemodynamics is well-recognized in the brain, especially during stroke³⁵¹. Similarly, blood components are toxic, even at low concentrations, to oligodendrocytes, OPCs, neurons, and other spinal constituents^{95,352,353}. The toxicity of blood to oligodendrocytes and OPCs is particularly

poignant given decreased frank myelin pathology in *Acomys*. Iron in the blood also induces a pro-inflammatory state in macrophages³⁵⁴, leading to further exacerbation of CNS tissue damage.

Hemodynamics in the CNS are further complicated by coagulopathy—improper balance of the coagulation and fibrinolysis—which is readily apparent after CNS injury³⁵⁵⁻³⁵⁸. A leading theory for the cause of coagulopathy in CNS injury posits that the CNS is rich in tissue factor, which can overactivate fibrinolysis early after injury³⁵⁹. The early overactivation of fibrinolysis, known as consumptive coagulation, prevents proper clotting initially and consumes enzymes necessary for proper fibrinolysis later in the wound healing process^{358,360,361}. The overall dysregulation of hemodynamics in the injured CNS sets the stage for improper wound healing processes through its direct and indirect effects on cellular facilitators of injury responses.

Hemodynamics are likely to play a role in divergent secondary injury responses seen in *Mus* compression-contusion vs. contusion-only injuries. Previous studies show that compression increases hemorrhage, thus, altering the fluid dynamics of the contused spinal cord^{290,296,353}. Additionally, residual compression alters acute hypoxia and cellular bioenergetics with significantly higher lactate:pyruvate ratios compared to contusion alone, likely due to hemorrhage-induced ischemia²⁹¹. In chapter 5, we observed that residual compression drives a potentially destructive inflammatory response. As late as two weeks after the initial insult, acute residual compression (for 20 seconds) at the time of contusion SCI increased the relative ratio of pathological/pro-inflammatory to purportedly-reparative macrophages/microglia compared to contusion-alone SCI. These subacute phase differences between injury groups imply that some sustainable microenvironmental shift is

induced by compression at the time of injury, and previous studies support the hypothesis that this change may be, at least in part, driven by hemodynamics. Further studies of the effect of hemorrhage after residual compression are warranted to better understand this potential mechanistic driver of macrophage dynamics in the subacute spinal cord.

Notably, we utilized a thoracic spinal crush with a short (1sec) sustained compression in our *Acomys* studies. While the SCI itself mostly shows blood/edema as a bruise in the injured cord, there is some minor bleeding during the procedure while exposing the spinal cord. Interestingly, during our surgeries in *Acomys* our two surgeons independently noted a less bleeding in the *Acomys* compared to *Mus*. Considering the importance of hemodynamics in compression-involving SCI, and the potential link between hemodynamics, inflammation, and fibrosis, I decided to perform a histological analysis of fibrin/fibrinogen, a key component of coagulation and fibrinolysis. After creating a ROI around the entire SCI site and setting threshold values to distinguish positive versus background fluorescent staining, I evaluated the density of fibrin/fibrinogen staining in injured *Mus* and *Acomys* spinal cords. These preliminary results show a trend for more fibrin/fibrinogen in the *Acomys* spinal cord at 3dpi and 7dpi, with a species effect across both timepoints (two-way ANOVA $p < 0.05$). In the typical clotting response, circulating fibrinogen is cleaved by thrombin to create fibrin, which then polymerizes to form a fibrin clot. This fibrin clot is then degraded by plasmin in a process known as fibrinolysis. The increased fibrin/fibrinogen staining in the injured *Acomys* spinal cord may reflect more circulating fibrinogen, more initial fibrin clot formation, or less degradation of established fibrin clots. Follow-up studies are necessary to evaluate which step of the clotting process

this trend reflects, and to evaluate if/how this phenomenon contributes to the hemodynamics of the injured *Acomys* spinal cord.

Gene expression post-SCI in *Acomys* vs. *Mus* also indicates unique clotting control. Streeter et al. show that both *Mus* and *Acomys* increase expression of *Plau*, *Timp1*, and *Serpine1* after injury, but *Mus* increase expression of these genes around 3-fold more than *Acomys*⁶¹. *Plau* encodes a urokinase activator, *Timp* encodes a metallopeptidase inhibitor, and *Serpine1* encodes a plasminogen activator. These three components of the fibrinolysis cascade are analogous to the gas and brakes, providing balancing control of plasmin activation and subsequent breakdown of fibrin clots³⁶². The overproduction of these fibrinolysis-regulating factors potentially represents an out-of-control coagulation cascade that leads to dysfunctional control of hemodynamics and coagulopathy in the *Mus* spinal cord after injury.

Previous studies suggest that there is a tight window for anti-fibrinolytic therapies to elicit positive effects in CNS injury. While acute anti-fibrinolytic therapy with tranexamic acid (TXA) decreases hemorrhage and improves outcomes from CNS injury, delayed treatment results in a loss of efficacy and poor outcomes^{363,364}. Evidence suggests that this loss of efficacy when not administered early is due to early consumption of naturally occurring regulators of plasmin activity³⁶⁵. Cessation of anti-fibrinolytic therapies also needs to be properly timed. Using a genetic knockout or TXA to inhibit fibrinolysis, Shiraishi and colleagues show that short-term inhibition of fibrinolysis limited short-term vascular dysfunction and improved early functional recovery from mouse SCI, but sustained inhibition prevented tissue remodeling and wound healing³⁶⁶. Collectively, evidence suggests that inhibiting early consumption of coagulation-regulating enzymes by

inhibiting early fibrinolysis can improve outcomes of CNS injury, but fibrinolysis must be allowed to proceed at later time points to facilitate clot dissolution and proper wound repair.

Mus and human neurotrauma result in coagulopathy that worsens outcomes from injury, but that *Acomys* respond to SCI with a unique coagulation/fibrinolysis profile. Evidence suggest that *Acomys* may exhibit a more controlled coagulation cascade which decreases bleeding at the time of injury, leads to greater fibrin/fibrinogen clotting at early time points after injury, and requires less coagulation cascade regulators. However, additional studies are necessary to investigate this possibility. These investigations are important to inform future therapeutic development efforts. Indeed, early intervention to stabilize hemodynamics in the injured spinal cord is likely to not only improve acute spinal damage, but also improve subsequent injury responses, particularly inflammation. This avenue of biomedical research is important for therapeutic development, particularly in compression SCI.

6.4 Summary of conclusions

These studies describe novel mammalian models of spinal cord injury that were developed to shed light on the secondary injury responses that shape the progression of spinal damage and repair. *Acomys* were identified as a unique adult mammalian model of enhanced recovery from SCI, and histological and *in vitro* analysis shows that this enhanced recovery is likely facilitated by a dampened inflammatory and fibrotic response that leads to decreased frank tissue pathology in the subacute and chronic windows after injury. A novel compression-contusion injury model also identified that compression at the time of injury dictates a more pro-inflammatory macrophage profile in the subacute window, which leads to decreased functional recovery and increased tissue pathology after

injury. Together, these studies identify the importance of the subacute inflammatory and fibrotic responses in contributing to the overall functional and anatomical outcomes of SCI.

Moving forward, understanding the factors that dictate these injury responses could enable therapeutics that enhance endogenous repair. Early antifibrinolytic therapy may optimize hemodynamics to prevent out-of-control bleeding and inflammatory activation, especially in SCIs that involve compression. Delayed PDGFR β inhibition may decrease cellular migration and proliferation, leading to a dampened inflammatory and fibrotic profile that mimics the *Acomys* spinal cord. Potentially, intervening in both of these processes would be necessary to establish the delicate balance necessary to facilitate proper wound repair.

These studies provide a solid foundation for future investigations using these novel models of SCI, and hopefully pave the way to therapeutic developments that will improve the lives of people living with SCI.

APPENDICES

1 Appendix 1: Supplementary Figures

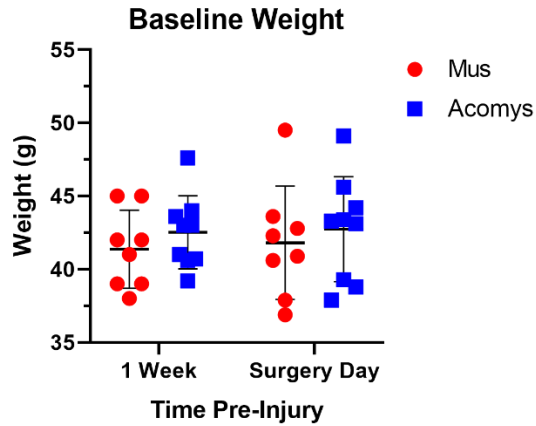


Figure A1.1: *Acomys* and *Mus* had similar and stable body weight before spinal crush surgery.

Animals were weighed before baseline functional measurements (1 week pre-injury) and on the surgery day as a matter of routine animal care. After injury, these animals were part of the cohort used for functional recovery data (chapter 2, section 2.3) and for chronic 12wpi histology (chapters 2, 3, and 4). Two-way ANOVA with Sidak's multiple comparisons test shows no statistical difference in weight by species or by time within each species.

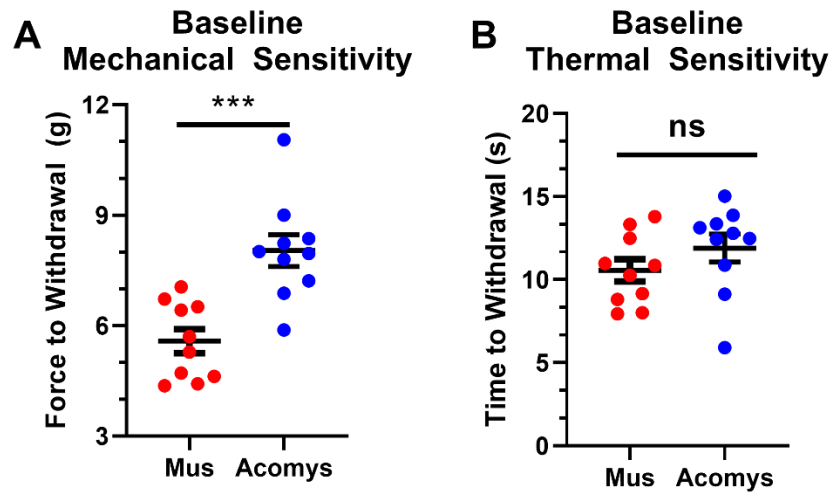


Figure A1.2: *Mus* and *Acomys* baseline sensory sensitivity.

Mechanical sensitivity was measured using an electronic von-frey filament, which measures the amount of pressure applied to the paw before the animal voluntarily withdraws from the stimulus. Thermal sensitivity was measured using Hargreave's test, which measures the amount of time before the animal voluntarily withdraws its paw from an infrared thermal stimulus. A) Greater force stimulus was required to evoke *Acomys* paw withdrawal ($p < 0.001$). B) However, *Mus* and *Acomys* withdrew paws around the same time during graded increases in heat stimulus. These results are typically used to calibrate post-injury returns to a baseline sensitivity, but animals did not reach a level of functional recovery to enable reliable paw withdrawal.

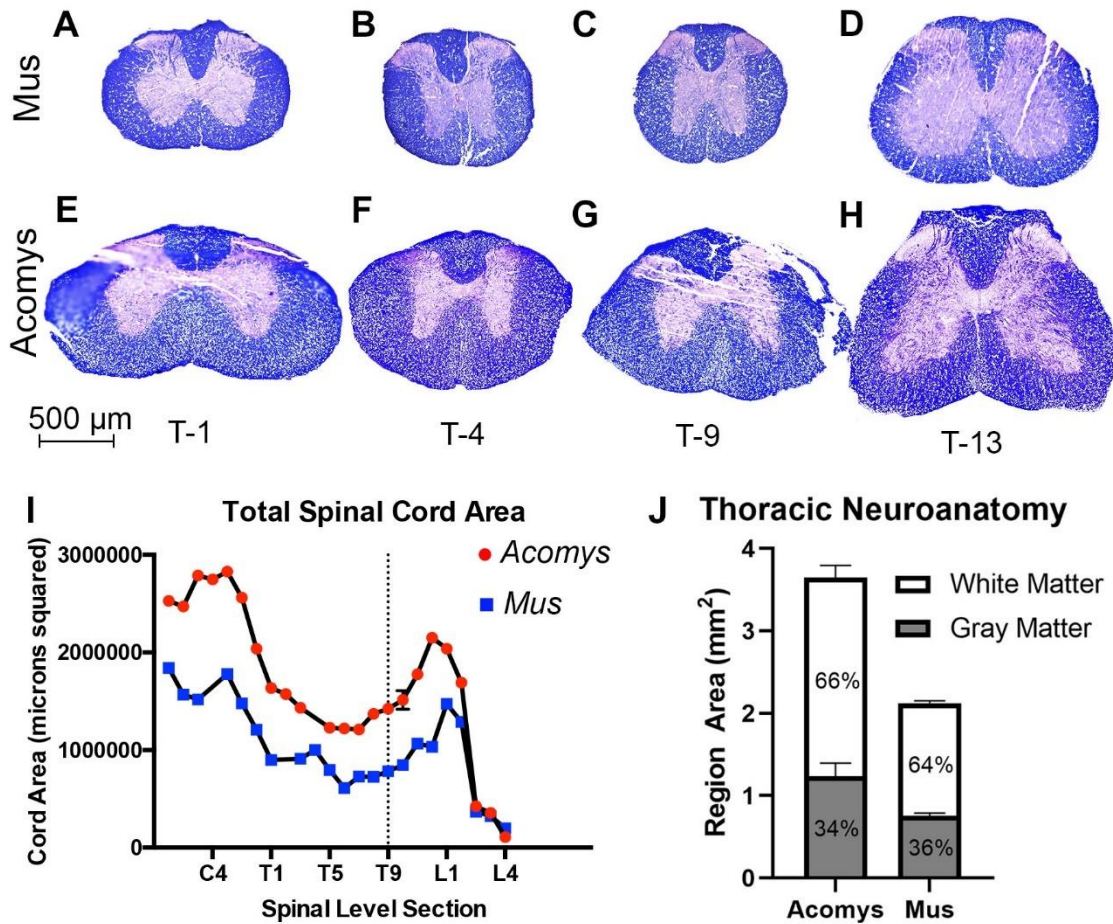


Figure A1.3: Gross neuroanatomy is similar in naïve *Mus* and *Acomys* spinal cord.

The entire spinal column was removed from a *Mus* and *Acomys*. Both *Acomys* and *Mus* had the same number of spinal vertebrae with similar vertebral morphology. These vertebrae were used to categorize the spinal cord into cervical, thoracic, and lumbar sections. Cords were stained for myelin (eriochrome cyanine, blue) and nuclei (fast red, red) to visualize grey and white matter in the *Mus* (A-D) and *Acomys* (E-H) cord. This histological analysis shows qualitatively similar gross neuroanatomy between species, with internal grey matter adopting a structure with apparent dorsal and ventral horns. Quantification shows that both species also have a similar proportion of grey:white matter in the thoracic (T9) cord (J; *Acomys* ~34%, *Mus* ~36%). While *Acomys* have consistently larger spinal cords than *Mus* (I) including at T9 (J), both species have similar patterning of cervical and lumbar enlargements with a smaller thoracic cord (I).

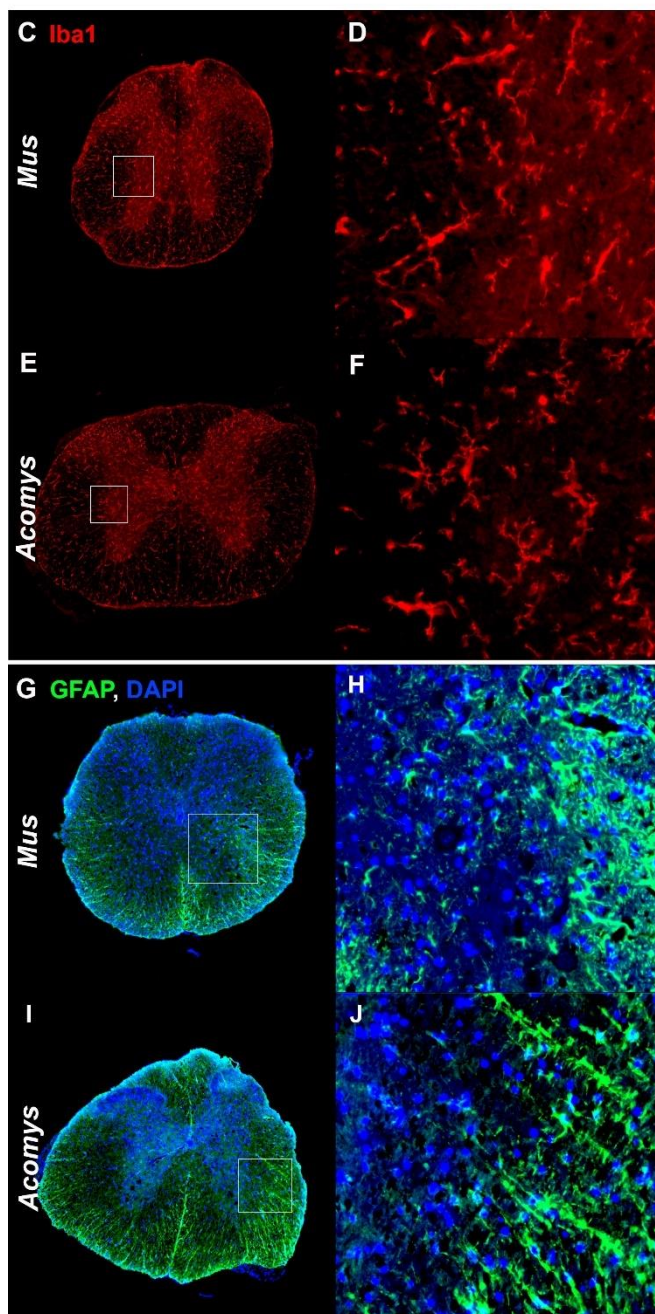
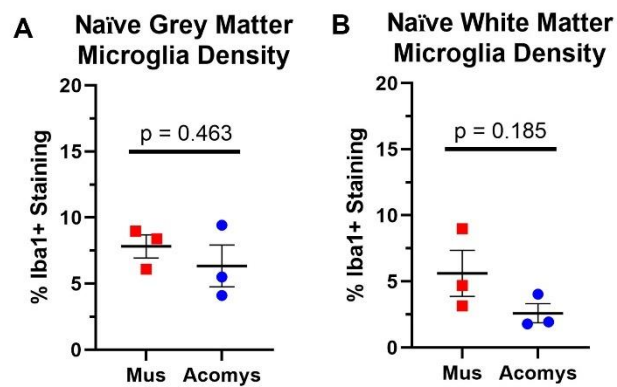
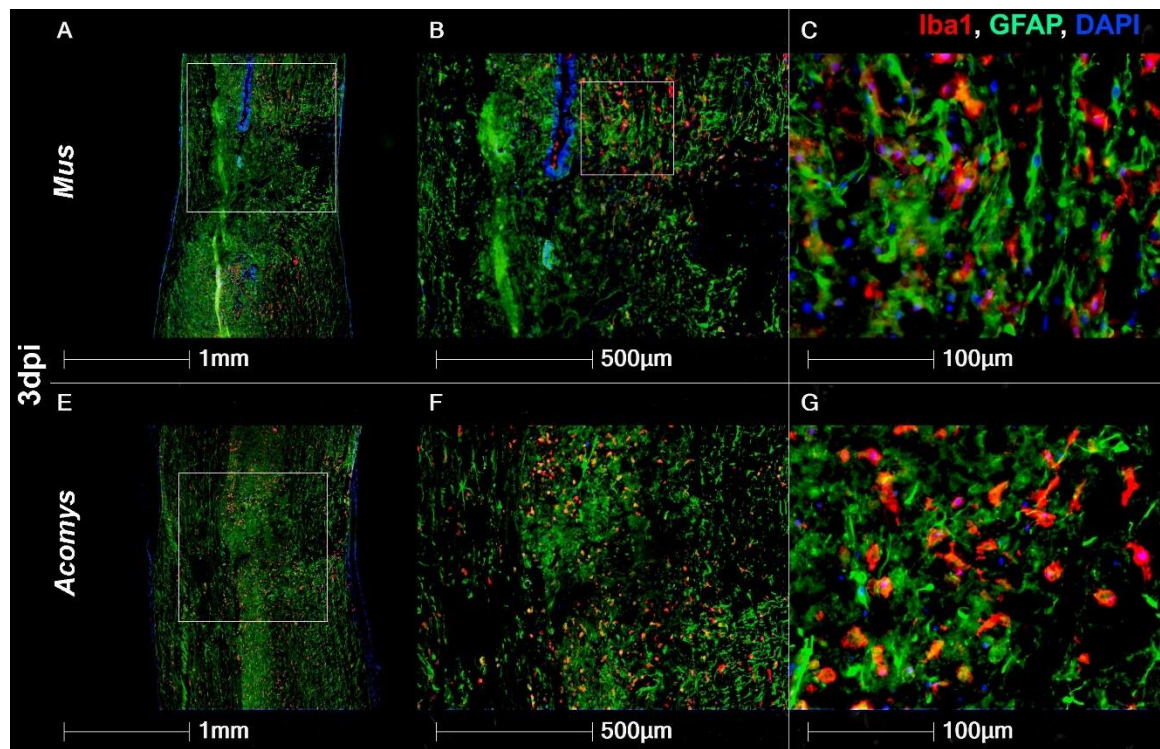


Figure A1.4: Naïve glia are similar in *Mus* and *Acomys*.

Spinal cords were collected from uninjured animals and histologically evaluated for baseline glial density and morphology. Both *Mus* and *Acomys* have similar macrophage/microglia density according to Iba1 staining (A, B) and similar ramified macrophage/microglia morphology (C-F). Astrocyte patterning and morphology also appears similar between species (G-J).



G Spinal Macrophages/Microglia 3dpi

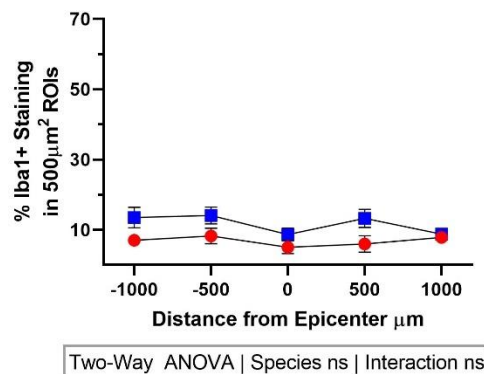


Figure A1.5: *Acomys* and *Mus* have similar acute inflammatory responses to spinal crush injury.

Histological analysis of macrophage/microglia marker (Iba1, red) in sagittal spinal sections isolated 3dpi show similar levels and patterning of Iba1+ staining density in *Acomys* and *Mus* spinal cords. At this acute time point, Iba1+ staining shows the typical amoeboid shape of activated macrophages/microglia.

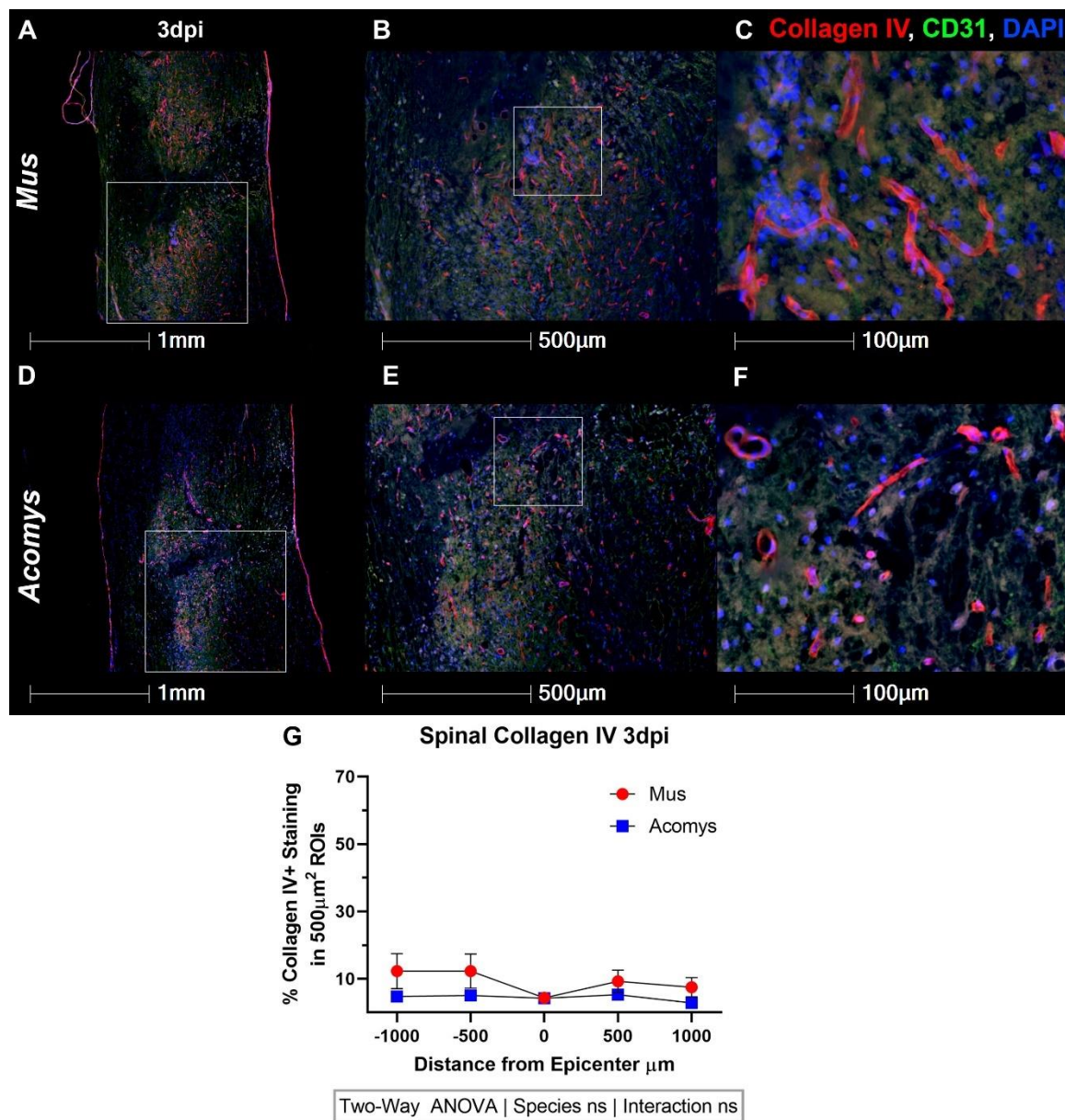


Figure A1.6: *Acomys* and *Mus* have similar collagen IV levels and patterning in acute spinal crush injury.

Histological analysis of collagen IV (red) in sagittal spinal sections isolated 3dpi show similar patterning and staining density in *Acomys* and *Mus* spinal cords. At this acute time point, collagen IV staining is sparse and appears in a vessel-like morphology.

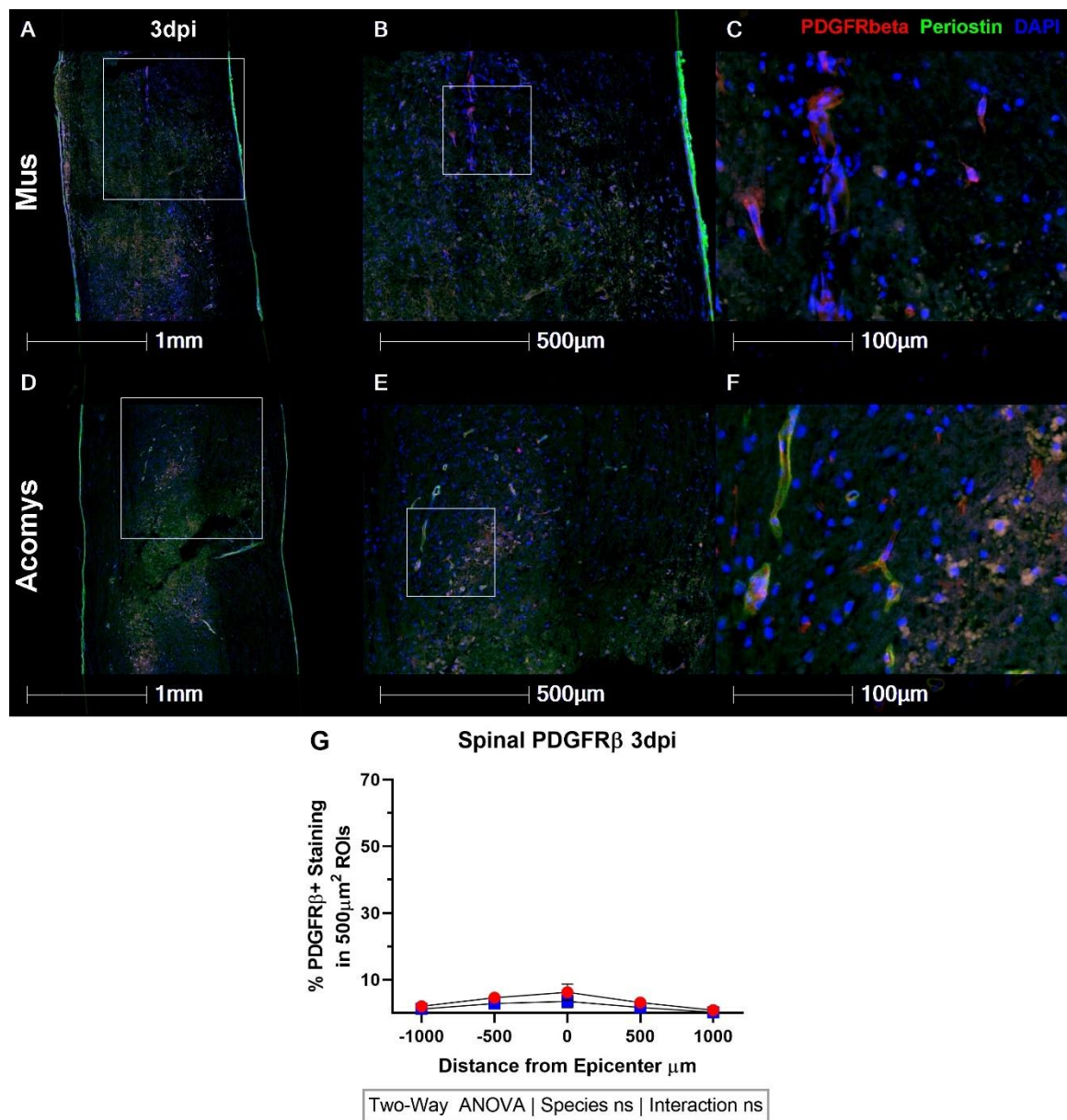


Figure A1.7: *Acomys* and *Mus* have similar PDGFRβ patterning in acute spinal crush injury.

Histological analysis of PDGFRβ (red) and periostin (green) in sagittal spinal sections isolated 3dpi show similar patterning and staining density in *Acomys* and *Mus* spinal cords. At this acute time point, both PDGFRβ and periostin staining are sparse and appear in a vessel-like morphology.

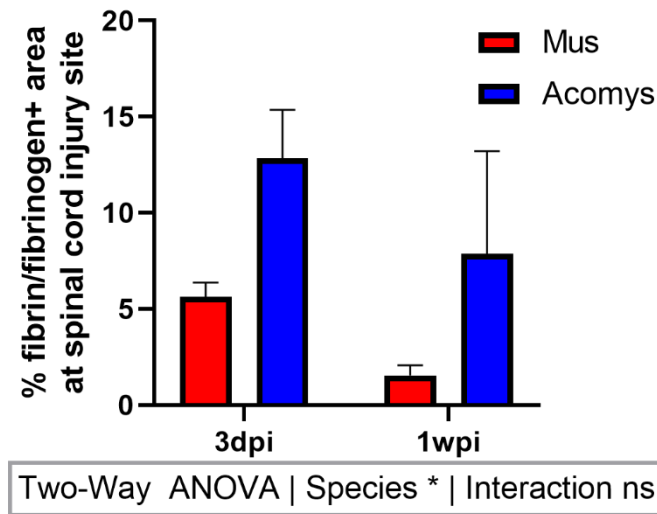


Figure A1.8: *Acomys* have more clot-promoting protein, fibrin/fibrinogen, in the acutely-injured.

Immunohistological analysis of sagittal spinal sections isolated from animals 3 days and 1 week after spinal crush shows that *Acomys* have significantly more fibrin/fibrinogen than *Mus*. These results may suggest that *Acomys* have more clotting and/or more propensity to clot early after SCI. * $p < 0.05$.

2 APPENDIX 2: Methods

*Recipes for solutions created in-house and specific product information for bought materials are detailed in Appendix 2: Materials.

2.1 Animal Husbandry

Acomys cahirinus (*Acomys*) and Swiss Webster Mus *Musculus* (*Mus*) were housed at the University of Kentucky, Lexington, KY in a vivarium managed by Dr. Ashley Seifert and the Department of Laboratory Animal Research. Aco were bred in-house while Mus were obtained from Charles River Laboratories. Animals were kept on an ambient light cycle with the primary light source being exterior vivarium windows. Before SCI, *Acomys* were housed at a density of 10–15 animals per cage in metal wire cages (24 inch x18 inch x16 inch, height x width x depth) with dry pellet bedding and fed a 3:1 mixture by volume of 14% protein mouse chow and black-oil sunflower seeds with ad libitum access to food and water.

Before spinal cord injury, *Mus* were housed at a density of 5 individuals per cage in Allentown Mouse Tub HTPC Cages (11 in x 7 in, width x depth) with sani-chip bedding and fed 14% protein mouse chow with ad libitum access to food and water. Animals were assessed for weight and health 3 days before SCI and were transferred to individual housing in Allentown Mouse Tub HTPC Cages with sani-chip bedding and ad libitum access to food and water. Animals were individually housed because preliminary studies showed a proclivity for *Acomys* cannibalization and autophagy after SCI. Throughout the study, cages were regularly rotated to compensate for any unlikely effects of disproportionate access to light from windows.

Table A2.1.1: Animals per experiment for comparative study (Ch 2-4)

Experiment ID	Intended Time Post Injury	<i>Mus</i> at time of spinal crush Surgery	<i>Acomys</i> at time of spinal crush Surgery
01202020	3dpi	6	6
03182020	3dpi	4	4
01162020	1wpi	6	6
03142020	1wpi	4	4
09102019	2wpi	7	7
08262019	12wpi	10	10

2.2 Spinal Cord Injury and Spinal Isolation

The only method currently available to accurately recapitulated the SCI responses and progression is to produce a SCI in an animal. Therefore, we administered spinal crush, unilateral spinal hemisection, or spinal contusion injuries to rodents. Animals were anesthetized with isoflurane, using 3% isoflurane in a chamber for induction and 1-2% isoflurane in a nose cone throughout the procedure. Before injury, animals were weighed, then the surgery site was shaved and sanitized with betadine and sterile alcohol wipes. Skin, fat, and muscle were cut and opened to provide access to the 9th thoracic (T9) vertebra. The dorsal aspect of the vertebra was removed to the most lateral-extent of the vertebra. For spinal crush injuries, we crushed the entire T9 spinal cord for 1 sec using Dumont #5 forceps that were modified with a spacer that physically restricts the maximum closure distance to 0.5mm. For unilateral spinal hemisection injuries, we cut the spinal dura on 1 lateral half of the spinal cord using microscissors then inserting a 29 gauge needle at the spinal midline and dragging the needle laterally, repeating the 3 times; this process effectively cuts the entire dorsal-ventral extent of 1 lateral side of the spinal cord. For

spinal contusion injuries, we stabilized the spinal cord with a stereotactic device clamped on T8 and T9 then impacted the spinal cord using the metal pneumatic impactor tip of Infinite Horizons (IH) injury device, elicits injuries based on pre-defined impact force and dwell times. Specific impact parameters are detailed in Chapter 7.

Each injury was verified immediately afterward by the surgeon, then the surgery site was closed by discontinuous stitches in the overlying muscle, followed by continuous stitches in the skin. *Acomys* skin tears at low tensile force and are able to regenerate damaged skin quickly and reliably, so stitches were placed slightly further from the surgery site and with slightly more slack than standard rodent stitching; injury sites for all animals were monitored at least twice daily for the first 2 weeks post injury.

Spinal cords were collected from animals 3dpi, 1wpi, 2wpi, and 12wpi to perform histological assessment of SCI progression and injury responses. At each specified timepoint, animals were euthanized with a lethal dose of CO₂, then transcardially perfused with cold phosphate-buffered saline (PBS) (0.1 M, pH 7.4), followed by perfusion with cold 4% paraformaldehyde (PFA). Dissected spinal cords (~1 cm) were post-fixed for 2 h in 4% PFA, then rinsed and stored in cold phosphate buffer (0.2 M, pH 7.4) overnight at 4°C. Tissue was cryoprotected in 30% sucrose in dH₂O at 4°C for 5 days (when the cords sunk to the bottom of their container), then oriented for sagittal or coronal sectioning in optimal cutting temperature compound and rapidly frozen using dry ice. Each OCT block contained 2-3 spinal cords with at least 1 animal from each group in each block to ensure uniformity of staining across groups. Tissue was stored at -80°C before sectioning. Tissue blocks were cut in serial sections and mounted onto Colorfrost plus slides. Tissue was cut

to 10 μm thickness for experiments except the chronic, 12 wpi time point, which was cut to 25 μm in an effort to visualize full axons and to evaluate anatomical repair.

Table A2.2.1: Summary of Animal Characteristics

Endpoint	Injury Type	Species	Sex	Animals Injured	Age at Injury	Weight at Injury
3dpi	Crush	Mus	Male	4 or 6	3-6mo	39.6 ± 1.1 or $36.3 \pm 3.2\text{g}$
3dpi	Crush	Acomys	Male	4 or 6	3-6mo	43.4 ± 5.8 or $42.3 \pm 4.1\text{g}$
7dpi	Crush	Mus	Male	4 or 6	3-4 mo	39.0 ± 1.9 or $36.5 \pm 2.5\text{g}$
7dpi	Crush	Acomys	Male	4 or 6	3-5 mo	43.6 ± 2.6 or $41.2 \pm 3.4\text{g}$
14dpi	Crush	Mus	Male	7	4-5mo	$42.0 \pm 1.9\text{g}$
14dpi	Crush	Acomys	Male	7	4-6mo	$41.6 \pm 2.8\text{g}$
12wpi	Crush	Mus	Male	10	3-4mo	$43.4 \pm 3.8\text{g}$
12wpi	Crush	Acomys	Male	10	3-5mo	$43.3 \pm 5.3\text{g}$

For our 14dpi analysis of Acomys and Mus SCI, 5 of 14 animals did not survive to the endpoint and 1 was excluded from analysis: 1 Acomys died unexpectedly before the endpoint; 2 Acomys exhibited autophagy 1dpi and were euthanized; 2 Mus were euthanized 1dpi to match tissue for histological analysis; 1 Mus was excluded for an incomplete injury (hindlimb function 1dpi and 3dpi was >1 standard deviation better than all other animals, according to BMS).

For our chronic analysis of Acomys and Mus SCI, 3 of 20 animals did not survive to the endpoint; 1 Acomys was euthanized after becoming lethargic 14dpi, 1 mouse died for unknown reasons overnight between 1-2dpi, and 1 mouse died during bladder care 22dpi.

All procedures were performed in accordance with the guidelines of the Office of Responsible Research Practices and with the approval of the Institutional Animal Care and Use Committee at the University of Kentucky.

2.3 Functional Analysis

Bladder voiding was analyzed as a Survival curve using the log-rank Mantel-Cox test, where the species difference is $p < 0.0001$ (displayed as ****).

Locomotor hindlimb function was assessed longitudinally using a battery of functional tests. All animals were tested using an open field test based on the Basso Mouse Scale, as described previously by Basso and colleagues⁶², to verify a consistent injury within and between groups and to gain general insight into functional recovery. Briefly, two trained observers observed and scored mice in an open field for 4 min at each specified time point. Each hindlimb was scored separately based on movement (e.g., ankle placement and stepping), coordination, and trunk stability, then averaged to generate a single score for each animal. Each aspect of movement may serve as an outcome measure for functional recovery, or a composite score designed by Basso et al., where a score of 0 indicates complete paralysis while a score of 9 indicates normal locomotion, may summarize overall hindlimb functional recovery. When using this scale, though, it is important to considering that the BMS was specifically designed for *Mus*. Hindlimb functional recovery was analyzed using BMS 3dpi, 1wpi, 2wpi, and 12wpi to determine initial functional deficits from SCI and to follow functional recovery.

During the 4 minutes of free roaming for BMS, distinct hindlimb functions are recorded on the BMS scoring sheet (Table A2.3.1). These distinct hindlimb functions can be further analyzed as BMS subscores, as described by Basso and colleagues in the study originally describing the BMS⁶². In this study I analyze specific hindlimb functions using

subscores derived Basso and colleagues, specifically analyzing hindlimb plantar placement, plantar stepping, and coordination. It is important to note that these subscores are particularly informative because the BMS was designed to measure the functional recovery progression in *Mus*, but *Acomys* may follow a distinct progression through particular hindlimb function⁶². Furthermore, these BMS subscores are much easier to interpret as they specifically measure and report a particular hindlimb function rather than an ordinal scale that reflects a collection of hindlimb functions. Therefore, while the BMS benefits from showing the progression of animals through a range of functional recovery states, these BMS subscores are more informative for particular aspects of recovery.

To evaluate rearing, animals were placed in a translucent plexiglass activity box with an array of infrared beams to track animal movement. Two rows of beams are arranged such that “beam breaks” on the first row can identify both horizontal movement across the ground, while beam breaks on the second row can discriminate rearing. The plexiglass box is further subdivided into 2 small compartments so that 2 animals can be run concurrently. We placed 1 animal of each species in the activity box, engaged the infrared beam activity tracker, and allowed free movement for 10 minutes. We collected pre-injury baseline rearing data, but only began collecting rearing data after animals began to recover stepping ability (before the animals were able to step, none of them were able to rear on their hindlimbs). The resultant data are analyzed as vertical/horizontal movement (top/bottom row beam breaks), to normalize rearing movements to total animal movement.

Rearing and BMS data after injury were analyzed by two-way ANOVA using species and time as independent variables, and multiple comparisons using Sidak’s test

were used to compare hindlimb function between species at each time point. Baseline rearing, BMS 3dpi, and BMS subscores were analyzed using a t-test.

Table A2.3.1: Basso Mouse Scale Grading Criteria (adapted from Basso et al., 2006⁶²)

Score	Operational Definitions
0	No ankle movement
1	Slight ankle movement
2	Extensive ankle movement
3	Plantar placing of the paw with or without weight support *OR* Occasional, frequent, or consistent dorsal stepping but no plantar stepping
4	Occasional plantar stepping
5	Frequent or consistent plantar stepping, no coordination *OR* Frequent or consistent plantar stepping, <i>some</i> coordination, paws <i>rotated</i> at initial contact <u>and</u> lift off
6	Frequent or consistent plantar stepping, <i>some</i> coordination, paws <i>parallel</i> at initial contact (P/R) *OR* Frequent or consistent plantar stepping, <i>mostly</i> coordinated, paw <i>rotated</i> at initial contact <u>and</u> lift off
7	Frequent or consistent plantar stepping, <i>mostly</i> coordinated, paws <i>parallel</i> at initial contact and <i>rotated</i> at lift off *OR* Frequent or consistent plantar stepping, <i>mostly</i> coordinated, paws <i>parallel</i> at initial contact <u>and</u> lift off, and <i>severe</i> trunk instability.
8	Frequent or consistent plantar stepping, <i>mostly</i> coordinated, paws <i>parallel</i> at initial contact <u>and</u> lift off, and <i>mild</i> trunk instability *OR* Frequent or consistent plantar stepping, <i>mostly</i> coordinated, paws <i>parallel</i> at initial contact <u>and</u> lift off, <i>normal</i> trunk stability, and tail <i>down</i> or <i>up & down</i>
9	Frequent or consistent plantar stepping, <i>mostly</i> coordinated, paws <i>parallel</i> at initial contact <u>and</u> lift off, <i>normal</i> trunk stability, and tail <i>always</i> up.

2.4 Spinal Cord Histology

2.4.1 Acomys SCI Studies (Ch. 2, 3, 4)

Before staining, slides were warmed for >1hr at 37C; for immunohistological procedures antigen retrieval was performed in hot (approaching, but not reaching boiling) Citrate Buffer pH 6. Massons Trichrome staining to visualize collagen fibers and gross cellular/extracellular morphology followed routine protocol with Masson's trichrome (Richard-Allen Scientific, Kalamazoo, MI). PicoSirius Red staining to enhance

birefringence and enable polarized light imaging of collagen fibrils followed standard protocol using a PicoSirius Red Stain Kit (StatLab, McKinney, TX). As validated and described previously, lesion size and spared tissue was identified using a combination of eriochrome cyanine (EC) and neuro-filament (NF) (Aves Labs, #NFH) to label myelin and axons, respectively^{69,70}. For immunohistochemical measures, slides underwent antigen retrieval in hot (close to, but not actually boiling) citrate buffer pH 6. To block non-specific binding sites, slides were incubated in blocking buffer (0.1M PBS with 5% normal donkey serum, 1% BSA and 0.1% Triton X-100) for 1hr, in blocking buffer with avidin for 15min, and blocking buffer with biotin for 15min (Vector Labs, Burlingame, CA). Antibodies were also diluted in blocking buffer. Slides were incubated in primary antibodies (listed in Table A3.3.3) overnight at 4°C. Slides were incubated in secondary antibodies for 1hr at room temperature. In the case of using biotinylated secondary antibodies, streptavidin was diluted in 0.1M PB with 0.1% Triton X-100 and slides were incubated in this streptavidin for 1hr at room temperature.

For lesion measurements, I used HALO image analysis software to delineate the spinal lesion by tracing EC-negative regions. The pixel-to- μm^+ conversion was performed automatically using the software, and the “ruler” function was used to determine the length between the most-rostral and most-caudal points of the lesion. These measurements gave a lesion area and a lesion length for each spinal section. The final value for each animal was determined by the average value of the 3 central-most sections from each animal.

For quantification of injury responses, I used HALO image analysis software to create. The first step of the process was to hide the channel of interest (Iba1, collagen IV, PDGFR β , etc.) to prevent biased ROI placement based on that staining. Then 500 μm^2

square ROIs were created and specifically placed on 3 spinal sections closest to the center of the cord, as determined by the central canal and/or grey matter shape. An exclusion tool was used to exclude any areas of autofluorescence or artificial tissue damage produced in the tissue preparation process from analysis. The central ROI were placed at the injury epicenter using other stains (usually GFAP and DAPI) as a guide, then ROIs were placed rostral and caudal to the epicenter with edges abutting the injury epicenter ROI, and then additional ROIs were placed rostral and caudal to those ROIs with edges abutting. Collectively, this produced a series of five $500\mu\text{m}^2$ ROIs with their center at the injury epicenter, $500\mu\text{m}$ rostral, $500\mu\text{m}$ caudal, $1000\mu\text{m}$ rostral, and $1000\mu\text{m}$ caudal to the injury epicenter. Subsequent to ROI placement, the channel of interest was turned on and threshold values were set to determine weak, moderate, and strong staining in the spinal sections. The HALO software then ran an analysis of staining intensity across all regions of interest, and produced a quantification of % staining at each intensity. Data reported are %moderate + %strong staining in each ROI. Whole cord values were calculated as $((\text{total moderate area} + \text{total strong area})/\text{total ROI area}) \times 100$.

Data were analyzed by a 2-way ANOVA to see overall species and interaction (species x time) effects. Post-hoc analysis with Sidak's multiple comparison test was used to evaluate species effects at individual time points. Statistical significance is displayed as * $p < 0.05$, ** $p < 0.01$, *** $p < 0.001$, **** $p < 0.0001$.

2.4.2 Compression Studies (Ch. 5)

As validated and described previously, spared tissue was identified using a combination of eriochrome cyanine (EC) and neurofilament (NF) to label myelin and axons, respectively 31,176. For immunohistochemical analyses of macrophage phenotypes, sections were incubated with goat anti-CD206 (1:100dilution, AF2535, R&D

Systems, Minneapolis, MN), goat anti-Arg1(1:100, SC-18354, Santa Cruz Biotechnology, Dallas, TX), rat anti-CD86 (1:100, 553689, BD Biosciences, San Jose, CA), or rat anti-MARCO (1:1000, MCA1849, BioRad, Hercules, CA). Slides were incubated with these primary antibodies overnight at 4°C in 0.1M PBS with 5% normal donkey serum, 1% FBS and 0.1% Triton X-100. Sections were subsequently incubated with a biotinylated tomato lectin (1:1000,L0651; Sigma-Aldrich, St. Louis, MO) to counterstain for total macrophage numbers.

Detection of primary antibodies was performed with donkey anti-rat Alexa Fluor (AF) 488, donkey anti-rabbit AF 568, and streptavidin AF 647 (all secondaries at 1:1000 dilution, LifeTechnologies, Carlsbad, CA) for 1 h at room temperature. To validate antibody staining, negative controls were run without primary antibody, and full dilution curves were analyzed.

The EC/NF images were captured using an Olympus AX-80 and Aperio Scanscope. To quantify spared tissue, the regions of dense EC staining were outlined and measured using the MetaMorph analysis program (Molecular Devices, Sunnyvale, CA). To quantify macrophage activation, three or four regions of interest (ROI) were captured per subject using an Axioplan 2 imaging microscope(Carl Zeiss) at 20 \times magnification. The ROI were taken from within the lesion epicenter using NF/EC stained serial sections as references (Fig. 5.5.2A). Threshold based area measures of positive signal within the ROI were performed using MetaMorph to determine total area of positive signal. The total area of positive signal of macrophage markers (Arg1, CD206, MARCO, CD86) was then normalized to total tomato lectin (TomL) positive area for each ROI to determine proportion of positive macrophages within the lesion.

Because of unknown, at the time, temperature inconsistencies during tissue processing and sectioning, some cross sections were lost or folded during staining, making analysis impossible. Mice without an obvious and fully intact epicenter were not included for histological analysis, decreasing the total number of mice analyzed for histological analyses from 88 to 71.

2.5 In vitro macrophage neurotoxicity

Data in Figure 5.3 represent 1 of 3 biological replicates, each of which show similar trends. For each biological replicate experiment, 1 *Acomys* and 1 *Mus* were euthanized, then skin and muscle were removed to access and collect intact femurs and tibias. Bones were stored in ice-cold RPMI 1640 supplemented media before moving to an aseptic cell culture hood for sterile isolation of bone marrow stem cells. To collect cells, we clip off the ends of each of the bones and flush bone marrow into separate 50mL conical tubes using syringes filled with RPMI 1640 supplemented media. After cells have been flushed from all bones, cells were titrated and centrifuged (all centrifugation steps for switching media were performed at 300 g for 5 min). To remove red blood cells, cells were resuspended in red blood cell lysis buffer* for 3-5 min. After diluting and removing red blood cell lysis buffer, the cell pellet was resuspended in BMDM culture media*. Cell counts were acquired using a hemocytometer and a 10uL sample diluted 1:1 in trypan blue and cells were plated at a density of $8-10 \times 10^6$ cells/10mL in a T75 flask.

We stimulated bone marrow stem cells to become macrophages, then activated these cells in vitro. The BMDM culture media contains supernatant from L929 cells, which is rich in macrophage colony stimulating factor (MCSF) that promotes the differentiation of pluripotent bone marrow stem cells into macrophages. T75 flasks were allowed to differentiate into macrophages for 7 days in a cell culture incubator at 5% CO₂ and 37°C,

replacing fresh media 2, 4, and 6 days after plating. After the 7 days, we shocked macrophages with cold phosphate buffered saline (PBS) before using a cell scraper to lift the cells off of the flask. These floating macrophages were centrifuged and resuspended in warm BMDM replating media*, counted, replated at a density of 3×10^6 cells/3mL in 6-well cell culture plates. BMDMs were seeded into 4 separate 6-well plate replicates. Plates were incubated overnight to prevent cell death and allow macrophage adherence to the plate. The next day, supernatant was removed and replaced with warm replating media with or without activating stimuli. Macrophages were activated in warm BMDM activating media* containing 50ng/mL lipopolysaccharide (LPS) + 20ng/mL interleukin 4 (IL-4) for 32 hr before supernatant macrophage conditioned media (MCM) was collected and filtered. Control unactivated macrophages were kept in warm BMDM activating media without additional stimulants for 32 hr before collecting and filtering MCM.

Mouse neuroblastoma cells (Neuro-2a or N2A) cells were stored in liquid nitrogen in a suspension of N2A growth media with 10% DMSO. We thawed cells from frozen stock warm N2A growth media, centrifuged at 200 g for 5min to pellet cells and remove toxic DMSO, and resuspended cells in 10-15mL N2A growth media in a T75 flask and placed the flask in a cell culture incubator at 5% CO-2 and 37°C. When cells reached confluence, we detached cells with 3mL Trypsin for 2-5min, resuspending in N2A growth media, and adding a small aliquot to a new T75 flask. N2A cells were grown and split for 1 week prior to counting cells using an aliquot in a 1:1 suspension with Trypan Blue and a hemocytometer, then replating 5×10^4 cells in 100uL of serum-free N2A growth media (no FBS). N2A cells were seeded into 2 separate 96-well plates and a total of 70 wells. Two plates were used in an effort to avoid evaporative loss from cells seeded on the edges

of 96-well plates. After 24hr, supernatant was removed and 100μL MCM collected from activated or unactivated BMDMs was applied to N2A Cells. N2A cells remained in MCM for 32 hr before performing the MTT assay. Stimulation included 4-5 technical replicates for each sample of collected MCM (4-5 N2A replicates x 4 MCM replicates = 18 total wells per stimulation type). N2A cells were incubated in MCM in a cell culture incubator 5% CO₂ and 37°C.

To test N2A cell health, we performed the MTT assay. After 32hr incubation in MCM, 10μL thiazolyl blue tetrazolium bromide (MTT substrate) solution was added to each well and the plate was incubated for 2hr in cell culture incubator at 5% CO₂ and 37°C. Mitochondrial dehydrogenases in viable cells cleave the tetrazolium ring of MTT substrate to yield purple formazan crystals. These crystals were then dissolved in 100μL acidified isopropanol (MTT solvent) using a multichannel pipette. After adding solvent to each well, the solution was mixed well by pipetting up and down at least 10 times. The purple solution created by the MTT assay was analyzed spectrophotometrically at 570nm in an Epoch microplate reader using 690nm as a background absorbance.

Data were analyzed compared to the unactivated Mus MCM control. All data were normalized to the mean value for unactivated Mus MCM absorbance to give relative neurotoxicity. These data were analyzed by two-way ANOVA for overall species and activation effects. For within-group analysis, we used Sidak's multiple comparisons test.

2.6 *In vitro* neurite growth

Data presented are from 1 of 2 biological replicates, each of which show similar trends. For each biological replicate, 1 animal from each species was euthanized, then the skin, fat, fascia, and muscle were removed to visualize the spinal column. The dorsal half of vertebrae were removed to allow access to the entire spinal cord and peri-spinal dorsal

root ganglia. The spinal cord was periodically doused with cold 1X HBSS to prevent drying and maintain cell health. Dorsal root ganglia were removed from the cervical, lumbar, and thoracic cord by cutting nerve fiber projections with a pair of microscissors, then ganglia were placed in a petri dish filled with cold 1X HBSS. This process was performed quickly (<1hr) to preserve cellular integrity.

Isolated ganglia were further processed to remove any remaining nerve fiber projections, then a small cut in the edge of the ganglia was made to facilitate later dissociation and transferred to a 1.5mL conical tube. Allowed DRGs to sink to the bottom of the conical tube before carefully removing excess liquid with a micropipette. DRG dissociation was facilitated by collagenase/dispase enzymatic digestion of connective tissues overnight at room temperature on a shaker plate. After enzymatic digestion, excess liquid was carefully removed with a micropipette and 475 μ L of 1X HBSS was added. The digested DRGs were lightly triturated with a fire-polished pipette for 1-3min until cells were dissociated, as evident by cloudiness of solution. The resultant cell solution was centrifuged at 200 g for 3min and supernatant was discarded before resuspending cells in 100 μ L DRG media*. DRG neurons were counted by diluting a sample from the cell solution 1:1 in trypan blue and using a hemocytometer under a phase-contrast microscope, and appropriate volumes of the cell solution and DRG media were combined to reach 250 cells/150 μ L/coverslip.

Coverslip preparation began 1 day before plating DRG neurons. Circular coverslips sized to fit in 24-well cell culture plates were handled in sterile conditions for the preparation process. Coverslips were sterilized with 3 treatments of 70% alcohol and 3 washes dH₂O before placing on parafilm to serve as a hydrophobic barrier to maintain

liquid atop the coverslip. Coverslips were incubated in 157 μ L poly-D-lysine (PDL; 25 μ g/mL in dH₂O) overnight in the cell culture hood to coat coverslips in PDL. The next day, 3-4hr before time for plating DRG neurons, coverslips were washed 3x with sterile dH₂O then allowed to dry. Coverslips were incubated in 160 μ L of the ECM substrate for 2-3hr before time for plating DRG neurons in a cell culture incubator 5% CO₂ and 37°C. Laminin was added at a concentration of 10 μ g/mL, while fibronectin, collagen IV, and aggrecan were added at a concentration of 5 μ g/mL.

After coverslips were coated with the appropriate substrates and DRG neurons were dissociated and suspended at the appropriate concentration, the ECM solution was aspirated from the coverslips and immediately replaced by 150 μ L of cell solution containing 250 cells. Cells from each species were placed on 3 technical replicates of each substrate type. Neurons were allowed to settle and adhere onto the coverslip with ECM substrates for 15min in the cell culture hood before being transferred to a 24-well plate with 500 μ L DRG media in each well. Neurons were maintained in these 24-well plates for 36hr before fixation with 500 μ L 4% paraformaldehyde. After 10min of fixation, each coverslip was carefully removed, washed 3 times in 1X PBS, and placed on parafilm cell-side up for staining.

For the staining procedure, parafilm was used as a hydrophobic barrier to maintain liquid atop the coverslips. For each step, about 150 μ L of liquid was added to each coverslip by gentle droppers or removed by aspirating at a low suction force to prevent cell or neurite damage during the staining process. Coverslips were blocked for 1hr at room temperature in blocking buffer*. Blocking buffer was replaced with primary antibodies targeted to β -tubulin (1:2000 rabbit anti- β -tubulin) and neurofilament (1:2000 rat anti-NFH) and

incubated for 1hr at room temperature. After 3 washes with 1X PBS, coverslips were incubated for 1hr at room temperature in fluorescently-conjugated secondary antibodies targeted to primary host species (1:2000 goat anti-rabbit alexa fluor 546 binding rabbit anti- β -tubulin; goat anti-rat alexa fluor 488 binding rat anti-NF). After 3 washes with 1X PBS, coverslips were incubated in 1:95 DAPI for 10min at room temperature, washed 3 more times in dH₂O. Coverslips were carefully removed from parafilm with forceps and mounted to colorfrost slides cell-side down using immumount mounting media. A blinded colleague then assigned coding numbers to each slide, which was stored and not viewed until analysis was completed.

Stained coverslips were imaged using an Axioscan ScanScope to collect 20x magnification images of the entire coverslip. These large images were then analyzed using HALO software, where the analyst transposed a premade grid over top of the coverslip to select a reproducible and unbiased selection of neurons to analyze. Any neurons with soma or neurites interacting with premade-boxes were imaged using the HALO software. If multiple images were required for a single neuron, these images were stitched together using Adobe Photoshop 6 software. Final images of each neuron were analyzed using Metamorph software and a Sholl Analysis program to analyze neurite length. In sholl analysis, an array of concentric rings with diameters of $((n-1)*25)+25\mu\text{m}$ diameters, where n equals the number in sequence of the rings, are placed centered on the neuron soma. Automated software then detects the number of times a neurite crosses each of the concentric rings. Therefore the primary output has 2 vectors: 1) the number of crossings at a ring of 2) a given distance from the neural soma. The area under the curve is then extrapolated from the number of crossings at each given distance, to give a single neurite

growth value for each neuron. Data in Figure 4.3.1 represent the mean and standard error of the mean for each analyzed neuron from a given species and substrate type. Data were analyzed by a two-way ANOVA with Sidak's multiple comparison test to determine the effect of each coverslip substrate on neurite growth of DRG neurons from a single species. To compare growth between species, multiple Student's T tests were conducted to compare *Mus* vs. *Acomys* within a single coverslip substrate type (laminin, fibronectin, collagen IV, or Aggrecan).

3 APPENDIX 3: Materials

3.1 Animal Husbandry

Table A3.1.1: Animal Product Information

Names	Abbrev.	Source	Catalogue #
Swiss Webster <i>Mus musculus</i>	<i>Mus</i>	Charles Rivers	CFW
14% protein mouse chow		Teklad Global	
Black-oil sunflower seeds		Pennington Seed Inc., Madison, GA	
Allentown Mouse Tub HTPC Cages		Labex of MA, Worcester, MA	
Metal wire cages		Quality Cage Company Portland, OR	
Teklad Sani-chip bedding	Sani-chip bedding	Envigo, Indianapolis, IN	7090
Dry pellet bedding		Southern States, Richmon VA	10001915

3.2 Spinal Cord Injury and Spinal Isolation

Recipes:

- 4% Paraformaldehyde: dH₂O with 20% 5X PBS, 4% weight by volume paraformaldehyde powder. Dissolved powder by adding <1% NaOH and stirring at 55°C. Adjusted to pH 7.4 at room temperature and filtered for final solution.
- 30% Sucrose: dH₂O with 30% weight by volume sucrose powder, stirred until dissolved.

Table A3.2.1: Spinal cord injury and spinal isolation product information

Names	Abbrev.	Source	Catalogue #
Isoflurane	Iso		
Betadine			
Sterile Alcohol Wipes			
Baytril			
Infinite Horizons Injury Device	IH	Precision Systems and Instruments	

Biosyn Monofilament Absorbable Suture	Absorbable suture	Covidien	GM875
6-0 Dermalon Blue 18" P-10 Cutting	Non-absorbable suture	Esutures.com	1754-13
Optimum Cutting Temperature Compound	OCT	Sakura Finetek	
Colorfrost plus slides		Fisher	12-550-17

3.3 Spinal Macrophage Histology

Recipes

- Antigen Retrieval/Citrate Buffer: dH₂O with 10mM Sodium Citrate, 0.05% Tween 20. Stirred til dissolved and pH adjusted to 6.0.
- Blocking Buffer: 1X PBS with 5% N₂S (goat or donkey serum, to match secondary host species), 1% FBS, 0.1% Triton X-100
- Avidin Blocking Buffer: Blocking buffer with 4 drops/mL avidin (from avidin/biotin blocking kit)
- Biotin Blocking Buffer: Blocking buffer with 4 drops/mL biotin (from avidin/biotin blocking kit)

Table A3.3.1: General staining supplies

Name	Abbrev	Source	Catalogue #
Normal Donkey Serum	NDS	Sigma-Aldrich	D9663-10ML
Normal Goat Serum	NGS	Sigma-Aldrich	G9023-10ML
Fetal Bovine Serum	FBS	Life Technologies	10082147
Triton X-100			
Avidin/Biotin Blocking Kit		Vector Laboratories	SP-2001
Eriochrome Cyanine	EC		
Picrosirius Red Stain Kit	Picrosirius	Statlab	
Massons Trichrome Stain Kit		Richard-Allen Scientific	
DAB Peroxidase (HRP) Substrate Kit	DAB	Vector Laboratories	SK-4100
ImmPACT SG Peroxidase (HRP) Substrate	SG	Vector Laboratories	SK-4705

Table A3.3.2: Antibodies and Lectins for Acomys Histology (Chs 2-4)

Abbrev.	Target	Host	Conjugate	Dilution	Company	Cat #
---------	--------	------	-----------	----------	---------	-------

GFAP	Glial Fibrillary Acidic Protein	Chicken		1:500	Aves Labs	GFAP
NF-H	High Molecular Weight Neurofilament	Chicken		1:1000	Aves Labs	NFH
NF-H	High molecular weight neurofilament	Rat		1:5000	Millipore Sigma	MAB5448
NeuN	NeuN	Rabbit		1:4000	Abcam	Ab177487
5-HT	Serotonin	Rabbit		1:5000	ImmunoStar	20080
Iba1	Allograft inflammatory factor 1	Rabbit		1:500	Wako Chemicals	019-19741
ColIV	Collagen IV	Rabbit		1:250	Abcam	Ab6586
	Fibronectin	Rabbit		1:500	EMD Millipore	AB2033
	Laminin	Rabbit		1:500	Sigma-Aldrich	L9393-100UL
PDGFR β	Platelet Derived Growth Factor Receptor β	Rabbit		1:500	Abcam	Ab32570
	Periostin	Goat		1:200	R&D Systems	AF2955
α SMA	α smooth muscle actin			1:200	Abcam	Ab5694
	Chicken Ab	Goat	Alexa Fluor 488	1:1000		
	Rat Ab	Goat	Biotinylated	1:1000		
	Rabbit Ab	Goat	Alexa Fluor 546	1:500	Life Technologies	A11010
	Biotin	Streptavidin	Alexa Fluor 405	1:1000	Life Technologies	S32351

	Biotin	Streptavidin	Alexa Fluor 568	1:1000	Life Technologies	S-11226
	Goat Ab	Donkey	Alexa Fluor 488	1:500	Thermo Fisher Scientific	A-11055
	Rabbit Ab	Donkey	Alexa Fluor 568	1:500	Life Technologies	A10042

Table A3.3.3: Antibodies and Lectins for Compression Histology (Ch. 5)

Abbrev.	Target	Host	Conjugate	Dilution	Company	Cat #
NF-H	High molecular weight neurofilament	Chicken	Biotinylated	1:1000	Aves Labs	NFH
CD206	Mannose Receptor	Goat		1:100	R&D Systems	AF2535
Arg1	Arginase 1	Goat		1:100	Santa Cruz Biotechnology	SC-18354
CD86	Cluster of differentiation 86	Rat		1:100	BD Biosciences	553689
MARCO	Macrophage receptor with collagenous structure	Rat		1:1000	BioRad	MCA1849
TomL	Tomato Lectin		Biotinylated	1:1000	Sigma-Aldrich	L0651
AF488	Goat Ab	Donkey	Alexa Fluor 488	1:1000	Thermo Fisher Scientific	A-11055
AF568	Rat Ab	Donkey	Alexa Fluor 568	1:1000	Life Technologies	
AF647	Biotin	Streptavidin	Alexa Fluor 647	1:1000	Thermo Fisher Scientific	S-21374

3.4 *In Vitro* Macrophage Neurotoxicity

Recipes:

- Red blood cell lysis buffer: 155 mM NH₄Cl + 10 mM KHCO₃ + 0.13 mM Na₄EDTA in dH₂O
- BMDM culture media: RPMI 1640 supplemented media with 10% FBS, 1% HEPES, 1% pen/strep, 0.001% β-mercaptoethanol, and 20% supernatant from L929 cells
 - Supernatant from L929 Cells: L929 cells grown to confluency in T75 flasks in L929 media, supernatants removed from cells and stored at -20°C until needed
 - L929 media: RPMI 1640 supplemented media with 10% fetal bovine serum, 1% FBS, 1% penicillin/streptomycin, 1% glutamax
- BMDM replating media: DMEM with 10% FBS, 1% Glutamax, and 1% pen/strep
- BMDM activating media: DMEM with 10% FBS, 1% Glutamax, 1% pen/strep, 50ng/mL LPS, and 20ng/mL IL-4
- N2A growth media: Half OPTI-MEM and half DMEM with 10% FBS, 1% pen/strep

Table A3.4.1: *In Vitro* Macrophage Neurotoxicity Product Information

Name	Abbrev	Source	Catalogue #
RPMI 1640 supplemented media	RMPI	Thermo Fisher Scientific	21870-092
Fetal bovine serum	FBS	Thermo Fisher Scientific	10082147
L929		Dr. Phil Popovich, The Ohio State University	
4-(2-hydroxyethyl)-1-piperazineethanesulfonic acid	HEPES	Sigma-Aldrich Corporation	83264-100ML-F
Penicillin and streptomycin	Pen/strep	Thermo Fisher Scientific	15140122
β-mercaptoethanol (55mM)		Thermo Fisher Scientific	21985023
Glutamax		Thermo Fisher Scientific	35050061
Dulbecco's Modified Eagle's Medium	DMEM	Fisher	10-313-039
Lipopolysaccharide	LPS	Invivogen	tlrl-b5lps
Interleukin 4	IL-4	R&D Systems	404-ML-010
Opti-MEM Reduced-Serum Medium	Opti-MEM	Life Technologies	31985-070
Trypan Blue			
Cell Culture Flask, T75	T75	Eppendorf	0030711122
Dimethyl Sulfoxide	DMSO		
Trypsin-EDTA (0.05%), phenol red	Trypsin	Thermo Fisher Scientific	25300-062

Cell Growth Determination Kit, MTT based	MTT Assay	Sigma-Aldrich	CGD1-1KT
Epoch Microplate Reader			

3.5 *In Vitro* Neurite Growth

Recipes:

- DRG Media: Neurobasal A + 2% B-27 Supplement + 1% Pen/Strep + 1% Glutamax
- Blocking Buffer: 1X PBS + 5% NGS + 1% FBS + 0.1% Triton X-100
- Laminin coverslip coating mixture: 10µg/mL laminin
- Fibronectin coverslip coating mixture: 10µg/mL laminin + 5µg/mL fibronectin
- Collagen IV coverslip coating mixture: 10µg/mL laminin + 5µg/mL collagen IV
- Aggrecan coverslip coating mixture: 10µg/mL laminin + 5µg/mL aggrecan

Table A3.5.1: *In Vitro* Neurite Growth Product Information

Name	Abbrev	Source	Catalogue #
Hank's Buffered Saline Solution	HBSS		
Poly-d-lysine	PDL	EMD Millipore	A-003-E
Laminin		Invitrogen	23017-015
Fibronectin		EMD Millipore	FC010
Collagen IV		EMD Millipore	CC076
Aggrecan		Sigma-Aldrich	A1960-1MG
Collagenase/Dispase		Sigma-Aldrich	A1960-1MG
0.5oz Circular Coverslips			
24-well plates			
Parafilm			
Phosphate buffered saline	PBS		

Table A3.5.2: *In Vitro* Neurite Growth Antibody Product Information

Abbrev.	Target	Host	Conjugate	Dilution	Company	Cat #
---------	--------	------	-----------	----------	---------	-------

β -tubulin	β -tubulin	Rabbit		1:2000	Thermo Fisher	PA5-16863
NF-H	Neurofilament heavy chain	Chicken		1:2000	Aves Labs	NFH
AF546	Rabbit Ab	Goat	Alexa fluor 546	1:2000	Life Technologies	A11010
AF488	Chicken antibody	Goat	Alexa Fluor 488	1:2000	Life Technologies	A11039

4 APPENDIX 4: Sample Sizes and Statistics

Table A4.1: *Acomys* Functional Recovery (Chapter 2, Appendix 1)

Figure #s	Outcome Measure	Species	Timepoint(s)	n	Analysis method
2.3.1A	Bladder Voiding	<i>Mus</i>	Daily 1dpi – 84dpi	8	Log-rank (Mantel-Cox) test
2.3.1A	Bladder Voiding	<i>Acomys</i>	Daily 1dpi – 84dpi	9	Log-rank (Mantel-Cox) test
2.3.1B, A1.1	Body Weight	<i>Mus</i>	Weekly -1wpi – 12wpi	8	Two-way ANOVA, Sidak's multiple comparison correction
2.3.1B, A1.1	Body Weight	<i>Acomys</i>	Weekly -1wpi – 12wpi	9	Two-way ANOVA, Sidak's multiple comparison correction
2.3.2A	Rearing Baseline	<i>Mus</i>	1 week pre-injury	8	Student's T-Test
2.3.2A	Rearing Baseline	<i>Acomys</i>	1 week pre-injury	9	Student's T-Test
2.3.2B	Acute Basso Mouse Scale	<i>Mus</i>	3dpi	8	Student's T-Test
2.3.2B	Acute Basso Mouse Scale	<i>Acomys</i>	3dpi	9	Student's T-Test
2.3.3A	Basso Mouse Scale	<i>Mus</i>	1dpi, 3dpi, 1wpi, 2wpi, 11wpi	8	Two-way ANOVA, Sidak's multiple comparison correction

2.3.3A	Basso Mouse Scale	<i>Acomys</i>	1dpi, 3dpi, 1wpi, 2wpi, 11wpi	9	Two-way ANOVA, Sidak's multiple comparison correction
2.3.3B	Rearing	<i>Mus</i>	4wpi, 5wpi, 6wpi, 7wpi, 9wpi, 10wpi	8	Two-way ANOVA, Sidak's multiple comparison correction
2.3.3B	Rearing	<i>Acomys</i>	4wpi, 5wpi, 6wpi, 7wpi, 9wpi, 10wpi	9	Two-way ANOVA, Sidak's multiple comparison correction
2.3.3C	Hindlimb Paw Placement	<i>Mus</i>	11wpi	8	Student's T-Test
2.3.3C	Hindlimb Paw Placement	<i>Acomys</i>	11wpi	9	Student's T-Test
2.3.3D	Hindlimb Stepping	<i>Mus</i>	11wpi	8	Student's T-Test
2.3.3D	Hindlimb Stepping	<i>Acomys</i>	11wpi	9	Student's T-Test
2.3.3E	Hindlimb Coordination	<i>Mus</i>	11wpi	8	Student's T-Test
2.3.3E	Hindlimb Coordination	<i>Acomys</i>	11wpi	9	Student's T-Test
A1.2A	Baseline Von Frey	<i>Mus</i>	-1wpi	10	Student's T-Test
A1.2A	Baseline Von Frey	<i>Acomys</i>	-1wpi	10	Student's T-Test
A1.2B	Baseline Hargreaves	<i>Mus</i>	-1wpi	10	Student's T-Test
A1.2B	Baseline Hargreaves	<i>Acomys</i>	-1wpi	10	Student's T-Test

Table A4.2: Compression Functional Recovery (Chapter 5)

Figure #s	Outcome Measure	Injury Group	Timepoint(s)	n	Analysis method
-----------	-----------------	--------------	--------------	---	-----------------

5.3.1 5.3.2	Basso Mouse Scale and Subscores	50kdyn	1dpi, 3dpi, 7dpi, 14dpi, 21dpi, 28dpi	11	Two-way ANOVA, Sidak's multiple comparison correction
5.3.1 5.3.2	Basso Mouse Scale and Subscores	50kdyn + 20s	1dpi, 3dpi, 7dpi, 14dpi, 21dpi, 28dpi	9	Two-way ANOVA, Sidak's multiple comparison correction
5.3.1 5.3.2	Basso Mouse Scale and Subscores	75kdyn	1dpi, 3dpi, 7dpi, 14dpi, 21dpi, 28dpi	9	Two-way ANOVA, Sidak's multiple comparison correction
5.3.1 5.3.2	Basso Mouse Scale and Subscores	75kdyn + 20s	1dpi, 3dpi, 7dpi, 14dpi, 21dpi, 28dpi	10	Two-way ANOVA, Sidak's multiple comparison correction

Table 4.3: *Acomys* histology (Chapters 2-4, Appendix 1)

Figure #s	Outcome Measure	Species	3dpi n	1wpi n	2wpi n	12wpi n	Analysis method
2.5.5	Soma Pathology Length (NeuN)	<i>Mus</i>	4	7	4		Two-way ANOVA, Sidak's multiple comparison correction
2.5.5	Soma Pathology Length (NeuN)	<i>Acomys</i>	8	8	4		Two-way ANOVA, Sidak's multiple comparison correction
3.5.6A	Lesion Size (EC/NF)	<i>Mus</i>	4	10	4	8	Two-way ANOVA, Sidak's multiple comparison correction
2.5.6A	Lesion Size (EC/NF)	<i>Acomys</i>	8	8	4	9	Two-way ANOVA, Sidak's multiple comparison correction
2.5.6B	Lesion Length (EC/NF)	<i>Mus</i>	3	10	5	8	Two-way ANOVA, Sidak's multiple comparison correction
2.5.6B	Lesion Length (EC/NF)	<i>Acomys</i>	8	8	4	9	Two-way ANOVA, Sidak's multiple comparison correction

3.4.1, 3.4.3	Macrophages/ microglia (Iba1)	<i>Mus</i>	7	6	5	7	Two-way ANOVA, Sidak's multiple comparison correction
3.4.1, 3.4.3	Macrophages/ microglia (Iba1)	<i>Acomys</i>	6	5	4	9	Two-way ANOVA, Sidak's multiple comparison correction
4.4.2	Collagen IV	<i>Mus</i>	5	8	5	8	Two-way ANOVA, Sidak's multiple comparison correction
4.4.2	Collagen IV	<i>Acomys</i>	8	8	4	9	Two-way ANOVA, Sidak's multiple comparison correction
4.5.2M, N; 4.5.1; 4.5.3G	PDGFR β	<i>Mus</i>	6	8	5	8	Two-way ANOVA, Sidak's multiple comparison correction
4.5.2M, N; 4.5.1; 4.5.3G	PDGFR β	<i>Acomys</i>	8	7	4	9	Two-way ANOVA, Sidak's multiple comparison correction
4.5.4B, D	Periostin	<i>Mus</i>		8	4		Two-way ANOVA, Sidak's multiple comparison correction
4.5.4B, D	Periostin	<i>Acomys</i>		7	4		Two-way ANOVA, Sidak's multiple comparison correction
4.4.3A- C	Collagen Fibrils (Picrosirius Red)	<i>Mus</i>			4		Two-way ANOVA, Sidak's multiple comparison correction
4.4.3A- C	Collagen Fibrils (Picrosirius Red)	<i>Acomys</i>			4		Two-way ANOVA, Sidak's multiple comparison correction
4.4.3D- F	Laminin	<i>Mus</i>			4		Two-way ANOVA, Sidak's multiple comparison correction

4.4.3D-F	Laminin	<i>Acomys</i>			4		Two-way ANOVA, Sidak's multiple comparison correction
4.4.3G-I	Fibronectin	<i>Mus</i>			4		Two-way ANOVA, Sidak's multiple comparison correction
4.4.3G-I	Fibronectin	<i>Acomys</i>			4		Two-way ANOVA, Sidak's multiple comparison correction

Table A4.4: Compression Histology (Chapter 5)

Figure #	Outcome Measure	Injury Group	3dpi n	1wpi n	2wpi n	12wpi n	Analysis method
5.4.1, 5.4.2	Anatomical pathology (EC/NF)	50kdyn	3	3	5	8	Two-way ANOVA, Sidak's multiple comparison correction
5.4.1, 5.4.2	Anatomical pathology (EC/NF)	50kdyn + 20s	4	3	5	8	Two-way ANOVA, Sidak's multiple comparison correction
5.4.1, 5.4.2	Anatomical pathology (EC/NF)	75kdyn	3	3	5	9	Two-way ANOVA, Sidak's multiple comparison correction
5.4.1, 5.4.2	Anatomical pathology (EC/NF)	75kdyn + 20s	2	3	5	9	Two-way ANOVA, Sidak's multiple comparison correction
5.5.2, 5.5.3, 5.5.4	MARCO mac. phenotype	50kdyn		3	5		Two-way ANOVA, Sidak's multiple

							comparison correction
5.5.2, 5.5.3, 5.5.4	MARCO mac. phenotype	50kdyn + 20s		3	5		Two-way ANOVA, Sidak's multiple comparison correction
5.5.2, 5.5.3, 5.5.4	MARCO mac. phenotype	75kdyn		3	4		Two-way ANOVA, Sidak's multiple comparison correction
5.5.2, 5.5.3, 5.5.4	MARCO mac. phenotype	75kdyn + 20s		3	5		Two-way ANOVA, Sidak's multiple comparison correction
5.5.2, 5.5.3, 5.5.4	Arg1 mac. phenotype	50kdyn		3	5		Two-way ANOVA, Sidak's multiple comparison correction
5.5.2, 5.5.3, 5.5.4	Arg1 mac. phenotype	50kdyn + 20s		3	5		Two-way ANOVA, Sidak's multiple comparison correction
5.5.2, 5.5.3, 5.5.4	Arg1 mac. phenotype	75kdyn		3	4		Two-way ANOVA, Sidak's multiple comparison correction
5.5.2, 5.5.3, 5.5.4	Arg1 mac. phenotype	75kdyn + 20s		3	5		Two-way ANOVA, Sidak's multiple

							comparison correction
5.5.2, 5.5.3, 5.5.4	CD86 mac. phenotype	50kdyn		3	5		Two-way ANOVA, Sidak's multiple comparison correction
5.5.2, 5.5.3, 5.5.4	CD86 mac. phenotype	50kdyn + 20s		3	5		Two-way ANOVA, Sidak's multiple comparison correction
5.5.2, 5.5.3, 5.5.4	CD86 mac. phenotype	75kdyn		3	5		Two-way ANOVA, Sidak's multiple comparison correction
5.5.2, 5.5.3, 5.5.4	CD86 mac. phenotype	75kdyn + 20s		3	5		Two-way ANOVA, Sidak's multiple comparison correction
5.5.2, 5.5.3, 5.5.4	CD206 mac. phenotype	50kdyn		3	5		Two-way ANOVA, Sidak's multiple comparison correction
5.5.2, 5.5.3, 5.5.4	CD206 mac. phenotype	50kdyn + 20s		3	5		Two-way ANOVA, Sidak's multiple comparison correction
5.5.2, 5.5.3, 5.5.4	CD206 mac. phenotype	75kdyn		3	5		Two-way ANOVA, Sidak's multiple

							comparison correction
5.5.2, 5.5.3, 5.5.4	CD206 mac. phenotype	75kdyn + 20s		3	5		Two-way ANOVA, Sidak's multiple comparison correction

Table A4.5: Macrophage Neurotoxicity *in vitro* (Chapter 3)

Figure #	BMDM Species	BMDM Stimulation	Neuron n	Analysis Method
3.5.1	<i>Mus</i>	Activated	10	Two-way ANOVA with Sidak's multiple comparison correction
3.5.1	<i>Mus</i>	Unactivated	10	Two-way ANOVA with Sidak's multiple comparison correction
3.5.1	<i>Acomys</i>	Activated	10	Two-way ANOVA with Sidak's multiple comparison correction
3.5.1	<i>Acomys</i>	Unactivated	10	Two-way ANOVA with Sidak's multiple comparison correction

Table A4.5: DRG Neurite Growth *in vitro* (Chapter 4)

Figure #	DRG Species	ECM Stimulant	DRG n	Analysis Method
4.3.1	<i>Mus</i>	Laminin	38	One-way ANOVA with Tukey's multiple comparison Correction
4.3.1	<i>Mus</i>	Laminin + Fibronectin	64	One-way ANOVA with Tukey's multiple comparison Correction
4.3.1	<i>Mus</i>	Laminin + Collagen IV	51	One-way ANOVA with Tukey's multiple comparison Correction
4.3.1	<i>Mus</i>	Laminin + Aggrecan	63	One-way ANOVA with Tukey's multiple comparison Correction
4.3.1	<i>Acomys</i>	Laminin	13	One-way ANOVA with Tukey's multiple comparison Correction

4.3.1	<i>Acomys</i>	Laminin + Fibronectin	47	One-way ANOVA with Tukey's multiple comparison Correction
4.3.1	<i>Acomys</i>	Laminin + Collagen IV	24	One-way ANOVA with Tukey's multiple comparison Correction
4.3.1	<i>Acomys</i>	Laminin + Aggrecan	39	One-way ANOVA with Tukey's multiple comparison Correction

Table A4.6: *Acomys* Naïve Anatomy (Appendix 1)

Figure #	Outcome Measure	Species	n	Analysis method
A1.3	Naïve neuroanatomy (EC/NF)	<i>Mus</i>	3	Two-way ANOVA, Sidak's multiple comparison correction
A1.3	Naïve neuroanatomy (EC/NF)	<i>Acomys</i>	3	Two-way ANOVA, Sidak's multiple comparison correction
A1.4	Naïve glia (Iba1)	<i>Mus</i>	3	Two-way ANOVA, Sidak's multiple comparison correction
A1.4	Naïve glia (Iba1)	<i>Acomys</i>	3	Two-way ANOVA, Sidak's multiple comparison correction

BIBLIOGRAPHY

- 1 Center, N. S. C. I. S. Spinal Cord Injury Facts and Figures at a Glance. (Birmingham, AL, 2019).
- 2 Orr, M. B. & Gensel, J. C. Spinal Cord Injury Scarring and Inflammation: Therapies Targeting Glial and Inflammatory Responses. *Neurotherapeutics* **15**, 541-553, doi:10.1007/s13311-018-0631-6 PMID - 29717413 (2018).
- 3 Lee, J. K. & Zheng, B. Axon regeneration after spinal cord injury: insight from genetically modified mouse models. *Restor Neurol Neuros* **26**, 175-182 (2008).
- 4 David, S. & Aguayo, A. Axonal elongation into peripheral nervous system "bridges" after central nervous system injury in adult rats. *Science* **214**, 931-933, doi:10.1126/science.6171034 PMID - 6171034 (1981).
- 5 Alilain, W. J., Horn, K. P., Hu, H., Dick, T. E. & Silver, J. Functional regeneration of respiratory pathways after spinal cord injury. *Nature* **475**, 196-200, doi:10.1038/nature10199 PMID - 21753849 (2011).
- 6 Liu, K. *et al.* PTEN deletion enhances the regenerative ability of adult corticospinal neurons. *Nat Neurosci* **13**, 1075-1081, doi:10.1038/nn.2603 PMID - 20694004 (2010).
- 7 Godwin, J., Kuraitis, D. & Rosenthal, N. Extracellular matrix considerations for scar-free repair and regeneration: Insights from regenerative diversity among vertebrates. *Int J Biochem Cell Biology* **56**, 47-55, doi:10.1016/j.biocel.2014.10.011 PMID - 25450455 (2014).
- 8 Gonzalez-Perez, F., Udina, E. & Navarro, X. Chapter Ten Extracellular Matrix Components in Peripheral Nerve Regeneration. *Int Rev Neurobiol* **108**, 257-275, doi:10.1016/b978-0-12-410499-0.00010-1 PMID - 24083438 (2013).
- 9 Joosten, E. A. J., Bär, P. R. & Gispen, W. H. Collagen implants and cortico-spinal axonal growth after mid-thoracic spinal cord lesion in the adult rat. *J Neurosci Res* **41**, 481-490, doi:10.1002/jnr.490410407 PMID - 7473879 (1995).
- 10 Deister, C., Aljabari, S. & Schmidt, C. E. Effects of collagen 1, fibronectin, laminin and hyaluronic acid concentration in multi-component gels on neurite extension. *J Biomaterials Sci Polym Ed* **18**, 983-997, doi:10.1163/156856207781494377 PMID - 17705994 (2007).
- 11 Wanner, I. B. *et al.* Glial Scar Borders Are Formed by Newly Proliferated, Elongated Astrocytes That Interact to Corral Inflammatory and Fibrotic Cells via STAT3-Dependent Mechanisms after Spinal Cord Injury. *J Neurosci* **33**, 12870-12886, doi:10.1523/jneurosci.2121-13.2013 PMID - 23904622 (2013).
- 12 Waller, A. Experiments on the section of the glossopharyngeal and hypoglossal nerves of the frog, and observations of the alterations produced thereby in the structure of their primitive fibres. *Abstr Pap Commun Royal Soc Lond* **140**, 924-925, doi:10.1098/rspl.1843.0224 (1851).
- 13 Hon, A. J. & Kraus, P. Spasticity Management After Spinal Cord Injury. *Current Physical Medicine and Rehabilitation Reports* **8**, 159-171, doi:10.1007/s40141-020-00280-6 (2020).

- 14 Rabchevsky, A. G. & Kitzman, P. H. Latest approaches for the treatment of spasticity and autonomic dysreflexia in chronic spinal cord injury. *Neurotherapeutics* **8**, 274-282, doi:10.1007/s13311-011-0025-5 (2011).
- 15 Oyinbo, C. A. Secondary injury mechanisms in traumatic spinal cord injury: a nugget of this multiply cascade. PMID - 21731081. *Acta Neurobiol Exp* **71**, 281-299 (2011).
- 16 Beck, K. D. *et al.* Quantitative analysis of cellular inflammation after traumatic spinal cord injury: evidence for a multiphasic inflammatory response in the acute to chronic environment. *Brain* **133**, 433-447, doi:10.1093/brain/awp322 PMID - 20085927 (2010).
- 17 Sroga, J. M., Jones, T. B., Kigerl, K. A., McGaughy, V. M. & Popovich, P. G. Rats and mice exhibit distinct inflammatory reactions after spinal cord injury. *J Comp Neurol* **462**, 223-240, doi:10.1002/cne.10736 PMID - 12794745 (2003).
- 18 Fleming, J. C. *et al.* The cellular inflammatory response in human spinal cords after injury. *Brain* **129**, 3249-3269, doi:10.1093/brain/awl296 PMID - 17071951 (2006).
- 19 Soderblom, C. *et al.* Perivascular Fibroblasts Form the Fibrotic Scar after Contusive Spinal Cord Injury. *J Neurosci* **33**, 13882-13887, doi:10.1523/jneurosci.2524-13.2013 PMID - 23966707 (2013).
- 20 Göritz, C. *et al.* A Pericyte Origin of Spinal Cord Scar Tissue. *Science* **333**, 238-242, doi:10.1126/science.1203165 PMID - 21737741 (2011).
- 21 Plemel, J. R. *et al.* A Graded Forceps Crush Spinal Cord Injury Model in Mice. *J Neurotraum* **25**, 350-370, doi:10.1089/neu.2007.0426 PMID - 18373484 (2008).
- 22 Basso, D. M., Beattie, M. S. & Bresnahan, J. C. Graded Histological and Locomotor Outcomes after Spinal Cord Contusion Using the NYU Weight-Drop Device versus Transection. *Exp Neurol* **139**, 244-256, doi:10.1006/exnr.1996.0098 PMID - 8654527 (1996).
- 23 Gruner, J. A., Yee, A. K. & Blight, A. R. Histological and functional evaluation of experimental spinal cord injury: evidence of a stepwise response to graded compression. *Brain Res* **729**, 90-101, doi:10.1016/0006-8993(96)00366-6 PMID - 8874880 (1996).
- 24 Kloos, A. D., Fisher, L. C., Detloff, M. R., Hassenzahl, D. L. & Basso, D. M. Stepwise motor and all-or-none sensory recovery is associated with nonlinear sparing after incremental spinal cord injury in rats. *Exp Neurol* **191**, 251-265, doi:10.1016/j.expneurol.2004.09.016 PMID - 15649480 (2005).
- 25 Ghasemlou, N., Kerr, B. J. & David, S. Tissue displacement and impact force are important contributors to outcome after spinal cord contusion injury. *Exp Neurol* **196**, 9-17, doi:10.1016/j.expneurol.2005.05.017 PMID - 16023101 (2005).
- 26 Lemmon, V. What does “Disruptive” mean? Thoughts on the NIH SCI 2020 meeting. *Neural Regen Res* **14**, 1527, doi:10.4103/1673-5374.255969 PMID - 31089050 (2019).
- 27 LaPlaca, M. C., Simon, C. M., Prado, G. R. & Cullen, D. K. CNS injury biomechanics and experimental models. *Prog Brain Res* **161**, 13-26, doi:10.1016/s0079-6123(06)61002-9 PMID - 17618967 (2007).
- 28 Chen, K. *et al.* Differential Histopathological and Behavioral Outcomes Eight Weeks after Rat Spinal Cord Injury by Contusion, Dislocation, and Distraction

- Mechanisms. *J Neurotraum* **33**, 1667-1684, doi:10.1089/neu.2015.4218 PMID - 26671448 (2016).
- 29 Swartz, K. R., Scheff, N. N., Roberts, K. N. & Fee, D. B. Exacerbation of spinal cord injury due to static compression occurring early after onset. *J Neurosurg Spine* **11**, 570-574, doi:10.3171/2009.5.spine08588 PMID - 19929360 (2009).
 - 30 Biase, A. D. *et al.* Gene expression profiling of experimental traumatic spinal cord injury as a function of distance from impact site and injury severity. *Physiol Genomics* **22**, 368-381, doi:10.1152/physiolgenomics.00081.2005 PMID - 15942019 (2005).
 - 31 Choo, A. M., Liu, J., Dvorak, M., Tetzlaff, W. & Oxland, T. R. Secondary pathology following contusion, dislocation, and distraction spinal cord injuries. *Exp Neurol* **212**, 490-506, doi:10.1016/j.expneurol.2008.04.038 PMID - 18561916 (2008).
 - 32 Bloom, O. Non-mammalian model systems for studying neuro-immune interactions after spinal cord injury. *Exp Neurol* **258**, 130-140, doi:10.1016/j.expneurol.2013.12.023 PMID - 25017894 (2014).
 - 33 Brant, J. O., Yoon, J. H., Polvadore, T., Barbazuk, W. B. & Maden, M. Cellular events during scar-free skin regeneration in the spiny mouse, *Acomys*. *Wound Repair Regen* **24**, 75-88, doi:10.1111/wrr.12385 PMID - 26606280 (2016).
 - 34 Gawriluk, T. R. *et al.* Comparative analysis of ear-hole closure identifies epimorphic regeneration as a discrete trait in mammals. *Nat Commun* **7**, 11164, doi:10.1038/ncomms11164 PMID - 27109826 (2016).
 - 35 Santos, D. M. *et al.* Ear wound regeneration in the African spiny mouse *Acomys cahirinus*. *Regen* **3**, 52-61, doi:10.1002/reg2.50 PMID - 27499879 (2016).
 - 36 Maden, M. *et al.* Perfect chronic skeletal muscle regeneration in adult spiny mice, *Acomys cahirinus*. *Sci Rep-uk* **8**, 8920, doi:10.1038/s41598-018-27178-7 PMID - 29892004 (2018).
 - 37 Okamura, D. M. *et al.* Scarless repair of acute and chronic kidney injury in African Spiny mice (*Acomys cahirinus*). *Biorxiv*, 315069, doi:10.1101/315069 (2018).
 - 38 Simkin, J., Gawriluk, T. R., Gensel, J. C. & Seifert, A. W. Macrophages are necessary for epimorphic regeneration in African spiny mice. *Elife* **6**, e24623, doi:10.7554/elife.24623 PMID - 28508748 (2017).
 - 39 Shechter, R. & Schwartz, M. CNS sterile injury: just another wound healing? *Trends Mol Med* **19**, 135-143, doi:10.1016/j.molmed.2012.11.007 PMID - 23279948 (2012).
 - 40 Gurtner, G. C., Werner, S., Barrandon, Y. & Longaker, M. T. Wound repair and regeneration. *Nature* **453**, 314-321, doi:10.1038/nature07039 PMID - 18480812 (2008).
 - 41 David, S. & Kroner, A. Neural Regeneration. *Sect Iv Neural Regen Cns*, 245-261, doi:10.1016/b978-0-12-801732-6.00016-1 (2015).
 - 42 Stokes, B. T. & Jakeman, L. B. Experimental modelling of human spinal cord injury: a model that crosses the species barrier and mimics the spectrum of human cytopathology. *Spinal Cord* **40**, 101-109, doi:10.1038/sj.sc.3101254 PMID - 11859436 (2002).

- 43 Seifert, A. W. *et al.* Skin shedding and tissue regeneration in African spiny mice (Acomys). *Nature* **489**, 561-565, doi:10.1038/nature11499 PMID - 23018966 (2012).
- 44 Eldahan, K. C. & Rabchevsky, A. G. Autonomic dysreflexia after spinal cord injury: Systemic pathophysiology and methods of management. *Autonomic Neurosci* **209**, 59-70, doi:10.1016/j.autneu.2017.05.002 PMID - 28506502 (2018).
- 45 Krause, J. S., Cao, Y. & Clark, J. M. R. Pain Intensity, Interference, and Medication Use After Spinal Cord Injury: Association With Risk of Mortality After Controlling for Socioeconomic and Other Health Factors. *Arch Phys Med Rehabil* **98**, 2464-2470, doi:10.1016/j.apmr.2017.05.024 (2017).
- 46 Lo, C., Tran, Y., Anderson, K., Craig, A. & Middleton, J. Functional Priorities in Persons with Spinal Cord Injury: Using Discrete Choice Experiments To Determine Preferences. *J Neurotraum* **33**, 1958-1968, doi:10.1089/neu.2016.4423 PMID - 27080545 (2016).
- 47 Fowler, C. J., Griffiths, D. & de Groat, W. C. The neural control of micturition. *Nat Rev Neurosci* **9**, 453-466, doi:10.1038/nrn2401 (2008).
- 48 Taweel, W. A. & Seyam, R. Neurogenic bladder in spinal cord injury patients. *Res Rep Urol* **7**, 85-99, doi:10.2147/RRU.S29644 (2015).
- 49 Ruffion, A. *et al.* Systematic review of the epidemiology of urinary incontinence and detrusor overactivity among patients with neurogenic overactive bladder. *Neuroepidemiology* **41**, 146-155, doi:10.1159/000353274 (2013).
- 50 Hicken, B. L., Putzke, J. D. & Richards, J. S. Bladder Management and Quality of Life After Spinal Cord Injury. *Am J Phys Med Rehab* **80**, 916-922, doi:10.1097/00002060-200112000-00008 PMID - 11821674 (2001).
- 51 Roberts, T. T., Leonard, G. R. & Cepela, D. J. Classifications In Brief: American Spinal Injury Association (ASIA) Impairment Scale. *Clin Orthop Relat Res* **475**, 1499-1504, doi:10.1007/s11999-016-5133-4 PMID - 27815685 (2017).
- 52 Gundogdu, I., Akyuz, M., Ozturk, E. A. & Cakci, F. A. Can spinal cord injury patients show a worsening in ASIA impairment scale classification despite actually having neurological improvement? The limitation of ASIA Impairment Scale Classification. *Spinal Cord* **52**, 667-670, doi:10.1038/sc.2014.89 (2014).
- 53 Basso, D. M., Beattie, M. S. & Bresnahan, J. C. A Sensitive and Reliable Locomotor Rating Scale for Open Field Testing in Rats. *J Neurotraum* **12**, 1-21, doi:10.1089/neu.1995.12.1 PMID - 7783230 (1995).
- 54 Basso, D. M. *et al.* Basso Mouse Scale for Locomotion Detects Differences in Recovery after Spinal Cord Injury in Five Common Mouse Strains. *J Neurotraum* **23**, 635-659, doi:10.1089/neu.2006.23.635 PMID - 16689667 (2006).
- 55 Barth, A. M., Domonkos, A., Fernandez-Ruiz, A., Freund, T. F. & Varga, V. Hippocampal Network Dynamics during Rearing Episodes. *Cell Rep* **23**, 1706-1715, doi:10.1016/j.celrep.2018.04.021 (2018).
- 56 Formento, E. *et al.* Electrical spinal cord stimulation must preserve proprioception to enable locomotion in humans with spinal cord injury. *Nat Neurosci* **21**, 1728-1741, doi:10.1038/s41593-018-0262-6 PMID - 30382196 (2018).
- 57 Takeoka, A. & Arber, S. Functional Local Proprioceptive Feedback Circuits Initiate and Maintain Locomotor Recovery after Spinal Cord Injury. *Cell Rep* **27**, 71-85 e73, doi:10.1016/j.celrep.2019.03.010 (2019).

- 58 Covarrubias-Escudero, F., Rivera-Lillo, G., Torres-Castro, R. & Varas-Diaz, G. Effects of body weight-support treadmill training on postural sway and gait independence in patients with chronic spinal cord injury. *J Spinal Cord Med* **42**, 57-64, doi:10.1080/10790268.2017.1389676 (2019).
- 59 Houghton, C. L., Gawriluk, T. R. & Seifert, A. W. The Biology and Husbandry of the African Spiny Mouse (*Acomys cahirinus*) and the Research Uses of a Laboratory Colony. *J Am Assoc Laboratory Animal Sci Jaalas* **55**, 9-17 (2016).
- 60 Kadekawa, K. *et al.* Characterization of bladder and external urethral activity in mice with or without spinal cord injury--a comparison study with rats. *Am J Physiol Regul Integr Comp Physiol* **310**, R752-758, doi:10.1152/ajpregu.00450.2015 (2016).
- 61 Streeter, K. A. *et al.* Molecular and histologic outcomes following spinal cord injury in spiny mice, *Acomys cahirinus*. *J Comp Neurol* **528**, 1535-1547, doi:10.1002/cne.24836 PMID - 31820438 (2020).
- 62 Basso, D. M. *et al.* Basso Mouse Scale for Locomotion Detects Differences in Recovery after Spinal Cord Injury in Five Common Mouse Strains. **23**, 635-659, doi:10.1089/neu.2006.23.635 PMID - 16689667 (2006).
- 63 Fouad, K., Popovich, P. G., Kopp, M. A. & Schwab, J. M. The neuroanatomical-functional paradox in spinal cord injury. *Nat Rev Neurol* **17**, 53-62, doi:10.1038/s41582-020-00436-x (2021).
- 64 Tator, C. H. & Fehlings, M. G. Review of the secondary injury theory of acute spinal cord trauma with emphasis on vascular mechanisms. *J Neurosurg* **75**, 15-26, doi:10.3171/jns.1991.75.1.0015 PMID - 2045903 (1991).
- 65 Beal, M. F. Mechanisms of excitotoxicity in neurologic diseases. *Faseb J* **6**, 3338-3344, doi:10.1096/fasebj.6.15.1464368 PMID - 1464368 (1992).
- 66 Liddelow, S. A. *et al.* Neurotoxic reactive astrocytes are induced by activated microglia. *Nature* **541**, 481-487, doi:10.1038/nature21029 PMID - 28099414 (2017).
- 67 Eftekharpour, E. *et al.* Myelination of Congenitally Dysmyelinated Spinal Cord Axons by Adult Neural Precursor Cells Results in Formation of Nodes of Ranvier and Improved Axonal Conduction. *J Neurosci* **27**, 3416-3428, doi:10.1523/jneurosci.0273-07.2007 PMID - 17392458 (2007).
- 68 Hagg, T. & Oudega, M. Degenerative and Spontaneous Regenerative Processes after Spinal Cord Injury. *J Neurotraum* **23**, 263-280, doi:10.1089/neu.2006.23.263 PMID - 16629615 (2006).
- 69 Rabchevsky, A. G., Fugaccia, I., Sullivan, P. G. & Scheff, S. W. Cyclosporin A Treatment Following Spinal Cord Injury to the Rat: Behavioral Effects and Stereological Assessment of Tissue Sparing. **18**, 513-522, doi:10.1089/089771501300227314 PMID - 11393254 (2001).
- 70 Orr, M. B. *et al.* Compression Decreases Anatomical and Functional Recovery and Alters Inflammation after Contusive Spinal Cord Injury. *J Neurotraum* **34**, 2342-2352, doi:10.1089/neu.2016.4915 PMID - 28381129 (2017).
- 71 Zhang, B. *et al.* Azithromycin drives alternative macrophage activation and improves recovery and tissue sparing in contusion spinal cord injury. *J Neuroinflamm* **12**, 218, doi:10.1186/s12974-015-0440-3 PMID - 26597676 (2015).

- 72 Anderson, M. A. *et al.* Astrocyte scar formation aids central nervous system axon regeneration. *Nature* **532**, 195-200, doi:10.1038/nature17623 PMID - 27027288 (2016).
- 73 Yuan, A., Rao, M. V., Veeranna & Nixon, R. A. Neurofilaments at a glance. *J Cell Sci* **125**, 3257-3263, doi:10.1242/jcs.104729 PMID - 22956720 (2012).
- 74 Ghosh, M. & Pearse, D. D. The role of the serotonergic system in locomotor recovery after spinal cord injury. *Front Neural Circuits* **8**, 151, doi:10.3389/fncir.2014.00151 (2014).
- 75 Rajaoetra, N., Sandillon, F., Geffard, M. & Privat, A. Pre- and post-natal ontogeny of serotonergic projections to the rat spinal cord. *J Neurosci Res* **22**, 305-321, doi:10.1002/jnr.490220311 PMID - 2709447 (1989).
- 76 Hornung, J. P. The human raphe nuclei and the serotonergic system. *J Chem Neuroanat* **26**, 331-343, doi:10.1016/j.jchemneu.2003.10.002 (2003).
- 77 Martin, G. F., Cabana, T. & Humbertson, A. O. Evidence for collateral innervation of the cervical and lumbar enlargements of the spinal cord by single reticular and raphe neurons. Studies using fluorescent markers in double-labeling experiments on the North American opossum. *Neurosci Lett* **24**, 1-6, doi:[https://doi.org/10.1016/0304-3940\(81\)90349-9](https://doi.org/10.1016/0304-3940(81)90349-9) (1981).
- 78 Kiehn, O. & Kullander, K. Central Pattern Generators Deciphered by Molecular Genetics. *Neuron* **41**, 317-321, doi:10.1016/s0896-6273(04)00042-x PMID - 14766172 (2004).
- 79 McKillop, W. M., Dragan, M., Schedl, A. & Brown, A. Conditional Sox9 ablation reduces chondroitin sulfate proteoglycan levels and improves motor function following spinal cord injury. *Glia* **61**, 164-177, doi:10.1002/glia.22424 PMID - 23027386 (2012).
- 80 Geremia, N. M. *et al.* CD11d Antibody Treatment Improves Recovery in Spinal Cord-Injured Mice. *J Neurotraum* **29**, 539-550, doi:10.1089/neu.2011.1976 PMID - 22044160 (2012).
- 81 Zhou, H., Liu, Y., Sun, L., Fu, M. & Zhao, Y. Salvianolic acid B activates Wnt/beta-catenin signaling following spinal cord injury. *Exp Ther Med* **19**, 825-832, doi:10.3892/etm.2019.8292 (2020).
- 82 Chen, H. S., Holmes, N., Liu, J., Tetzlaff, W. & Kozlowski, P. Validating myelin water imaging with transmission electron microscopy in a rat spinal cord injury model. *Neuroimage* **153**, 122-130, doi:10.1016/j.neuroimage.2017.03.065 (2017).
- 83 Vedantam, A. *et al.* Diffusion tensor imaging of the spinal cord: insights from animal and human studies. *Neurosurgery* **74**, 1-8; discussion 8; quiz 8, doi:10.1227/NEU.0000000000000171 (2014).
- 84 Guest, J. D., Hiester, E. D. & Bunge, R. P. Demyelination and Schwann cell responses adjacent to injury epicenter cavities following chronic human spinal cord injury. *Exp Neurol* **192**, 384-393, doi:10.1016/j.expneurol.2004.11.033 PMID - 15755556 (2005).
- 85 Beattie, M. S. *et al.* Endogenous Repair after Spinal Cord Contusion Injuries in the Rat. *Exp Neurol* **148**, 453-463, doi:10.1006/exnr.1997.6695 PMID - 9417825 (1997).

- 86 Inman, D. M. & Steward, O. Physical Size Does Not Determine the Unique Histopathological Response Seen in the Injured Mouse Spinal Cord. *J Neurotraum* **20**, 33-42, doi:10.1089/08977150360517164 PMID - 12614586 (2003).
- 87 Hayes, K. C. & Kakulas, B. A. Neuropathology of Human Spinal Cord Injury Sustained in Sports-related Activities. *J Neurotraum* **14**, 235-248, doi:10.1089/neu.1997.14.235 PMID - 9151772 (1997).
- 88 Zhang, Z., Fujiki, M., Guth, L. & Steward, O. Genetic influences on cellular reactions to spinal cord injury: A wound-healing response present in normal mice is impaired in mice carrying a mutation (WldS) that causes delayed Wallerian degeneration. *J Comp Neurology* **371**, 485-495, doi:10.1002/(sici)1096-9861(19960729)371:3<485::aid-cne10>3.0.co;2-i PMID - 8842901 (1996).
- 89 Forgiione, N. *et al.* Bilateral Contusion-Compression Model of Incomplete Traumatic Cervical Spinal Cord Injury. *J Neurotraum* **31**, 1776-1788, doi:10.1089/neu.2014.3388 PMID - 24949719 (2014).
- 90 Stewart, A. N. *et al.* Transplantation of mesenchymal stem cells that overexpress NT-3 produce motor improvements without axonal regeneration following complete spinal cord transections in rats. *Brain Res* **1699**, 19-33, doi:10.1016/j.brainres.2018.06.002 (2018).
- 91 Sipski, M. L., Jackson, A. B., Gomez-Marin, O., Estores, I. & Stein, A. Effects of gender on neurologic and functional recovery after spinal cord injury. *Arch Phys Med Rehabil* **85**, 1826-1836, doi:10.1016/j.apmr.2004.04.031 (2004).
- 92 Kostyk, S. K., Popovich, P. G., Stokes, B. T., Wei, P. & Jakeman, L. B. Robust axonal growth and a blunted macrophage response are associated with impaired functional recovery after spinal cord injury in the MRL/MpJ mouse. *Neuroscience* **156**, 498-514, doi:10.1016/j.neuroscience.2008.08.013 PMID - 18786615 (2008).
- 93 Thuret, S., Thallmair, M., Horky, L. L. & Gage, F. H. Enhanced Functional Recovery in MRL/MpJ Mice after Spinal Cord Dorsal Hemisection. *Plos One* **7**, e30904, doi:10.1371/journal.pone.0030904 PMID - 22348029 (2012).
- 94 Hesp, Z. C., Goldstein, E. A., Miranda, C. J., Kaspar, B. K. & McTigue, D. M. Chronic Oligodendrogenesis and Remyelination after Spinal Cord Injury in Mice and Rats. *J Neurosci* **35**, 1274-1290, doi:10.1523/jneurosci.2568-14.2015 PMID - 25609641 (2015).
- 95 Juliet, P. A., Frost, E. E., Balasubramaniam, J. & Del Bigio, M. R. Toxic effect of blood components on perinatal rat subventricular zone cells and oligodendrocyte precursor cell proliferation, differentiation and migration in culture. *J Neurochem* **109**, 1285-1299, doi:10.1111/j.1471-4159.2009.06060.x (2009).
- 96 Wang, G. *et al.* Microglia/Macrophage Polarization Dynamics in White Matter after Traumatic Brain Injury. *J Cereb Blood Flow Metabolism* **33**, 1864-1874, doi:10.1038/jcbfm.2013.146 PMID - 23942366 (2013).
- 97 Ren, Y. & Young, W. Managing inflammation after spinal cord injury through manipulation of macrophage function. *Neural Plast* **2013**, 945034, doi:10.1155/2013/945034 PMID - 24288627 (2013).
- 98 Chun, S. J., Rasband, M. N., Sidman, R. L., Habib, A. A. & Vartanian, T. Integrin-linked kinase is required for laminin-2-induced oligodendrocyte cell spreading and CNS myelination. *J Cell Biology* **163**, 397-408, doi:10.1083/jcb.200304154 PMID - 14581460 (2003).

- 99 Buttery, P. C. & French-Constant, C. Laminin-2/Integrin Interactions Enhance Myelin Membrane Formation by Oligodendrocytes. *Mol Cell Neurosci* **14**, 199-212, doi:10.1006/mcne.1999.0781 PMID - 10576890 (1999).
- 100 Hinks, G. L. & Franklin, R. J. M. Distinctive Patterns of PDGF-A, FGF-2, IGF-I, and TGF- β 1 Gene Expression during Remyelination of Experimentally-Induced Spinal Cord Demyelination. *Mol Cell Neurosci* **14**, 153-168, doi:10.1006/mcne.1999.0771 PMID - 10532806 (1999).
- 101 Jiang, F., Frederick, T. J. & Wood, T. L. IGF-I Synergizes with FGF-2 to Stimulate Oligodendrocyte Progenitor Entry into the Cell Cycle. *Dev Biol* **232**, 414-423, doi:10.1006/dbio.2001.0208 PMID - 11401402 (2001).
- 102 Maegele, M., Miller, S., Wernig, A., Edgerton, V. R. & Harkema, S. J. Recruitment of Spinal Motor Pools during Voluntary Movements versus Stepping after Human Spinal Cord Injury. *J Neurotraum* **19**, 1217-1229, doi:10.1089/08977150260338010 PMID - 12427330 (2002).
- 103 Wilcox, J. T. *et al.* Generating level-dependent models of cervical and thoracic spinal cord injury: Exploring the interplay of neuroanatomy, physiology, and function. *Neurobiol Dis* **105**, 194-212, doi:10.1016/j.nbd.2017.05.009 PMID - 28578003 (2017).
- 104 Muir, G. D. & Webb, A. A. Assessment of behavioural recovery following spinal cord injury in rats. *Eur J Neurosci* **12**, 3079-3086, doi:10.1046/j.1460-9568.2000.00205.x PMID - 10998091 (2000).
- 105 Wheaton, B. J., Callaway, J. K., Ek, C. J., Dziegielewska, K. M. & Saunders, N. R. Spontaneous Development of Full Weight-Supported Stepping after Complete Spinal Cord Transection in the Neonatal Opossum, *Monodelphis domestica*. *Plos One* **6**, e26826, doi:10.1371/journal.pone.0026826 PMID - 22073202 (2011).
- 106 Norenberg, M. D., Smith, J. & Marcillo, A. The Pathology of Human Spinal Cord Injury: Defining the Problems. *J Neurotraum* **21**, 429-440, doi:10.1089/089771504323004575 PMID - 15115592 (2004).
- 107 Gensel, J. C. & Zhang, B. Macrophage activation and its role in repair and pathology after spinal cord injury. *Brain Res* **1619**, 1-11, doi:10.1016/j.brainres.2014.12.045 PMID - 25578260 (2015).
- 108 Kigerl, K. A. *et al.* Identification of Two Distinct Macrophage Subsets with Divergent Effects Causing either Neurotoxicity or Regeneration in the Injured Mouse Spinal Cord. *J Neurosci* **29**, 13435-13444, doi:10.1523/jneurosci.3257-09.2009 PMID - 19864556 (2009).
- 109 Novak, M. L. & Koh, T. J. Phenotypic transitions of macrophages orchestrate tissue repair. *Am J Pathology* **183**, 1352-1363, doi:10.1016/j.ajpath.2013.06.034 PMID - 24091222 (2013).
- 110 Greaves, N. S., Ashcroft, K. J., Baguneid, M. & Bayat, A. Current understanding of molecular and cellular mechanisms in fibroplasia and angiogenesis during acute wound healing. *J Dermatol Sci* **72**, 206-217, doi:10.1016/j.jdermsci.2013.07.008 PMID - 23958517 (2013).
- 111 Kigerl, K. A. & Popovich, P. G. Current Topics in Microbiology and Immunology. *Curr Top Microbiol* **336**, 121-136, doi:10.1007/978-3-642-00549-7_7 PMID - 19688331 (2009).

- 112 Kigerl, K. A., Vaccari, J. P. d. R., Dietrich, W. D., Popovich, P. G. & Keane, R. W. Pattern recognition receptors and central nervous system repair. *Exp Neurol* **258**, 5-16, doi:10.1016/j.expneurol.2014.01.001 PMID - 25017883 (2014).
- 113 Sofroniew, M. V. Molecular dissection of reactive astrogliosis and glial scar formation. *Trends Neurosci* **32**, 638-647, doi:10.1016/j.tins.2009.08.002 PMID - 19782411 (2009).
- 114 David, S. & Kroner, A. Repertoire of microglial and macrophage responses after spinal cord injury. *Nat Rev Neurosci* **12**, 388-399, doi:10.1038/nrn3053 PMID - 21673720 (2011).
- 115 Guerrero, A. R. *et al.* Blockade of interleukin-6 signaling inhibits the classic pathway and promotes an alternative pathway of macrophage activation after spinal cord injury in mice. *J Neuroinflamm* **9**, doi:10.1186/1742-2094-9-40 (2012).
- 116 Schnell, L., Fearn, S., Schwab, M. E., Perry, V. H. & Anthony, D. C. Cytokine-induced Acute Inflammation in the Brain and Spinal Cord. *J Neuropath Exp Neurol* **58**, 245-254, doi:10.1097/00005072-199903000-00004 PMID - 10197816 (1999).
- 117 Bao, F., Chen, Y., Schneider, K. A. & Weaver, L. C. An integrin inhibiting molecule decreases oxidative damage and improves neurological function after spinal cord injury. *Exp Neurol* **214**, 160-167, doi:10.1016/j.expneurol.2008.09.006 PMID - 18926823 (2008).
- 118 Donnelly, D. J. *et al.* Deficient CX3CR1 Signaling Promotes Recovery after Mouse Spinal Cord Injury by Limiting the Recruitment and Activation of Ly6Clo/iNOS+ Macrophages. *J Neurosci* **31**, 9910-9922, doi:10.1523/jneurosci.2114-11.2011 PMID - 21734283 (2011).
- 119 Mabon, P. J., Weaver, L. C. & Dekaban, G. A. Inhibition of Monocyte/Macrophage Migration to a Spinal Cord Injury Site by an Antibody to the Integrin α D: A Potential New Anti-inflammatory Treatment. *Exp Neurol* **166**, 52-64, doi:10.1006/exnr.2000.7488 PMID - 11031083 (2000).
- 120 Carlson, S. L., Parrish, M. E., Springer, J. E., Doty, K. & Dossett, L. Acute Inflammatory Response in Spinal Cord Following Impact Injury. *Exp Neurol* **151**, 77-88, doi:10.1006/exnr.1998.6785 PMID - 9582256 (1998).
- 121 Taoka, Y. *et al.* Role of neutrophils in spinal cord injury in the rat. *Neuroscience* **79**, 1177-1182, doi:10.1016/s0306-4522(97)00011-0 PMID - 9219976 (1997).
- 122 Yang, L. *et al.* Early Expression and Cellular Localization of Proinflammatory Cytokines Interleukin-1 β , Interleukin-6, and Tumor Necrosis Factor- α in Human Traumatic Spinal Cord Injury. *Spine* **29**, 966-971, doi:10.1097/00007632-200405010-00004 PMID - 15105666 (2004).
- 123 Kigerl, K. A., McGaughy, V. M. & Popovich, P. G. Comparative analysis of lesion development and intraspinal inflammation in four strains of mice following spinal contusion injury. *J Comp Neurology* **494**, 578-594, doi:10.1002/cne.20827 PMID - 16374800 (2005).
- 124 Kubota, K. *et al.* Myeloperoxidase Exacerbates Secondary Injury by Generating Highly Reactive Oxygen Species and Mediating Neutrophil Recruitment in Experimental Spinal Cord Injury. *Spine* **37**, 1363-1369, doi:10.1097/brs.0b013e31824b9e77 PMID - 22322369 (2012).

- 125 Castro, R. d. *et al.* Evidence that infiltrating neutrophils do not release reactive oxygen species in the site of spinal cord injury. *Exp Neurol* **190**, 414-424, doi:10.1016/j.expneurol.2004.05.046 PMID - 15530880 (2004).
- 126 Gensel, J. C. & Popovich, P. G. in *Traumatic Brain and Spinal Cord Injury* (eds C. Morganti-Kossmann, R. Raghupathi, & A. Maas) Ch. 23, 272-279 (Cambridge University Press, 2012).
- 127 Prüss, H. *et al.* Non-resolving aspects of acute inflammation after spinal cord injury (SCI): indices and resolution plateau. *Brain Pathology Zurich Switz* **21**, 652-660, doi:10.1111/j.1750-3639.2011.00488.x PMID - 21418368 (2011).
- 128 Schwab, J. M., Zhang, Y., Kopp, M. A., Brommer, B. & Popovich, P. G. The paradox of chronic neuroinflammation, systemic immune suppression, autoimmunity after traumatic chronic spinal cord injury. *Exp Neurol* **258**, 121-129, doi:10.1016/j.expneurol.2014.04.023 PMID - 25017893 (2014).
- 129 Donnelly, D. J. & Popovich, P. G. Inflammation and its role in neuroprotection, axonal regeneration and functional recovery after spinal cord injury. *Exp Neurol* **209**, 378-388, doi:10.1016/j.expneurol.2007.06.009 PMID - 17662717 (2008).
- 130 Chao, C. C., Hu, S., Molitor, T. W., Shaskan, E. G. & Peterson, P. K. Activated microglia mediate neuronal cell injury via a nitric oxide mechanism. *J Immunol Baltim Md 1950* **149**, 2736-2741 (1992).
- 131 Mawhinney, L. A. *et al.* Differential Detection and Distribution of Microglial and Hematogenous Macrophage Populations in the Injured Spinal Cord of lys-EGFP-ki Transgenic Mice. *J Neuropathology Exp Neurology* **71**, 180-197, doi:10.1097/nen.0b013e3182479b41 PMID - 22318123 (2012).
- 132 Greenhalgh, A. D. *et al.* Arginase-1 is expressed exclusively by infiltrating myeloid cells in CNS injury and disease. *Brain Behav Immun* **56**, 61-67, doi:10.1016/j.bbi.2016.04.013 PMID - 27126514 (2016).
- 133 Popovich, P. G. *et al.* Depletion of Hematogenous Macrophages Promotes Partial Hindlimb Recovery and Neuroanatomical Repair after Experimental Spinal Cord Injury. *Exp Neurol* **158**, 351-365, doi:10.1006/exnr.1999.7118 PMID - 10415142 (1999).
- 134 Shechter, R. *et al.* Infiltrating Blood-Derived Macrophages Are Vital Cells Playing an Anti-inflammatory Role in Recovery from Spinal Cord Injury in Mice. *Plos Med* **6**, e1000113, doi:10.1371/journal.pmed.1000113 PMID - 19636355 (2009).
- 135 Rabchevsky, A. G. & Streit, W. J. Grafting of cultured microglial cells into the lesioned spinal cord of adult rats enhances neurite outgrowth. *J Neurosci Res* **47**, 34-48, doi:10.1002/(sici)1097-4547(19970101)47:1<34::aid-jnr4>3.0.co;2-g PMID - 8981236 (1997).
- 136 Rapalino, O. *et al.* Implantation of stimulated homologous macrophages results in partial recovery of paraplegic rats. *Nat Med* **4**, 814-821, doi:10.1038/nm0798-814 PMID - 9662373 (1998).
- 137 Schwartz, M. & Yoles, E. Immune-Based Therapy for Spinal Cord Repair: Autologous Macrophages and Beyond. *J Neurotraum* **23**, 360-370, doi:10.1089/neu.2006.23.360 PMID - 16629622 (2006).
- 138 Boje, K. M. & Arora, P. K. Microglial-produced nitric oxide and reactive nitrogen oxides mediate neuronal cell death. *Brain Res* **587**, 250-256, doi:10.1016/0006-8993(92)91004-x PMID - 1381982 (1992).

- 139 Liu, B. & Hong, J.-S. Role of Microglia in Inflammation-Mediated Neurodegenerative Diseases: Mechanisms and Strategies for Therapeutic Intervention. *J Pharmacol Exp Ther* **304**, 1-7, doi:10.1124/jpet.102.035048 PMID - 12490568 (2003).
- 140 Hesketh, M., Sahin, K. B., West, Z. E. & Murray, R. Z. Macrophage Phenotypes Regulate Scar Formation and Chronic Wound Healing. *Int J Mol Sci* **18**, 1545, doi:10.3390/ijms18071545 PMID - 28714933 (2017).
- 141 McTigue, D. M., Popovich, P. G., Morgan, T. E. & Stokes, B. T. Localization of Transforming Growth Factor- β 1 and Receptor mRNA after Experimental Spinal Cord Injury. *Exp Neurol* **163**, 220-230, doi:10.1006/exnr.2000.7372 PMID - 10785461 (2000).
- 142 Buss, A. *et al.* TGF- β 1 and TGF- β 2 expression after traumatic human spinal cord injury. *Spinal Cord* **46**, 364-371, doi:10.1038/sj.sc.3102148 PMID - 18040277 (2008).
- 143 Stout, R. D. & Suttles, J. Functional plasticity of macrophages: reversible adaptation to changing microenvironments. *J Leukocyte Biol* **76**, 509-513, doi:10.1189/jlb.0504272 PMID - 15218057 (2004).
- 144 Novak, M. L. & Koh, T. J. Macrophage phenotypes during tissue repair. *J Leukocyte Biol* **93**, 875-881, doi:10.1189/jlb.1012512 PMID - 23505314 (2013).
- 145 Zhang, B., Bailey, W. M., McVicar, A. L. & Gensel, J. C. Age increases reactive oxygen species production in macrophages and potentiates oxidative damage after spinal cord injury. *Neurobiol Aging* **47**, 157-167, doi:10.1016/j.neurobiolaging.2016.07.029 PMID - 27596335 (2016).
- 146 Griot, C., Bürge, T., Vandeveld, M. & Peterhans, E. Antibody-induced generation of reactive oxygen radicals by brain macrophages in canine distemper encephalitis: a mechanism for bystander demyelination. *Acta Neuropathol* **78**, 396-403, doi:10.1007/bf00688176 PMID - 2782050 (1989).
- 147 Whetstone, W. D., Hsu, J. Y. C., Eisenberg, M., Werb, Z. & Noble-Haeusslein, L. J. Blood-spinal cord barrier after spinal cord injury: Relation to revascularization and wound healing. *J Neurosci Res* **74**, 227-239, doi:10.1002/jnr.10759 PMID - 14515352 (2003).
- 148 Schnell, L., Fearn, S., Klassen, H., Schwab, M. E. & Perry, V. H. Acute inflammatory responses to mechanical lesions in the CNS: differences between brain and spinal cord: Inflammatory responses in brain and spinal cord. *Eur J Neurosci* **11**, 3648-3658, doi:10.1046/j.1460-9568.1999.00792.x PMID - 10564372 (1999).
- 149 Gris, D. *et al.* Transient Blockade of the CD11d/CD18 Integrin Reduces Secondary Damage after Spinal Cord Injury, Improving Sensory, Autonomic, and Motor Function. *J Neurosci* **24**, 4043-4051, doi:10.1523/jneurosci.5343-03.2004 PMID - 15102919 (2004).
- 150 Aurora, A. B. *et al.* Macrophages are required for neonatal heart regeneration. *J Clin Invest* **124**, 1382-1392, doi:10.1172/jci72181 PMID - 24569380 (2014).
- 151 Godwin, J. W., Debuque, R., Salimova, E. & Rosenthal, N. A. Heart regeneration in the salamander relies on macrophage-mediated control of fibroblast activation and the extracellular landscape. *Npj Regen Medicine* **2**, 22, doi:10.1038/s41536-017-0027-y PMID - 29201433 (2017).

- 152 Godwin, J. W., Pinto, A. R. & Rosenthal, N. A. Macrophages are required for adult salamander limb regeneration. *Proc National Acad Sci* **110**, 9415-9420, doi:10.1073/pnas.1300290110 PMID - 23690624 (2013).
- 153 Shifman, M. I. & Selzer, M. E. Differential expression of Class 3 and 4 semaphorins and netrin in the lamprey spinal cord during regeneration. *J Comp Neurology* **501**, 631-646, doi:10.1002/cne.21283 PMID - 17278142 (2007).
- 154 Lau, B. Y. B., Fogerson, S. M., Walsh, R. B. & Morgan, J. R. Cyclic AMP promotes axon regeneration, lesion repair and neuronal survival in lampreys after spinal cord injury. *Exp Neurol* **250**, 31-42, doi:10.1016/j.expneurol.2013.09.004 PMID - 24041988 (2013).
- 155 Becker, T. & Becker, C. G. Regenerating descending axons preferentially reroute to the gray matter in the presence of a general macrophage/microglial reaction caudal to a spinal transection in adult zebrafish. *J Comp Neurology* **433**, 131-147, doi:10.1002/cne.1131 PMID - 11283955 (2001).
- 156 Zukor, K. A., Kent, D. T. & Odelberg, S. J. Meningeal cells and glia establish a permissive environment for axon regeneration after spinal cord injury in newts. *Neural Dev* **6**, 1, doi:10.1186/1749-8104-6-1 PMID - 21205291 (2011).
- 157 Shifman, M. I., Yumul, R. E., Laramore, C. & Selzer, M. E. Expression of the repulsive guidance molecule RGM and its receptor neogenin after spinal cord injury in sea lamprey. *Exp Neurol* **217**, 242-251, doi:10.1016/j.expneurol.2009.02.011 PMID - 19268666 (2009).
- 158 Kyritsis, N. *et al.* Acute inflammation initiates the regenerative response in the adult zebrafish brain. *Sci New York N Y* **338**, 1353-1356, doi:10.1126/science.1228773 PMID - 23138980 (2012).
- 159 Goldshmit, Y. *et al.* Blockage of Lysophosphatidic Acid Signaling Improves Spinal Cord Injury Outcomes. *Am J Pathology* **181**, 978-992, doi:10.1016/j.ajpath.2012.06.007 PMID - 22819724 (2012).
- 160 Kirkham, M., Berg, D. A. & Simon, A. Microglia activation during neuroregeneration in the adult vertebrate brain. *Neurosci Lett* **497**, 11-16, doi:10.1016/j.neulet.2011.04.007 PMID - 21515337 (2011).
- 161 Wynn, T. A., Chawla, A. & Pollard, J. W. Macrophage biology in development, homeostasis and disease. *Nature* **496**, 445-455, doi:10.1038/nature12034 PMID - 23619691 (2013).
- 162 Leskovar, A., Moriarty, L. J., Turek, J. J., Schoenlein, I. A. & Borgens, R. B. The macrophage in acute neural injury: changes in cell numbers over time and levels of cytokine production in mammalian central and peripheral nervous systems. *J Exp Biology* **203**, 1783-1795 (2000).
- 163 Hampton, D. W., Seitz, A., Chen, P., Heber-Katz, E. & Fawcett, J. W. Altered CNS response to injury in the MRL/MpJ mouse. *Neuroscience* **127**, 821-832, doi:10.1016/j.neuroscience.2004.05.057 PMID - 15312895 (2004).
- 164 Yoon, J. H., Cho, K., Garrett, T. J., Finch, P. & Maden, M. Comparative Proteomic Analysis in Scar-Free Skin Regeneration in *Acomys cahirinus* and Scarring *Mus musculus*. *Sci Rep-uk* **10**, 166, doi:10.1038/s41598-019-56823-y PMID - 31932597 (2020).
- 165 Brant, J. O., Lopez, M.-C., Baker, H. V., Barbazuk, W. B. & Maden, M. A Comparative Analysis of Gene Expression Profiles during Skin Regeneration in

- Mus and Acomys. *Plos One* **10**, e0142931, doi:10.1371/journal.pone.0142931 PMID - 26606282 (2015).
- 166 Brant, J. O. *et al.* Comparative transcriptomic analysis of dermal wound healing reveals de novo skeletal muscle regeneration in Acomys cahirinus. *Plos One* **14**, e0216228, doi:10.1371/journal.pone.0216228 PMID - 31141508 (2019).
- 167 Zhu, Y. *et al.* Hematogenous macrophage depletion reduces the fibrotic scar and increases axonal growth after spinal cord injury. *Neurobiol Dis* **74**, 114-125, doi:10.1016/j.nbd.2014.10.024 PMID - 25461258 (2015).
- 168 Gensel, J. C. *et al.* Macrophages Promote Axon Regeneration with Concurrent Neurotoxicity. *J Neurosci* **29**, 3956-3968, doi:10.1523/jneurosci.3992-08.2009 PMID - 19321792 (2009).
- 169 Lammertse, D. P. *et al.* Autologous incubated macrophage therapy in acute, complete spinal cord injury: results of the phase 2 randomized controlled multicenter trial. *Spinal Cord* **50**, 661-671, doi:10.1038/sc.2012.39 PMID - 22525310 (2012).
- 170 Zhang, B. *et al.* Macrolide derivatives reduce proinflammatory macrophage activation and macrophage-mediated neurotoxicity. *Cns Neurosci Ther* **25**, 591-600, doi:10.1111/cns.13092 PMID - 30677254 (2019).
- 171 Longbrake, E. E., Lai, W., Ankeny, D. P. & Popovich, P. G. Characterization and modeling of monocyte-derived macrophages after spinal cord injury. *J Neurochem* **102**, 1083-1094, doi:10.1111/j.1471-4159.2007.04617.x PMID - 17663750 (2007).
- 172 Ghassabeh, G. H. *et al.* Identification of a common gene signature for type II cytokine-associated myeloid cells elicited in vivo in different pathologic conditions. *Blood* **108**, 575-583, doi:10.1182/blood-2005-04-1485 PMID - 16556895 (2006).
- 173 Gensel, J. C. & Orr, M. B. Reflections on Data Sharing Practices in Spinal Cord Injury Research. *Neuroinformatics*, doi:10.1007/s12021-020-09498-0 (2021).
- 174 Bracken, M. B. *et al.* Administration of Methylprednisolone for 24 or 48 Hours or Tirilazad Mesylate for 48 Hours in the Treatment of Acute Spinal Cord Injury. *Surv Anesthesiol* **42**, 197, doi:10.1097/00132586-199808000-00011 (1998).
- 175 Lawrence, T. & Gilroy, D. W. Chronic inflammation: a failure of resolution? *Int J Exp Pathol* **88**, 85-94, doi:10.1111/j.1365-2613.2006.00507.x (2007).
- 176 Serhan, C. N. *et al.* Resolution of inflammation: state of the art, definitions and terms. *Faseb J* **21**, 325-332, doi:10.1096/fj.06-7227rev (2007).
- 177 Francos-Quijorna, I. *et al.* Maresin 1 Promotes Inflammatory Resolution, Neuroprotection, and Functional Neurological Recovery After Spinal Cord Injury. *J Neurosci* **37**, 11731-11743, doi:10.1523/JNEUROSCI.1395-17.2017 (2017).
- 178 Basso, D. M. Neuroanatomical Substrates of Functional Recovery After Experimental Spinal Cord Injury: Implications of Basic Science Research for Human Spinal Cord Injury. *Phys Ther* **80**, 808-817, doi:10.1093/ptj/80.8.808 PMID - 10911417 (2000).
- 179 Grossman, S. D., Rosenberg, L. J. & Wrathall, J. R. Temporal-Spatial Pattern of Acute Neuronal and Glial Loss after Spinal Cord Contusion. *Exp Neurol* **168**, 273-282, doi:10.1006/exnr.2001.7628 PMID - 11259115 (2001).
- 180 Keirstead, H. S. & Blakemore, W. F. Identification of Post-mitotic Oligodendrocytes Incapable of Remyelination within the Demyelinated Adult

- Spinal Cord. *J Neuropathology Exp Neurology* **56**, 1191-1201, doi:10.1097/00005072-199711000-00003 PMID - 9370229 (1997).
- 181 Tripathi, R. & McTigue, D. M. Prominent oligodendrocyte genesis along the border of spinal contusion lesions. *Glia* **55**, 698-711, doi:10.1002/glia.20491 PMID - 17330874 (2007).
- 182 Renault-Mihara, F. *et al.* Regulation of RhoA by STAT3 coordinates glial scar formation. STAT3-regulated RhoA drives glial scar formation. *J Cell Biology* **216**, 2533-2550, doi:10.1083/jcb.201610102 PMID - 28642362 (2017).
- 183 Bruce, J. H. *et al.* Schwannosis: Role of Gliosis and Proteoglycan in Human Spinal Cord Injury. *J Neurotraum* **17**, 781-788, doi:10.1089/neu.2000.17.781 PMID - 11011818 (2000).
- 184 Buss, A. *et al.* Growth-modulating molecules are associated with invading Schwann cells and not astrocytes in human traumatic spinal cord injury. *Brain* **130**, 940-953, doi:10.1093/brain/awl374 PMID - 17314203 (2006).
- 185 Zhang, S.-X., Huang, F., Gates, M. & Holmberg, E. G. Role of endogenous Schwann cells in tissue repair after spinal cord injury. *Neural Regen Res* **8**, 177-185, doi:10.3969/j.issn.1673-5374.2013.02.011 PMID - 25206489 (2013).
- 186 Goldshmit, Y. *et al.* Fgf-Dependent Glial Cell Bridges Facilitate Spinal Cord Regeneration in Zebrafish. *J Neurosci* **32**, 7477-7492, doi:10.1523/jneurosci.0758-12.2012 PMID - 22649227 (2012).
- 187 Kimura-Kuroda, J. *et al.* An in vitro model of the inhibition of axon growth in the lesion scar formed after central nervous system injury. *Mol Cell Neurosci* **43**, 177-187, doi:10.1016/j.mcn.2009.10.008 PMID - 19897043 (2010).
- 188 Fitch, M. T., Doller, C., Combs, C. K., Landreth, G. E. & Silver, J. Cellular and Molecular Mechanisms of Glial Scarring and Progressive Cavitation: In Vivo and In Vitro Analysis of Inflammation-Induced Secondary Injury after CNS Trauma. *J Neurosci* **19**, 8182-8198, doi:10.1523/jneurosci.19-19-08182.1999 PMID - 10493720 (1999).
- 189 Logan, A. *et al.* Effects of Transforming Growth Factor β 1, on Scar Production in the Injured Central Nervous System of the Rat. *Eur J Neurosci* **6**, 355-363, doi:10.1111/j.1460-9568.1994.tb00278.x PMID - 8019673 (1994).
- 190 East, E., Golding, J. P. & Phillips, J. B. A versatile 3D culture model facilitates monitoring of astrocytes undergoing reactive gliosis. *J Tissue Eng Regen M* **3**, 634-646, doi:10.1002/term.209 PMID - 19813215 (2009).
- 191 Faulkner, J. R. *et al.* Reactive Astrocytes Protect Tissue and Preserve Function after Spinal Cord Injury. *J Neurosci* **24**, 2143-2155, doi:10.1523/jneurosci.3547-03.2004 PMID - 14999065 (2004).
- 192 Bott, K. *et al.* The effect of matrix characteristics on fibroblast proliferation in 3D gels. *Biomaterials* **31**, 8454-8464, doi:10.1016/j.biomaterials.2010.07.046 PMID - 20684983 (2010).
- 193 Harris, G. M. *et al.* Nerve Guidance by a Decellularized Fibroblast Extracellular Matrix. *Matrix Biol* **60**, 176-189, doi:10.1016/j.matbio.2016.08.011 PMID - 27641621 (2017).
- 194 Franze, K., Janmey, P. A. & Guck, J. Mechanics in Neuronal Development and Repair. *Annu Rev Biomed Eng* **15**, 227-251, doi:10.1146/annurev-bioeng-071811-150045 PMID - 23642242 (2013).

- 195 Kalembeyi, I. *et al.* Tenascin-C upregulates matrix metalloproteinase-9 in breast cancer cells: Direct and synergistic effects with transforming growth factor β 1. *Int J Cancer* **105**, 53-60, doi:10.1002/ijc.11037 PMID - 12672030 (2003).
- 196 Tremble, P., Chiquet-Ehrismann, R. & Werb, Z. The extracellular matrix ligands fibronectin and tenascin collaborate in regulating collagenase gene expression in fibroblasts. *Mol Biol Cell* **5**, 439-453, doi:10.1091/mbc.5.4.439 PMID - 7519905 (1994).
- 197 Trebaul, A., Chan, E. K. & Midwood, K. S. Regulation of fibroblast migration by tenascin-C. *Biochem Soc T* **35**, 695-697, doi:10.1042/bst0350695 PMID - 17635125 (2007).
- 198 Ogier, C. *et al.* Matrix metalloproteinase-2 (MMP-2) regulates astrocyte motility in connection with the actin cytoskeleton and integrins. *Glia* **54**, 272-284, doi:10.1002/glia.20349 PMID - 16845676 (2006).
- 199 Goussev, S. *et al.* Differential temporal expression of matrix metalloproteinases after spinal cord injury: relationship to revascularization and wound healing. *J Neurosurg Spine* **99**, 188-197, doi:10.3171/spi.2003.99.2.0188 PMID - 12956462 (2003).
- 200 Tezel, G., Hernandez, M. R. & Wax, M. B. In vitro evaluation of reactive astrocyte migration, a component of tissue remodeling in glaucomatous optic nerve head. *Glia* **34**, 178-189, doi:10.1002/glia.1052 PMID - 11329180 (2001).
- 201 Zhang, H. *et al.* Matrix metalloproteinase-9 and stromal cell-derived factor-1 act synergistically to support migration of blood-borne monocytes into the injured spinal cord. *J Neurosci Official J Soc Neurosci* **31**, 15894-15903, doi:10.1523/jneurosci.3943-11.2011 PMID - 22049432 (2011).
- 202 Zhu, Y., Soderblom, C., Trojanowsky, M., Lee, D.-H. & Lee, J. K. Fibronectin Matrix Assembly after Spinal Cord Injury. *J Neurotraum* **32**, 1158-1167, doi:10.1089/neu.2014.3703 PMID - 25492623 (2015).
- 203 Shechter, R., Raposo, C., London, A., Sagi, I. & Schwartz, M. The Glial Scar-Monocyte Interplay: A Pivotal Resolution Phase in Spinal Cord Repair. *Plos One* **6**, e27969, doi:10.1371/journal.pone.0027969 PMID - 22205935 (2011).
- 204 Rolls, A. *et al.* Two Faces of Chondroitin Sulfate Proteoglycan in Spinal Cord Repair: A Role in Microglia/Macrophage Activation. *Plos Med* **5**, e171, doi:10.1371/journal.pmed.0050171 PMID - 18715114 (2008).
- 205 Clark, P., Britland, S. & Connolly, P. Growth cone guidance and neuron morphology on micropatterned laminin surfaces. *J Cell Sci* **105** (Pt 1), 203-212 (1993).
- 206 Hari, A., Djohar, B., Skutella, T. & Montazeri, S. Neurotrophins and extracellular matrix molecules modulate sensory axon outgrowth. *Int J Dev Neurosci* **22**, 113-117, doi:10.1016/j.ijdevneu.2003.12.002 PMID - 15036386 (2004).
- 207 Wood, M. D. & Willits, R. K. Applied electric field enhances DRG neurite growth: influence of stimulation media, surface coating and growth supplements. *J Neural Eng* **6**, 046003, doi:10.1088/1741-2560/6/4/046003 PMID - 19494423 (2009).
- 208 Rogers, S. L., Letourneau, P. C., Palm, S. L., McCarthy, J. & Furcht, L. T. Neurite extension by peripheral and central nervous system neurons in response to substratum-bound fibronectin and laminin. *Dev Biol* **98**, 212-220, doi:10.1016/0012-1606(83)90350-0 PMID - 6862106 (1983).

- 209 Bukhari, N., Torres, L., Robinson, J. K. & Tsirka, S. E. Axonal Regrowth after Spinal Cord Injury via Chondroitinase and the Tissue Plasminogen Activator (tPA)/Plasmin System. *J Neurosci* **31**, 14931-14943, doi:10.1523/jneurosci.3339-11.2011 PMID - 22016526 (2011).
- 210 Jones, L. L., Margolis, R. U. & Tuszynski, M. H. The chondroitin sulfate proteoglycans neurocan, brevican, phosphacan, and versican are differentially regulated following spinal cord injury. *Exp Neurol* **182**, 399-411, doi:10.1016/s0014-4886(03)00087-6 PMID - 12895450 (2003).
- 211 Bradbury, E. J. *et al.* Chondroitinase ABC promotes functional recovery after spinal cord injury. *Nature* **416**, 636-640, doi:10.1038/416636a PMID - 11948352 (2002).
- 212 Bartus, K. *et al.* Large-scale chondroitin sulfate proteoglycan digestion with chondroitinase gene therapy leads to reduced pathology and modulates macrophage phenotype following spinal cord contusion injury. *J Neurosci Official J Soc Neurosci* **34**, 4822-4836, doi:10.1523/jneurosci.4369-13.2014 PMID - 24695702 (2014).
- 213 Manwaring, M. E., Walsh, J. F. & Tresco, P. A. Contact guidance induced organization of extracellular matrix. *Biomaterials* **25**, 3631-3638, doi:10.1016/j.biomaterials.2003.10.043 PMID - 15020137 (2004).
- 214 Buss, A. *et al.* Gradual loss of myelin and formation of an astrocytic scar during Wallerian degeneration in the human spinal cord. *Brain* **127**, 34-44, doi:10.1093/brain/awh001 PMID - 14534158 (2004).
- 215 Buss, A. *et al.* NG2 and phosphacan are present in the astroglial scar after human traumatic spinal cord injury. *Bmc Neurol* **9**, 32, doi:10.1186/1471-2377-9-32 PMID - 19604403 (2009).
- 216 Shen, D., Wang, X. & Gu, X. Scar-modulating treatments for central nervous system injury. *Neurosci Bull* **30**, 967-984, doi:10.1007/s12264-013-1456-2 PMID - 24957881 (2014).
- 217 Faissner, A. *et al.* Contributions of astrocytes to synapse formation and maturation - Potential functions of the perisynaptic extracellular matrix. *Brain Res Rev* **63**, 26-38, doi:10.1016/j.brainresrev.2010.01.001 PMID - 20096729 (2010).
- 218 Rehmann, M. I., Santiñaque, F. F., López-Carro, B., Russo, R. E. & Trujillo-Cenóz, O. Cell proliferation and cytoarchitectural remodeling during spinal cord reconnection in the fresh-water turtle *Trachemys dorbignyi*. *Cell Tissue Res* **344**, 415-433, doi:10.1007/s00441-011-1173-y PMID - 21574060 (2011).
- 219 Mokalled, M. H. *et al.* Injury-induced *ctgfa* directs glial bridging and spinal cord regeneration in zebrafish. *Science* **354**, 630-634, doi:10.1126/science.aaf2679 PMID - 27811277 (2016).
- 220 Yu, Y. M. *et al.* The extracellular matrix glycoprotein tenascin-C promotes locomotor recovery after spinal cord injury in adult zebrafish. *Neuroscience* **183**, 238-250, doi:10.1016/j.neuroscience.2011.03.043 PMID - 21443931 (2011).
- 221 Chernoff, E. A. G., O'Hara, C. M., Bauerle, D. & Bowling, M. Matrix metalloproteinase production in regenerating axolotl spinal cord. *Wound Repair Regen* **8**, 282-291, doi:10.1046/j.1524-475x.2000.00282.x PMID - 11013020 (2000).

- 222 Tom, V. J., Doller, C. M., Malouf, A. T. & Silver, J. Astrocyte-Associated Fibronectin Is Critical for Axonal Regeneration in Adult White Matter. *J Neurosci* **24**, 9282-9290, doi:10.1523/jneurosci.2120-04.2004 PMID - 15496664 (2004).
- 223 Bozkurt, A. *et al.* In Vitro Assessment of Axonal Growth Using Dorsal Root Ganglia Explants in a Novel Three-Dimensional Collagen Matrix. *Tissue Eng* **13**, 2971-2979, doi:10.1089/ten.2007.0116 PMID - 17937537 (2007).
- 224 Smith, D. S. & Skene, J. H. P. A Transcription-Dependent Switch Controls Competence of Adult Neurons for Distinct Modes of Axon Growth. *J Neurosci* **17**, 646-658, doi:10.1523/jneurosci.17-02-00646.1997 PMID - 8987787 (1997).
- 225 Colognato, H. & Yurchenco, P. D. Form and function: The laminin family of heterotrimers. *Dev Dynam* **218**, 213-234, doi:10.1002/(sici)1097-0177(200006)218:2<213::aid-dvdy1>3.0.co;2-r PMID - 10842354 (2000).
- 226 Chen, Z.-L. & Strickland, S. Laminin $\gamma 1$ is critical for Schwann cell differentiation, axon myelination, and regeneration in the peripheral nerve. *J Cell Biology* **163**, 889-899, doi:10.1083/jcb.200307068 PMID - 14638863 (2003).
- 227 Weidner, N., Grill, R. J. & Tuszynski, M. H. Elimination of Basal Lamina and the Collagen “Scar” after Spinal Cord Injury Fails to Augment Corticospinal Tract Regeneration. *Exp Neurol* **160**, 40-50, doi:10.1006/exnr.1999.7200 PMID - 10630189 (1999).
- 228 Loy, D. N. *et al.* Temporal progression of angiogenesis and basal lamina deposition after contusive spinal cord injury in the adult rat. *J Comp Neurol* **445**, 308-324, doi:10.1002/cne.10168 PMID - 11920709 (2002).
- 229 Frisén, J. *et al.* Spinal axons in central nervous system scar tissue are closely related to laminin-immunoreactive astrocytes. *Neuroscience* **65**, 293-304, doi:10.1016/0306-4522(94)00467-j PMID - 7753403 (1995).
- 230 Singh, P., Carraher, C. & Schwarzbauer, J. E. Assembly of fibronectin extracellular matrix. *Annu Rev Cell Dev Biol* **26**, 397-419, doi:10.1146/annurev-cellbio-100109-104020 (2010).
- 231 Cooper, J. G. *et al.* Fibronectin EDA forms the chronic fibrotic scar after contusive spinal cord injury. *Neurobiol Dis* **116**, 60-68, doi:10.1016/j.nbd.2018.04.014 PMID - 29705186 (2018).
- 232 Ghosh, K., Ren, X.-D., Shu, X. Z., Prestwich, G. D. & Clark, R. A. F. Fibronectin Functional Domains Coupled to Hyaluronan Stimulate Adult Human Dermal Fibroblast Responses Critical for Wound Healing. **12**, 601-613, doi:10.1089/ten.2006.12.601 PMID - 16579693 (2006).
- 233 Egan, R. A. & Vijayan, V. K. Fibronectin immunoreactivity in neural trauma. *Brain Res* **568**, 330-334, doi:10.1016/0006-8993(91)91421-v PMID - 1814578 (1991).
- 234 Shearer, M. C. & Fawcett, J. W. The astrocyte/meningeal cell interface – a barrier to successful nerve regeneration? *Cell Tissue Res* **305**, 267-273, doi:10.1007/s004410100384 PMID - 11545264 (2001).
- 235 Klapka, N. & Müller, H. W. Collagen Matrix in Spinal Cord Injury. *J Neurotraum* **23**, 422-436, doi:10.1089/neu.2006.23.422 PMID - 16629627 (2006).
- 236 Klapka, N. *et al.* Suppression of fibrous scarring in spinal cord injury of rat promotes long-distance regeneration of corticospinal tract axons, rescue of primary motoneurons in somatosensory cortex and significant functional recovery. *Eur J*

- Neurosci* **22**, 3047-3058, doi:10.1111/j.1460-9568.2005.04495.x PMID - 16367771 (2005).
- 237 Stichel, C. C. *et al.* Basal membrane-depleted scar in lesioned CNS: characteristics and relationships with regenerating axons. *Neuroscience* **93**, 321-333, doi:10.1016/s0306-4522(99)00112-8 PMID - 10430496 (1999).
- 238 Stichel, C. C. *et al.* Inhibition of collagen IV deposition promotes regeneration of injured CNS axons. *Eur J Neurosci* **11**, 632-646, doi:10.1046/j.1460-9568.1999.00466.x PMID - 10051764 (1999).
- 239 Lemons, M. L., Sandy, J. D., Anderson, D. K. & Howland, D. R. Intact aggrecan and chondroitin sulfate-depleted aggrecan core glycoprotein inhibit axon growth in the adult rat spinal cord. *Exp Neurol* **184**, 981-990, doi:10.1016/s0014-4886(03)00383-2 (2003).
- 240 Rowlands, D. *et al.* Aggrecan directs extracellular matrix mediated neuronal plasticity. *J Neurosci* **38**, 1122-1118, doi:10.1523/jneurosci.1122-18.2018 PMID - 30282728 (2018).
- 241 Grimpe, B. & Silver, J. Progress in Brain Research. *Prog Brain Res* **137**, 333-349, doi:10.1016/s0079-6123(02)37025-0 PMID - 12440376 (2002).
- 242 Fitch, M. T. & Silver, J. CNS injury, glial scars, and inflammation: Inhibitory extracellular matrices and regeneration failure. *Exp Neurol* **209**, 294-301, doi:10.1016/j.expneurol.2007.05.014 PMID - 17617407 (2008).
- 243 Tang, X., Davies, J. E. & Davies, S. J. A. Changes in distribution, cell associations, and protein expression levels of NG2, neurocan, phosphacan, brevican, versican V2, and tenascin-C during acute to chronic maturation of spinal cord scar tissue. *J Neurosci Res* **71**, 427-444, doi:10.1002/jnr.10523 PMID - 12526031 (2003).
- 244 Condic, M. L., Snow, D. M. & Letourneau, P. C. Embryonic Neurons Adapt to the Inhibitory Proteoglycan Aggrecan by Increasing Integrin Expression. *J Neurosci* **19**, 10036-10043, doi:10.1523/jneurosci.19-22-10036.1999 PMID - 10559411 (1999).
- 245 Johnson, W. E. *et al.* Human intervertebral disc aggrecan inhibits nerve growth in vitro. *Arthritis Rheum* **46**, 2658-2664, doi:10.1002/art.10585 (2002).
- 246 Gensel, J. C., Schonberg, D. L., Alexander, J. K., McTigue, D. M. & Popovich, P. G. Semi-automated Sholl analysis for quantifying changes in growth and differentiation of neurons and glia. *J Neurosci Meth* **190**, 71-79, doi:10.1016/j.jneumeth.2010.04.026 PMID - 20438758 (2010).
- 247 Binley, K. E., Ng, W. S., Tribble, J. R., Song, B. & Morgan, J. E. Sholl analysis: A quantitative comparison of semi-automated methods. *J Neurosci Meth* **225**, 65-70, doi:10.1016/j.jneumeth.2014.01.017 PMID - 24485871 (2014).
- 248 Inman, D. M. & Steward, O. Ascending sensory, but not other long-tract axons, regenerate into the connective tissue matrix that forms at the site of a spinal cord injury in mice. *J Comp Neurol* **462**, 431-449, doi:10.1002/cne.10768 PMID - 12811811 (2003).
- 249 Dong, X., Han, S.-k., Zylka, M. J., Simon, M. I. & Anderson, D. J. A Diverse Family of GPCRs Expressed in Specific Subsets of Nociceptive Sensory Neurons. *Cell* **106**, 619-632, doi:10.1016/s0092-8674(01)00483-4 PMID - 11551509 (2001).

- 250 Shi, T.-J. S., Winzer-Serhan, U., Leslie, F. & Hökfelt, T. Distribution and regulation of $\alpha 2$ -adrenoceptors in rat dorsal root ganglia. *Pain* **84**, 319-330, doi:10.1016/s0304-3959(99)00224-9 PMID - 10666537 (2000).
- 251 Persohn, E., Malherbe, P. & Richards, J. G. In situ hybridization histochemistry reveals a diversity of GABAA receptor subunit mRNAs in neurons of the rat spinal cord and dorsal root ganglia. *Neuroscience* **42**, 497-507, doi:10.1016/0306-4522(91)90392-2 PMID - 1654537 (1991).
- 252 Tong, X.-j. *et al.* Sciatic nerve regeneration navigated by laminin-fibronectin double coated biodegradable collagen grafts in rats. *Brain Res* **663**, 155-162, doi:10.1016/0006-8993(94)90473-1 PMID - 7850464 (1994).
- 253 Vu, L. T., Jain, G., Veres, B. D. & Rajagopalan, P. Cell Migration on Planar and Three-Dimensional Matrices: A Hydrogel-Based Perspective. *Tissue Eng Part B Rev* **21**, 67-74, doi:10.1089/ten.teb.2013.0782 PMID - 25011932 (2015).
- 254 Hakkinen, K. M., Harunaga, J. S., Doyle, A. D. & Yamada, K. M. Direct Comparisons of the Morphology, Migration, Cell Adhesions, and Actin Cytoskeleton of Fibroblasts in Four Different Three-Dimensional Extracellular Matrices. *Tissue Eng Pt A* **17**, 713-724, doi:10.1089/ten.tea.2010.0273 PMID - 20929283 (2011).
- 255 Lee, J., Cuddihy, M. J. & Kotov, N. A. Three-Dimensional Cell Culture Matrices: State of the Art. *Tissue Eng Part B Rev* **14**, 61-86, doi:10.1089/ten.teb.2007.0150 PMID - 18454635 (2008).
- 256 Marquardt, L. & Willits, R. K. Student award winner in the undergraduate's degree category for the society for biomaterials 35th annual meeting, Orlando, Florida, April 13-16, 2011: Neurite growth in PEG gels: Effect of mechanical stiffness and laminin concentration. *J Biomed Mater Res A* **98A**, 1-6, doi:10.1002/jbm.a.33044 PMID - 21538826 (2011).
- 257 Koppes, A. N. *et al.* Neurite outgrowth on electrospun PLLA fibers is enhanced by exogenous electrical stimulation. *J Neural Eng* **11**, 046002, doi:10.1088/1741-2560/11/4/046002 PMID - 24891494 (2014).
- 258 Li, Y. *et al.* Engineering cell alignment in vitro. *Biotechnol Adv* **32**, 347-365, doi:10.1016/j.biotechadv.2013.11.007 PMID - 24269848 (2014).
- 259 Wang, W. *et al.* MicroRNA-21-5p mediates TGF- β -regulated fibrogenic activation of spinal fibroblasts and the formation of fibrotic scars after spinal cord injury. *Int J Biol Sci* **14**, 178-188, doi:10.7150/ijbs.24074 PMID - 29483836 (2018).
- 260 Hulmes, D. J. Building collagen molecules, fibrils, and suprafibrillar structures. *J Struct Biol* **137**, 2-10, doi:10.1006/jsbi.2002.4450 (2002).
- 261 Rittié, L. Fibrosis, Methods and Protocols. *Methods Mol Biology* **1627**, 395-407, doi:10.1007/978-1-4939-7113-8_26 PMID - 28836216 (2017).
- 262 Goodpaster, T. *et al.* An Immunohistochemical Method for Identifying Fibroblasts in Formalin-fixed, Paraffin-embedded Tissue. *J Histochem Cytochem* **56**, 347-358, doi:10.1369/jhc.7a7287.2007 PMID - 18071065 (2008).
- 263 Hesp, Z. C. *et al.* Proliferating NG2-Cell-Dependent Angiogenesis and Scar Formation Alter Axon Growth and Functional Recovery After Spinal Cord Injury in Mice. *J Neurosci* **38**, 1366-1382, doi:10.1523/jneurosci.3953-16.2017 PMID - 29279310 (2018).

- 264 Göritz, C. *et al.* A pericyte origin of spinal cord scar tissue. *Sci New York N Y* **333**, 238-242, doi:10.1126/science.1203165 PMID - 21737741 (2011).
- 265 Reeves, C., Pradim-Jardim, A., Sisodiya, S. M., Thom, M. & Liu, J. Y. W. Spatiotemporal dynamics of PDGFRbeta expression in pericytes and glial scar formation in penetrating brain injuries in adults. *Neuropathol Appl Neurobiol* **45**, 609-627, doi:10.1111/nan.12539 (2019).
- 266 Rajkumar, V. S. *et al.* Platelet-Derived Growth Factor- β Receptor Activation Is Essential for Fibroblast and Pericyte Recruitment during Cutaneous Wound Healing. *Am J Pathology* **169**, 2254-2265, doi:10.2353/ajpath.2006.060196 PMID - 17148686 (2006).
- 267 Zhu, S. *et al.* Immunolocalization of Periostin-like factor and Periostin during embryogenesis. *J Histochem Cytochem* **56**, 329-345, doi:10.1369/jhc.7A7321.2007 (2008).
- 268 Conway, S. J. *et al.* The role of periostin in tissue remodeling across health and disease. *Cell Mol Life Sci* **71**, 1279-1288, doi:10.1007/s00018-013-1494-y (2014).
- 269 Snider, P. *et al.* Origin of cardiac fibroblasts and the role of periostin. *Circ Res* **105**, 934-947, doi:10.1161/CIRCRESAHA.109.201400 (2009).
- 270 Shimamura, M. *et al.* Long-term expression of periostin during the chronic stage of ischemic stroke in mice. *Hypertens Res* **37**, 494-499, doi:10.1038/hr.2014.36 (2014).
- 271 Yokota, K. *et al.* Periostin Promotes Scar Formation through the Interaction between Pericytes and Infiltrating Monocytes/Macrophages after Spinal Cord Injury. *Am J Pathology* **187**, 639-653, doi:10.1016/j.ajpath.2016.11.010 PMID - 28082119 (2017).
- 272 Riew, T.-R., Choi, J.-H., Kim, H. L., Jin, X. & Lee, M.-Y. PDGFR- β -Positive Perivascular Adventitial Cells Expressing Nestin Contribute to Fibrotic Scar Formation in the Striatum of 3-NP Intoxicated Rats. *Front Mol Neurosci* **11**, 402, doi:10.3389/fnmol.2018.00402 PMID - 30455628 (2018).
- 273 Morita, S., Hourai, A. & Miyata, S. Changes in pericytic expression of NG2 and PDGFRB and vascular permeability in the sensory circumventricular organs of adult mouse by osmotic stimulation. *Cell Biochem Funct* **32**, 51-61, doi:10.1002/cbf.2971 (2014).
- 274 Cuttler, A. S. *et al.* Characterization of Pdgfrb-Cre transgenic mice reveals reduction of ROSA26 reporter activity in remodeling arteries. *Genesis* **49**, 673-680, doi:10.1002/dvg.20769 (2011).
- 275 Shen, J. *et al.* PDGFR-beta as a positive regulator of tissue repair in a mouse model of focal cerebral ischemia. *J Cereb Blood Flow Metab* **32**, 353-367, doi:10.1038/jcbfm.2011.136 (2012).
- 276 Andrae, J., Gallini, R. & Betsholtz, C. Role of platelet-derived growth factors in physiology and medicine. *Gene Dev* **22**, 1276-1312, doi:10.1101/gad.1653708 PMID - 18483217 (2008).
- 277 Figley, S. A., Khosravi, R., Legasto, J. M., Tseng, Y.-F. & Fehlings, M. G. Characterization of Vascular Disruption and Blood-Spinal Cord Barrier Permeability following Traumatic Spinal Cord Injury. *J Neurotraum* **31**, 541-552, doi:10.1089/neu.2013.3034 PMID - 24237182 (2014).

- 278 Kamei, N. *et al.* Contribution of bone marrow-derived endothelial progenitor cells to neovascularization and astrogliosis following spinal cord injury. *J Neurosci Res* **90**, 2281-2292, doi:10.1002/jnr.23113 (2012).
- 279 Cullen, B., Silcock, D., Brown, L. J., Gosiewska, A. & Geesin, J. C. The differential regulation and secretion of proteinases from fetal and neonatal fibroblasts by growth factors. *Int J Biochem Cell Biology* **29**, 241-250, doi:10.1016/s1357-2725(96)00137-9 PMID - 9076959 (1997).
- 280 Werner, S. & Grose, R. Regulation of Wound Healing by Growth Factors and Cytokines. *Physiol Rev* **83**, 835-870, doi:10.1152/physrev.2003.83.3.835 PMID - 12843410 (2003).
- 281 Klingberg, F., Hinz, B. & White, E. S. The myofibroblast matrix: implications for tissue repair and fibrosis. *J Pathology* **229**, 298-309, doi:10.1002/path.4104 PMID - 22996908 (2013).
- 282 Smithmyer, M. E., Sawicki, L. A. & Kloxin, A. M. Hydrogel scaffolds as in vitro models to study fibroblast activation in wound healing and disease. *Biomater Sci-uk* **2**, 634-650, doi:10.1039/c3bm60319a PMID - 25379176 (2014).
- 283 Bear, J. E. & Haugh, J. M. Directed migration of mesenchymal cells: where signaling and the cytoskeleton meet. *Curr Opin Cell Biol* **30**, 74-82, doi:10.1016/j.ceb.2014.06.005 PMID - 24999834 (2014).
- 284 Dias, D. O. & Göritz, C. Fibrotic scarring following lesions to the central nervous system. *Matrix Biol* **68-69**, 561-570, doi:10.1016/j.matbio.2018.02.009 PMID - 29428230 (2018).
- 285 Kirshblum, S. *et al.* A Comparison of Diagnostic Stability of the ASIA Impairment Scale Versus Frankel Classification Systems for Traumatic Spinal Cord Injury. *Arch Phys Med Rehabil*, doi:10.1016/j.apmr.2020.05.016 (2020).
- 286 Scheff, S. W., Rabchevsky, A. G., Fugaccia, I., Main, J. A. & Lump, J. E. Experimental Modeling of Spinal Cord Injury: Characterization of a Force-Defined Injury Device. **20**, 179-193, doi:10.1089/08977150360547099 PMID - 12675971 (2003).
- 287 Ma, M., Basso, D. M., Walters, P., Stokes, B. T. & Jakeman, L. B. Behavioral and Histological Outcomes Following Graded Spinal Cord Contusion Injury in the C57Bl/6 Mouse. *Exp Neurol* **169**, 239-254, doi:10.1006/exnr.2001.7679 PMID - 11358439 (2001).
- 288 Choo, A. M. *et al.* Contusion, dislocation, and distraction: primary hemorrhage and membrane permeability in distinct mechanisms of spinal cord injury. *J Neurosurg Spine* **6**, 255-266 (2007).
- 289 Gordon, S. & Taylor, P. R. Monocyte and macrophage heterogeneity. *Nat Rev Immunol* **5**, 953-964, doi:10.1038/nri1733 PMID - 16322748 (2005).
- 290 Sjøvold, S. G. *et al.* Histological Effects of Residual Compression Sustained for 60 Minutes at Different Depths in a Novel Rat Spinal Cord Injury Contusion Model. *J Neurotraum* **30**, 1374-1384, doi:10.1089/neu.2013.2906 PMID - 23731342 (2013).
- 291 Okon, E. B. *et al.* Intraparenchymal Microdialysis after Acute Spinal Cord Injury Reveals Differential Metabolic Responses to Contusive versus Compressive Mechanisms of Injury. *J Neurotraum* **30**, 1564-1576, doi:10.1089/neu.2013.2956 PMID - 23768189 (2013).

- 292 Streijger, F. *et al.* Characterization of a Cervical Spinal Cord Hemicontusion Injury in Mice Using the Infinite Horizon Impactor. *J Neurotraum* **30**, 869-883, doi:10.1089/neu.2012.2405 PMID - 23360150 (2013).
- 293 Santiago, J. M. *et al.* Molecular, Anatomical, Physiological, and Behavioral Studies of Rats Treated with Buprenorphine after Spinal Cord Injury. *J Neurotraum* **26**, 1783-1793, doi:10.1089/neu.2007.0502 PMID - 19653810 (2009).
- 294 Motulsky, H. J. & Brown, R. E. Detecting outliers when fitting data with nonlinear regression – a new method based on robust nonlinear regression and the false discovery rate. *Bmc Bioinformatics* **7**, 123, doi:10.1186/1471-2105-7-123 PMID - 16526949 (2006).
- 295 Joshi, M. & Fehlings, M. G. Development and Characterization of a Novel, Graded Model of Clip Compressive Spinal Cord Injury in the Mouse: Part 1. Clip Design, Behavioral Outcomes, and Histopathology. *J Neurotraum* **19**, 175-190, doi:10.1089/08977150252806947 PMID - 11893021 (2002).
- 296 Dimar, J. R., Glassman, S. D., Raque, G. H., Zhang, Y. P. & Shields, C. B. The Influence of Spinal Canal Narrowing and Timing of Decompression on Neurologic Recovery After Spinal Cord Contusion in a Rat Model. *Spine* **24**, 1623, doi:10.1097/00007632-199908150-00002 PMID - 10472095 (1999).
- 297 Kubota, K. *et al.* Neurological recovery is impaired by concurrent but not by asymptomatic pre-existing spinal cord compression after traumatic spinal cord injury. *Spine (Phila Pa 1976)* **37**, 1448-1455, doi:10.1097/BRS.0b013e31824ffda5 (2012).
- 298 Ropper, A. E. *et al.* An efficient device to experimentally model compression injury of mammalian spinal cord. *Exp Neurol* **271**, 515-523, doi:10.1016/j.expneurol.2015.07.012 PMID - 26210871 (2015).
- 299 Zhang, Y.-K. *et al.* Different TLR4 expression and microglia/macrophage activation induced by hemorrhage in the rat spinal cord after compressive injury. *J Neuroinflamm* **10**, 112, doi:10.1186/1742-2094-10-112 PMID - 24015844 (2013).
- 300 Kroner, A. *et al.* TNF and increased intracellular iron alter macrophage polarization to a detrimental M1 phenotype in the injured spinal cord. *Neuron* **83**, 1098-1116, doi:10.1016/j.neuron.2014.07.027 (2014).
- 301 Batchelor, P. E., Tan, S., Wills, T. E., Porritt, M. J. & Howells, D. W. Comparison of Inflammation in the Brain and Spinal Cord following Mechanical Injury. *J Neurotraum* **25**, 1217-1225, doi:10.1089/neu.2007.0308 PMID - 18986223 (2008).
- 302 Andjelkovic, A. V., Nikolic, B., Pachter, J. S. & Zecevic, N. Macrophages/microglial cells in human central nervous system during development: an immunohistochemical study. *Brain Res* **814**, 13-25, doi:10.1016/s0006-8993(98)00830-0 PMID - 9838024 (1998).
- 303 Gazi, U. & Martinez-Pomares, L. Influence of the mannose receptor in host immune responses. *Immunobiology* **214**, 554-561, doi:10.1016/j.imbio.2008.11.004 PMID - 19162368 (2009).
- 304 Stahl, P. D. & Ezekowitz, R. A. B. The mannose receptor is a pattern recognition receptor involved in host defense. *Curr Opin Immunol* **10**, 50-55, doi:10.1016/s0952-7915(98)80031-9 PMID - 9523111 (1998).

- 305 Chang, C.-I., Liao, J. C. & Kuo, L. Arginase modulates nitric oxide production in activated macrophages. *Am J Physiology Hear Circulatory Physiology* **274**, H342-H348, doi:10.1152/ajpheart.1998.274.1.h342 PMID - 29591520 (1998).
- 306 Imagama, T. *et al.* Regulation of nitric oxide generation by up-regulated arginase I in rat spinal cord injury. *J Clin Biochem Nutr* **51**, 68-75, doi:10.3164/jcbn.d-11-00011 PMID - 22798716 (2012).
- 307 Wang, Z. *et al.* Recombinant human arginase I elicited immunosuppression in activated macrophages through inhibiting autophagy. *Appl Microbiol Biot* **103**, 4825-4838, doi:10.1007/s00253-019-09832-w PMID - 31053913 (2019).
- 308 Gensel, J. C., Kopper, T. J., Zhang, B., Orr, M. B. & Bailey, W. M. Predictive screening of M1 and M2 macrophages reveals the immunomodulatory effectiveness of post spinal cord injury azithromycin treatment. *Sci Rep-uk* **7**, 40144, doi:10.1038/srep40144 PMID - 28057928 (2017).
- 309 Nolan, A. *et al.* Differential Role for CD80 and CD86 in the Regulation of the Innate Immune Response in Murine Polymicrobial Sepsis. *Plos One* **4**, e6600, doi:10.1371/journal.pone.0006600 PMID - 19672303 (2009).
- 310 Perry, V. H., Andersson, P.-B. & Gordon, S. Macrophages and inflammation in the central nervous system. *Trends Neurosci* **16**, 268-273, doi:10.1016/0166-2236(93)90180-t PMID - 7689770 (1993).
- 311 Mukhopadhyay, S. *et al.* MARCO, an innate activation marker of macrophages, is a class A scavenger receptor for *Neisseria meningitidis*. *Eur J Immunol* **36**, 940-949, doi:10.1002/eji.200535389 PMID - 16525990 (2006).
- 312 Novakowski, K. E. *et al.* A naturally occurring transcript variant of MARCO reveals the SRCR domain is critical for function. *Immunol Cell Biol* **94**, 646-655, doi:10.1038/icb.2016.20 PMID - 26888252 (2016).
- 313 Bowdish, D. M. E. *et al.* MARCO, TLR2, and CD14 are required for macrophage cytokine responses to mycobacterial trehalose dimycolate and *Mycobacterium tuberculosis*. *Plos Pathog* **5**, e1000474, doi:10.1371/journal.ppat.1000474 PMID - 19521507 (2009).
- 314 Elomaa, O. *et al.* Cloning of a novel bacteria-binding receptor structurally related to scavenger receptors and expressed in a subset of macrophages. *Cell* **80**, 603-609, doi:10.1016/0092-8674(95)90514-6 PMID - 7867067 (1995).
- 315 Mukhopadhyay, S. *et al.* SR-A/MARCO-mediated ligand delivery enhances intracellular TLR and NLR function, but ligand scavenging from cell surface limits TLR4 response to pathogens. *Blood* **117**, 1319-1328, doi:10.1182/blood-2010-03-276733 PMID - 21098741 (2011).
- 316 Dahl, M. *et al.* Protection against inhaled oxidants through scavenging of oxidized lipids by macrophage receptors MARCO and SR-AI/II. *J Clin Invest* **117**, 757-764, doi:10.1172/jci29968 PMID - 17332894 (2007).
- 317 Zhang, B. & Gensel, J. C. Is neuroinflammation in the injured spinal cord different than in the brain? Examining intrinsic differences between the brain and spinal cord. *Exp Neurol* **258**, 112-120, doi:10.1016/j.expneurol.2014.04.007 PMID - 25017892 (2014).
- 318 Getts, D. R. *et al.* Therapeutic Inflammatory Monocyte Modulation Using Immune-Modifying Microparticles. *Sci Transl Med* **6**, 219ra217-219ra217, doi:10.1126/scitranslmed.3007563 PMID - 24431111 (2014).

- 319 Mukhopadhyay, S. *et al.* SR-A/MARCO-mediated ligand delivery enhances intracellular TLR and NLR function, but ligand scavenging from cell surface limits TLR4 response to pathogens. *Blood* **117**, 1319-1328, doi:10.1182/blood-2010-03-276733 (2011).
- 320 Carlson, G. D. *et al.* Early Time-Dependent Decompression for Spinal Cord Injury: Vascular Mechanisms of Recovery. *J Neurotraum* **14**, 951-962, doi:10.1089/neu.1997.14.951 PMID - 9475376 (1997).
- 321 Zhang, B., Bailey, W. M., Braun, K. J. & Gensel, J. C. Age decreases macrophage IL-10 expression: Implications for functional recovery and tissue repair in spinal cord injury. *Exp Neurol* **273**, 83-91, doi:10.1016/j.expneurol.2015.08.001 (2015).
- 322 Shah, J. M., Omar, E., Pai, D. R. & Sood, S. Cellular events and biomarkers of wound healing. *Indian J Plast Surg* **45**, 220-228, doi:10.4103/0970-0358.101282 (2012).
- 323 Desmouliere, A., Darby, I. A., Laverdet, B. & Bonté, F. Fibroblasts and myofibroblasts in wound healing. *Clin Cosmet Investigational Dermatology Volume* **7**, 301-311, doi:10.2147/ccid.s50046 PMID - 25395868 (2014).
- 324 Wynn, T. A. & Vannella, K. M. Macrophages in Tissue Repair, Regeneration, and Fibrosis. *Immunity* **44**, 450-462, doi:10.1016/j.immuni.2016.02.015 (2016).
- 325 Mescher, A. L. Macrophages and fibroblasts during inflammation and tissue repair in models of organ regeneration. *Regen* **4**, 39-53, doi:10.1002/reg2.77 PMID - 28616244 (2017).
- 326 Enzerink, A. & Vaheri, A. Fibroblast activation in vascular inflammation. *J Thromb Haemost* **9**, 619-626, doi:10.1111/j.1538-7836.2011.04209.x (2011).
- 327 Duan, L. *et al.* PDGFRbeta Cells Rapidly Relay Inflammatory Signal from the Circulatory System to Neurons via Chemokine CCL2. *Neuron* **100**, 183-200 e188, doi:10.1016/j.neuron.2018.08.030 (2018).
- 328 Beidler, S. K. *et al.* Inflammatory cytokine levels in chronic venous insufficiency ulcer tissue before and after compression therapy. *J Vasc Surg* **49**, 1013-1020, doi:10.1016/j.jvs.2008.11.049 (2009).
- 329 Gope, R. The effect of epidermal growth factor & platelet-derived growth factors on wound healing process. *Indian J Medical Res* **116**, 201-206 (2002).
- 330 Nishimura, S. L. Integrin-Mediated Transforming Growth Factor- β Activation, a Potential Therapeutic Target in Fibrogenic Disorders. *Am J Pathology* **175**, 1362-1370, doi:10.2353/ajpath.2009.090393 PMID - 19729474 (2009).
- 331 Humphries, J. D., Byron, A. & Humphries, M. J. Integrin ligands at a glance. *J Cell Sci* **119**, 3901-3903, doi:10.1242/jcs.03098 PMID - 16988024 (2006).
- 332 Cheah, M. *et al.* Expression of an Activated Integrin Promotes Long-Distance Sensory Axon Regeneration in the Spinal Cord. *J Neurosci* **36**, 7283-7297, doi:10.1523/jneurosci.0901-16.2016 PMID - 27383601 (2016).
- 333 Steffensen, B., Häkkinen, L. & Larjava, H. Proteolytic Events of Wound-Healing — Coordinated Interactions Among Matrix Metalloproteinases (MMPs), Integrins, and Extracellular Matrix Molecules. *Crit Rev Oral Biol M* **12**, 373-398, doi:10.1177/10454411010120050201 PMID - 12002821 (2001).
- 334 Noble, L. J., Donovan, F., Igarashi, T., Goussev, S. & Werb, Z. Matrix Metalloproteinases Limit Functional Recovery after Spinal Cord Injury by

- Modulation of Early Vascular Events. *J Neurosci* **22**, 7526-7535, doi:10.1523/jneurosci.22-17-07526.2002 PMID - 12196576 (2002).
- 335 Duchossoy, Y., Horvat, J.-C. & Stettler, O. MMP-Related Gelatinase Activity Is Strongly Induced in Scar Tissue of Injured Adult Spinal Cord and Forms Pathways for Ingrowing Neurites. *Mol Cell Neurosci* **17**, 945-956, doi:10.1006/mcne.2001.0986 PMID - 11414785 (2001).
- 336 Achterberg, V. F. *et al.* The Nano-Scale Mechanical Properties of the Extracellular Matrix Regulate Dermal Fibroblast Function. *J Invest Dermatol* **134**, 1862-1872, doi:10.1038/jid.2014.90 PMID - 24670384 (2014).
- 337 Ayala, P., Lopez, J. I. & Desai, T. A. Microtopographical Cues in 3D Attenuate Fibrotic Phenotype and Extracellular Matrix Deposition: Implications for Tissue Regeneration. *Tissue Eng Pt A* **16**, 2519-2527, doi:10.1089/ten.tea.2009.0815 PMID - 20235832 (2010).
- 338 Naik, P. K. *et al.* Periostin promotes fibrosis and predicts progression in patients with idiopathic pulmonary fibrosis. *Am J Physiol Lung Cell Mol Physiol* **303**, L1046-1056, doi:10.1152/ajplung.00139.2012 (2012).
- 339 Beer, H. D., Longaker, M. T. & Werner, S. Reduced expression of PDGF and PDGF receptors during impaired wound healing. *J Invest Dermatol* **109**, 132-138, doi:10.1111/1523-1747.ep12319188 (1997).
- 340 Ashcroft, G. S., Horan, M. A. & Ferguson, M. W. J. The effects of ageing on wound healing: immunolocalisation of growth factors and their receptors in a murine incisional model. *J Anat* **190**, 351-365, doi:10.1046/j.1469-7580.1997.19030351.x PMID - 9147222 (1997).
- 341 Antoniades, H. N. *et al.* Platelet-derived growth factor in idiopathic pulmonary fibrosis. *J Clin Invest* **86**, 1055-1064, doi:10.1172/jci114808 PMID - 2170444 (1990).
- 342 Bonner, J. C. Regulation of PDGF and its receptors in fibrotic diseases. *Cytokine Growth F R* **15**, 255-273, doi:10.1016/j.cytogfr.2004.03.006 PMID - 15207816 (2004).
- 343 Klement, W. *et al.* A pericyte-glia scarring develops at the leaky capillaries in the hippocampus during seizure activity. *Epilepsia* **60**, 1399-1411, doi:10.1111/epi.16019 (2019).
- 344 Kjell, J. *et al.* Delayed Imatinib Treatment for Acute Spinal Cord Injury: Functional Recovery and Serum Biomarkers. *J Neurotraum* **32**, 1645-1657, doi:10.1089/neu.2014.3863 PMID - 25914996 (2015).
- 345 Abrams, M. B. *et al.* Imatinib Enhances Functional Outcome after Spinal Cord Injury. *Plos One* **7**, e38760, doi:10.1371/journal.pone.0038760 PMID - 22723886 (2012).
- 346 Su, E. J. *et al.* Imatinib treatment reduces brain injury in a murine model of traumatic brain injury. *Front Cell Neurosci* **9**, 385, doi:10.3389/fncel.2015.00385 PMID - 26500491 (2015).
- 347 Sharp, K. G., Yee, K. M. & Steward, O. A re-assessment of treatment with a tyrosine kinase inhibitor (imatinib) on tissue sparing and functional recovery after spinal cord injury. *Exp Neurol* **254**, 1-11, doi:10.1016/j.expneurol.2013.12.019 PMID - 24440639 (2014).

- 348 Abrams, M. B. *et al.* Response to the report, “A re-assessment of treatment with a tyrosine kinase inhibitor (imatinib) on tissue sparing and functional recovery after spinal cord injury” by Sharp *et al.* *Exp Neurol* **257**, 182-185, doi:10.1016/j.expneurol.2014.04.025 PMID - 24825370 (2014).
- 349 Cesarman-Maus, G. & Hajjar, K. A. Molecular mechanisms of fibrinolysis. *Brit J Haematol* **129**, 307-321, doi:10.1111/j.1365-2141.2005.05444.x PMID - 15842654 (2005).
- 350 Syrovets, T., Lunov, O. & Simmet, T. Plasmin as a proinflammatory cell activator. *J Leukocyte Biol* **92**, 509-519, doi:10.1189/jlb.0212056 PMID - 22561604 (2012).
- 351 Braughler, J. & Hall, E. Central nervous systems trauma and strokeI. Biochemical considerations for oxygen radical formation and lipid peroxidation. *Free Radical Bio Med* **6**, 289-301, doi:10.1016/0891-5849(89)90056-7 PMID - 2663662 (1989).
- 352 Losey, P., Young, C., Krimholtz, E., Bordet, R. & Anthony, D. C. The role of hemorrhage following spinal-cord injury. *Brain Res* **1569**, 9-18, doi:10.1016/j.brainres.2014.04.033 PMID - 24792308 (2014).
- 353 Gaasch, J. A., Lockman, P. R., Geldenhuys, W. J., Allen, D. D. & Van der Schyf, C. J. Brain iron toxicity: differential responses of astrocytes, neurons, and endothelial cells. *Neurochem Res* **32**, 1196-1208, doi:10.1007/s11064-007-9290-4 (2007).
- 354 Kroner, A. *et al.* TNF and Increased Intracellular Iron Alter Macrophage Polarization to a Detrimental M1 Phenotype in the Injured Spinal Cord. *Neuron* **83**, 1098-1116, doi:10.1016/j.neuron.2014.07.027 PMID - 25132469 (2014).
- 355 Younan, D. *et al.* Early Trauma-Induced Coagulopathy is Associated with Increased Ventilator-Associated Pneumonia in Spinal Cord Injury Patients. *Shock* **45**, 502-505, doi:10.1097/shk.0000000000000531 PMID - 26863121 (2016).
- 356 Stein, S. C. & Smith, D. H. Coagulopathy in traumatic brain injury. *Neurocrit Care* **1**, 479-488, doi:10.1385/ncc:1:4:479 PMID - 16174954 (2004).
- 357 Samuels, J. M. *et al.* Severe traumatic brain injury is associated with a unique coagulopathy phenotype. *J Trauma Acute Care* **Publish Ahead of Print**, &NA;, doi:10.1097/ta.00000000000002173 PMID - 30601456 (2018).
- 358 Lustenberger, T. *et al.* Time course of coagulopathy in isolated severe traumatic brain injury. *Inj* **41**, 924-928, doi:10.1016/j.injury.2010.04.019 PMID - 20471013 (2010).
- 359 Flössel, C., Luther, T., Müller, M., Albrecht, S. & Kasper, M. Immunohistochemical detection of tissue factor (TF) on paraffin sections of routinely fixed human tissue. *Histochemistry* **101**, 449-453, doi:10.1007/bf00269495 PMID - 7960944 (1994).
- 360 Hijazi, N. *et al.* Endogenous plasminogen activators mediate progressive intracerebral hemorrhage after traumatic brain injury in mice. *Blood* **125**, 2558-2567, doi:10.1182/blood-2014-08-588442 PMID - 25673638 (2015).
- 361 Laroche, M., Kutcher, M. E., Huang, M. C., Cohen, M. J. & Manley, G. T. Coagulopathy After Traumatic Brain Injury. *Neurosurgery* **70**, 1334-1345, doi:10.1227/neu.0b013e31824d179b PMID - 22307074 (2012).
- 362 Cesarman-Maus, G. & Hajjar, K. A. Molecular mechanisms of fibrinolysis. *Br J Haematol* **129**, 307-321, doi:10.1111/j.1365-2141.2005.05444.x (2005).

- 363 collaborators, C. *et al.* The importance of early treatment with tranexamic acid in
bleeding trauma patients: an exploratory analysis of the CRASH-2 randomised
controlled trial. *Lancet* **377**, 1096-1101.e1092, doi:10.1016/s0140-6736(11)60278-
x PMID - 21439633 (2011).
- 364 Study, C.-C. Effect of tranexamic acid in traumatic brain injury: a nested
randomised, placebo controlled trial (CRASH-2 Intracranial Bleeding Study). *Bmj*
343, d3795, doi:10.1136/bmj.d3795 PMID - 21724564 (2011).
- 365 Longstaff, C. & Locke, M. Increased urokinase and consumption of α 2-antiplasmin
as an explanation for the loss of benefit of tranexamic acid after treatment delay. *J*
Thromb Haemost **17**, 195-205, doi:10.1111/jth.14338 PMID - 30451372 (2019).
- 366 Shiraishi, Y. *et al.* Short-term inhibition of fibrinolytic system restores locomotor
function after spinal cord injury in mice. *Sci Rep-uk* **9**, 16024, doi:10.1038/s41598-
019-52621-8 PMID - 31690812 (2019).

VITA

Michael B Orr

Education

B.S. Biology 2010-2014
Centre College, Danville Ky

Professional Experience

Healthcare Research Project Manager 2020-present
Vanderbilt Institute for Clinical and Translational Research, VUMC Nashville, TN

Graduate Research Assistant 2015-2021
Physiology Department, University of Kentucky Lexington, Ky

Commercialization Fellow Jan-Dec 2018
Office of Technology Commercialization, University of Kentucky Lexington, Ky

Laboratory Technician 2014-2015
Spinal Cord and Brain Injury Research Center, University of Kent. Lexington, Ky

Research Assistant Jun-Oct 2014
Biochemistry Department, Centre College Danville, Ky

Scholastic and Professional Honors

NIH F31 NS110264-O1A1 – nationally-competitive research training fellowship 2019-20
Graduate Poster Award – International Symposium for Neural Regeneration 2020
NIH 5T32 NS077889 – competitive intra-institutional training fellowship 2018-2019
Fellowship for Graduate Excellence – Uky College of Medicine 2017
Travel Award – University of Kentucky College of Medicine 2017, 2019
Selected Speaker – Comparative Biology of Tissue Regeneration Symposium 2017
Travel Award – Spinal Cord and Brain Injury Research Center 2016
Graduate Travel Award – International Symposium for Neural Regeneration 2015
Lab Tech Poster Award – Bluegrass Society for Neuroscience 2015

Professional Publications

John C. Gensel and **Michael B. Orr**. Reflections on Data Sharing Practices in Spinal Cord Injury Research. *Neuroinformatics*, 2021. DOI: <https://doi.org/10.1007/s12021-020-09498-0>

Chao Ma, Jerry B. Hunt, Maj-Linda B. Selenica, Awa Sanneh, Leslie Sandusky-Betran, Mallory Watler, Rana Daas, Andrii Kovalenko, Huimin Liang, Devon Placides, Chuanhai Cao, Xiaoyang Lin, **Michael B. Orr**, Bei Zhang, John C. Gensel, David J. Feola, Marcia

N. Gordon, Dave Morgan, Paula C. Bickford, and Daniel C. Lee. Arginase 1 Insufficiency Precipitates Amyloid- β Deposition and Hastens Behavioral Impairment in a Mouse Model of Amyloidosis. *Frontiers in Immunology*, 2020. DOI: 10.3389/fimmu.2020.582998

Timothy J Kopper, Katelyn E McFarlane, William M Bailey, **Michael B. Orr**, Bei Zhang, and John C Gensel. Delayed azithromycin treatment improves recovery after mouse spinal cord injury. *Frontiers in Cellular Neuroscience*, 2019. 13: 490. DOI: 10.3389/fncel.2019.00490

Michael B. Orr and John C. Gensel. Spinal cord injury scarring and inflammation: therapies targeting glial and inflammatory responses. Invited Review, *Neurotherapeutics*, 2018. 68(3): 409-422, 2018. DOI: 10.1016/j.neurother.2018.03.002

Michael B. Orr and John C. Gensel. Interactions of primary insult biomechanics and secondary cascades in spinal cord injury, implications for therapy. *Neural Regeneration Research*, 2017. (12)10:1618-1619, 2017. DOI: 10.4103/1673-5374.217332.

Michael B. Orr, Jennifer Simkin, William M. Bailey, Neha S. Kadambi, Anna Leigh McVicar, Amy K. Veldhorst, and John C. Gensel. Compression decreases anatomical and functional recovery and alters inflammation after contusive spinal cord injury. *Journal of Neurotrauma*, 2017. DOI: 10.1089/neu.2016.4915.

John C. Gensel, Bei Zhang, **Michael B. Orr**, William M. Bailey. Predictive screening of M1 and M2 macrophages reveal the immunomodulatory effectiveness of post spinal cord injury azithromycin treatment. *Scientific Reports*, 2017. DOI: 10.1038/srep40144

Bei Zhang, William M. Bailey, Timothy J. Kopper, **Michael B. Orr**, David J. Feola, and John C. Gensel. Azithromycin drives alternative macrophage activation and improves recovery and tissue sparing in contusion spinal cord injury. *Journal of Neuroinflammation*, 2015. 12:218, DOI: 10.1186/s12974-015-0440-3